The Development and Optimisation of a Fast Pyrolysis Process for Bio-oil Production

ABBA SANI KALGO

Doctor of Philosophy

ASTON UNIVERSITY

June 2011

Aston University

The Development and Optimisation of a Fast Pyrolysis Process for Bio-Oil Production

Abba Sani Kalgo
Doctor of Philosophy
2011

THESIS SUMMARY

A two-tier study is presented in this thesis. The first involves the commissioning of an extant but at the time, unproven bubbling fluidised bed fast pyrolysis unit. The unit was designed for an intended nominal throughput of 300 g/h of biomass. The unit came complete with solids separation, pyrolysis vapour quenching and oil collection systems. Modifications were carried out on various sections of the system including the reactor heating, quenching and liquid collection systems. The modifications allowed for fast pyrolysis experiments to be carried out at the appropriate temperatures. Bio-oil was generated using conventional biomass feedstocks including Willow, Beechwood, Pine and Miscanthus.

Results from this phase of the research showed however, that although the rig was capable of processing biomass to bio-oil, it was characterised by low mass balance closures and recurrent operational problems. The problems included blockages, poor reactor hydrodynamics and reduced organic liquid yields. The less than optimal performance of individual sections, particularly the feed and reactor systems of the rig, culminated in a poor overall performance of the system.

The second phase of this research involved the redesign of two key components of the unit. An alternative feeding system was commissioned for the unit. The feed system included an off the shelf gravimetric system for accurate metering and efficient delivery of biomass. Similarly, a new bubbling fluidised bed reactor with an intended nominal throughput of 500g/h of biomass was designed and constructed. The design leveraged on experience from the initial commissioning phase with proven kinetic and hydrodynamic studies. These units were commissioned as part of the optimisation phase of the study.

Also as part of this study, two varieties each, of previously unreported feedstocks namely Jatropha *curcas* and Moringa *olifiera* oil seed press cakes were characterised to determine their suitability as feedstocks for liquid fuel production via fast pyrolysis. Consequently, the feedstocks were used for the production of pyrolysis liquids. The quality of the pyrolysis liquids from the feedstocks were then investigated via a number of analytical techniques. The oils from the press cakes showed high levels of stability and reduced pH values.

The improvements to the design of the fast pyrolysis unit led to higher mass balance closures and increased organic liquid yields. The maximum liquid yield obtained from the press cakes was from African Jatropha press cake at 66 wt% on a dry basis.

Key words: Biomass, Jatropha *curcas*, Moringa *olifiera*, Press cakes, Fluidised bed reactor

"We must all aspire to intellectual honesty. Intellectual honesty demands that when you meet a very powerful argument or come across counter evidence, you have to accept it, take it into the equation and adjust your own views accordingly."

A.C Grayling

"Nothing in the world can take the place of persistence. Talent will not; nothing is more common than unsuccessful men with talent. Genius will not; unrewarded genius is almost a proverb. Education will not; the world is full of educated derelicts. Persistence and determination are omnipotent. The slogan press on has solved and always will solve the problems of the human race. No person was ever honoured for what he received. Honour has been the reward for what he gave."

Calvin Coolidge (1872-1933)

"It is a capital mistake to theorise before one has data. Insensibly one begins to twist facts to suit theories instead of theories to suit facts."

Mr. Sherlock Holmes of 221B, Baker Street
Fictional character created by
Sir Arthur Conan Doyle (1859 – 1930)

ACKNOWLEDGEMENTS

For Habiba

One good mother is worth a hundred schoolmasters

TABLE OF CONTENTS

LIST OF FIGURES

LIST OF TABLES

1 INTRODUCTION

1.1 BACKGROUND

The oil embargoes of the 1970's disrupted the global energy supplies. A consequence of the embargoes was a fluctuation in global energy prices. This led to a renewed search for energy from alternative sources. The disruption coupled with a realisation that conventional fossil fuels are finite and their continued use cannot be sustained caused many industries to look to new and sustainable technologies for energy.

Similarly, concerns arising from global warming and ever tightening legislation on emissions have also led to an increase in energy research from alternative sources. The two earth summits held in Rio and New York in 1992 and 1997 highlighted the growing international concern over the nefarious effects of carbon dioxide emissions on the environment. The developed nations which took part in the summits reached an accord to achieve reductions in carbon emissions. Sequel to those summits, the Kyoto protocol drew a commitment from 37 developed countries to cut their greenhouse gas emissions. The protocol entered into force in 2005. It has been signed and ratified by 192 countries as of June 2011 [1] . The global community has realised that the long term strategy to meet emissions targets must be based on energy from renewable and sustainable sources.

One area which has seen an increase in interest is energy production through biomass conversion. The term biomass refers to organic matter that may be converted to energy. Biomass may take the form of energy crops, agricultural wastes, domestic and industrial waste which include sewage sludge and Municipal solid waste. Energy from biomass, does however pose a challenge as most forms of biomass have low energy contents, high moisture contents and a wide range of variability in terms of size and shape translating into problems of feed handling. Issues of transportation of feedstock to the point of production also pose a challenge to the production of energy from biomass. These issues have led researchers to seek means of mitigating these problems and increase the attractiveness of biomass as a sustainable source of energy production.

1.2 BIOMASS CONVERSION TECHNOLOGIES

Technological advancements have led to the development of numerous kinds of technologies for the conversion of biomass to energy. They are characterised by conversion method which follow either biological or thermochemical routes [2, 3]. The Biological conversion processes include fermentation and anaerobic digestion of the biomass while the thermochemical methods include combustion, pyrolysis, gasification and liquefaction [4].

Biological conversion of biomass mainly refers to conversion of biomass into bio-fuels by employing the enzymatic action of bacteria and yeast. Biological conversion usually involves low temperature biological processes like fermentation and digestion. They are mostly applied to carbohydrate rich feedstocks high in moisture content (>40%). The major drawback to Biological conversion processes is the long reaction times associated with such processes that may last for numerous hours or days [5].

Thermochemical conversion processes on the other hand rely on heat, chemical reactions or a combination of both to convert biomass to bio-fuels. They are suited for biomass with lower moisture content (<20%) and high lignin contents which is more resistant to enzymatic actions. Figure 1-1 shows the four main thermochemical biomass conversion processes as presented by Bridgwater [6].

Aston University

Illustration removed for copyright restrictions

Figure 1-1 Thermochemical conversion routes [6]

It is widely accepted that thermochemical conversion technologies are able to achieve better utilisation of the energy content of biomass. This research is focused on fast pyrolysis, a thermochemical conversion process.

1.3 PYROLYSIS

Bridgwater and Bridge [7] define pyrolysis as thermal degradation of matter in the complete absence of an oxidising agent or with such a limited supply that gasification does not occur. There exist three principal kinds of pyrolysis namely slow, intermediate and fast pyrolysis [8].

1.3.1 Slow pyrolysis

The Slow pyrolysis process is a well established technology that has been used for hundreds of years for charcoal production [9]. More recently, it has been used for the production of methanol and tars. Slow pyrolysis is usually characterised by

- Low heating rates of 0-2 ℃/min
- Low rate of volatile release from biomass particles
- Long residence times that range from minutes to days
- Low temperatures of between 200-400 ℃

1.3.2 Intermediate pyrolysis

Intermediate pyrolysis unlike slow pyrolysis is used predominantly for liquid production. It produces gases and solids. It is known to produce similar amounts of solids and gases although liquid yields are usually the highest of the pyrolysis products. Typical yields are around 50% for liquids, 25% for solids and 25% for char. The liquid distribution is reported to be about half representing organic liquid yields and the other half being water [10]. Intermediate pyrolysis is characterised by

- Moderate temperatures 500 ℃
- Moderate residence times ranging from 10-30 seconds
- Low rates of volatiles evolution from biomass feed

1.3.3 Fast pyrolysis

Fast Pyrolysis is the thermochemical conversion of organic materials into mainly liquid fuel. It involves thermally decomposing the organic feedstock at moderate temperatures while rapidly quenching the vapours to form a liquid product commonly referred to as bio-oil [11]. In fast pyrolysis, the biomass feedstock is thermally decomposed using various reactor configurations via high heating rates. Bio-oil may be used for power, heat and electricity generation. It may also be further processed to speciality chemicals that may be put to other uses [10, 12]. Fast pyrolysis is characterised by

- High heating rates of more than 1000 ºC/min
- Moderate temperatures of between 400-550 ºC
- Short vapour residence times of between 0.5-2 seconds
- Rapid quenching of pyrolysis vapours

1.4 BIOMASS PRIMARY FEEDSTOCKS

Two feedstocks scarcely reported as feedstock for fast pyrolysis were chosen for use during the course of this research. Press cakes from the oil extraction process of Jatropha *curcas* and Moringa *olifiera* were chosen to be primary feedstocks. Two varieties of each feedstock were used. The first variety was of African origins while the second variety was of Asian origins.

The feedstocks chosen at the time needed to meet certain criteria to justify their use as feedstocks for fast pyrolysis processes. The criteria included but were not limited to

- Being a 2nd generation bio-fuel
- Being readily available with large scale production
- Not competing with conventional food sources
- Having acceptably high energy content
- Easily transportable

1.4.1 Introduction to Jatropha curcas

The Jatropha *curcas* plant is softwood specie belonging to the Euphorbiace family. Its native distributional range is known to be around Mexico, Brazil, Bolivia Peru and other Latin American countries [13]. Jatropha curcas has also spread to tropical regions of Africa and Asia including Western and Eastern Africa, India, Thailand and Cambodia. Acthen et al in a review paper on Jatropha curcas describes the plant as a small tree or shrub. Fully mature Jatropha plants are known to grow between 5-7 m depending on growth conditions. The Jatropha plant is reported to have a life span of up to 50 years with seed production starting as early as the second year after cultivation[14]. Jatropha curcas has more recently been cultivated for bio-diesel production via transesterification.

The earliest reported uses of Jatropha oil as an energy source is during the Second World War when crude Jatropha oil was used as fuel for driving German tanks. Crude Jatropha oil can also be used directly as a fuel for energy production [15, 16]. Figure 1-2 shows the parts of the Jatropha plant from a study by Dehgan [17].

a: stalk; b: stem; c: leaf; d: mature flower; e: young flower; f: pod cross section top; g: seed pods; h: pod cross section side ; i: seed

Figure 1-2 Anatomical parts of Jatropha *curcas* [17]

Jatropha is known to grow with a deep tap root and four shallow lateral roots for support. Leaves from the plant are smooth with 4-6 lobes ranging between 10-15 cm in length and width. Jatropha seeds from which oil for biodiesel is sourced are green and turn yellow at maturity. The seeds are covered in husks which can account for up to 40 % in mass. The seeds from Jatropha curcas are known to contain toxins including phorbol esters, curcin, lectins and phytates [18].

Figure 1-3 shows the typical input and outputs of a Jatropha cultivation process for energy production. Jatropha cultivation for bio-fuel purposes typically begin with the choice of proper cultivation sites with required characteristics.

Figure 1-3: Inputs and outputs of Jatropha exploitation for fuel purposes [13]

The required characteristics for growth of Jatropha curcas plants are less demanding when compared to other bio-fuel plants in terms of pest control, required rainfall and management needs. It is these characteristics that are known to make Jatropha a promising plant for alternative energy purposes. After the plants have grown to maturity, the seed production stage follows during which the seeds are collected and pressed for the oil. Many large scale Jatropha plantations are currently in place around the world some of which are shown in Figure 1-4.

Figure 1-4: Current commercial Jatropha developments around the world [19]

A knowledge gap has been identified in this stage of production that this research intends to cover. The use of the press cake residues from the pressing stage as a raw material for further liquid fuel production via fast pyrolysis is one objective of this research.

The seed yields for Jatropha plants reported in literature vary significantly from 0.4 ó 12 ton ha^{-1}yr^{-1}. The yields from the many different studies carried out are beyond the scope of this thesis although it is generally agreed that yields are a function of many parameters

including climatic conditions and agricultural practice. An excellent review has been published by Estrin [18].

The issue of yield is considered a difficult problem as claims can be exaggerated because of the economic potential [20]. Even by conservative yield estimates reported in literature, the yields of Jatropha curcas seeds for bio-oil production are enough for it to be considered as a potential raw material for fast a pyrolysis processes as annual seed production of between 0.2 ó2 kg per plant have been reported [21]. Tewari [22] reports yields of up to 3 ton $ha^{-1}yr^{-1}$ even in semi arid regions of cultivation.

The oil yield from Jatropha curcas is reported to range between 35-43%. Mechanical extraction using presses are known to be less efficient than chemical extraction processes although the former is preferred because of cost and environmental concerns. Achten et al [23] conclude from a study that oil extraction using solvents can only be economical in large scale processes of up to 50 ton day^{-1} of crude Jatropha oil.

The press cake of Jatropha curcas is reported to have a gross energy value of up to 18 MJ/kg [23]. The press cakes may contain up to 12% oil depending on the efficiency of the extraction method employed. Currently, press cakes of Jatropha processes are used as fertilizer and animal feed after detoxification. Jatropha press cake has also been used as a feed for biogas production via anaerobic digestion. Staubman [24] in a study produced bio-gas containing up to 70% CH_4. Lopez et al [25] also showed in another study that biogas may be produced from the husks of Jatropha curcas seeds. The relatively high energy content of the press cake however also makes it attractive as a raw material for further bio-oil production.

1.4.2   Introduction to Moringa olifiera

Moringa Olifiera is one of 14 known species of the Moringaceae single genus family. The Moringa Olifiera is a tree that can vary in height between 5-10 m. Of the 14 varieties of Moringa, Moringa olifiera is the most widely known and utilized as reported by Morton and Sengupta [26, 27]. It is native to the sub Himalayan regions of India, Sub Saharan Africa, South America and Cambodia [28].

Moringa Olifiera has been identified as source of oil for biodiesel production. A study by Rashid et al [29] makes a strong case for Moringa olifiera oil as a source of biodiesel production. Other uses of Moringa include fertilizer, pesticide, and animal fodder.

The seeds of the Moringa plant are stored in pods between 250 and 450 mm long. They typically contain up to 20 seeds in every pod. Inadvertently, the pressing of Moringa olifiera seeds for bio-oil production leaves significant quantities of by-products as press cake residue. Figure 1-5 shows parts of the Moringa plant including pods, seeds and leaves.
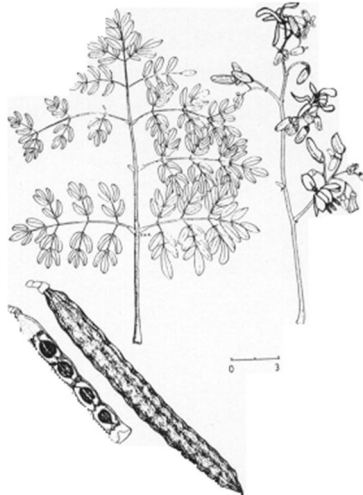
Figure 1-5: Anatomical parts of Moringa Olifiera plant

Although Moringa is not as widely cultivated as Jatropha, it is also increasingly being cultivated for bio-fuel purposes. Large scale cultivation of Moringa has been initiated in Malawi, Kenya, India, Tanzania and Nicaragua suggesting similar climates elsewhere should be suitable for Moringa cultivation [30]. The shaded areas in Figure 1-6 shows the global land mass currently reported to be suitable for large scale Moringa cultivation as reported by Foidi et al [31].

Figure 1-6: Global landmass suitable for Moringa cultivation for bio-fuel purposes [31]

Reported yields from Moringa plantations show that up to 3 tonnes of seeds per hectare of Moringa seeds can be obtained. The reported oil seed yields are between 30 and 40 wt%. These figures translate to press cake yields of up to 1.8 tonnes per hectare. Kibazohi et al [30] report oil yield from Moringa seeds of 38.1wt%. As with Jatropha curcas press cakes, this research intends to cover the knowledge gap in production of bio-fuels from Moringa olifiera press cakes.

1.5 RESEARCH OBJECTIVES

The main objectives of this research are:

I. To commission a laboratory scale bubbling fluidised bed fast pyrolysis unit for bio-oil production.
II. To operate, identify and rectify any shortcomings of the system including making improvements to the existing design if necessary.
III. To characterise Jatropha and Moringa press cakes as a means of assessing their suitability as feedstocks for fast pyrolysis.
IV. To investigate the effects of process parameters particularly temperature on the product yields from the fast pyrolysis of the Jatropha and Moringa feedstocks.

1.6 STRUCTURE OF THESIS

The rest of this thesis is structured into chapters as described below.

Chapter 2 introduces biomass thermal degradation and fast pyrolysis principles. This chapter looks at the thermal decomposition of biomass constituents. It also looks at the technological requirements of the fast pyrolysis process. Literature on the kinetic studies of biomass thermal degradation beneficial to process design and operation is also reviewed in this chapter.

Chapter 3 reviews various commercial and research reactor systems that have been used for the fast pyrolysis of biomass. It focuses on the different reactor configurations, modes of operation, and reported product yields. This chapter also looks briefly at laboratory scale fast pyrolysis systems for bio-oil production. It discusses the theory behind fluidised beds as a technology for achieving thermal degradation of matter. The key parameters that influence the hydrodynamics of fluid bed systems are introduced via a brief literature review.

Chapter 4 gives details of all the characterisation techniques and the feed processing methods employed. It also describes the methods used to characterise and assess pyrolysis liquid quality.

Chapter 5 details the results of biomass characterisation using the techniques introduced in chapter 4. The results of characterisation carried out on the commissioning and primary feedstocks are presented and discussed.

In chapter 6, a detailed breakdown and description of the commissioned 300g/h fast pyrolysis rig is given. Commissioning of this unit was one of the main objectives of this research and this chapter describes in detail the commissioned unit, and the efforts undertaken to commission the unit.

Chapter 7 details the experiments carried out with the commissioned unit. It gives a breakdown of the commissioning experiments and subsequent studies with varying particle size and temperature. The process performance and product yields are discussed within the chapter. Post commissioning problems are identified in this chapter. Chapter 7 also reports a cold model study carried out as part of the initial steps to redesign the new reactor.

In chapter 8, the development of an alternative feeding system for the unit is presented.

Chapter 9 reviews the reactor design methodology which formed the basis for the construction and commissioning of a new bubbling fluidised bed reactor for the system.

Chapter 10 of the thesis reports fast pyrolysis experiments using the optimised system. It discusses in details the experiments, the mass balance closures and characterisation of the fast pyrolysis products from the primary feedstocks.

The conclusions from this research and recommendations for future work relating to the entire research form the basis of chapter 11.

2 BIOMASS COMPOSITION, THERMAL DEGRADATION PATHWAYS AND FAST PYROLYSIS PRINCIPLES

This chapter focuses on the constituents of biomass, their thermal decomposition and whole biomass thermal degradation pathways. The technological requirements of the fast pyrolysis process are also reviewed. Chapter 2 also gives an introduction to the products of fast pyrolysis as well as discussing the factors that should be considered during the operation of fast pyrolysis units.

2.1 BIOMASS CONSTITUENTS AND THEIR THERMAL DEGRADATION

Biomass which includes wood, grasses and agricultural crops have been identified as a renewable source of energy. The structure of biomass species determines the ease or difficulty in breaking them down. About 30-60 % of biomass is cellulose, 20-35 % is hemicellulose and 15-30 % is lignin. Resins and minerals are also present in biomass depending on the specie. Figure 2-1 shows a typical composition of plant biomass as reported by Mohan et al [32].

Aston University

Illustration removed for copyright restrictions

Figure 2-1 Typical Composition of plant biomass [32]

The major elemental constituents of biomass are hydrogen, carbon and oxygen while other elements like sulphur and nitrogen may be present in lesser quantities. Woody biomass typically has a lower heating value of 19.8-21.0 MJ/kg [33]. Table 2-1 gives typical compositions of some biomass species in terms of their major constituents.

Table 2-1 Ratios of biomass constituents in different feedstocks (wt% dry) [34].

Biomass	Ash	Lignin	Hemicellulose	Cellulose	Others
Beechwood	0.5	23.2	26.8	40.1	9.4
Hardwood	0.3	19.5	35.0	39.0	6.2
Softwood	0.4	27.8	24.0	41.0	6.8
Wheat straw	6.6	16.7	28.2	39.9	8.6
Bagasse	1.6	20.2	38.5	38.1	1.6

The varying extent of stability of biomass constituents coupled with the diversity and heterogeneity make the pyrolysis of biomass a very complex set of reactions [35, 36]. Goos [37] speculated that the pyrolysis of wood as a whole would yield similar products from the proportional pyrolysis of its individual components. The individual components of biomass govern the degradation pathways and determine the primary and secondary reactions taking place. The major components of biomass and their degradation during pyrolysis are discussed below.

2.1.1 Cellulose and its pyrolysis

Cellulose is the main component of plant cell walls and consists of anhydroglucose units connected by glycoside bonds. It is also the major constituent of most woods. Cellulose is represented by the formula $(C_6H_{12}O_5)_n$ and is a linear polymer as can be seen in Figure 2-2 [33, 38].

Aston University

Illustration removed for copyright restrictions

Figure 2-2: Cellulose Structure [32]

The functional groups on the cellulose molecules are known to have a significant effect on the chemical and physical properties of biomass. Cellulose pyrolysis is the most studied and understood of the lignocellulosic materials of biomass. The first model for cellulose pyrolysis was proposed by Madorskey as reviewed by Byrne [39]. The model suggested that cellulose pyrolysis progressed via 2 competing pathways dependent on temperature. The first pathway formed at below 280 ºC gave rise to the formation of water and volatiles

while the second pathway occurred at above 280 ºC and gave rise to the formation of tars. The Madorskey Model is shown in Figure 2-3.

Figure 2-3: Madorskey model of cellulose pyrolysis [40]

A different study on the cellulose pyrolysis model was conducted by Kilzer [41] in which he agreed with Madorskey.

Shafizadeh [42] also carried out extensive research on cellulose thermal degradation. His studies suggested that the formation of pyrolysis products were dependent upon process parameters and other effects including the influence of ash, degree of depolymerisation and morphology. As such, the Shafizadeh model proposed in 1968 [42] is more detailed when compared to the Madorskey model. The Shafizadeh model shown in Figure 2-4 is a 3 path model dependent on temperature.

Figure 2-4 Shafizadeh model of cellulose pyrolysis [42]

The model suggests that pathway 1 occurs at temperatures less than 280 ºC from which water, char, CO_2 and CO are evolved. This pathway is representative of dehydration reactions. Pathway 2 which occurs at temperatures between 300 -500 ºC is representative of depolymerisation with the main product being levoglucosan. The third and final pathway occurs at temperatures > 500 ºC with the evolution of low molecular gases and volatiles. Shafizadeh suggested that the formation of pyrolysis volatiles and permanent gases are as a result of a combination of different reactions including dehydration, disproponation, decarbonylation and decarboxylation [42].

The Waterloo mechanism of thermal degradation proposed by Scott et al [43] is also widely accepted to be a representation of the reaction pathway of cellulose through competing reactions. The waterloo mechanism depicted in Figure 2-5 proposes that cellulose pyrolysis occurs through three competing reactions which are fragmentation, depolymerisation and dehydration [44, 45].

Aston University

Illustration removed for copyright restrictions

Figure 2-5 Waterloo pathway of cellulose degradation [5, 46]

The Waterloo model also acknowledges that feedstock characteristics in conjunction with process parameters determine the choice of pathway. The fragmentation reaction occurs via the breakdown of the glucose monomer from the cellulose polymer while depolymerisation occurs via the breaking of the bonds that hold the monomers together [33, 46]. Fragmentation involves cellulose conversion to hydroxyacetaldehyde, other carbonyls, acids and alcohols while depolymerisation involves the forming of levoglucosan and other primary anhydrousugars. Depolymerisation and fragmentation occur at higher temperatures. Depolymerisation occurs at between 300 and 450 °C while fragmentation occurs optimally at 600 °C. Figure 2-6 shows the breakdown of cellulose polymers via fragmentation and depolymerisation.
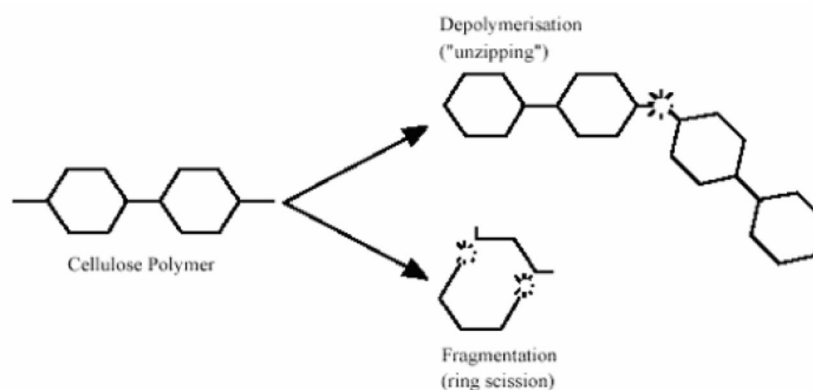
Figure 2-6 Fragmentation and depolymerisation of cellulose polymer [2, 12]

2.1.2 Hemicellulose and its pyrolysis

Hemicellulose is made up of non-cellulosic polysaccharides formed from pentosans and hexosans. They are usually based on a variety of sugars like D-glucose, D-xylose, D-galactose and L-arabinose. Hemicellulose is closely linked with cellulose in the plant cell wall where they act as support structures [32]. Hemicellulose can also be linked with lignin in the middle lamella of plant cells where it is crossed within the matrix of the plant structure. Components of hemicellulose are shown in Figure 2-7.
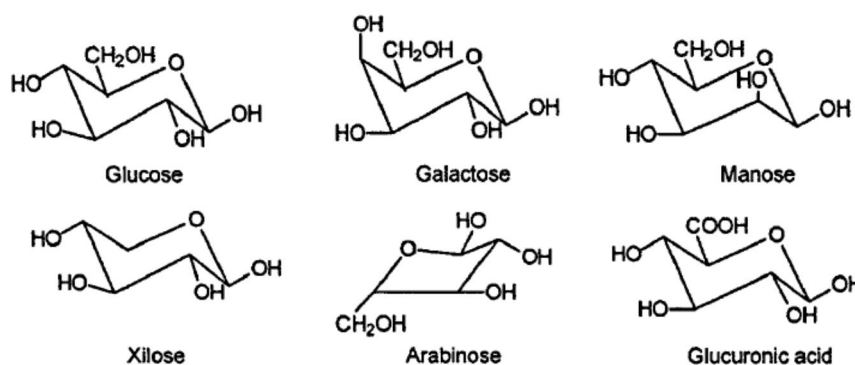
Figure 2-7 Main components of hemicellulose [32]

From Figure 2-7, it can be seen that hemicellulose displays branched structures unlike the linear structure of cellulose. It is these differences in monomers that cause hemicellulose to be physically and chemically different from cellulose. Quantitatively, hemicellulose is less abundant than cellulose and is accepted to be more reactive because of its lower thermal stability when compared to cellulose [47, 48]. Peacocke [33] suggests that its lower abundance is the reason why it has received less attention than cellulose. Typically, hemicellulose undergoes rapid thermal degradation at temperatures between 150-350 ℃ [33, 46]. Like cellulose, it also undergoes fragmentation and dehydration when being thermally decomposed although the extent of depolymerisation is reduced due to its lack of crystallinity [49]. Hemicellulose is known to be a source of furan derivatives and has been directly linked to higher yields of char, water and acetic acid during fast pyrolysis [50, 51].

2.1.3 Lignin and its pyrolysis

Nowakowski et al., [52] assert that lignin is the second most abundant and the only renewable source of aromatics in nature. Lignin is an amorphous material that surrounds cellulose fibres in the middle lamella of a plant cell which holds them together. Lignin structure of European Beech is shown in Figure 2-8. It is the strengthening component of the cell wall and is mainly present in woody biomass. Lignin is a polymer that consists of

hydroxyl and methoxy substituted propyl phenol units. Lignin is composed of C_3-C_6 phenyl propane units. The phenyl propane units can consist of guaicyl, syringl or hydroxyl units as shown in Figure 2-9 [5]. The highly complex structure of lignin depends on plant species and as such, no standard structure for lignin can be hypothesised accurately [33]. Lignin units are known to be commonly joined with - or - linkages. Lignin is also known to yield various products including catechols, vanillins and aromatic carbohydrates. At lower temperatures <500 ºC, lignin decomposes by dehydration while a diversity of monomers are formed at higher temperatures. At temperatures higher than 700 ºC, lignin monomers decompose to the vapour phase. Lignin is known to be more thermally stable than cellulose and hemicellulose and leads to higher char yields but also higher aromatic compounds [47, 49].

Figure 2-8 Partial structure of lignin from European Beech [32]

Figure 2-9 Lignin monomers [8]

The complex structure of lignin has not allowed for extensive studies into the mechanism of its thermal decomposition. There have been however some studies on the pyrolysis of lignin. One of the widely reported models of lignin pyrolysis is the one proposed by Antal [53] depicted in Figure 2 -10.

Aston University

Illustration removed for copyright restrictions

Figure 2-10 Antal's proposed lignin decomposition pathway [53]

The model proposes distinct pathways followed by different pyrolysis products. It suggests that the first three pathways indicated by number 1, 2 and 3 in Figure 2-10 occur at lower temperatures while pathways 4 and 5 indicate further cracking of the monomers at higher temperatures from which condensables and permanent gases are formed at higher temperatures above 500 ºC. The Antal model of lignin pyrolysis also suggests that pathway number 3 which leads eventually to the formation of vapours, and secondary char occur at high rates [5, 40, 53].

Nunn et al [54] have also carried out work on Lignin pyrolysis and pathways from which they concluded that the formation of oxygenated liquids occur at around 500 ºC. The conclusions of their study show areas of agreement with the Antal model. It must be mentioned however that the area of lignin pyrolysis is less understood requiring extensive research before researchers reach an agreement on clearly defined pathways of its pyrolysis [54].

Finally, Chin and Shafizadeh [55] reached a number of conclusions as regards the pyrolysis of biomass components which are that

- Hemicellulose is the most reactive component degrading at temperature between 225 and 325 ºC
- Lignin is the most thermally stable component degrading between 250and 500 ºC
- Cellulose decomposes between 325 and 375 ºC and is intermediate in its reactivity.

2.2 BIOMASS FAST PYROLYSIS

Fast Pyrolysis as a thermochemical conversion route of biomass particles produces numerous complex compounds as can be deduced from the discussions section 2.1. This section intends to look at the pathways of biomass degradation as a whole.

Chemical engineering applications tend to categorise the products of biomass pyrolysis into three broad groups namely permanent gases, pyrolytic liquid (bio-oil) and chars. These products are a result of the primary decomposition of the biomass particles as well as the secondary decomposition of volatile condensable organic vapour products into low molecular weight gases and char [56].

The very complex nature of the reactions taking place during a fast pyrolysis process means that many homogenous and heterogeneous reactions occur simultaneously and consecutively. These reactions are governed and directed primarily by the reaction conditions [35, 36]. The overall kinetic studies of fast pyrolysis reactions are undertaken as a means of representing them as individual and distinct reaction pathways. This allows for the study of reaction parameters on the yields and compositions of the process.

The complexity of the numerous fast pyrolysis reactions that occur under process conditions makes it a fairly difficult field to study. Consequently, simplifications must be incorporated to kinetic studies.

Fast pyrolysis kinetic studies serve as an important part of the design engineering applications for liquid production. As pointed out by Boukis [5], the study of process kinetics play an important role in

- The development of diagnostic tools in order to evaluate the importance of process parameters on the products
- The prediction of the effect of process parameters such as heating rates, reactor temperature, particle size and residence time on the product yield and characteristics in order to aid the optimisation of the process
- The development of better reactor design techniques
- The optimisation of the parameters for the desired end product.

Three major categorisations in literature exist for kinetic studies of wood pyrolysis. Di Blasi gives a comprehensive explanation of the kinetic models [46, 57]. The major kinetic models of wood pyrolysis are

Overall decomposition models: Overall decomposition models of wood pyrolysis employ a single reaction to describe the thermal degradation of solid biomass to char and volatiles. This is achieved by measuring the weight loss of the biomass particles as a function of time and temperature.

One stage multi reaction models: Kinetic Models in this category employ step wise degradation of biomass to primary vapour products, char and gaseous species. These reactions are used to determine rate constants for the formation of the products.

Two stage semi global models: Kinetic models in this category are used when the aim of the study is to determine rate constants for primary pyrolysis reactions and secondary reactions of the evolved volatile products.

Several researchers including Di Blasi, Graham and Peacocke [33, 56, 57] have produced detailed and insightful reviews into the many kinetic studies of wood pyrolysis undertaken over six decades. The individual review of each kinetic study is well beyond the established scope of this thesis. The reader is again referred to their excellent reviews. A brief summary of the biomass kinetic reaction models follow.

2.2.1 Overall decomposition models

The overall decomposition model of thermal degradation of biomass can be represented by the reaction shown in equation 2-1

$$\rightarrow \quad \square \quad + \qquad\qquad\qquad \textbf{Eq 2-1}$$
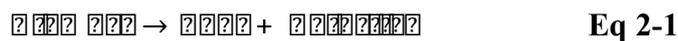
A common technique used to fit this kinetic model is Thermogravimatric Analysis (TGA). TGA measures the weight loss of wood samples as a function of time and temperature. The technique does not allow for the collection of volatile pyrolysis products and as such, only an overall decomposition rate. TGA studies may be carried out in conjunction with Differential Thermal Analysis (DTA) or Differential Scanning Calorimetry (DSC) which can be used to determine the heat of reactions.

Liden [58] points out that though the overall decomposition models are applicable to kinetic studies, the kinetic parameters obtained from them can vary tremendously even for similar feedstocks under similar conditions for a number of reasons which include:

- The use of the steady state temperature as the overall reaction temperature

- Failure to take into account the feedstock composition (impurities, inorganic compounds, morphology)

- The simplistic nature of the model as it does not take into account secondary reaction pathways

- The failure to incorporate the effects of heating rates and its role in determining the extent of fast and slow pyrolysis reactions. This is especially important when modelling has been carried out using large biomass samples.

Models used to predict weight loss cannot be employed for the prediction of product distribution. Similarly, they assume that the decomposition of particles occur over an infinite period of time [59]. This assumption is particularly flawed because the fast pyrolysis process is limited by the time required for decomposition of biomass particles.

2.2.2 One stage multi reaction models

As cellulose is the most abundant component in most woods and biomass species, many of the early kinetic models relating to biomass fast pyrolysis are based on the decomposition of cellulose. One of the earliest step wise degradation models was proposed by Bradbury [60]. It was a model for the step wise degradation using a three reaction model as shown in Figure 2-11. The model was proposed to account for the variations in product yields that may occur during pyrolysis.

Aston University

Illustration removed for copyright restrictions

Figure 2-11 Bradbury model for pyrolysis of cellulose [60]

The Bradbury model indicates the initial change of wood to intermediates before formation of final products. A first order initiation reaction occurs that leads to the formation of ‑active celluloseø The active cellulose as an intermediate has a high activation energy [60]. Diebold theorised further that though the state of the active cellulose is not known, it is considered to be in a liquid like state and has significantly lower degree of polymerisation than the initial cellulose particle.

The resulting intermediate is further decomposed via two competitive first order reactions whereby one of the reactions yields pyrolysis volatiles and the other permanent gases and char. The concept of Bradbury's model suggests that the cellulose molecule is not directly converted to low molecular weight vapours, gases and char but undergoes and intermediate physical and chemical transition. The hypothesis of this model is supported by research carried out by Back and Shafizadeh [5, 42, 61].

2.2.3 Two stage semi global models

Models in this category were developed from the need to quantitatively assess the rate of formation of pyrolysis products as a function of time. Though this approach is generally regarded as the most complex of kinetic studies, it is accepted as the one that best fits the fast pyrolysis process because it considers the residence time of the vapours. This is vital in ensuring maximum liquid yields. Other simpler models fail to consider the impact of residence time which makes them less suitable for studying yields during fast pyrolysis [56].

Simpler models also suggest that an increase in temperature should favour the increase in liquid yields. This is however not the case with fast pyrolysis processes as they liquid yield is reduced when temperatures are significantly higher than the optimum reaction temperature of 500 °C. Researchers are of the opinion that for a model to accurately represent biomass pyrolysis in terms of yields, it must take into account the secondary reactions. These secondary reactions are primarily in the form of cracking and carbon deposition with the conversion of oils to char and gases [56]. This is in line with pyrolysis principles since secondary reactions in the form of vapour cracking are responsible for the reduced liquid yield at higher temperatures.

Liden [58] and Diebold [62] proposed two similar models based on the explanation given. Their kinetic models take into account the secondary decomposition of primary tars formed. One of the key assumptions of their models was that the primary formation of tars and their subsequent decomposition were all first order reactions. The liquid yield arising from the vapours were estimated as a function of temperature and vapour residence time in the reaction zone [63]. The model proposed by both Diebold and Liden is shown in Figure 2-12.

Figure 2-12 Diebold and Liden pathways for wood pyrolysis [62]

In the same vein, Gorton and Knight [64] also proposed a kinetic model shown in Figure 2-13 that takes into account the secondary reactions of biomass pyrolysis. The assumptions of the model were the same as that used by Liden and Diebold.

Figure 2-13 Gorton and Knight pathways for wood pyrolysis [64]

Scott et al [43] in related studies successfully used the Liden and Diebold model to predict the liquid yield of products within a temperature range of between 450 and 800 ºC. The results from that study showed that the model agreed with achieved yields within ±10% for a temperature range of between 500 and 700 ºC and a residence time of up to 1s.

2.3   FAST PYROLYSIS PRODUCTS

The relative proportions of products from fast pyrolysis processes are subject to a combination of factors including reactor configuration, vapour residence time and temperatures. Key parameters which influence the fast pyrolysis process are described later in this chapter.

2.3.1   Bio-oil

Bio-oils produced from fast pyrolysis are usually mixtures of char, water and complex organic compounds. The compounds are products formed during the decomposition of macro polymers of cellulose, lignin and hemicellulose that constitute the original biomass feedstock.

The ratios of the components are dependent on complex relationships between the configuration of the pyrolysis process, reaction conditions, extent of char removal, condensation method and the composition of the initial feedstock. Table 2-2 shows the major physical and chemical characteristics of a typical bio-oil in comparison to heavy fuel oil

Table 2-2 Typical composition of bio-oil compared to heavy fuel oil [9].

Physical Property	Bio-Oil	Heavy fuel oil
Water Content, (wt %)	15-30	0.1
pH	2.5	(-)
Specific Gravity	1.2	0.94
Elemental composition (wt %)		
Carbon	54-58	85
Hydrogen	5.5-7.0	11
Oxygen	35-40	1.0
Nitrogen	0-0.2	0.3
HHV (MJ/kg)	16-19	40
Viscosity (at 50C), cp	40 -100	180
Solids (wt%)	0.2-1	1

Bio-oils are reported to resemble the original feedstock based on elemental comparisons and because of this, usually contain highly oxygenated compounds. Table 2-3 shows the composition of bio-oil from white spruce and poplar as reported by Piskorz et al [65].

Table 2-3 Composition of bio-oil from white Spruce and Poplar [65]

Bio-oil Composition (wt%)	White Spruce	Poplar
Sachharides	3.3	2.4
Anhydrosugars	6.5	6.8
Aldehydes	10.1	14.0
Furans	0.35	-
Ketones	1.24	1.4
Alcohols	2.0	1.2
Carboxylic acids	11.0	8.5
Pyrolytic lignin	20.6	16.2
Unaccounted fractions	11.4	15.2

From Table 2-3, it can be seen that carboxylic acids can constitute up to 11% mass fraction of bio-oil. This in turn makes most bio-oils highly acidic with pH values ranging between 2- 4. Diebold [66] reports that the major organic components of bio-oil are continuously reacting in order to attain chemical equilibrium. The continuous organic reactions taking place even after the formation of the bio-oils are responsible for the aging witnessed in bio-

oil during storage. These can alter the physical and chemical characteristics of the product [67]. The components of bio-oil can be classified into water soluble and water insoluble categories. The water soluble phase of most bio-oils is composed of lighter organic compounds while the water insoluble phase is composed of larger and heavy compounds commonly referred to as pyrolytic lignin [68].

Pyrolytic lignin consists primarily of tri- and tetramers of lignin sub units (hydroxyphenyl, guaiacyl and syrigyl units) as was shown in Figure 2-9. These compounds can represent up to 80 % of the original biomass and have molecular weights of between 650 and 1300 kg/kmol [69]. The high molecular weight compounds are known to be responsible for the high viscosity of bio-oil although the viscosity is also a function of the pyrolysis process configuration and the initial water content of the actual biomass feed [69].

The components of bio-oil make its properties very likely to change over time dependent on storage conditions. Polymerisation reactions within bio-oils are known to continue until heavy lignin rich fractions separate from other components into sludge like liquids [70]. An increase in bio-oil molecular weight will be observed as the product ages due to the reaction of carbohydrate based constituents. These constituents such as aldehydes and ketones can jointly account for up to 25 % of its composition [71, 72].

Bio-oil fuel properties compare differently to conventional crude because of the presence of highly oxygenated compounds. The heating values are relatively lower when compared to that of crude which is a mixture of only hydrocarbons. The high amount of water and the acidity of the product make it corrosive. The presence of water also makes it likely that bio-oil may catalyse the formation of hydrated iron (III) oxide [73]. The presence of solid fines in the oil also makes it likely to clog up fuel and injection systems.

Notwithstanding the drawbacks highlighted, bio-oil is reported to be an attractive source of high specialty chemicals when fractionated. Compounds like acetic acid, formaldehyde, hydroxyacetaldehyde and maltol can all be derived from bio-oil [74].

2.3.2 Char

Fast pyrolysis processes leave a residue of high carbon content char with relatively low amounts of oxygen and hydrogen. Char is usually removed as a by-product of the pyrolysis process using cyclones because it is known to reduce the yields of liquids by catalysing cracking reactions in pyrolysis vapours. Some pyrolysis configurations like circulating fluidised beds are known to utilise the char as a fuel to provide energy for the actual pyrolysis process. Many processes however collect the char product as a by-product and use it for other energy purposes as chars from fast pyrolysis can have heating values of up to 23 MJ/kg [74, 75].

2.3.3 Non condensable gases

The final product of pyrolysis processes are the non-condensable gases formed as a consequence of the thermal degradation of the biomass. The amount of non condensable gases produced from any fast pyrolysis process is dependent on numerous factors including process temperature and reactor configuration [9]. The efficiency of the vapour quenching process will also impact the amount of non condensable gases produced with very efficient quenching producing less gases. Pyrolysis gases mainly consist of carbon monoxide, carbon dioxide, methane, hydrogen, ethane and propane. The gases can be utilised for energy purposes but their use is dependent on process scale because of relatively low energy content [74]. A 7kg/h fluid bed fast pyrolysis rig at Aston University recycles the process gas through a compressor and reuses it as the fluidising gas in order to reduce costs. This is an example of effective use of pyrolysis process gases.

2.4 PROCESS REQUIREMENTS FOR FAST PYROLYSIS

The fast pyrolysis process of biomass feed to liquid may be defined as a two stage process defined by significant changes in temperatures. The first stage involves heating the biomass feed to pyrolysis temperature and the second stage involves rapid quenching of the formed vapours [6]. Bridgwater reports that the key essential features of any fast pyrolysis process are

- High heating and heat transfer rates
- Carefully controlled temperatures of around 500 ºC
- Rapid cooling of pyrolysis vapours to bio-oil product

2.4.1 High heating rates

High heating rates are essential to the fast pyrolysis process. Several researchers have agreed on high heating rates as a requirement of the fast pyrolysis process mainly to minimise char formation [76, 77]. The transfer of heat to the biomass particle is mainly through conduction and convection depending on reactor configuration. Convection happens mostly between any hot fluidising gas and the biomass particle while conduction occurs between the heat transfer medium and the biomass particle. The high heating rate during the fast pyrolysis process in fluidised beds (like the one commissioned during this study) is made more efficient via the 3 methods discussed below.

Preheated fluidising gas: The fluidising gas used for the fast pyrolysis process is usually pre heated to reduce the temperature gradient that would be caused by a cold stream of gas entering a reactor operating at pyrolysis temperature 550 °C.

Fluidising medium: In fluid bed systems, the process is not started until the fluidising medium is at pyrolysis temperature and this is mainly to ensure that the high heating rate required by the process is achievable.

Small biomass particles: As discussed earlier, the liquid yield of the process is due to the release of volatiles caused by thermal degradation. The thermal conductivity of biomass particles is relatively low and as such, to ensure complete devolatisation of the particles in minimal time, the particle sizes are kept to a minimum as bigger particles would reduce the heating rates and increase residence times

2.4.2 Optimum reaction temperature

Several researches have reported the optimum fast pyrolysis process temperature for maximum oil yield to be in the region of 500-600 °C for several types of biomass [6, 11, 78-84]. This temperature is important for achieving high oil yields. Temperatures significantly higher than this range results in the extended cracking of pyrolysis vapours. Samolada [78] concluded that process temperature is the parameter that significantly affects the yields of pyrolysis products. It is therefore essential that during any design and operation considerations, the ability of the system to reach and maintain this temperature range is achieved. Figure 2-14 shows the typical impact of temperature on fast pyrolysis product yields
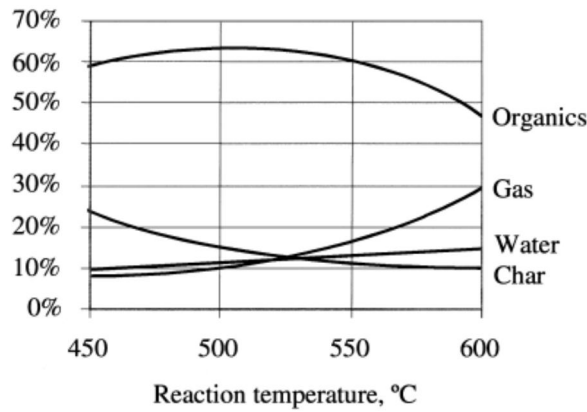
Figure 2-14 Typical fast pyrolysis product distribution as a function of reaction temperature [9]

2.4.3 Rapid vapour quenching

The collection of the liquid product is another key stage of the fast pyrolysis process. Quenching to the liquid product is usually achieved through contact with a liquid which is immiscible with the bio-oil. Bridgewater reports that though the method is effective, careful considerations need to be given to design parameters and temperature control to avoid differential condensation of heavy ends. Light ends collection is also important to reduce oil viscosity. [6, 9, 11].

2.4.4 Short vapour residence time

The time taken between the formation and quenching of the fast pyrolysis vapours is known to impact on the composition and quality of the liquid product. High temperatures facilitate vapour cracking and the longer the vapours are exposed to high temperature, the greater the extent to which cracking will occur. Vapour residence times of few milliseconds to about 2 seconds are known to be the optimum for high liquid yields from fast pyrolysis. Longer residence times are known to impact negatively on organic liquid yields due to cracking reactions [6, 12, 33].

2.4.5 Char and ash removal

Char as a by-product of the pyrolysis process contributes to secondary cracking in the vapours from the degrading biomass particles [46]. This is because it contains metals from the original biomass feedstock that catalyse cracking reactions. Char is also known to contribute to instability in the cooled liquid as it accelerates polymerisation which increases the viscosity of the oil product [85]. Almost all the ash produced in the process is retained in the char. The removal of char from the process is therefore important to maintain a high product quality. In many fluidised bed systems as is the case in the unit to

be commissioned, char is removed by a cyclone although the use of hot vapour filtration is also gaining popularity [6, 86].

2.5 FACTORS IMPACTING ON PYROLYSIS PRODUCTS YIELDS AND QUALITY

The following factors have been shown over the course of several research studies to have a direct impact on product yield, quantity and quality. They are discussed in more detail as they are taken into account during the course of this research.

2.5.1 Type of feedstock

The type of feedstock used in the process determines to a large extent the composition of the oil product. The distribution of the 3 main components of biomass i.e. cellulose, hemicellulose and lignin are mainly responsible for this. Different anatomical parts of the biomass may also favour char, oil and gaseous products in different compositions [87]. In standard woody biomass, cellulose is the most abundant component accounting for half its composition. The remaining 2 components lignin and hemicellulose are sometimes evenly distributed though in most cases, lignin is more abundant. In grasses however, lignin is the least abundant component.

Similarly, different biomass species will vary in composition of the 3 major components leading to different compositions of the pyrolysis products. Hague [12] in the course of his research, showed that agricultural residues tend to have high lignin contents which translate to low organic yields while standard woody biomass, gives high organic yields resulting from increased cellulose quantity in the composition of the feedstock.

2.5.2 Feed particle size

Heat transfer in biomass particles is mainly achieved through conduction and convection. Most biomass particles are irregularly shaped and tend to have lengths several times their thickness [67, 88]. During fluidised bed fast pyrolysis, more than 90% of the heat requirement for a biomass particle is achieved via conduction through contact with the fluidising medium [9]. In a decomposing porous biomass particle, there is a pressure build up due to vapour formations that increase to a maximum within the core of the particle as shown in Figure 2-15. Vapours formed are subject to further cracking which promotes formations of char, gases and thermally stable chars [89]. Biomass also, has low thermal conductivity (usually 0.1 W/m^{2}K) [90]. This means that to achieve the high heating rates and low residence times required for complete thermal degradation, smaller biomass

45

particles are essential to the process [91]. In most pilot and lab scale units, particle sizes are usually limited to between 2-3mm to mitigate the effect of incomplete devolatization and meet requirements for short vapour residence times and minimal cracking of formed vapours. In a study of Aspen Poplar biomass using particle size ranges of 44-105 µm, 105-250 µm and 250-500 µm, Scott et al [92] obtained organic yields of 51.0, 58.9 and 53.0 mf wt % for the fraction sizes respectively. The conclusion from the study was that the smaller particles were either overheated or blown out too quickly while the larger particle sizes liquid yields were reduced because of incomplete pyrolysis and increased vapour residence time. The study indicated clearly that the yields from pyrolysis process are a function of particle size [92].

Figure 2-15 Decomposing Wood Particle including reactions [89]

2.5.3   Moisture content

The moisture in the biomass material eventually ends up in the products of the process mainly the liquid product. As water is an unwanted compound in most bio-oil, due to its lowering effect on the heating values, most feedstocks are dried to less than 10% moisture. Kelbon [93] pyrolysed feedstock with 10%, 60% and 110 wt% particles. She showed that the onset of pyrolysis can be delayed by up to 150 seconds depending on the moisture content of the feed. This is because the moisture in the feed must be evaporated before the thermal degradation of the particle will begin. The presence of water has also been shown to cause secondary reactions in some cases. Further research has also backed up the claim that moisture in the feedstock usually ends up in the oil product as discovered by Maniatis [94] during pyrolysis of bone dry samples and particles with 10 % moisture. A moderate amount of moisture is known to impact positively on the viscosity of the oil product.

Bridgewater [6] recommends that the moisture content for biomass for fast pyrolysis processes be around 10 %.

2.6 SUMMARY

This chapter has introduced the major constituents of most biomass materials and reviewed their thermal decomposition under pyrolysis conditions. Similarly, existing kinetic models describing the fast pyrolysis process and biomass thermal degradation have been reviewed and explained. The major products of fast pyrolysis processes and their characteristics have been reviewed. This chapter has also explained in detail the process parameters and factors required for optimal operation of any fast pyrolysis process.

3 FAST PYROLYSIS CONFIGURATIONS AND FLUIDISATION THEORY

Various systems for achieving fast pyrolysis have developed over the years with some of them moving from the bench scale to pilot scale and commercialisation. Some systems are more popular than others. Most notable amongst the systems currently used for research and commercial purposes include entrained flow systems, fluidised bed systems, ablative systems, vacuum systems and circulating fluidised bed systems. This chapter reviews the literature on fast pyrolysis configurations.

3.1 INTRODUCTION

Fast Pyrolysis for liquid production has come a long way since the early experiments started in the 1970øs. Many kinds of reactors and technologies for biomass processing via fast pyrolysis have been developed and the process is now widely accepted as a viable route for obtaining renewable fuels. Bridgwater [6] asserts in a review of existing fast pyrolysis processes that there is currently no best method as most processes achieve between 65-75 % liquid yields on a dry wood basis. The matrix in Figure 3-1 from a review by Van den Velden [95] showed the market attractiveness of fast pyrolysis technologies relative to current technological strengths.

Aston University

Illustration removed for copyright restrictions

Figure 3-1 Technological Strengths and attractiveness of Fast Pyrolysis Technologies [95]

Chapter 2 has reviewed the requirements for successful operation of fast pyrolysis processes, naming controlled reaction temperature, vapour residence time and high heat transfer rates as the most important requirements of fast pyrolysis.

Generally, the process parameters of vapour residence time and reactor temperature for most pyrolysis reactor technologies can be readily controlled. The third key requirement which is the high heating rates and heat transfer to the biomass particles is usually dependent on the reactor configuration employed for the process. In terms of the heat transfer, any technology employed must be able to provide the heat flux required to match the high heat transfer rates to the energy requirements for the thermal degradation of the biomass particles.

The two dominant modes of heat transfer during fast pyrolysis are conduction and convection. Bridgwater [6] reports that each mode of heat transfer may be maximised or contribute to the total heat requirements depending on the reactor configuration. The modes of heat transfer are also known to impose limitations in terms of operation. They can also increase the complexity of the system. Table 3-1 summarises the features of some fast pyrolysis technologies.

Table 3-1 Fast Pyrolysis Reactor Configurations, modes of heat transfer and features [9]

Reactor Type	Suggested heat transfer mode	Features
Ablative	95 % Conduction, 4 % Convection, 1 % Radiation	Large Particle size up to 6 mm, High char abrasion, minimal requirements for heat transfer gas, complex mechanical design
Circulating Fluidised Bed	80 % Conduction, 19 % Convection, 1 % Radiation	High heat transfer rates, high char abrasion, solid recycle, complex hydrodynamics
Fluidised Bed	90 % Conduction, 9 % Convection, 1 % Radiation	High heat transfer rates, good solid mixing, particle size <2 mm,
Entrained Flow	4 % Conduction, 95 % Convection, 1 % Radiation	Low heat transfer rates, particle size limit <2 mm, limited gas solid mixing.

3.2 FLUIDISED BED SYSTEMS (WFPP)

3.2.1 Background

The waterloo fast pyrolysis programme for biomass pyrolysis originated at the University of Waterloo in the 1980s. A shallow fluidised bed concept for thermal processing was used for the systems. Four of the fast pyrolysis units including the 300 g/h unit commissioned as part of this research at the Bio-Energy Research Group (BERG) operate on the principle of the waterloo system. Bridgewater reports that the University of Waterloo can be credited

with laying the foundation of modern fast pyrolysis. Research from the University of Waterloo is regarded as the most extensively published and publicised [8].

Early experiments employed a continuous fast pyrolysis unit using a fluidised bed at atmospheric pressure. The early units used particle sizes of between 105 and 250 µm. Feed rates were at 50 g/h in a nitrogen atmosphere over a temperature range between 400-600 ºC. Liquid yields of up to 70 % for hardwoods like aspen, poplar and maple on dry basis have been achieved using this system. The system was also used to process agricultural wastes like wheat, straw and corn stover with yields of between 40-60 wt% obtained [44].

Results from a Waterloo process was the basis for the construction of a 200 kg/h pilot plant for Union Fenosa in Spain [96].

3.2.2 Description and process yields

The 3 kg/h variant of the fluidised bed reactor shown in Figure 3-2 is a unit equipped with a loss in weight feed hopper capable of recording continuous weight loss and feeder mounted on a platform. The process begins with wood dried to about 7 % moisture content. The feed is then milled and screened to a size of 595 µm. The dried and milled feed is subsequently conveyed to from a storage hopper by a variable speed twin screw feeder where it is fed into the reactor unit by the recycled product gas which has been passed through a compressor [6].

Aston University

Illustration removed for copyright restrictions

Figure 3-2 Waterloo fast pyrolysis process [7]

Sand is used as the reactor bed material for heat transfer and the biomass injection point into the fluidised bed is within the bed itself. The bed is fluidised by a recycled stream of CO-CO_2-CH_4 mixture preheated after passing through controlled electric heaters. Additional heating coils are wrapped around the reactor to facilitate heating of the bed or freeboard if needed.

The design of the fluidised bed operates on the principle that allows the char formed in the reactor to be ejected from the fluid bed while ensuring that the fluidised sand bed collapses back retaining the bed material for heat transfer. This is achieved by careful selection of the process parameters including bed material size and fluid velocity adaptable to the fluidisation requirements [44].

Control of the reaction temperature is achieved by a thermocouple fixed in the fluidised bed that regulates the reactor heaters and heating coils through which the fluidising gas passes. Reactor pressure is monitored by differential and absolute bellows type gauges and is kept at 125 kPa [44].

Product vapours from the process are passed through a cyclone where char and particulates are removed. The oil product is collected by passing the vapours through two condensers in series. The condensers are equipped with collection pots at the bottom. The first condenser is held at 60 ºC and the second one operates at about 0 ºC. That temperature is achieved by passing chilled water through the condenser.

Effluent gases are filtered to remove tar and mist after passing through a filter and then passed through a compressor where part of it is recycled back to the reactor and the remaining is vented through a gas analysis system and gas meter. The product gas is analysed for CO and CO_2 through an on-line infra-red gas analyser-recorder. Periodical samples of the product gas are also taken for analysis using gas chromatography.

Using the 3 kg/h unit, high liquid yields were obtained at temperatures around 500 ºC which is believed to be as a result of minimum secondary decomposition reactions which occur at lower temperatures. Highly oxygenated liquids are obtained with no phase separation. The liquids have low viscosity with water content reported to be between 10-20% wt. The gases reported have heating values of 14.4 MJ/m^3 [6].

3.2.3   Other fluidised bed systems

The success of the Waterloo fast pyrolysis system led to the development of other fluidised bed units that operate on the same principle. Similar units have been built at universities and research centres across the world including NREL, University of Stuttgart, Technical Research Centre, Finland and Aston University [44]. The systems vary in sizes and capacity from 0.1-2 kg/h units.

Aston University currently has four fast pyrolysis units including the 150 g/h, the 300 g/h (commissioning primary objective of this research), the 1 kg/h and the 7 kg/h units. The 5 kg/h and 1.5 kg/h variant changed the cooling method of vapours from an indirect system to cooling by direct contact with a quench liquid. The cooling system was replaced by a quench unit with a disk and doughnut system. The unrecovered vapours are passed through a cotton filter before being metered and vented. The 1.5 kg/h unit was also used as part of a 2009 study employing hot vapour filtration unit for the pyrolysis vapours as a means of upgrading oil quality [97].

3.3   ABLATIVE SYSTEM (ASTON UNIVERSITY)

3.3.1   Background

Ablative pyrolysis may be defined as the melting or thermal erosion of biomass via contact with a hot solid or surface. This contact against the hot surface facilitates the thermal decomposition of the biomass. An ablative system was successfully operated at Aston University with a designed throughput of 3 kg/h by Peacocke [8, 33].

3.3.2   Description and process yields

The initial reactor used by Peacocke [33] had a circular base and internal diameter of 256 mm. The reactor had a volume of 0.00138 m^3 and the height from base to lid was 28 mm. The system layout is shown in Figure 3-3. The principle of Peacocke's ablative pyrolysis system was the use of high pressure on biomass particles against a hot surface at a temperature of not more than 600 ºC. A rotating blade moving at relatively high speeds was used. The angled blades also ensure the horizontal movement of the particles across the heated surface [33].

Figure 3-3 Ablative pyrolysis reactor and solids Collection system [33]

Up to 6.35 mm particle size of dried biomass were fed into reactor vessel from a screw feeder that is sealed and purged with nitrogen. Four asymmetric blades rotating at speeds of up to 200 rpm apply significant pressures on the biomass particles crushing them against the heated reactor base [33]. Thermal erosion of the particles is initiated by the quick blade motion and the hot reactor surface. The produced vapours and gases are removed from the reactor by diluted nitrogen while char is removed via a cyclone.

While nitrogen purging or the use of any inert gas is not a necessity, it is used in this process for control purposes particularly for the residence time and safety in the feed system. Primary liquid products are collected in a counter-current quench unit with stable products in the non condensable gases removed via an electrostatic precipitator. Gas samples are taken periodically for analysis after passing through a gas meter. Ablative pyrolysis systems are known to produce very fine chars that can be difficult to remove using conventional cyclones [98] .

Process yields from the process show that up to 78 % liquid yield was obtained using the ablative unit [99].

3.3.3 Other ablative pyrolysis systems

Robinson [8] also employed ablative pyrolysis using a 10 kg/h unit for bio-oil production at temperatures ranging between 450 °C-600 °C. The system employed for his study was designed with a direct contact liquid collection system and a wet walled electrostatic precipitator. Liquid yields of up to 64 % on dry feed basis have been reported using this configuration. Scholl et al [100] have also reported an ablative pyrolysis system with a nominal capacity of 15 kg/h. Average yields from this system were 68, 22 and 10 wt% for

liquid, gas and char yields respectively. Results from this unit formed the basis for the design and construction of a 6 ton per day pilot unit for processing whole wood chips.

3.4 TRANSPORT BED SYSTEMS (ENSYN)

3.4.1 Background

The University of Western Ontario undertook research on fast pyrolysis of biomass for Ensysnøs Rapid Thermal Processing technology. The initial term for the process was Ultrapyrolysis. This development happened in the late 1970øs and the early 1980øs. The aim of the project was to produce chemicals, gaseous and liquid fuels through fast pyrolysis although most work reported on this project focuses on ethylene and propylene production. Commercialisation of the process happened in 1989 [6].

Liquid fuel production from the process prompted the sale of a commercial plant to Red Arrow in the USA for recovery of food flavourings. Ensysn technology is currently operational in six plants. Further facilities are being developed including a 350 ton per day capacity [101].

3.4.2 Description and process yields

Four different variations of the patented Ensysn technology have existed referred to as RTP-I, RTP-II, RTP-III and RTP-IV. The Figure 3-4 below shows the RTP-III variation as is operational in an Italian plant for ENEL in Bastardo Italy. The system is operated as a transport bed reactor which contacts hot re-circulated sand with biomass in an up-flowing gas stream through the reactor. In all variations of the technology, the feed is kept to a size of less than 6 mm and moisture content does not exceed 10 % [102].

Aston University

Illustration removed for copyright restrictions

Figure 3-4 Ensyn RTP III fast pyrolysis ENEL plant [6, 101]

The gaseous products pass through two cyclones to facilitate solids separation before eventual quenching is carried out rapidly in a multiple stage quench system. The system is able to operate at residence times of hundreds of milliseconds and this is known to almost eliminate thermally unstable liquid intermediates of pyrolysis. These low residence times are used mainly for chemical production while longer residence times are used for liquid production. The system has been run with a wide range of feeds including pure cellulose, lignin, agricultural residues heavy distillates, heavy oils, asphalt and bitumen [102].

The products and yields from the Ensysn process vary with feedstock, reactor configuration and process parameters. Yields of up to 83% have been reported for woody biomass on a dry basis [6].

3.4.3   Other transport systems
The RTP I transport plant was designed to operate at a nominal feed rate of 10 kg/h. It was the first scale up of the initial ultrapyrolysis unit developed at the University of Western Ontario. The scale up represented a 30 times magnitude [5]. Similarly, the second configuration the RTP II developed in 1989 was built to have a nominal feed processing capability of 30 kg/h. The reactor was an up-flow transport system with residence times of less than 1.5 seconds. Success of the RTP II system gave rise to the RTP III system already described and a later variation tagged RTP IV.

3.5   ENTRAINED FLOW SYSTEM (EGEMIN)

3.5.1   Background
An entrained flow fast pyrolysis pilot unit for bio-oil production was commissioned in 1991 for Egemin in Belgium. The project was funded by the EEC as part of the Joule programme. The process was capable of handling 200 kg/h of fine wood particles using a down-flowing entrained flow. The Egemin research ended in 1993 and the project was discontinued due to financial constraints and unfavourable results. Figure 3-5 shows a schematic of the process discussed.

Figure 3-5 Egemin entrained flow flash pyrolysis process [6]

3.5.2   Description and process yields

Wood particles were transported form storage silos to a smaller hopper before being pyrolysed in an entrained flow reactor via a water cooled screw auger purged with a stream of nitrogen gas. The wood particles were of 1 and 5 mm sizes with moisture and ash content being 16 and 0.57 wt% respectively. The reactor was designed to operate at residence times of 0.6 second. The wood particles were entrained into the down flowing vertical reactor in a stream of hot gas at a temperature between 700-800 ℃. The gas was heated by a 90% sub-stoichiometric burner fuelled by propane and diluted by nitrogen as a means of temperature control. The reactor diameter was 0.4 m and the height was 1.2 m [8].

Pyrolysis products exited the reactor at 490 ℃ and passed through a nitrogen purged cyclone. Liquid collection was achieved via a Venturi scrubber using product oil as the scrubbing medium. The vapours entering the scrubber were at 400 ℃ and the scrubber liquid exit temperature was 55 ℃. Oil being recycled was cooled via a water cooled heat exchanger. One unique feature of the process was the use of mineral oil to start the scrubbing system. The oil was allowed to accumulate in a disentrainment tank before being drained at the end of a run [8].

A number of problems were encountered during the operation of the Egemin unit worthy of note. The feed was not completely pyrolysed particularly at feed rates exceeding 100 kg/h. This was disappointing as the unit was designed to operate at 200 kg/h. This was due to insufficient heat transfer to the particles in the short residence time designed for the

process. The primary means of heat transfer was convection. The partially pyrolysed particles continued to be pyrolysed in the cyclones and char pots potentially contaminating the primary products produced with the secondary ones being formed [103].

Other problems included the char carryover from the cyclone in the liquid lines and caused blockages in the pipework and heat exchangers as well as poor bio-oil separation from the non-condensable gas confirmed by the poor bio-oil yields in the results.

The bio-oil from the process was collected at three points namely the primary collection vessel, the secondary collection vessel and the drain at the fan. The mass flowrate of the gases were not measured and the value was obtained by difference. Liquid yields of up to 54 wt% were recorded using this system with gases accounting for 29 wt% of biomass input. The reported char yield from the process was 16.2 wt% [6].

3.5.3   Other entrained flow systems

An upflow process development unit for fast pyrolysis was also commissioned at the Georgia Tech Research Institute (GTRI). Entrained flow pyrolysis of biomass was studied in a unit capable of processing 45 kg/h of hardwood species available in the South Eastern United States of America. The Process Development Unit was completed in 1983 and the conditions for maximum pyrolysis yields were experimentally investigated. Results reported liquid yields of 50 wt% on a moisture and ash free basis. The unit was modified in 1984 and finally in 1987 to improve liquids collection and quality. Yields of liquids improved to 60 wt% for certain feedstocks. The use of catalysts was explored using the system but as the results of tests were inconclusive, the data was not reported [56]. The programme was discontinued in 1989 due to shrinking budgets [5].

3.6   CIRCULATING FLUIDISED BEDS (CRES)

3.6.1   Background

European interest in the generation of energy from renewable sources led to the start of a project in 1990 at the Centre for Renewable Energy Sources in Greece. This programme was one of six projects started as part of the EEC joule programme at the time. The others being spread across Europe in Aston University and University of Twente, amongst others [6, 96].

3.6.2   Description and process yields

The process at CRES was developed to have a nominal throughput of 10 kg/h. The process described herein is a transport bed system in its own right. The process was unique however, in the sense that the char produced from the pyrolysis of the biomass would be burned off to provide energy for the continuation of the process. The system operated as one unit instead of having to separate reactors. A flow diagram of the process is shown in Figure 3-6. The principle of operation was the burning of char in a conventional bubbling fluid bed below the fast pyrolysis reactor to provide energy to the heat transfer medium (sand). The sand is subsequently transported through a recirculation bed with the hot gases from the combustion stage to decompose the biomass particles [5, 104, 105].

Aston University

Illustration removed for copyright restrictions

Figure 3-6 Circulating fluidised bed System at CRES [5, 6]

Problems associated with this unit include short runs, coupled with the complexity of integrating a combustion unit with a pyrolysis unit. The unit also reports low mass balance closures with significant agglomeration and uncertainties with the reliability of the volumetric feed system [5].

Liquid yields of up to 60 wt% have been reported using this unit although the yields from the system are significantly lower than liquid yields of other fast pyrolysis systems [5].

3.7   VACUUM SYSTEMS (PYROVAC)

3.7.1   Background

Vacuum pyrolysis is a process that has been under development at the Universities of Laval and Sherbrooke since the early 1980øs. Vacuum pyrolysis is not fast pyrolysis in the

conventional sense since it has relatively low heating rates for the biomass particles. This however, does not restrict the process as the primary liquid products are drawn quickly from the reacting surface on which they are formed. Bench scale units at Sherbrooke and Laval universities resulted in a 25 kg/h process development unit being tested. A 200 kg/h unit was initiated but discontinued due to financial difficulties [6, 98].

A commercialised vacuum pyrolysis unit shown in Figure 3-7 was however established in Canada. The Pyrocycling process is a product of research carried out at the universities already mentioned [6].

Aston University

Illustration removed for copyright restrictions

Figure 3-7 Pyrocycling vacuum pyrolysis process [6]

3.7.2   Description and process yields

The pyrocycling ^{TM} process is a patented technology that processes organic material by thermal decomposition under reduced pressure conditions, high heating rates and temperature for producing useful products. The process usually operates at about 450 °C and a pressure of 15 kPa. These conditions are what enable the recovery of large quantities of pyrolysis liquids and solid carbonaceous materials [106].

The feedstock is dried and shredded before being fed into the reactor called a pyrocycler under vacuum conditions. The feed is carried through horizontal plates heated by a mixture of molten salts. The temperature is maintained at 530 °C and the molten salts are heated by burning the non condensable waste gases from the process. The vapours produced from passing the feed over the heated plates are instantly removed via a vacuum pump subsequently sent to a two condenser unit where they are cooled into heavy and light oils together with an aqueous phase. The solid products from the process exit via the reactor outlet after they have been cooled [106].

The Pyrovac process has been commercialised and is capable of being used in other industries that process biomedical, municipal solid and other wastes with organic components. In most cases, the wastes are completely transformed into pyrolytic oils, water, solid residues and non condensable gases. The Pyrovac process also has potential to be used in remediation of soils contaminated with hydrocarbons to extract bitumen from sands [106].

The problems associated with this process include the mechanically complex systems that make it more liable to failure. Vacuum technology as a process is a very expensive and may not be cost-effective. The reaction products are significantly cracked with a loss of organic liquids despite the use of a vacuum [6].

Yields for the Pyrocycling process for woody biomass show up to 55 wt% liquid yield with char accounting for 34 wt% of input. The gas yields from the process is reported to be 11% [6].

3.7.3   Other vacuum pyrolysis systems

The University of Laval undertook research for the generation of bio-oil using pyrolysis at low pressures. The system employed selective condensation of vapours for extraction of specialty chemicals. The study involved using Aspen Poplar as feedstock from which they obtained a maximum oil liquid yield of 60 wt%. The optimum temperature lies between 425-450 ºC. The reactor is a 2 m high and 0.7 m diameter multiple-hearth furnace which is hermetically sealed. The operating pressure of the process is around 10.7 kPa [107]. Bridgwater reports that the temperature profile of the unit ranges between 200 and 465 ºC. The generated vapours are removed from the reactor system using a vacuum pump while the char falls to the bottom of the reactor where it is collected on a load cell [7].

The quenching occurs in different units where the primary condenser is a shell and tube quenching unit followed by a series of secondary condensers. The first secondary condenser is water ethylene glycol mixture while the next two are dry ice acetone cooled. The final condenser is a glass wool filter at room temperature. One unique feature of the unit was its ability to fractionate the products of pyrolysis by the use of outlets at different levels as shown in Figure 3-8.

Figure 3-8 University of Laval vacuum pyrolysis process [7]

The results showed that oils from the primary condensing unit have little moisture content while the secondary condensing unit having high water content fractions as is found in conventional systems.

Problems associated with the system include clogging of the quench system at high throughputs >30 kg/h. The use of large volume reactors and large vacuum pumps reduce its potential for scale up [7].

3.8 ROTATING CONE SYSTEMS (UNIVERSITY OF TWENTE)

3.8.1 Background

Two European sponsored research projects led to the development of the rotating cone concept for biomass fast pyrolysis between 1989 and 1997. The aim of the research was the development of an intensive reactor where the biomass particles slide on a heated surface like the ablative reactor already discussed. Subsequent development of the ideas led to the development of the rotating cone concept. The process was developed at the University of Twente in the Netherlands [108].

3.8.2 Description and process yields

The principle of operation of the rotating cone pyrolysis reactor shown as Figure 3-9 is that the biomass particles are fed from the base of a reactor onto a heated rotating cone. The centrifugal motion of the cone imparts pressure on the biomass particle with a resultant ablative effect on the particles to achieve thermal degradation [108].

Figure 3-9 Rotating cone concept for biomass pyrolysis [6]

The development of the concept began with a see through cold model to facilitate visual inspection and photography. The cold model was operated with two cones of 60 and 90º angles. Rotation speeds of up to 1800 rpm were achieved. Data from the cold model runs were used to determine the effect of gas flow on particle residence time [108].

Consequently, a rig was built that was capable of operating at pyrolysis temperatures with a cone angle of 60º as shown in Figure 3-10. Initial experiments indicated that smaller particle sizes of less than 250 µm had the tendency to stick to the heated surface reducing throughput. Based on the findings, it was decided that the process be operated with a heat transfer medium where sand was selected [6].

Figure 3-10 Rotating cone reactor at University of Twente [6, 108]

The developed reactor is capable of throughputs of up to 3 kg/h. The resulting vapours from the reactor are cooled in a quench system. The nature of the reactor means that only isothermal operation may be achieved leading to significant cracking of vapour products. Reported yields are 60 wt% for liquids, 25 wt% for gases and 15 wt% for char at vapour residence times of 1 s. Mass balance closures are reported to be around 90% [6, 108].

3.8.3 Other rotating cone systems

A company called BTG has recently commercialised the rotating cone fast pyrolysis concept. Detailed mass balances are not available but the company website claims liquid yields of 70 % with char and gases accounting for the remaining 30 % [109].

The commercial RTR system recycles char and sand from the rotating cone reactor into an air fed combustor where the char is burned to heat up the sand which is recycled back into the reactor. The pyrolysis vapours are fed into a direct contact quench column where the bio-oil is condensed and collected. A cyclone is located after the combustor for ash collection while the flue gases are vented.

3.9 LABORATORY SCALE FAST PYROLYSIS UNITS

Different researchers have also looked at fast pyrolysis of biomass on a laboratory scale basis similar to the one to be commissioned during this research. These researchers have used various reactor configurations some of which are described below.

A detailed description of a typical laboratory scale pyrolysis process is given by Luo et al [110] and depicted in Figure 3-11. Employing the depicted system, they explored the production of bio-oil from feedstocks including rice husk.

Aston University

Illustration removed for copyright restrictions

Figure 3-11 Laboratory fluidised bed fast pyrolysis process as reported by Luo et al [110]

The reactor was a bubbling fluidised bed with an internal diameter of 80 mm and a height of 1200 mm. The reactor was equipped with a cyclone and char pot for collection of process char ejected from the fluidised bed. Heat for pyrolysis of the biomass was supplied by three electric heaters of 2 kW rating. The throughput of the fluidised bed reactor was 3

kg/h with a volumetric flowrate of nitrogen for fluidising the sand bed between 3-6 m^{3}/h. The flowrate equates to a value of between 3-4 times the minimum fluidising velocity of the bed material. The fluidising gas was passed through a pre heating vessel with another nitrogen inlet through the biomass feeder. The study reports that the pipe inlet from the reactor to the quenching unit was kept at a steady temperature above 300 ºC to reduce the likelihood of condensation of pyrolysis vapours prior to reaching the quenching unit. The principle of operation involved preheating the fluidised bed to temperatures between 450 and 700 ºC. Pyrolysis vapours were cooled to bio-oil product using water cooled quenching unit and the product gases were analysed using a GC. The results from their study was the basis for design of a larger process shown in Figure 3-12. A similar unit capable of 20 kg/h nominal throughput was developed. The main variation was the use of a multi stage product collection unit on the developed process [110].

Aston University

Illustration removed for copyright restrictions

Figure 3-12 Developed fast pyrolysis process from laboratory scale data [110]

The developed unit highlights one importance of laboratory scale processes in the development of newer and more efficient processes in the area of fast pyrolysis.

Zheng et al [111] carried out fast pyrolysis of cotton stalk using a fluidised bed unit. As part of the study, they modified a fast pyrolysis unit by introducing a dual screw feed system and incorporating a spray medium to the quench system to improve energy performance. A schematic of the process used is shown in Figure 3-13

Figure 3-13 Fluidised bed lab scale fast pyrolysis process as modified by Zheng et al [111]

The initial process used a single screw feed system but the study reports thermal degradation of biomass prior to reactor entry. This caused them to modify the system to a dual screw feed system with one acting as a metering screw and the other as the transport screw into the reactor. Similarly, the initial process employed the use of indirect cooling for cooling pyrolysis vapours but was modified to a direct contact system using the product bio-oil for quenching. The modified process began with ethanol as the quench liquid but its high volatility ensured complete removal depending on the duration of the run. The results of the study concluded that the optimum pyrolysis temperature for maximum liquid yield was between 480 and 530 ºC. Maximum liquid yield was 56 wt% [111]. As with many laboratory scale fast pyrolysis units, the fluidising gas was preheated by passing it through a heated vessel. The system was equipped with 2 cyclones and char pots for solid product removal and storage.

A Fluidised bed reactor was developed at Imperial College London by Weerasinghe [112]. The reactor with dimensions of 52 mm internal diameter and 200 mm height was equipped with a quartz sintered plate as the bed support and gas distributor. The heat transfer medium of the bed was acid washed sand of particle size between 180 and 425 µm. The reactor was heated in a furnace with a solid state temperature controller. Feeding into the reactor was through a gas cooled feeding probe that went into the fluid bed through which materials were fed. The bed was operated at between 3-3.7 times the minimum fluidising velocity of the bed material. The fluidising gas used was nitrogen part of which was passed through the feed hop as means of entrain. Tar collection form the process was achieved through a liquid nitrogen cooled tar trap at the exit of the reactor.

Zhou [113] commissioned and further developed an existing high pressure fluidised bed reactor for the pyrolysis of coal and biomass in a 1999 Ph.D. study at Imperial College London. The reactor used was 34 mm diameter and 504 mm length. As part of the process development, modifications were made to the reactor assembly, heating system, feeding system and gas supply to improve performance and the range of pyrolysis experiments to be carried out. The reactor employed acid washed sand as fluidising medium. It was operated at operating at 4 times the minimum fluidising velocity of the bed material. By the conclusion of the study the system had been used for pyrolysis, gasification and combustion experiments to determine yields from biomass, coal and co-processing.

3.10 FLUIDISATION THEORY AND LITERATURE REVIEW

One of the primary objectives of this study was to commission a bubbling fluidised bed reactor to process biomass via fast pyrolysis hence the need to review fluidisation theory. The operation of a fluidised bed involves certain parameters that have been studied for many decades. The content of this section of the thesis presents and reviews literature on parameters relevant to the successful operation of a fluidised bed reactor. It is pertinent to state at this point however, that the literature reviewed herein is selective and covers material relevant to this research. For a detailed review of fluidisation literature, the reader is referred to work published by Kunii and Levenspiel [114].

One of the earliest reported uses of fluidised bed technology dates back to the 1920s when a fluidised bed gasifier was used in Germany by BASF to supply raw gas to the synthetic chemical industry [114]. The fast pyrolysis process has been introduced as a moderately high temperature process occurring optimally at 500 ℃. Factors like elevated temperatures and pressures are known to impact the behaviour of fluidised beds. As the process occurs at atmospheric pressure, only the effect on temperature on the selected fluidisation parameters will be reviewed. Different regimes of fluidisation exist as shown in Figure 3-14.

Figure 3-14 Different regimes of fluidisation [114]

3.10.1 Geldart classification of particles

Particles of different sizes, shapes and densities behave differently during fluidisation. A general and widely accepted system of classification of particles based on sizes and densities is the Geldart classification as shown in Figure 3-15. The Geldart system categorises particles into four classes based on the difference in the densities mean particle sizes. Particles of each category exhibit certain characteristics as detailed below [115].

A) Particles in this category fluidise easily. They are typically in the range of 20-100 µm with densities less than 1400 kg/m^3. The catalysts used in fluid catalytic cracking fall in this category and are some of the most studied particles in fluidisation

B) Most sand particles are known to fall in this category. The particles in this class are mostly in the size range of 500-2000 µm and have densities greater than 1400 kg/m^3.

C) Particles of this category show very unsatisfactory fluidisation behaviour. Examples of these particles are flour and starch. The inter-particle forces are stronger than the forces of the fluid causing poor fluidisation behaviour and characteristics

D) These are large particles such as grains and larger sand particles. They exhibit erratic bed behaviour such as channelling and spouting and are common particularly in deep beds.

Figure 3-15 Geldart classification of particles [115]

3.10.2 Minimum fluidisation velocity

The minimum fluidising velocity U_{mf} , is the minimum velocity at which the flow of the fluid will cause a packed bed of loose materials to behave like a liquid. During fluidisation, as the upward velocity of fluid flow through a packed bed is increased, a point is reached at which the weights of the particles are just freely supported by the fluid flow. This point is known as incipient fluidisation [116]. The relationship between fluid flow through a fixed and fluidised beds is shown in Figure 3-16.

Figure 3-16 Relationship between superficial velocity and pressure drop across fixed and fluidised beds[117]

There is a close relationship between fluid velocity and the pressure drop across the bed. In fluidised bed technology, there is an increase in the pressure drop for fluid flow through packed beds until the point of incipient fluidisation [118]. The pressure drop across a packed bed is given by the Ergun equation shown in equation 3-1.

$$ — = 150\frac{(\quad)}{(\quad)} + 1.75\frac{(\quad)}{} \qquad \textbf{Eq 3-1} $$

At that point, any increase in the fluid velocity passing through the bed has little impact on the pressure drop across the bed until the point of entrainment at which the bed materials are blown off. Many correlations are available for predicting the minimum fluidising velocity of particles. Subramani et al [119] report 15 correlations that may be used to determine the minimum fluidisation velocity of particles. Most of them are related to the particle voidage, density, sphericity and the fluid density and viscosity. The minimum fluidising velocity is usually derived from the correlation shown in equation 3-2

$$ = 150\frac{(\quad)}{} + \frac{\cdot}{} \qquad \textbf{Eq 3-2} $$

Where Ar is the Archimedes number given by equation 3-3

$$ = \frac{\qquad}{\qquad} \qquad \textbf{Eq 3-3} $$

Re_{mf} is given by the equation 3-4

$$ = \frac{\qquad}{} \qquad \textbf{Eq 3-4} $$

Where

p	pressure drop across bed	[N/m2]
L	bed height	[m]
Ar	Archimedes number	[-]
Re_{mf}	Reynolds number at minimum fluidisation velocity	[-]
s	Particle density	[Kg/m^3]
g	Gas Density	[Kg/m^3]

μ$_g$	Gas Viscosity	[-]
⬚	Voidage	[-]
	Sphericity	[-]
U$_{mf}$	particle minimum fluidisation velocity	[m/s]

It is important to note that if there are sufficiently accurate values of ε$_{mf}$ and dm, then the minimum fluidising velocity for fluidised beds can be obtained from any of many empirical correlations. Experiments have however shown that ε$_{mf}$ varies in a complex manner with bed temperature and as such, the accuracy of values obtained using this correlation and others may vary [118].

3.10.2.1 *Impact of elevated temperature on Minimum fluidisation velocity*

The density of a gas is inversely proportional to its temperature. In line with this principle, the density of a gas will reduce as the temperature increases. Rowe [120] in a study showed the effects of increasing temperature on the minimum fluidisation velocities. The results of the study shown in Figure 3-17 shows that for group B particles as used during this study, an initial rise in minimum fluidising velocity is noted before a slight decline in the values [116, 121].

Figure 3-17 Effect of temperature on minimum fluidisation velocity of particles [116, 121]

3.10.3 Particle terminal velocity

The particle terminal velocity Ut. is defined as the final steady velocity at which a particle will remain steady in an upward flow of a fluid. The particle terminal velocity is important for determining entrainment of particles in an upward flow of a fluid through a fluidised bed. At $U_0 = U_t$, the particle floats in the upward fluid flow. At $U_0 > U_t$, the particle will rise with the upward flow of the fluid. Like the minimum fluidising velocity, the particle terminal velocity is dependent on the particle density, sphericity and voidage It is also related to the fluid density and viscosity [114]. The particle terminal velocity is obtained by the correlation in equation 3-5

$$\overline{\qquad} \cdot \qquad\qquad \textbf{Eq 3-5}$$

3.10.3.1 Impact of elevated temperature on terminal velocity

As with the minimum fluidisation velocity, elevated temperatures can to lower the values of terminal velocities of particles. A review by Werther [122] showed a decline in the values of terminal velocities of Group A particles as temperature increased (Figure 3-18). This study is focused on group B particles. Nevertheless, the same trend is expected [116, 120, 121].

Aston University

Illustration removed for copyright restrictions

Figure 3-18 Effect of temperature on terminal velocity of Group A particles [116, 121]

3.10.4 Minimum bubbling velocity

The minimum bubbling velocity U_{mb} is the fluid velocity at which bubbles are first observed through a packed bed. In a liquid-solid system, there is usually smooth fluidisation through a bed so the minimum bubbling velocity is of little impact [114]. In gas-solid systems (group B particles), like the ones used in this research, bubbles start to form as soon as the fluid velocity exceeds minimum fluidisation velocity[114]

3.10.5 Entrainment and elutriation

Entrainment as regards fluidised bed technology refers to the flux of solids carried out of the fluidised bed by the fluidising gas in kilograms per unit cross sectional area and second. Elutriation on the other hand refers to the classifying effect of the fluidised bed entrainment. Elutriation characterises the selective removal of certain particles of individual sizes and characteristics from the fluidised bed [122, 123]. An important variable with regards entrainment and elutriation is the Transport Disengaging Height. The TDH refers to the point in a fluidised bed at which no further material returns to the bed and which the maximum solid loading of the fluidising gas is determined by its capacity to transport the solid pneumatically [124].

With regards to fast pyrolysis, char is known to catalyse cracking reactions, and reduces liquid yields. This makes controlled elutriation and entrainment particularly important for fluidised bed fast pyrolysis units. The process requires that char particles are ejected from the fluidised bed while ensuring that the bed material collapses back. A typical fluidised bed consists of two regions. The bottom region is where the dense bed is situated and the region above that is referred to as the free board region. For fluidised bed reactors used in fast pyrolysis, it is important that the height of the reactor freeboard should be at least the height of the TDH. This is to ensure that the extent of carryover of heat transfer particles i.e. the bed material is minimal or in an ideal situation, nonexistent. This guarantees a continuous process as the sand will continue to provide heat transfer while the char particles are ejected from the reactor. Figure 3-19 shows the relationship between solids hold up and TDH. It shows that the rate of hold up becomes constant at freeboard heights exceeding the TDH.

Figure 3-19 Bed and freeboard relationship to TDH in a fluidised bed [122]

There exists in literature correlations for the determination of rates of elutriation and entrainment. One of the correlations proposed by Kunii and Levenspiel was tested as part of an MEng project by Thong at Aston University [125]. Results obtained showed wide variations including negative values for entrainment. Thong's study showed the limitations of empirical correlations when used at different conditions from which they were derived.

3.11 HEAT TRANSFER IN FLUIDISED BEDS

Heat transfer in externally heated fluidised beds as used for this research occurs as combination of three individual mechanisms. They occur in the form of gas to particle heat transfer, particle to particle heat transfer and wall to bed heat transfer.

In the first case, heat is transferred from the gas to the bed particles depending on the temperature difference. For most processes, the fluidising gas is usually preheated thus facilitating a rise in the temperature of the bed solids by their interaction with the preheated gas supply. Pioneering work on the effects of gas to particle heat transfer was carried out by Kettering, Mansfield and Smith [126]where they employed a 6cm diameter column to study the effect of gas to particle heat transfer. This study did not measure the temperature in the bed but only took into account the outlet temperature of the gas [126]. Further work by Heertjes et al [127] studied the effect of heat transfer in fluidised beds where the effect of the distributor on heat transfer between gas and particles were measured. They concluded that gas to particle heat transfer occurred only up to 5mm above the distributor above which the impact was reduced. This study suggested that the solids temperature is higher at the bottom of the bed than at the top because of the effect of the distributor [128].

Botterill [129] showed that although the heat transfer coefficient between gas and particles is usually in the range of between 6-23 W/m^{2}K, they are compensated for by high heat transfer rates because of the large heat transfer surface area that can be achieved even by small particles. This study further showed that there is a rapid temperature change at the point of entry of the gas into the vessel and showed the difficulty in being able to accurately measure the temperature at that point [129]. Overall, numerous studies have been undertaken to study the effect of heat transfer between gas and solid particles in fluidised beds. The scope of this thesis does not include detailed reviews of all the studies undertaken though the reader is referred to a study undertaken by Mostafa [130] where excellent reviews of many of the studies are given.

The second case is where heat transfer occurs between higher temperature particles and lower temperature particles. This kind of heat transfer occurs in externally heated vessels where particles acquire heat from the heated walls and transfer them to cooler particles because bodies in contact which each other will exchange heat until thermal equilibrium is reached. However, in bubbling fluidised beds tend to have a high degree of mixing with uniform temperature across the bed such that particle to particle heat transfer is usually insignificant when compared to the other two heat transfer mechanisms occurring [130].

In the third and final mechanism of heat transfer, particles acquire heat from the heated walls of the vessel because of the bubble induced solid movements where the particles come in contact with the heated walls exchange heat before being pushed away. The repetitive nature of this mechanism coupled with the high degree of mixing makes this the dominant means of heat transfer between fluidised bed contents [129]. One of the earliest studies covering heat transfer between bed and wall is the one conducted by Baerg, Klassen and Gishler [131]. The study was conducted in 14 cm diameter column and bed heights of 25cm. The study focused on different bed materials including sand, glass and alumina. At the conclusion of the study, it was seen that the heat transfer coefficient reduced with increasing particle size. This conclusion relating reduced heat transfer coefficient with increasing particle size was further buttressed by Levenspiel [114]. Botterill [129] again carried out another study on the heat transfer between bed and wall heat transfer and concluded that heat transfer between wall and bed is more as a result of the frequency of the number of times the bed particles meets the heated wall rather than conduction because the contact time between the bed materials and the walls are minimal. Again, many studies have reviewed the different studies carried over the years by several

researchers and the reader is again referred to work by Mostafa [130] where excellent reviews of these studies are given.

Later studies however showed that heat although there is a decrease in heat transfer coefficient with increasing particle size, the effect reverses when the particles become larger than 3000 µm at which point an increase in heat transfer coefficient with increasing particle size is noticed [132] . This research will not use particle sizes up to 3000 µm.

3.11.1   Heat transfer in bubbling fluidised beds for fast pyrolysis processes

 Most definitions of fast pyrolysis as the one earlier presented define the process in terms of vapour residence time and quenching to oil product. While this is fundamentally true, the basic definitions do not take into account the more complex process of heat transfer to the biomass particles.

Graham [56] postulates two possibilities during the thermal decomposition of biomass particles. In the first, the resistance to heat and mass transfer in the biomass is negligible to such an extent that no temperature gradients are present within the particle. This scenario is best suited for fast pyrolysis and is seen where the rates of heat transfer to the particle is adequate. In the second scenario where the extent of heat transfer to the particle is inadequate, temperature gradients are present within the biomass particles between the surfaces and centre such that a fraction of the biomass particle will remain unreacted for a period of time that will allow for slow pyrolysis to take place or alternative reaction pathways to occur. The second scenario is undesirable for a fast pyrolysis process. As biomass has low thermal diffusivity, it is possible that while the surfaces of the particles undergo fast pyrolysis, the cores of the particles are undergoing slow or intermediate pyrolysis. This is one of the reasons that smaller biomass particles are preferred for fast pyrolysis processes.

The heat gained by a biomass particle during fast pyrolysis is related to its mass, its specific heat capacity and the temperature change between the cold particle and temperature during pyrolysis. Peacocke [33] reports that although specific heat capacity of the biomass particle is dependent on temperature, it is assumed to be constant until the biomass particle decomposes. Such that a particle exposed to an external heat flux is heated up but not instantly. This is because the heating rate is governed by the rate of heat flow inside the particle on the one hand, and a resistance layer on the surface of the

particle. The extent of the described phenomenon can be given by the dimensionless parameter known as the Biot number given by equation 3-6

$$= \frac{(\qquad)}{(\qquad)} \qquad \text{Eq 3-6}$$

Where

h_t Overall heat transfer coefficient   [w/m²K]

d_p particle diameter   [m]

$_b$ biomass thermal conductivity   [w/mK]

The Biot number as a heat transfer parameter is able to give a measure of the resistance to heat transfer. The Biot number compares the magnitude of convection at the surface of the particle to the magnitude of internal conduction taking place in the reacting biomass particle giving an overall measure of resistance to heat transfer.

With reference to the discussions so far, Scott et al [133, 134] presented a more quantitative definition of fast pyrolysis. They defined fast pyrolysis as a pyrolysis process during which the biomass particle attains 95 % of reaction temperature in less than 20 % of the vapour residence time. The definition is based on work in a fluidised bed where they estimated that a 600µm particle reaches a temperature of 450 ℃ in 618 ms where the target temperature was 500 ℃.

To further emphasise the suitability of bubbling fluidised beds to meet the high rates of heat transfer required for fast pyrolysis, reference is made to work carried out by Liden [58] where the heat transfer coefficient hot of a bed of sand to biomass was determined to lie between 300 and 510 W/m²K. The study involved silica sizes of 450 µm and a voidage of 0.4. The study arrived at these figures from correlations applied to immersed surfaces assuming particles to be 1mm in size. The temperature profiles which they obtained from the study showed that even for a worst case scenario where the heat transfer coefficient is 300 W/m²K, the wood particle centre is able to attain a temperature of 400 ℃ within 2 seconds.

From the results of Scott and Liden, it can be concluded that the rate of heat transfer in a bubbling fluidised bed of small sand particles to biomass is sufficient to meet the criterion of high heat transfer rates within the shortest possible time for biomass particles up to 1 mm in size.

3.12 SUMMARY

The literature reviewed in this chapter looked at a number of past and present fast pyrolysis configurations that have been used on laboratory, pilot and commercial scales. The literature reviewed has shown that fast pyrolysis has developed since its inception as a thermal processing route for converting biomass to energy.

Literature concerning hydrodynamics and heat transfer in fluidised beds has also been reviewed. The literature has helped to explain the mechanisms of heat transfer in fluidised beds. It has also introduced hydrodynamic parameters relevant to fluidised bed design and operation. In terms of fluidised bed hydrodynamics and heat transfer for fast pyrolysis, the literature has shown that bubbling fluidised beds are capable of meeting the heating and technological requirements for the process.

4 BIOMASS AND FAST PYROLYSIS PRODUCTS CHARACTERISATION METHODS

This chapter introduces the feedstocks used during this research. Feedstocks were categorised as commissioning feedstocks and primary feedstocks. The methods of characterisation are described in detail. This chapter also reviews the methods used to characterise and assess bio-oil quality in later chapters.

4.1 COMMISSIONING FEEDSTOCKS

A variety of feed types were used in the course of this research. During the commissioning of the 300g/h fast pyrolysis unit, previously reported feedstocks were used. This allowed for comparison of experimental data with already published results. The feedstocks used during commissioning stage of the 300 g/h unit were Beechwood, Willow, Pine and Miscanthus. Existing data on the feedstocks was used for comparison purposes in order to assess the process performance and product yield distribution of the commissioned unit. The feedstocks were readily available at the Bio-Energy Research Group (BERG).

4.2 PRIMARY FEEDSTOCKS

Two unreported feedstocks were chosen as primary feedstocks. Press cakes from the oil extraction process of Jatropha curcas and Moringa olifiera seeds were chosen. Two varieties of each feedstock were used. The first variety had African origins while the second was of Asian origins. An introduction to the primary feedstocks has already been given in a previous chapter. The Indian Jatropha and Indian Moringa press cakes used were supplied by Asian Greenfields based in India. African Moringa was sourced from Earth oil based in Kenya while African Jatropha was obtained from Jatropha Africa based in Ghana. Figures 4-1, 4-2, 4-3 and 4-4 shows photographs of the primary feedstocks as received.

Figure 4-1 Indian Moringa press cake as received

Figure 4-2 Indian Jatropha press cake as received

Figure 4-3 African Jatropha press cake as received

Figure 4-4 African Moringa press cake as received

The feedstock characterisations performed has where possible, tried to follow standard test methods. However, due to limitations of equipment, availability, time and budget constraints, this was not always feasible. Therefore, some tests have been adapted or developed to suit the equipment available.

4.3   FEED PROCESSING

Most of the feedstocks used came in different forms, shapes and sizes as was the case with the primary feedstocks. It was necessary that the feedstocks be processed due to limitations of the feed system of the fast pyrolysis unit. It was also necessary for the feedstock particles to be of certain sizes for analytical studies. To meet these criteria, the feedstocks were subjected to size reduction procedures and size separations.

4.3.1   Milling and sieving

The biomass samples were milled with a knife mill with interchangeable screens of varying sizes (1-10 mm). The choice of screen was based on the requirement of each experiment but limited to <1 mm to prevent blockages and feeding problems during Fast pyrolysis experiments. The milled particles were then sieved to separate the biomass particles according to sizes. This was achieved using a stack of sieves of different wire mesh sizes. The principle of operation involved vibrating the sieves. Smaller particle sizes were collected at the bottom and the larger were retained higher up.

4.3.2   Sampling

Biomass particles are known to be inhomogeneous. This lack of homogeneity impacts on characterisation results and analytical pyrolysis where small amounts of biomass are used. This lack of homogeneity occurs because different plant parts have differing ratios of cellulose, hemicellulose, lignin and extractives. This was not expected to be the case with the primary feedstocks but because limited information was provided by the suppliers, a method of obtaining a representative sample of the biomass feedstock had to be employed. Random samples were taken from the biomass particles after grinding and sieving. For analytical experiments and characterisation methods requiring small amounts, up to 5 mg of the sample was obtained and this procedure was replicated three times. This sampling method reduces the deviation that may be caused when using a single sample.

4.4 BIOMASS CHARACTERISATION METHODS

The pyrolysis process is affected by the characteristics of the feed. The moisture content of the feedstock is a major parameter that influences the water content and composition of the bio-oil product. The particle size distribution influences the reaction times for complete thermal decomposition of the biomass particles. The density and shape of the biomass particles will affect the fluidisation characteristics and influence bed hydrodynamics of the biomass and char in a fluidised bed reactor. The volatile matter content of the feedstock will have an effect on the product yields of any pyrolysis process. The ash content may impact side reactions and act as a catalyst for unwanted reactions that impact negatively on oil product quality and yields. For these reasons, it is pertinent to characterise the feedstocks both physically and chemically in order that reasonable conclusions can be drawn from experimental results.

4.4.1 Proximate analysis

The proximate analysis of samples involved the determination of the moisture, ash and fixed carbon contents.

The moisture contents were determined according to ASTM E1756-01 principles. The percentage weight loss of a pre weighed sample heated at 105 ℃ to constant weight is recorded. These measurements were taken using three crucibles with 3-4 g of the biomass sample placed in an oven at 105 ℃ for six hours. The lids are placed at an angle to allow for the escape of moisture. The samples are then cooled in desiccators and reweighed. The process is repeated hourly until constant weight is achieved.

The ash contents of different feedstocks were determined according to the ASTM E1755-01 method. Three samples of moisture free biomass are placed in an oven at 625 ℃ with the lids tilted at an angle to allow for the escape of volatiles. The samples are left for six hours and then cooled in desiccators for one hour. The ash content is then obtained by dividing the weight of the samples by the pre dried weight and expressed as a percentage. The average of three samples for each feedstock is taken to further reduce the deviation.

The percentage of fixed carbon was obtained by simple mass balance using equation 4-1

$$\% = 100 - (\qquad - \qquad \% + \quad \square(\%) \qquad \textbf{Eq 4-1}$$

4.4.2 Ultimate analysis

Ultimate analyses for the samples used were carried out by MEDAC ltd. The instrument employed for this analysis was a CE-440 elemental analyser. It works on the principle of combustion. The results for the ultimate analysis are given in terms of elemental composition of carbon, hydrogen, nitrogen and oxygen. The sulphur content for some of the feedstocks was also determined. Elemental Analysis was carried out by MEDAC laboratories in Surrey, United Kingdom.

4.4.3 Heating values

The heating values for the primary feedstocks i.e. African Moringa, African Jatropha, Indian Moringa and Indian Jatropha were determined to gauge the energy contents of the press cakes. A Carr 6100 bomb calorimeter was used for these experiments. It operates according to the ASTM D2015 standard test method. The principle of bomb calorimetry is the determination of heats of combustion when a sample is burned in excess oxygen. A known mass of the sample is burned in a steel vessel ensuring reaction occurs at constant volume. The change in temperature of the vessel is noted. The unit is calibrated with benzoic acid whose heat of combustion is 26.43 MJ/kg at 25 ºC. The heat capacity of the system can be obtained from the equation 4-2

$$ = \qquad\qquad\qquad \textbf{Eq 4-2}$$

Where Q, is the heat liberated from the combustion of the calibration material. Once the heat capacity of the calorimeter, C has been obtained, the materials whose heating values are to be determined are then burned in the unit while the change in temperature is noted. The heating values may then be determined by returning to the original equation 4-2.

The heat of combustion of obtained from the bomb calorimeter corresponds however, to the higher heating value HHV because the enthalpy change of the reaction assumes a temperature of 25 ºC at which water evolves in liquid form. As the HHV values for the samples are determined as received i.e. without drying, a HHV value for moisture free biomass was also calculated by the equation 4-3

$$ = \qquad (1 - \text{——}) \qquad\qquad \textbf{Eq 4-3}$$

The terms HHV_{ar} and HHV_{mf} represent the heating values on as received and moisture free basis respectively. Even though bomb calorimetry was employed to determine the energy contents, empirical formulas were also used.

Most of the empirical formulas for heating values use elemental compositions for their estimations. The Sheng and Azevedo formula shown in equation 4-4 was used [135].

$$= -1.3675 + 0.3137 \quad + 0.7009 \quad + 0.0318 \quad ^{*} \qquad \textbf{Eq 4-4}$$

The value given by this equation is based on the weight percentages of carbon and hydrogen on a dry basis. O* is representative of the oxygen content and other inorganic components in the sample. O* is obtained from equation 4-5

$$^{*} = 100 - \quad - \quad - \quad ⬚ \qquad \textbf{Eq 4-5}$$

Furthermore, there exist for fuels, the Lower heating values which are accepted to be more realistic energy values for thermochemical conversions. The lower heating values of fuels can be obtained from equation 4-6 [136] which presents it as a function of the HHV_{mf}.

$$= \quad - 2.442 * 8.936 \quad /100 \qquad \textbf{Eq 4-6}$$

Where H, represents the weight percentage of hydrogen on a dry basis.

4.4.4 Bulk density

Bulk density measurements were carried out to obtain data for fluidisation calculations for the commissioned 300 g/h unit. The bulk density measurements were carried out according to the method of Wang and Kinsella [137]. These values were obtained by dividing the weight of samples in a 100 ml measuring cylinder. The cylinder was tapped a sufficient number of time (>100) to ensure that the feed was settled. This was repeated five times for each feedstock to reduce the deviation and errors in the measurement. The bulk densities are presented as a ratio of sample weight to its volume. Values obtained are presented in section 5.2.3.

4.4.5 Specific density

Specific density data was obtained from literature for the commissioning feedstocks. With the primary feedstocks, density values were obtained by placing approximately 10 g of the samples in a 50 cm^3 measuring cylinder. The voids in the material were then filled using fine sand of a known bulk density. The specific density was then obtained using the formula in equation 4-7

$$= \frac{\rule{5cm}{0.4pt}}{\rule{2cm}{0.4pt}} \qquad \textbf{Eq 4-7}$$

4.4.6 Voidage

Knowing the absolute and bulk densities of the feedstocks, the voidage of the biomass particles were calculated using equation 4-8.

$$= \frac{\quad}{\quad} \qquad \textbf{Eq 4-8}$$

The voidage is a function of the specific density and the bulk density and the values obtained from the feedstocks are detailed in the characterisation results and discussions section 5.2.3.

4.4.7 Component analysis

Component analysis of the primary feedstocks were carried out during the course of this research. Wet chemistry methods including Acid digestible fibre, ADF, Neutral digestible fibre, NDF and Klason were used to determine the amounts of cellulose, hemicellulose and Lignin in the press cakes. The amount of extractives was also determined.

Lignocellulosic experiments were carried out by a colleague of the author at the European Bioenergy Research Institute (EBRI) based at Aston University

4.4.8 Determination of oil content in press cakes

The primary feedstocks used are all residues from oil seeds pressing. Invariably, the press cakes retain some oil from the pressing process the seeds are subjected to. The quantity of the oil retained in the press cakes is to a very large extent dependent on the efficiency of the extraction method [138]. The residual oil in the press cakes is expected to play a role in the thermal degradation behavior, heating values and final composition of the feedstocks. It is for these reasons that, it became necessary to determine the oil contents of all four primary feedstocks.

Oil contents of the press cakes were determined using an adapted solvent extraction method. Hexane, Toluene and Diethyl ether were used to treat samples of the press cakes. The samples were first dried overnight in an oven at 105 ºC to remove moisture. The samples were subsequently placed in sealed glass tubes. A 15:1 weight ratio of solvent to sample was used. The samples were then agitated vigorously in the glass vessels using a mechanical shaker for one hour. The resulting mass was then filtered through pre-weighed and pre-dried 0.1 µm Whatman filter papers. The mass left was then dried in a 60 ºC oven overnight before being weighed.

4.4.9 Estimation of protein content in press cakes

It was necessary to estimate the protein content of the primary feedstocks used because residues of oil pressing usually contain high amounts of crude protein. While some studies in literature have estimated the protein content in oil seeds by multiplying the total nitrogen content in the feedstocks by a conversion factor of 6.25 [13, 139], this research has not done so. This is because the estimation of protein content by a conversion factor of 6.25 assumes that protein contains 16% nitrogen. This may be true for animal proteins but is not necessarily valid for plant proteins. As such, it tends to overestimate the amounts of protein in samples [140]. Research conducted by Miton et al, Yeoh et al and Mosse [141-143] have all shown that protein conversion factor for plants based on nitrogen content is less than 6.25. As such, crude protein contents of the primary feedstocks have been estimated using a nitrogen conversion factor of 5.5 proposed by Ezeagu et al [144]. This conversion factor was derived based on experimental studies on tropical seeds. The primary feedstocks are all tropical seeds and the use of a conversion factor of 5.5 for nitrogen to protein content is understood to be a more accurate representation of the protein contents of the feedstocks. It should be stated however that this estimate is not a substitute for determining the true protein content experimentally. Protein determination is an expensive and time consuming process which is why a conversion factor has been used.

4.5 THERMOGRAVIMETRIC ANALYSIS

Thermogravimetric analysis is recognised as useful tool for determining kinetic and physical properties of fuels. A thermogravimetric analyser is able to measure the weight change of a given substance as a function of temperature and time [59].

Different biomass samples are expected to have different thermal degradation mechanisms because of differences in compositions. TGA has been employed as part of this research to study the thermal degradation of the primary fast pyrolysis feedstocks.

The TGA operating conditions are able to reach temperatures of up to 1000 ºC with a maximum heating rate of up to 200 ºC/min.

Aston University

Illustration removed for copyright restrictions

Figure 4-5 Pyris 1 TGA used during this research [145]

For TGA analysis, 2-3 mg of a sample is put on a ceramic crucible on the analyser tray. The sample crucible is then hung on a balance wire attached to a sensitive balance. As the program is started, the sample is subjected to heat from an external furnace at preset temperature and heating rates. Any weight loss as a result of thermal degradation is measured and recorded. The weight loss calculations are carried out by the program software. All pyrolysis TGA experiments are conducted in an inert atmosphere created by an inflow of nitrogen at 30 ml/min. Figure 4-5 shows a diagram of the Pyris 1 TGA used.

4.6 PY-GC/MS

PY-GC/MS looked at in its entirety is a combination of three techniques. The pyroprobe acts as the thermal degradation platform while gas chromatography and mass spectrometry are used for compound identification and quantification. The principle of operation of the PY-GC/MS is the breakdown of large molecules to smaller molecules using heat. The combined operation of the PY-GC/MS allows for assessments of formation of volatiles from the original biomass samples by observing the fragmented molecules. Mass spectroscopy operates by scanning and ion recordings of every sample passing through. Split ions that have the selected mass to charge ratio from the mass analyser are amplified by a low noise photometer by a factor of 10^5. Theoretically, if the parameters of temperature, time and heating rates are properly controlled, in a manner that is

reproducible, then the fragmentation of the bonds of the original biomass sample will be representative of the strengths of the bonds of the original sample.

During PY-GC/MS experiments, a micro controller is used to control the temperature and heating rate which are preset before the start of the experiment. The hold time of the experiments may be varied just as the heating rate and temperatures can be varied. Heating rates of up to 20000 ºC/s can be achieved with a maximum operation temperature of up to 1400 ºC. The hold time is usually kept as short as possible to mimic fast pyrolysis conditions. The PY-GC/MS is a valuable tool for studying analytical pyrolysis because it gives a near representation of an actual fast pyrolysis due to the very high heating rates, moderate temperatures that can be carefully controlled and relatively short holding time of the sample.

For PY-GC/MS during this research, a 5200 pyroprobe from CDS analytical was used. Up to 0.5 mg of the sample is placed in a quartz filler rod. The preset heating rate was 20 ºC/ms with a maximum set temperature of 500 ºC and hold time of 30 seconds. The vapours formed are then separated using a Varian 450 gas chromatograph with a Varian 220 Ion Trap mass spectrometer. The column for the gas chromatograph was a factor four capillary column VF-5ms 30 Mx0.25 mm I.D and 0.025 µ film thickness. Helium was employed as carrier gas at 38 cm/s velocity with a split ratio of 1:75. The oven programme operated at 45 ºC for 2.5 minutes and then the temperature was ramped up to 250 ºC at a rate of 5 ºC/min. The injector and detector temperatures were set to operate at 275 ºC.

The separated compounds by the gas chromatograph were then analysed by a mass spectrometer with electron impact mode. Chromatographic peak identification from the PY-GC/MS experiments was carried out using comparisons of mass ions of each peak with an NIST mass spectra database.

4.7   PYROLYSIS PRODUCTS CHARACTERISATION METHODS

Section 2.3 has already identified and reviewed the major products of a fast pyrolysis process. As part of the objectives of this research, it was necessary for the products from the pyrolysis process to be subjected to further characterisation studies in order that

- Mass balance calculations be accurately calculated to assess system efficiency
- A proper insight into the quality of the pyrolysis products be obtained
- Fuel qualities of the products be assessed since they may be of commercial value.

This section of the thesis details analytical methods used to assess the quality of the products. The extent of characterisation of pyrolysis products varies. The characterisation of pyrolysis products generated from the commissioning feedstocks are limited to the techniques required for obtaining a proper mass balance closure i.e. water content and solids content.

The pyrolysis product characterisation carried out for the primary feedstocks, i.e African Moringa, African Jatropha, Indian Moringa and Indian Jatropha however, are of a wider range primarily because the feedstocks were scarcely reported at the commencement of the research.

4.7.1   Pyrolysis liquid product quality

Fahmi [40] reports that there are currently 10 quality parameters that are assessed when characterising pyrolysis liquids. This research focuses on 7 of those parameters. The oil analysis deals primarily with the main bio-oil fraction although other liquids were also analysed. The bio-oil parameters assessed are

- pH
- Heating values
- Molecular weight distribution
- Compound identification and quantification using GC/MS
- Water content
- Solids content
- Elemental composition

Detailed descriptions of the analysis methods follow below

4.7.1.1 pH

Bio-oil is known to be composed of complex organic compounds. These compounds include acids like formic acid and acetic acid. As bio-oil may be employed as a fuel, the extent of its acidity is usually determined as it may speed up corrosion in fuel systems. The pH of pyrolysis liquids produced were measured using a Sartorius PB-11 pH meter. The pH meter works by measuring the amount of hydronium ions (H_3O^+) present in the bio-oil sample.

4.7.1.2 Molecular weight distribution

The molecular weight distribution of compounds in pyrolysis liquids produced were measured using gel permeation chromatography. The equipment used was an integrated PL-GPC 50 from polymer laboratories, UK, with a refractive index (RI) detector. The PL-GPC 50 is equipped with a PLgel 3 µm MIXED-E column, 300x1.5mm which operates at 40 ºC. Calibration of the GPC system was done using polystyrene calibration standards for a molecular weight range between 105 and 19880g/mol.

Sample preparation involved making a bio-oil solution in HPLC-grade tetrahydrofuran (THF) at a concentration of 0.01 g/ml. The bio-oil/THF solution was subsequently filtered through a milipore Millex-GN filter with a 0.1 µm pore size to remove solids and insoluble materials capable of causing blockages in the system. Approximately 100 µl was injected into the column via a PL-AS RT autosampler. Curves and data processing calculations were done using Cirrus 3.0 GPC software. The number average molecular weight (Mn), weight average molecular weight (Mw), molecular weight at highest peak (Mp) and polydipersity (PD) were calculated from the signal curves.

The stability of bio-oil could be measured from values obtained from the GPC as the presence of higher molecular weight as pyrolysis liquids age indicate a lack of stability.

4.7.1.3 Heating values

The principle of bomb calorimetry has already been explained in section 4.4.3. The same equipment a Parr 6100 bomb calorimeter was used to determine the heating values of the main pyrolysis liquids produced.

4.7.1.4 Compound identification and quantification: Liquid GC/MS

Bio-oils can contain up to 400 different compounds[66]. In order to properly identify and quantify the compounds in the bio-oil samples produced, the bio-oils were subjected to gas chromatography/ mass spectrometry analysis using a Varian 450 gas chromatograph with a Varian 220 Ion Trap mass spectrometer. The column for the gas chromatograph was a factor four capillary column VF-5ms 30 Mx0.25 mm I.D and 0.025 µ film thickness. A split ratio of 1:75 was used for compound separation and the injector temperature was maintained at 275 ℃. The carrier gas was helium at a flowrate of 1ml/min. The injector port was a 1079 programmable temperature vapourising injector (PTV) with a maximum temperature ramp rate of 200 ℃/min. Temperature program for the GC oven began at 45 ℃ with a 2 minute hold time before a steady rise to a final temperature of 250 ℃ at a heating rate of 5 ℃/min. Sample preparation involved creating a pyrolysis liquid solution at a ratio of 0.2 ml pyrolysis liquid to 0.8 ml of HPLC ethanol. The solution was filtered through a 0.2 µ filter to remove any solids before being injected into the column.

The separated compounds by the gas chromatograph were then analysed by a mass spectrometer with electron impact mode. Chromatographic peak identification from the GC/MS experiments was carried out using comparisons of mass ions of each peak with the NIST mass spectra database.

4.7.1.5 Water content

The water content analysis was necessary to complete mass balance calculations as well as measure the amount of water in the pyrolysis liquids produced since it is known to have an effect on heating values and viscosity. Water content of the pyrolysis liquids was determined using a Mettler Toledo V20 volumetric Karl-Fisher titration system. Calibration of the system was achieved using HPLC grade water (99%). Hydranal working medium K was used as the solvent and Hydranal Composite 5K as corresponding titer reagents. They have the specific ability to measure the water content of samples in the presence of ketones and aldehydes. The titration solution is composed of iodine, sulphur dioxide, pyridine and methanol. A known weight of the sample is injected into the system and inputted into the system computer. The titration is then carried out and results displayed. All water content determinations were done in triplicates to reduce the deviation between readings.

4.7.1.6   *Solid contents*

Cyclone systems are efficient from removing solids in gaseous streams. High efficiency cyclones however see a reduction in efficiency for small particle sizes <10 µm. This means that smaller fines from biomass processing invariably find their way into the pyrolysis liquids [86]. In order to properly quantify the amount of char produced during any experiment, the solid contents of pyrolysis liquids must be determined. A vacuum filtration technique suggested by Peacocke and Oasamaa [146] was used to determine the solid contents of the bio-oils. Approximately 5 g of the bio-oil was dissolved in ethanol and filtered through a Whatman GF/B micro glass Fiber filters with a maximum pore size of 0.1 µm. The oil sample was then washed with excess ethanol until a clear filtrate was observed indicating the complete removal of organics from the filter paper. The filter paper was then air dried for 15 minutes before being oven dried for 30 minutes at 105 ℃. The solids content could then be determined from the weight of the filter paper before and after filtration by presenting the mass retained in the filter paper as a fraction of the initial mass of the organic liquid.

4.7.1.7   *Elemental analysis*

The technique has already been described in section 4.4.2

4.7.2   Non condensable gas analysis

All the non condensable gases from experiments were analysed using an online Varian CP-4900 gas chromatograph. The unit took samples of the product gas every 3 minutes for quantitative analysis. The GC system is equipped with 2 columns. Column A (Molsieve 5A) is able to measure hydrogen, oxygen, nitrogen, methane and carbon monoxide. Column B (Poraplot Q) is able to detect nitrogen, methane, carbon dioxide, ethane, propene, propane and butane. Helium is used as carrier gas in the system. The system calibration is done with known composition standard gas mixtures.

4.8   SUMMARY

Biomass and pyrolysis product characterisation techniques used have been introduced. Thermogravimetric analysis and PY-GC/MS have also been reviewed. The techniques introduced in this chapter have all been used during this research as will be seen in later chapters.

5 BIOMASS CHARACTERISATION: RESULTS AND DISCUSSIONS

This chapter reports the results of the characterisation studies undertaken on the feedstocks used within this research. It employs some of the techniques introduced in chapter 4 of this thesis.

5.1 COMMISSIONING FEEDSTOCKS RESULTS

The extent of characterisation for the commissioning feedstocks was less than that of the primary feedstocks. This was because the characteristics of the commissioning feedstocks are already reported in literature [12, 117, 147-150]. Thus, a duplication of the results was deemed unnecessary. The characterisation of the commissioning feedstocks was limited to the proximate and ultimate analysis. The proximate analysis was more important because characteristics like the moisture content were subject to change depending on storage conditions. Table 5-1 reports the proximate and ultimate analysis of the commissioning feedstocks.

Table 5-1 Ultimate and proximate analysis data for commissioning feedstocks

Analysis	Beech	Willow	Pine	Miscanthus
Proxiamte (wt% as received)				
Combustible matter	89.45	90.37	87.4	90.85
Ash	1.0	1.38	0.98	3.32
Moisture	9.55	8.25	10.04	5.83
Ultimate (wt%, maf)				
C	48.395	45.75	50.485	46.40
H	5.955	5.2	6.535	5.75
N	<0.1	<0.1	<0.1	0.42
O*	45.65	49.05	42.98	47.43
S	ND	ND	ND	ND

*Oxygen determined by difference, ND: Not determined

The proximate and ultimate analysis of the commissioning feedstocks show all the feedstocks to be low ash content <1.5 wt% with the exception of Miscanthus. They were also found to have significantly high combustible matter. The commissioning feedstocks were also found to contain minute amounts of nitrogen undetectable by the elemental analyser. The only exception to this was Miscanthus where the nitrogen content was determined to be 0.42 %. From the results of the combustible matter and published literature, it is expected that yields of organic liquids from the commissioning feedstocks when subjected to fast pyrolysis should be relatively high (>50%) [12, 40, 117, 151].

5.2   PRIMARY FEEDSTOCKS RESULTS

5.2.1   Ultimate and proximate Analysis

Table 5-2 reports the results of the ultimate and proximate analysis of the four primary feedstocks as received. The data in the Table also reports the calculated calorific values as well as those obtained using bomb calorimetry. At the commencement of this research, there was no reported literature data for comparisons. At the time of writing this thesis however, a study had reported the use of Jatropha presscake as feedstock for fast pyrolysis where basic characterisation was undertaken [152]. As such, Table 5-2 also cites the data obtained from literature for comparisons. Characterisation of Moringa presscake remains unreported. This research for the first time, reports the characterisation of Moringa olifiera press cakes for fast pyrolysis.

Table 5-2 Ultimate and proximate analysis data for primary feedstocks

Analysis	African Jatropha	Indian Jatropha	Jatropha [152]	African Moringa	Indian Moringa
Proxiamte (wt% as received)					
Volatile matter	72.53	70.65	70.92	75.08	73.92
Ash	6.47	9.83	4.30	6.28	5.43
Fixed Carbon	10.97	8.36	16.06	8.26	14.32
Moisture	10.03	11.16	8.71	10.38	6.33
Ultimate (mf, wt%)					
C	44.42	52.51	59.17	45.59	46.97
H	6.23	7.35	6.52	6.49	6.85
N	4.33	3.25	0.38	6.47	8.44
O	44.51	36.30	33.93	41.45	34.71
S	0.51	0.59	<0.01	ND	3.03
Molecular Formula	$CH_{1.67}O_{0.75}S_{0.004}$	$CH_{1.67}O_{0.51}S_{0.004}$	$CH_{1.32}O_{0.43}$	$CH_{1.70}O_{0.68}$	$CH_{1.74}O_{0.55}S_{0.02}$
Inorganic components (ppm, mf basis)					
Ca	ND	7200	NA	ND	2650
K	ND	8800	NA	ND	9500
Mg	ND	5700	NA	ND	5300
Na	ND	500	NA	ND	150
Component Analysis (wt% ash, efb)					
Cellulose	23.27	18.81	NA	17.92	3.81
Hemicellulose	9.24	2.47	NA	1.84	2.14
Lignin	35.63	50.33	NA	24.95	6.29
Extractives	31.83	28.39	NA	55.27	87.76
Protein Content[a] mf, wt%	23.81	17.87	1.92	35.58	46.42
Heating Values (MJ/kg)					
Bomb Calorimetry (HHVar)	21.26	19.33	-	20.47	20.77
HHVmf	18.34	21.41	22.84	18.80	19.27
LHVmf	16.98	19.80	21.42	17.38	17.77

(a) Determined by multiplying nitrogen content by conversion factor of 5.5; **ND**-Not Determined; **NA**-Not Available, efb: extractives free basis; ar: as received; mf: moisture free;ppm:part per million

The data from Table 5-2 shows as expected, resemblances between African Jatropha and Indian Jatropha. The Jatropha feedstocks show similarities in the amount of fixed carbon and volatile matter with the only significant difference being in the ash contents. The Indian Jatropha value is about 30% higher than the value of the African Jatropha press cake. The ash content is known to be dependent on the inorganic components of the feedstocks which can be related to the soil and climatic conditions under which the feedstocks were grown [153-155]. The fact that the feedstocks were obtained from different geographical locations may well explain the differences recorded in ash content. The moisture contents reported in Table 5-2 are values of the different feedstocks as received. They show that in the case of the Jatropha feedstocks, the values differ very slightly although storage conditions will have played a part in the actual values.

When compared to the literature data on Jatropha press cakes which is from a study carried out in India by Raja [152] , the data on volatile matter for the Jatropha feedstocks show that they contain similar amounts of volatile matter (up to 70% as received). The amount indicates that the Jatropha feedstocks could be exploited as feedstocks for fast pyrolysis as higher volatile content feedstock is an early indicator of high liquid yields from fast pyrolysis. The values for fixed carbon for the primary Jatropha feedstocks are however, lower than the literature value [152].

The ash contents from the Jatropha feedstocks when compared to data presented in literature shows some discrepancies. The ash content from African Jatropha is 6.47 wt% while that from Indian Jatropha is higher at 9.83 wt%. When compared to the values from literature, the ash contents of both Jatropha feedstocks are higher. Though the values are higher, they cannot be considered unusual because as already stated; the ash from feedstock is a reflection of the inorganic components of the feedstocks. The discrepancies can be mainly attributed to different factors including growing conditions e.g. climate and soil contamination [156]. The highlighted factors may be responsible for the higher ash content of the feedstocks

The ultimate analysis of the Jatropha feedstocks show slight differences in elemental composition when the African and Indian varieties are compared. The carbon contents show that Indian Jatropha has a higher value of 52 wt% when compared to African Jatropha which has 44 wt%. The oxygen contents of the feedstocks also differ with African Jatropha having higher oxygen content of 44 wt% when compared to that of Indian Jatropha which stands at 36 wt%. The differences in nitrogen and hydrogen contents of African and Indian Jatropha

are less when compared to the major elements of carbon and oxygen. Again, these differences can be attributed to cultivation and climatic conditions. One immediate conclusion can be observation can be made from the elemental analysis, which is that both feedstocks have significantly high nitrogen content when compared to feedstocks from like maize stalk, pine and cotton stalk [84, 148, 157]. The nitrogen contents also serve as an indication of high protein content for both Jatropha feedstocks. The presence of nitrogen in higher proportions than conventional biomass feedstocks also raise a possibility of NOx compounds forming during the pyrolysis of the feedstocks [66]. This is undesirable in terms of environmental considerations. Both feedstocks showed a presence of sulphur in their compositions. Like in the case of nitrogen, the possibility of formation of oxides of sulphur exists during the pyrolysis of the Jatropha feedstocks.

In comparison to the literature values, it can be seen that the Indian Jatropha has more of an elemental resemblance to the Jatropha press cake reported in literature. This is not an unexpected result as both feedstocks were sourced from India. They might have been subjected to similar climate and soil compositions during cultivation. The main difference however lies in the nitrogen content for both feedstocks. Whereas both Indian and African Jatropha have closer nitrogen contents of 3.25 wt% and 4.33 wt% respectively, the nitrogen content for the Jatropha press cake reported in work published by Raja is 0.38 wt% [152]. It should be stated that the literature value is curious and unusually low. Residues of oil pressing are known to have high nitrogen content which is usually related to their protein content as reported by numerous researchers from other studies on press cakes of oil seeds [139, 158-164].

With regards to the primary Moringa feedstocks, the ultimate analysis shows a high level of resemblance between both feedstocks. In terms of volatile matter, the African Moringa has 75.08 wt% while the Indian Moringa has 73.92 wt%. The difference in volatile matter is small and is expected with feedstocks of the same genetic origins. Ash content values for African Moringa stand at 6.28 wt% while the ash content of Indian Moringa is 5.43 wt%. The difference between the ash contents of both Moringa feedstocks is small but is comparable to other oil press feedstocks like rape meal which was reported to be 6.30 wt% in a study by Ucar [165].

Comparing the ultimate analysis of the Moringa feedstocks, it can be seen that the resemblance between both feed stocks is higher than that seen in the case of Jatropha. The carbon content of African Jatropha stands at 45.59 wt% and that for Indian Moringa is 46.97%. Similar values of hydrogen can also be seen between the two Moringa feedstocks. African Moringa has a hydrogen content of 6.49 wt% and Indian Moringa has a value of 6.85 wt%. The highest variation in terms of elemental composition between the primary Moringa feedstocks is in terms of nitrogen and oxygen contents. The nitrogen contents are 8.44 wt% and 6.47 wt% for Indian and African Moringa respectively. The Moringa feedstocks show high nitrogen content which again is expected from press cakes of oil seeds. Like the case of Jatropha, high nitrogen content is indicative of high protein content in the feed stocks. The oxygen content which was determined by difference shows that Indian Moringa has less oxygen than its African counterpart. The quantity of oxygen in the Indian Moringa is 34.71% while that for African Moringa is 41.45 wt%. Worthy of mention with reference to Indian Moringa is the sulphur content which was found to be 3.03 wt%. This may become an issue in terms of its exploitation as a fuel for thermochemical processing because of the emission of sulphur oxides. The levels of sulphur in the African Moringa feedstock were not determined.

In comparing both feedstocks, i.e. Jatropha and Moringa, it can be seen that both feedstocks bear certain resemblances with each other. They all have ash contents between 5-10 wt%. This is higher than most lignocellulosic feedstocks. However, it is still lower than feedstocks like rice husk which have been reported to have ash contents between 11-18 wt% and are widely exploited as a fuel for thermochemical processes [166, 167]. The analysis shows that both Moringa feedstocks have higher nitrogen content than their Jatropha counterparts. Moringa also possesses more volatile matter than Jatropha which indicates that a higher liquid yield may be expected from the Moringa than Jatropha when they are subjected to fast pyrolysis. The energy contents of the feedstocks show that they all have similar values with the exception of Indian Jatropha which is significantly lower (by 5MJ/kg) than the other 3 feedstocks. Overall, the ash and nitrogen contents of the primary feedstocks fall within the range of most oil press residues reported in literature [83, 158, 161, 168, 169].

As per the structural composition of the primary feedstocks, it can be seen that they all contain small amounts of hemicellulose <10 wt% on an ash and extractives free basis. The cellulose contents of all the primary feedstocks to be less than 25 wt%. Indian Jatropha displays low cellulose content at of 3.81 wt%. The lignin contents of the feedstocks show that

Indian Jatropha has the highest lignin content of 50.33 wt%. African Jatropha has the second highest lignin content of 35.63 wt%. Like with the cellulose content, Indian Moringa has the lowest value of 6.29 wt%. Generally, biomass species with low lignin values are expected to produce lower molecular weight pyrolysis liquids as postulated by Ghetti et al [170]. All the feedstocks show high amount of extractives which is not surprising since they are residues of oil pressing and contain residual amounts of triglycerides. The Indian Moringa value for extractives stands at 87.76 wt% while African Moringa extractives are 55.27 wt%. The reason for the high extractive contents and the discrepancy in the extractives contents of the Moringa feedstocks cannot be theorised with certainty. The values can however be said to be high if compared to feedstocks like Corn cob [171]. Also, Smets et al [139] carried out work on rape seed press cake fast pyrolysis. They report cellulose, hemicellulose and lignin values of 9, 8 and 4 wt% respectively. Extractives values reported were also high (>65%). The press cake used by Smets shows similar characteristics to the Indian Moringa.

The values for the extractive contents of Indian and African Jatropha are closer. African Jatropha has a value of 31.83 wt% while Indian Jatropha has a value of 28.39 wt%.

The heating values of the press cakes show that they have reasonably acceptable energy contents of between 19 and 21 MJ/kg. This is an indication that pyrolysis liquids and bio-fuels with moderately high energy content may be obtained from the feedstocks.

5.2.2   Oil content

Table 5-3 shows the oil contents of the press cakes using the method described in section 4.4.8. The results of the oil content analysis of the press cakes show hexane as being the most effective in extracting oil from the cakes. This is expected since hexane is used industrially as a solvent for oil extraction from oil seeds [165]. Diethyl ether and toluene were also effective in oil extraction with all the solvents removing most of the oil in the press cake as seen in previous studies [139, 165].

Table 5-3 Oil content of primary feedstocks based on extracting solvent

Feedstock	unit	Hexane	Diethyl Ether	Toluene
Indian Moringa	mf (wt%)	17.91	16.30	15.31
Indian Jatropha	mf (wt%)	29.31	29.10	28.68
African Moringa	mf (wt%)	15.14	14.23	14.29
African Jatropha	mf (wt%)	14.33	ND	ND

ND: Not Determined due to later arrival of feedstock

The results show the Indian Jatropha as having the highest oil content. The oil content of the Indian Jatropha ranged between 28.68-29.31 wt% on a dry basis. One immediate conclusion that can be drawn from this result is that a less efficient method of pressing the oil out was used on Indian Jatropha. The Indian and African Moringa had similar oil contents 14.23-17.91 wt%. African Moringa was the last of the primary feedstocks to arrive. As such, only hexane was used to determine its oil content. The value obtained was 14.33 wt% on a dry basis.

5.2.3   Bulk and absolute density

The results of the absolute and bulk density measurements for the primary feedstocks are shown in Table 5-4. The Table shows that all the primary feedstocks have high bulk and absolute densities when compared to conventional feedstocks. This is because of the oil pressing the seeds were subjected to. As seen in a study of pelletisation of biomass feedstocks by Yoshida et al [172], it had little impact in changing the bulk density of Jatropha press cake when compared to other feedstocks like oil palm trunk and rice husk. This helps us to conclude that oil pressing does increase the bulk density of press cakes. The residual oil in the press cakes may also play a role in the high density of the feedstocks although this has not been determined.

Table 5-4 Bulk and absolute density data for primary feedstocks

Feedstock	Bulk Density (kg/m^3)	Absolute Density (kg/m^3)	Voidage
Indian Moringa	590	1220	0.51
Indian Jatropha	485	1010	0.52
African Moringa	430	890	0.51
African Jatropha	470	940	0.50

Voidage values show close relationships between all the feedstocks. They all range between 0.50-0.52.The results of the density measurements suggest that higher velocities will be required in fluidising the feedstocks if they are to be processed in a bubbling fluidised bed reactor.

5.2.4 TGA results

5.2.4.1 Indian Moringa

The TG and DTG curves of Indian Moringa are showed in Figure 5-1. Four major weight loss steps are evident from the DTG curve. The initial weight loss step which accounts for the removal of moisture from the Indian Moringa press cake occurs between 45 and 102 ℃. The second weight loss step happens between 105 and 282 ℃. This step happens as a result of the volatisation of hemicellulose. The inflection point of this step is at 248 ℃ and that shows the temperature at which weight loss of hemicellulose is at its maximum. The third weight loss step occurs between 290 and 650 ℃. This step is representative of the degradation of the cellulose and lignin components of the Indian Moringa press cake. The third step is the major pyrolysis process and has its inflection point at 355 ℃. There is a slight shoulder on the DTG curve with peak mass loss at 424 ℃. This is believed to represent the degradation of triglycerides which make up the most of the oil remaining in the press cakes. The TG-DTG curves show that all the major weight loss occurred between 90 and 650 ℃. The total weight loss as can be seen on the TG curve of the Indian Moringa stands at 71% between 45 and 900 ℃.
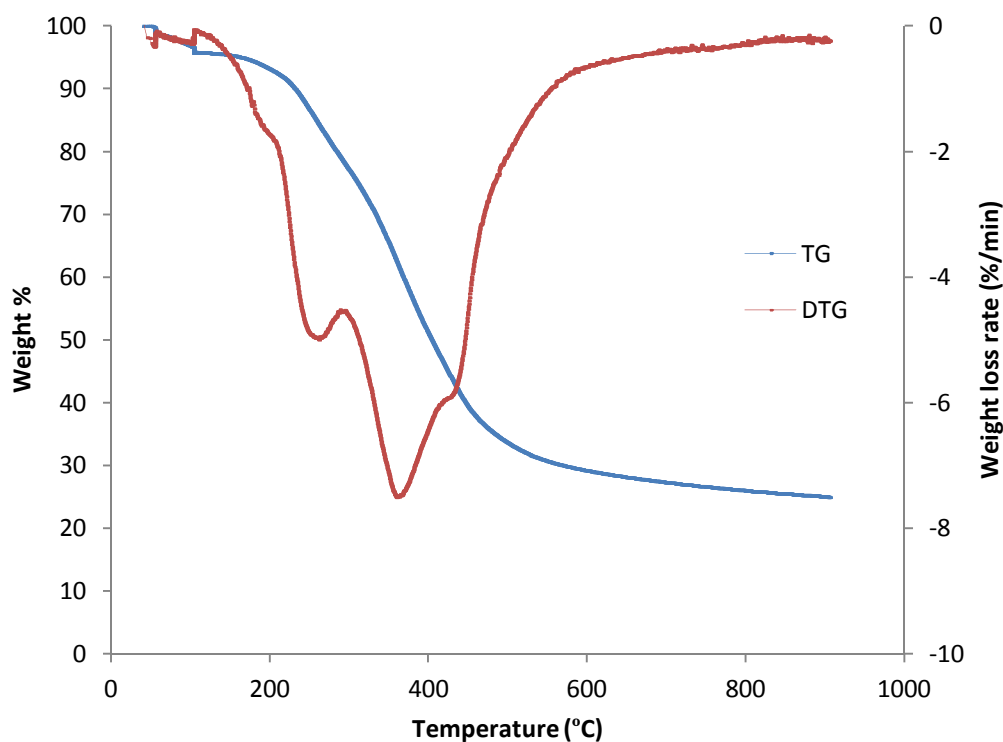
Figure 5-1 TG and DTG curves of Indian Moringa presscake

5.2.4.2 African Moringa

Figure 5-2 shows the TG-DTG curve of African Moringa seed cake. There are three major weight loss steps. The first step accounts for moisture removal and that occurred between 45 and 95 ºC. The second weight loss step represents the decomposition of hemicellulose and that occurred between 102 and 295 ºC. The temperature at which hemicellulose removal was at its maximum was at 278 ºC and that is shown by the inflection point on the DTG curve. The third and final major weight loss step happened between 290 and 650 ºC. This step is indicative of the decomposition of cellulose and lignin components of the African Moringa seed cake. The temperature at which mass loss peaked for this step was 368 ºC. No significant weight loss was recorded after 650 ºC as is evident from the DTG curve. The TG curve in Figure 5-2 shows that continuous weight loss for African Moringa occurred between 45 and 915 ºC. There was a 75% reduction in mass of the African Moringa press cake. Unlike the Indian Moringa, the removal of triglycerides in this feed stock is not as evident on the DTG curve.
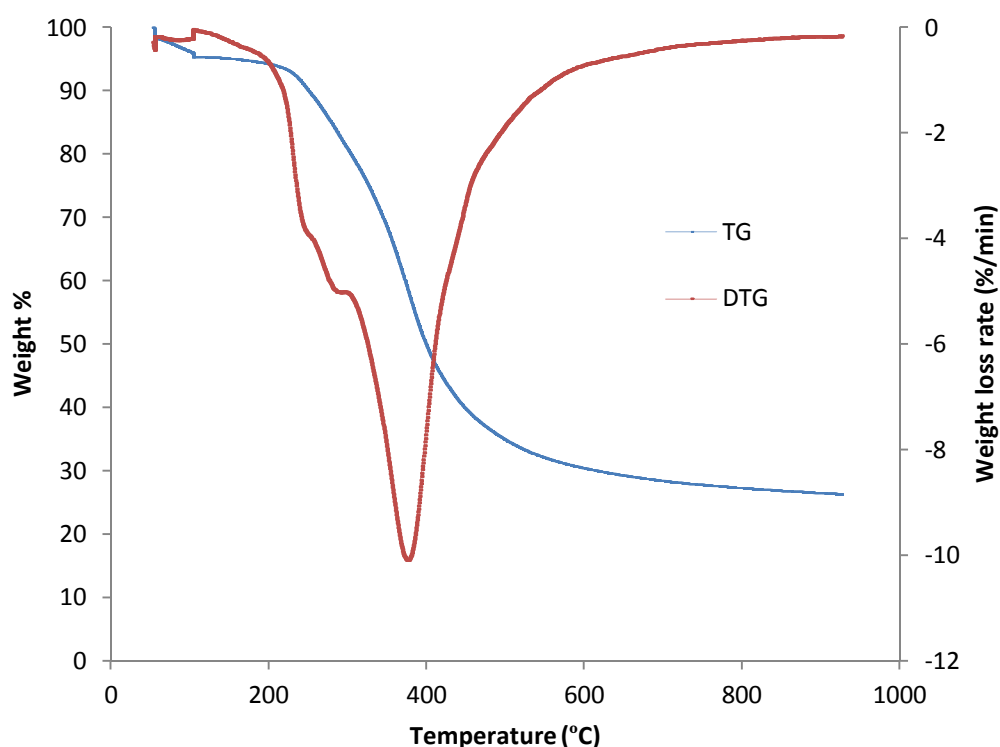
Figure 5-2 TG and DTG curves of African Moringa presscake

The TG-DTG curves presented in Figure 5-3 shows the major weight step losses for the Indian Jatropha press cake. Moisture was removed in the first major weight loss step between 45 and 95 ºC. The second step which portrays the degradation of hemicellulose occurred between 102 and 215 ºC. The third major weigh step loss occurred between 219 and 323 ºC. This step is believed to be representative of the removal of triglycerides. The temperature at which mass loss was highest for this step was 295 ºC. The irregular third step on the DTG curve can be explained by the high amounts of residual oil in the Indian Jatropha press cake as determined in section 4.4.8. The next major step happened between 323 and 640 ºC. This step shows the decomposition of lignin and cellulose although the lignin decomposition is likely to have begun since the previous step taking into account the wide temperature range at which lignin thermally degrades [173]. The temperature at which mass loss was highest for this step was 365ºC. This is indicated by the inflection point of the step as shown on the DTG curve. The TG curve shows continuous mass loss between 45 and 915 ºC with a 72% mass reduction of the initial Indian Jatropha press cake sample. This thermal degradation behaviour differs from the other samples analysed and is due to the high oil content (28%) in the Indian Jatropha press cake as found in section 5.2.1.
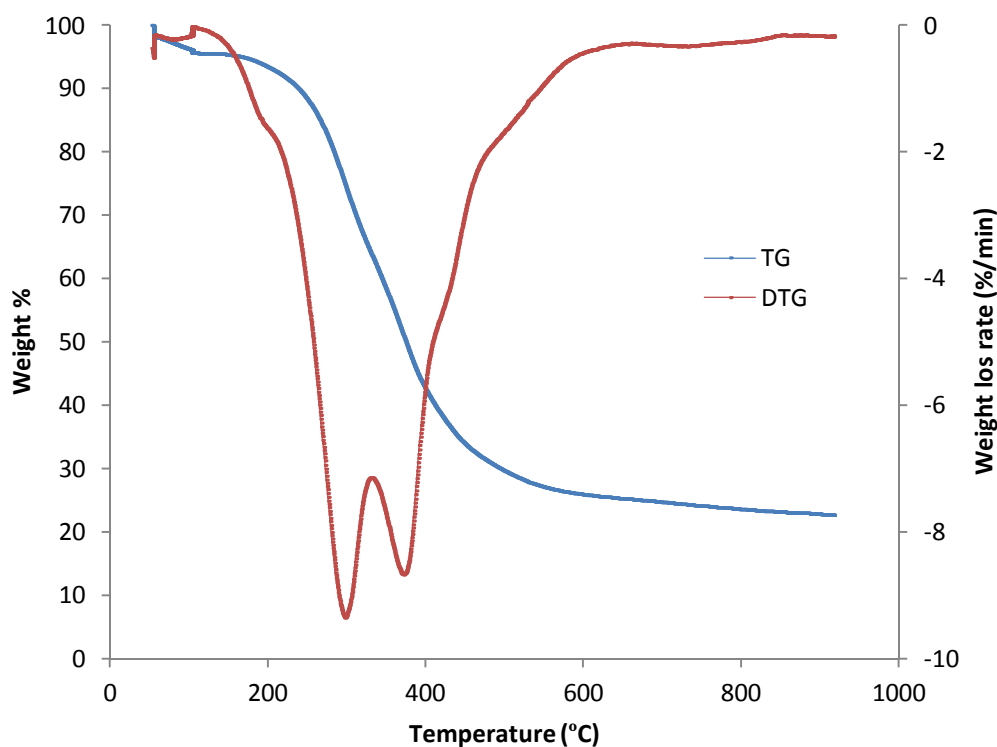
Figure 5-3 TG and DTG curves of Indian Jatropha presscake

5.2.4.4   *African Jatropha*

Figure 5-4 shows the TG-DTG curves of the thermal decomposition of African Jatropha press cake. The initial step on the TG-DTG curves shows the removal of moisture due to temperature increase. The moisture removal started at 45 ℃ and finished at 95 ℃. The next major weight loss step occurs between 105 ℃ and 303 ℃ with the highest rate of mass loss happening at 285 ℃. This step represents the decomposition of the hemicellulose fraction of the sample. The next major step occurs between 306 and 650 ℃ which shows the decomposition of cellulose and lignin. The highest rate of mass loss for this step occurred at 345 ℃. No major weight loss step occurred after 650 ℃. The TG curve shows that mass loss occurred between 45 and 950 ℃ with 77% mass of the initial sample lost between that temperature range.
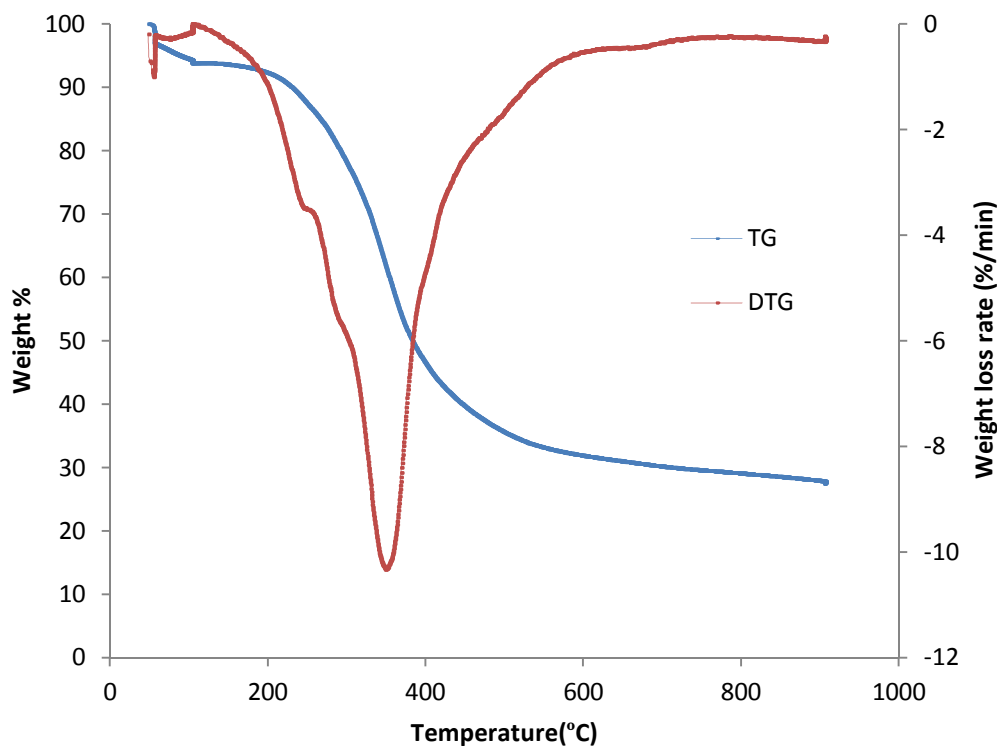
Figure 5-4 TG and DTG curves of African Jatropha presscake

A comparative thermogravimetric study of oiled and de-oiled primary feedstocks is presented in Appendix 2.

5.2.5 PY-GC/MS results

Table 5-5 gives a list of the major compounds identified from the PY-GC/MS of the primary feedstocks. The table also lists the quantities of the compounds as obtained from the area under the compound peaks in the chromatographs.

Table 5-5 Major compounds from PY-GC/MS of primary feedstocks (wt %)

Compound	African Moringa	Indian Moringa	Indian Jatropha	African Jatropha
Propanal 3-methylthio	2.019	0.544	1.087	0.00
Methanethiol	1.920	1.295	1.794	0.00
Furan 2 methyl	1.851	1.906	3.293	0.00
Acetohydroxamic acid	0.00	0.00	0.00	9.142
Methanecarbothiolic acid	0.00	6.842	2.831	8.582
Cyclobutene, 2-propenylidene	1.736	0.00	0.00	0.00
1 H-Pyrrole, 2-methyl-	0.928	0.240	0.114	0.266
2-Furanmethanol	0.753	0.00	0.00	1.764
Pyrazole-4-carboxaldehyde,1-methyl-	0.530	4.995	3.107	0.00
Pyrazole, 1, 4-dimethyl-	1.028	0.191	0.499	1.774
Furan 2,5 dimethyl	0.525	0.447	0.00	0.00
Carbamic acid phenyl ester	0.304	0.435	0.482	0.746
Toluene	1.670	0.149	0.851	1.887
Piperdino disulfide	0.393	0.00	3.590	0.00
Pyrrole, 2 methyl	0.895	0.458	0.272	0.147
Furfuryl alcohol	0.726	0.847	1.027	1.656
1H pyrrole	0.110	0.821	0.587	1.366
Pyrrolbutamide	0.641	3.125	2.879	2.970
Indolizine	0.00	0.00	0.00	0.550
Phenol	0.818	0.585	0.628	0.794
P cresol	2.290	2.163	1.454	2.174
Hex-5-noic acid methyl ester	1.445	0.00	0.138	0.00
4-Hydroxy-6-methylhexahydropyrimidin-2-thione	0.784	0.00	0.00	0.00
Phenol, 4-methoxy-acetate	2.385	1.417	1.652	1.486
2-Methoxy-4-vinylphenol	0.641	0.748	1.332	0.499
Phenol,4-ethyl-2-methoxy-	0.660	0.343	0.138	1.736
4-Amino-3,5-diethylpyridine	1.205	0.104	5.444	0.00
Phenol, 2, 6-dimethoxy-	1.190	1.073	1.080	0.135
Eugenol acetate	1.975	0.814	1.022	0.00
Phenol,2-methoxy-5-(1-propenyl)-, (E)-	1.615	0.317	2.378	2.093
Phenol,2-methoxy-4-(1-propenyl)-, (E)-	3.523	0.415	5.211	3.178
Benzeneacetonitrile, 4-hydroxy-	6.044	5.703	1.025	2.314
Methoxyeugenol	0.702	2.012	1.480	3.731
Pyridine-3-carbonitrile, 1,2-dihydro-4-[4,5,6,7-tetrahydro-benzothien-2y]-2-oxo-	6.897	7.617	2.018	7.144
Oleic acid	41.42	37.342	32.56	34.62
Phorbol	0.213	0.285	4.433	1.658
Total	**89.83**	**83.23**	**84.40**	**92.41**

The major compounds from the analytical pyrolysis of the press cakes show them to be products from the pyrolysis of triglycerides. The most abundant compound in all the press cakes is oleic acid. This finding is in line with a study by Vlahov et al [174] where they showed the major composition of Moringa oil to be oleic and vaccenic acid. The results also show compounds formed during degradation of the press cakes to contain organic compounds with nitrogen. The presence of pyridines, indoles, pyrazoles are in agreement with the elemental analysis of the press cakes since high amounts of nitrogen were present in the samples. The presence of phorbol is in line with the family of Euphorbiaceae plants [18] to which Jatropha belongs. The presence of phorbol in the Moringa samples is however unexpected. Results also show reduced amounts of aldehydes. This is due to the low cellulose content of the feedstocks from the component analysis in section 5.2.1.

5.3   SUMMARY

Characterisation studies have been conducted on the commissioning and primary feedstocks to be processed via fast pyrolysis. It has been found that all the press cakes contain residual amounts of oil from their oil extraction process. The thermal degradation behaviours of the primary feedstocks have also been studied using thermogravimetric analysis. Results show that fast pyrolysis is an appropriate technology to process the primary feedstocks. Analytical pyrolysis results show the presence of nitrogen containing compounds in the feedstocks. They also show the presence of compounds from the decomposition of triglycerides in addition to lignin and other cellulose based compounds.

6 300GRAMS PER HOUR FAST PYROLYSIS RIG

Chapter 6 describes the 300 g/h at the beginning of this research. It details the commissioning steps including calibration methods. The problems encountered prior to commissioning are reviewed. The modifications made to overcome the problems and relevant data from the commissioning stages of the rig are also presented.

6.1 INTRODUCTION TO 300 g/hr RIG

The original Aston University 300 g/h fast pyrolysis rig of which a photograph is shown in Figure 6-1 consists of a Feed hop, through which an auger screw is attached to a variable speed motor for feeding. A cylindrical reactor, a primary and secondary cyclone, a quench column and an electrostatic precipitator sitting on top of the oil collection tank make up the rest of the unit. The 300 g/h rig was designed and built to act as an intermediate rig between the existing 150 g/h rig and the bigger 1 kg/h and 5 kg/h rigs located at the BERG laboratory at Aston University [175]. The 300 g/h unit has never been commissioned. A total of 5 previous attempts at commissioning the unit were unsuccessful. For comparison purposes, the initial system description is based on the configuration at the commencement of this research. A flow sheet of the configuration of the 300 g/h unit is also shown as Figure 6-2.

Figure 6-1 Photograph of 300g/h Unit at commencement of this research
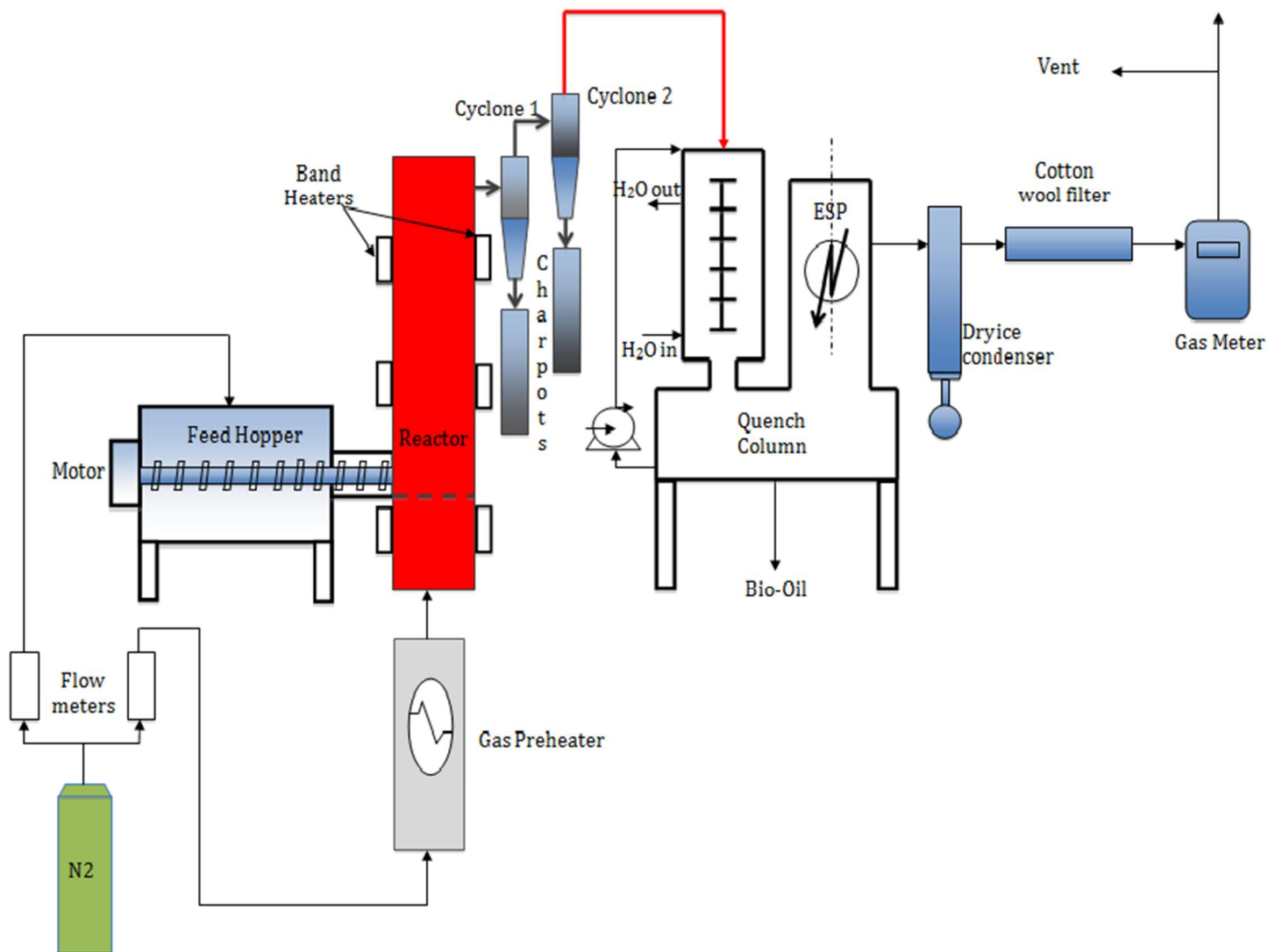
Figure 6-2 Flowsheet of 300g/h unit

6.1.1 Feeding

The 300 g/h rig feeding mechanism consists of a horizontal auger screw attached to a motor and gearbox. The set up is capable of feeding up to 3500 g/h of biomass depending on the speed setting of the motor. The feeding screw is encased in a feed hop of about 0.6 m^3 capable of housing about 1.6 kg of biomass at full capacity depending on the feedstock. The screw is 12 mm in diameter with a 3 mm pitch. The feeding screw attached to the motor is shown as Figure 6-3. It passes through a 14 mm diameter inlet into the fluidised bed reactor.
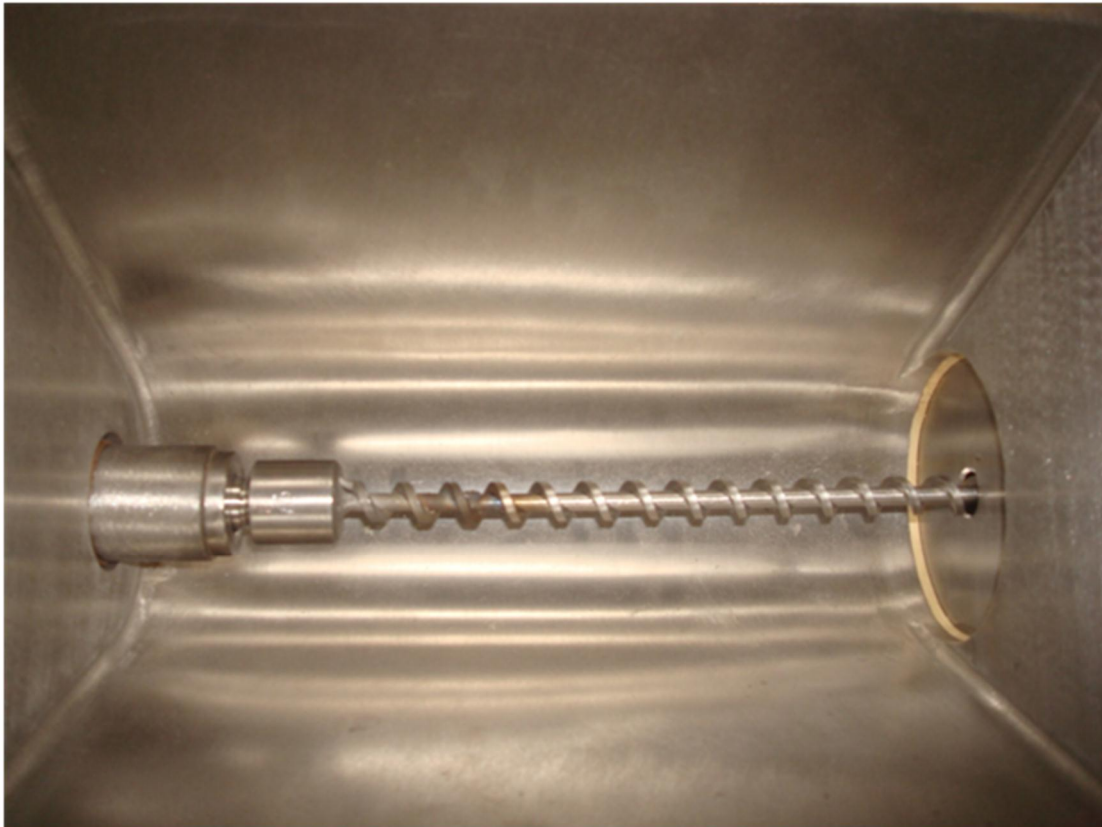
Figure 6-3 Top view of 300g/h feed hop showing feeding screw

The feed system also has attached to it through the cover of the feed hop, an inflow of nitrogen gas as a means of entrain for the feedstock and ensuring an oxygen free atmosphere. Table 6-1 details the relevant parameters for the feed system.

Table 6-1 Feed system parameters

Parameter	Unit	Value
Motor Power	kW	0.37
Feed Capacity	m^3	0.0068
Screw Length	mm	272
Screw Diameter	mm	12.00
Flight pitch	mm	3

The motor supplied by Brown Europe has a rating of 0.37 kW. It is controlled via a Siemens inverter with variable speed function. The maximum speed the motor is capable of reaching is 1500 rpm. A dimensional drawing of the feed hopper for biomass storage during operation is given in Figure 6-4 while the face plate that secures the reactor to the feed system is shown in Figure 6-5.
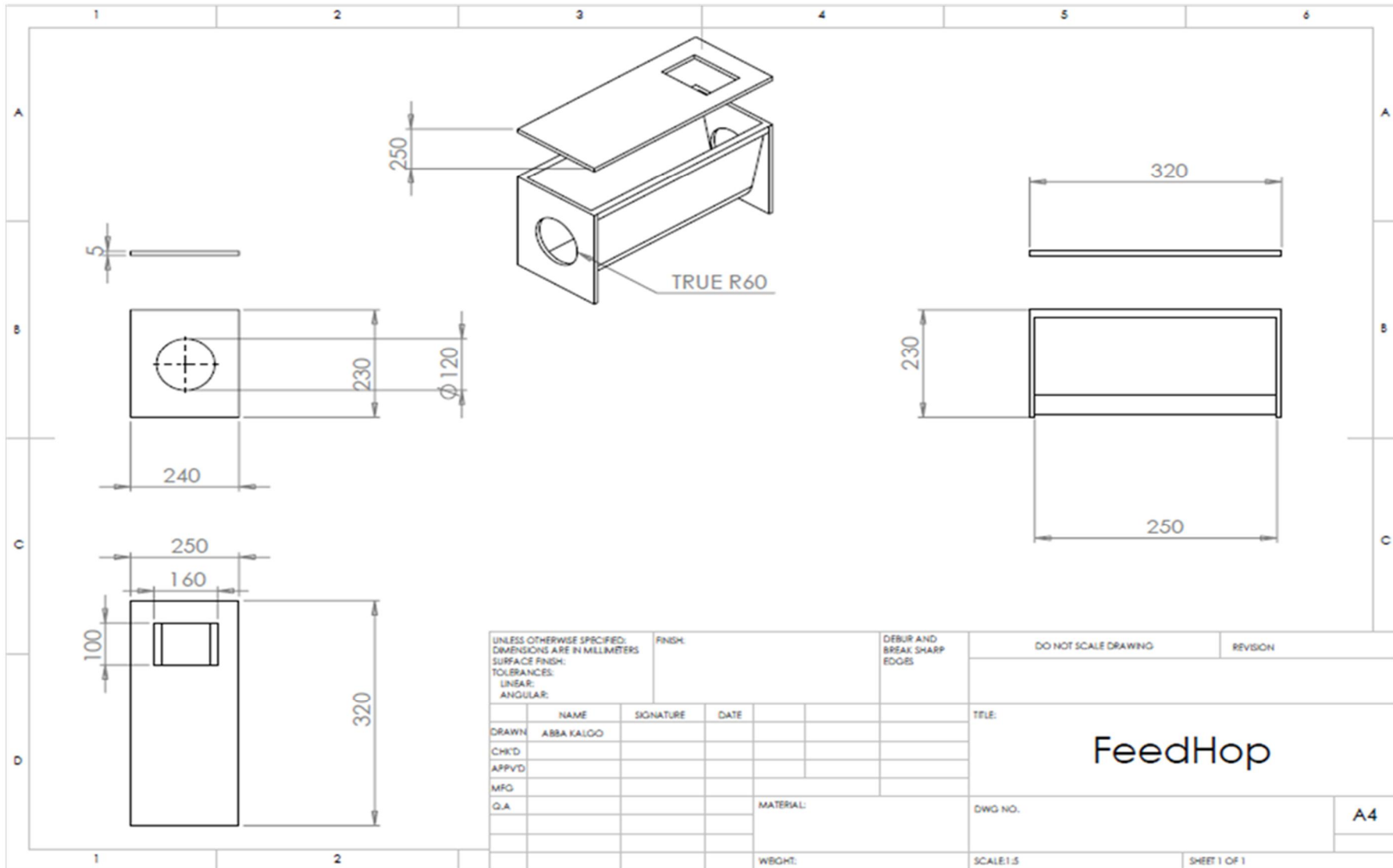
Figure 6-4 Feed hopper dimensional drawings

TRUE R6.50

DETAIL C

230
220
160
200
115

DETAIL B

B

160

230

8

6

8
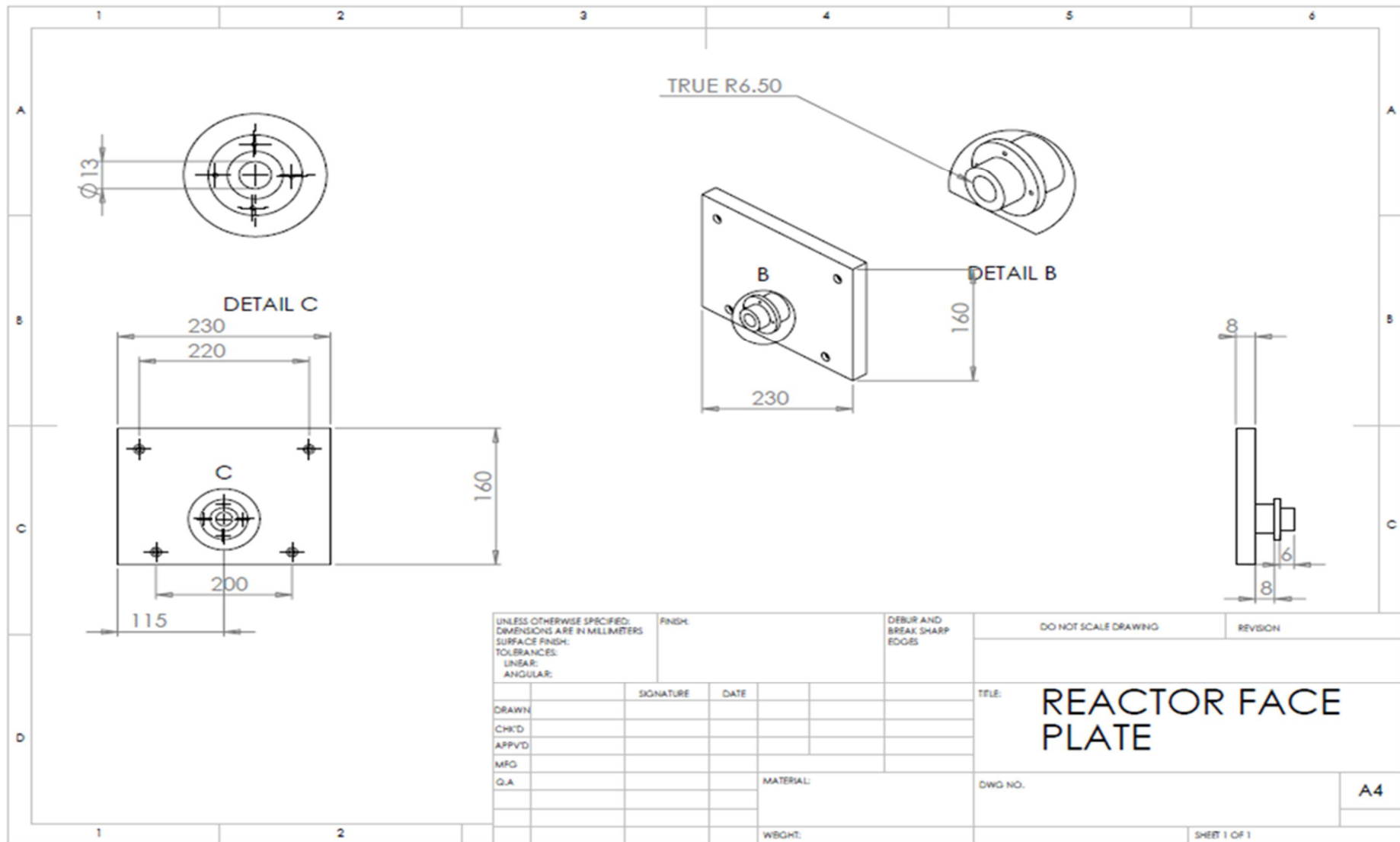
Figure 6-5 Reactor face plate dimensional drawings

6.1.2 Reactor system

A steel tubular reactor of 41mm internal diameter and 320 mm length is used as the reactor for the 300 g/h rig. The reactor is designed to operate at atmospheric pressure and pyrolysis temperatures of up to 700 ºC as a bubbling fluidised bed. All connections to the reactor have been made through the top and the bottom. The fluidising gas inlet is a centred 6.35 mm diameter pipe. The reactor consists of a screw top and a distribution plate 50 mm from the bottom of the vessel making the actual reaction chamber including freeboard 254 mm in length i.e. from distributor plate to reactor exit/cyclone inlet. The distributor plate is a sintered Inconel plate 3mm thick with an average pore size of 100 µm. The composition of the Inconel alloy used as the distributor plate is given in Table 6-2.

Table 6-2 Elemental composition of Inconel 600 [176]

Element	% composition
Nickel	72.00
Chromium	15.50
Iron	8.00
Silicon	0.50
Manganese	1.00
Carbon	0.15
Copper	0.50
Sulphur	0.015

The reactor is heated by three 250 W Watlow heaters. The heaters were attached to a temperature control box. The reactor system also consists of a gas pre-heating unit which is a Watlow Starflow circulation heater capable of reaching 650 ºC. It situated in a gas tight vessel through which the fluidising gas passes. The reactor system also consists of a primary and secondary cyclone in series each equipped with char pots below them. Figure 6-6 shows the dimensions of the reactor. The dimensions of the primary and secondary cyclones which are of the same size are shown in Figure 6-7.

Figure 6-6 Reactor dimensional drawings
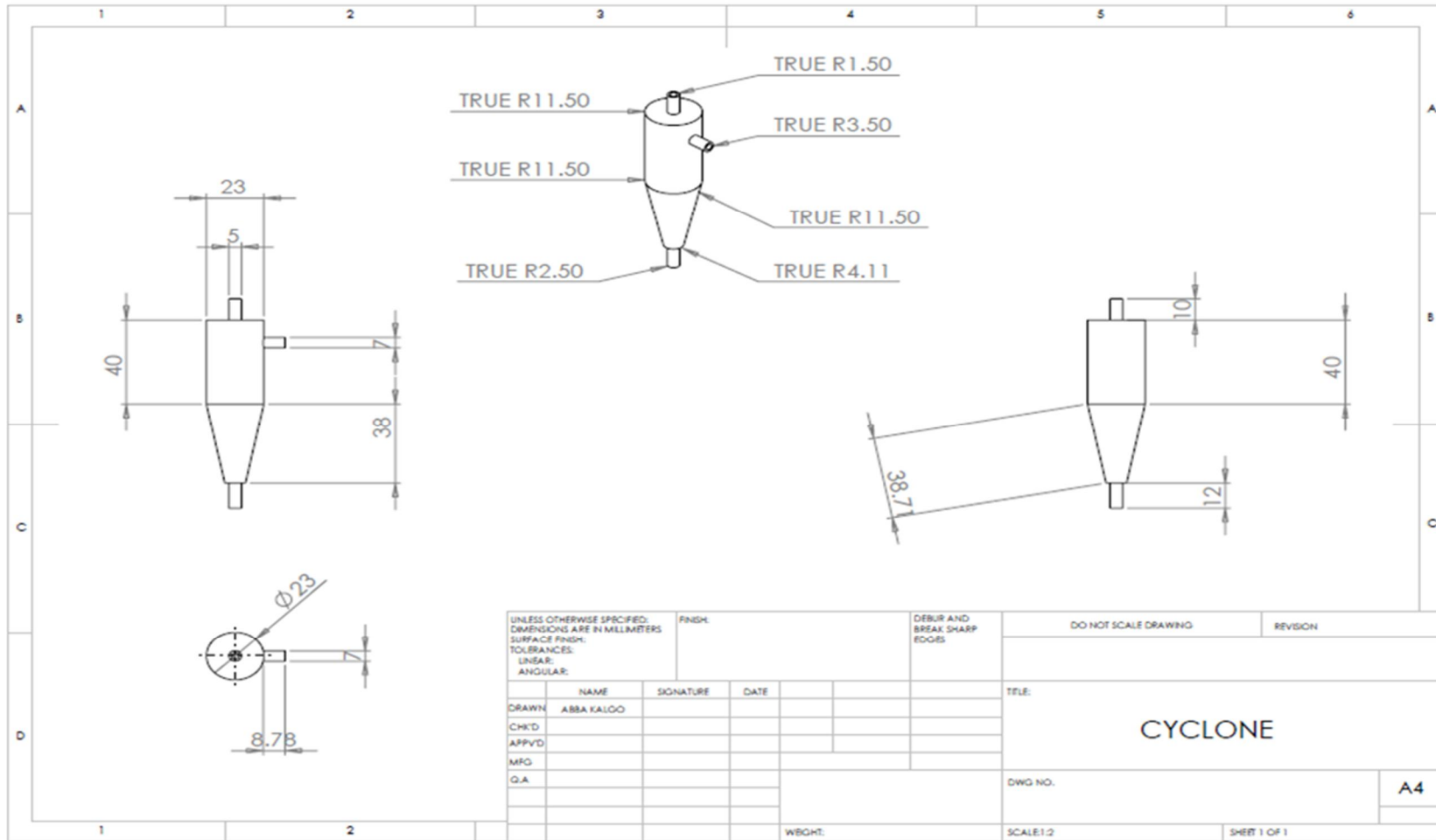
Figure 6-7 Cyclone dimensional drawings

6.1.3 Temperature control and indication

A 5 multizone Watlow temperature control unit shown in Figure 6-8 is used to control process temperatures for the reactor heaters, trace heating tapes, fluidising gas pre heater and heating rod on top of the quench column. The controller is a PID device operated using K type thermocouples for indication, feedback and set point control of process temperatures. Each heating zone is equipped with its own individual control thermocouple attached to the zone controller with a digital input interface. This allows the operator to set the required operating temperature. When the set point temperature of any zone is reached, the controller immediately cuts the heating to the particular zone. Conversely, if the temperature of a particular zone drops below the set point temperature, the controller restarts heating to the zone until the desired set point temperature is reached. This cycle is repetitive for all the heating zones.

Figure 6-8 Watlow multizone temperature controller

The fluidising gas temperature is controlled via a thermocouple inserted at the inlet of the preheating vessel. The thermocouple is horizontally immersed approximately 5 mm into the vessel. The fluidising gas enters the preheating vessel at room temperature and is preheated to the user defined temperature to reduce the energy demand from the band heaters.

117

For reactor heating and control, the control thermocouples are secured between the inner surface of the band heater and the outside surface of the reactor walls. This ensures that the control thermocouples are secure throughout the duration of any experiments. It should be noted that the setpoint for the reactor band heaters are deliberately set to higher temperature as there is a temperature difference between the reactor wall temperature and the temperature inside the fluidised bed reactor (reaction temperature). Experience has shown the temperature difference to range between 100 and 150 ºC. So that for an experiment requiring a reaction temperature of 500 ºC, the set point for the band heaters would be between 600 and 650 ºC.

In order that the pyrolysis vapours are maintained at the required temperatures until the point at which quenching begins, the process piping must be maintained at controlled temperatures (425 ºC). This is achieved by the use of trace heating tapes controlled via K type thermocouple attached to the multizone temperature controller. The thermocouple is wrapped in a spiral motion around the pipes going from the reactor to the quench column. The trace heating tapes are then wrapped around the thermocouple before being lagged to prevent excessive heat losses.

The temperature of the preheated fluidising gas leaving the preheating vessel is observed via a K type thermocouple inserted at the outlet of the preheating vessel. The set temperature of the gas is usually between 400 and 450 ºC although the unit is capable of operating temperatures of up to 550 ºC. If the temperature readings observed are below the required temperature, the set point of the preheating zone is increased to adjust for any discrepancies.

Data readings for the reactor prior to experiments are taken via two K-type thermocouples inserted into the reactor. The lower thermocouple situated 5 cm above the distributor plate of the reactor gives an indication of the temperature in the bubbling bed while a second thermocouple situated 25 cm above the distributor plate measures the temperature of the freeboard and by extension, the exit temperature of the generated pyrolysis vapours and product gases. These thermocouples are connected to a digital temperature indicator and readings during experiments are usually taken at 5 minute intervals.

6.1.4 Quench system

The quench system of the rig operates by direct contact with a quench liquid. The column is equipped with a shell side cooling jacket. The quench liquid is an Isoparrafin (ISOPAR^{TM}) recycled by a centrifugal pump. The stream continuously recycled from the oil collection tank to the top of the quench column where the vapours from the reactor are condensed to the liquid product. Table 6-3 shows the operating parameters of the quench unit and other relevant data.

Table 6-3 Quench column operating parameters

Parameter	Unit	Value
Vapour inlet Temperature	ºC	425-450
Column Diameter	mm	55
Number of plates		20
Plate Diameter	mm	54
Plate Area	m^2	0.00229
Plate Spacing	mm	12.5
Plate open area	%	4.71
Quench liquid Volumetric Flowrate	m^3/h	Variable

The outlet of the isopar stream is located 25 mm from the base of the quench tank to ensure that only the quench liquid is recycled to the top of the quench unit. The denser bio-oil product collects at the bottom of the tank.

A detailed dimensional drawing of the quench unit without the ESP at the beginning of this research is shown in Figure 6-9.
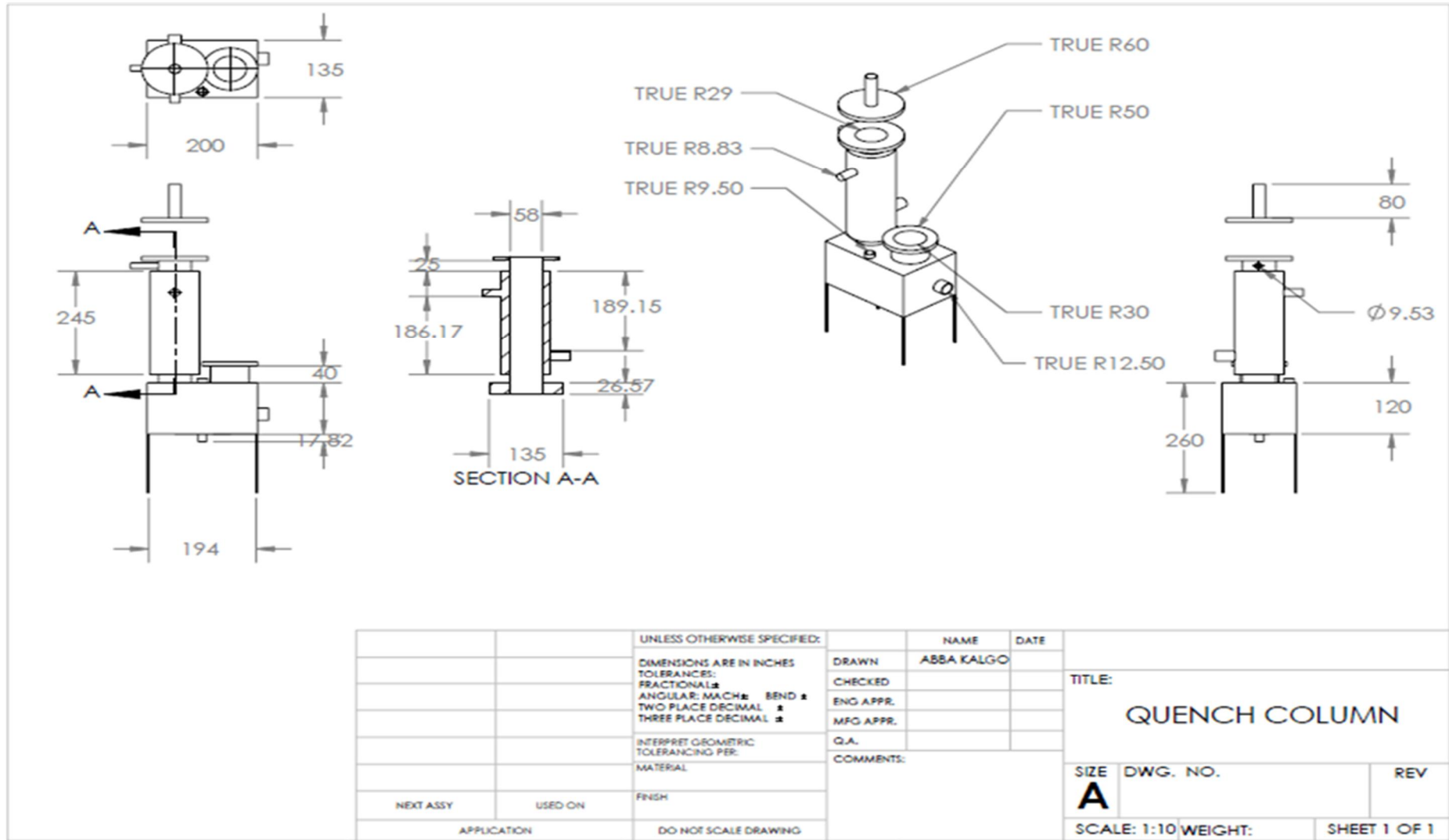
Figure 6-9 Dimensional drawings of quench column and oil collection sump

The inside of the quench column is equipped with 20 evenly spaced quench plates to aid adsorption of the vapours into the oil product. Each of the quench plates is fabricated with six 2 mm holes to allow for cascading of quench liquid and bio-oil mixture to the oil collection tank. Figure 6-10 shows a photograph of the plate arrangements. A 200 W Watlow heating rod is immersed into the top of the quench column. This is to also ensure that the vapours are maintained at the required temperature to prevent any condensation prior to contact with the quench liquid. The thermocouple for controlling the heating rod temperature is attached to the outer surface of a Swagelock fitting through which the heating rod is secured.

Figure 6-10 Quench Column Plates

6.1.5   Electrostatic precipitator

Electrostatic precipitation is employed on the 300 g/h unit as means of capturing fugitive aerosols that are not collected in the quench unit. Literature suggests that up to 70% of organic vapours are collected by the quench column leaving the remainder for collection by ESP and other downstream equipment [97] for a similar configuration. The Electrostatic precipitator for the 300 g/h rig is clear Perspex. The ESP is equipped with a stainless steel plate that acts as a positive electrode. A wire is passed through the centre of the ESP through which a high voltage (10-15 kV) is passed. The wire acts as the negative electrode. The specifications of the electrostatic precipitator are given in Table 6-4.

Table 6-4 ESP design and operational parameters

Parameter	Unit	Value
Diameter	mm	54
Length	mm	210
Collection plate Diameter	mm	52.5
Collection Plate length	mm	150
Collection Plate Area	m^2	0.0249
Electrode wire diameters	m	0.001
Operating Temperature	℃	30
Operating Voltage	kV	10-15
Residence time	s	0.6

The aerosols obtain negative charges as they pass through the electrodes and are deposited on the wall of ESP which is positively charged. The collected aerosols then slide down the walls of the electrostatic precipitator. They are then united with collected oil from the quench column in the collection tank. Figure 6-11 shows the dimensional drawings of the ESP.
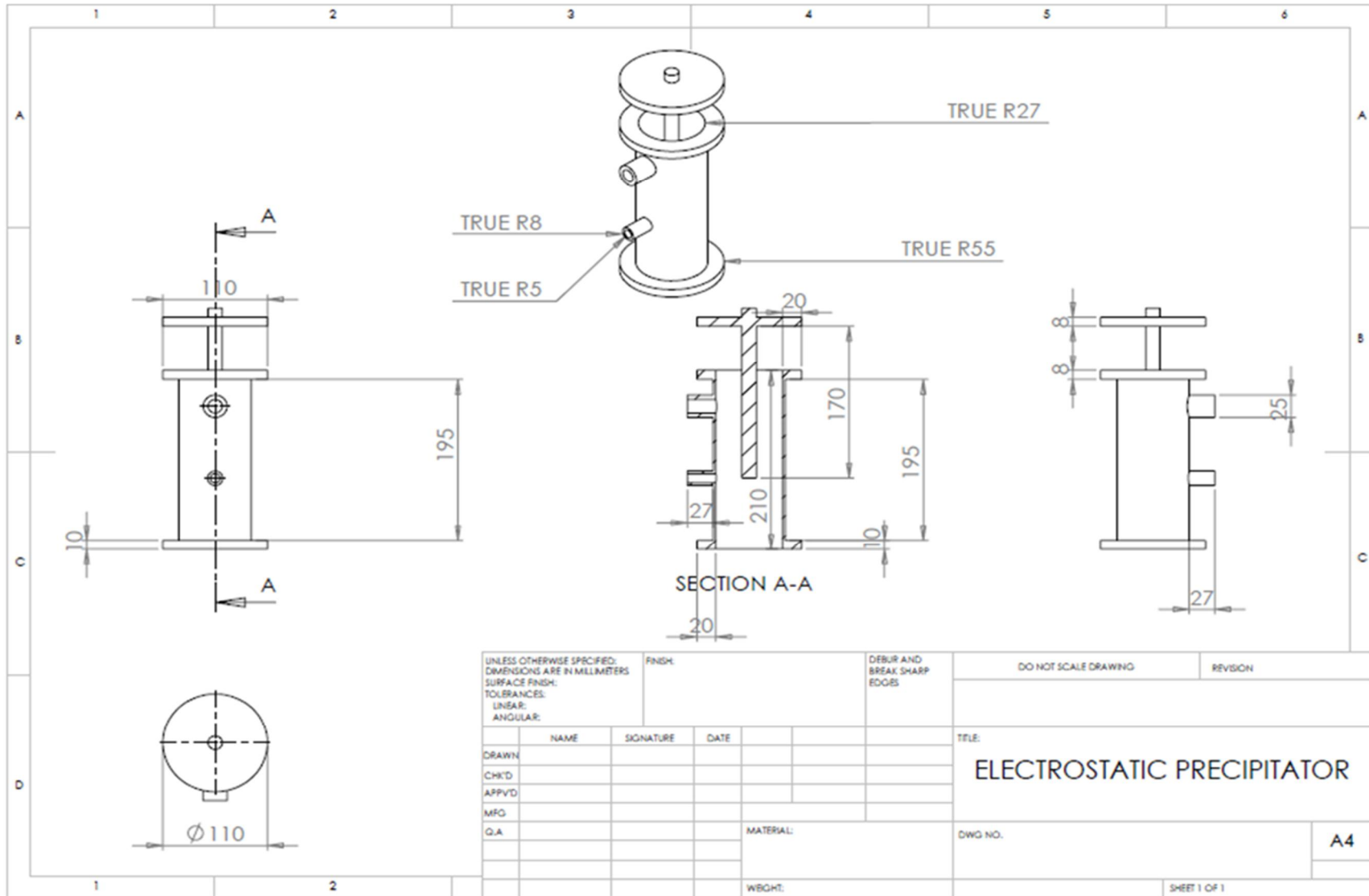
Figure 6-11 ESP dimensional drawings

123

6.1.6   Oil collection tank

The original oil collection Tank is a steel cuboid that sits below the quench column and the ESP shown as part of Figure 6-9.

6.1.7   Secondary condenser

The secondary condenser is a glass contraption that houses a mixture of dry ice and acetone. The condenser operates at a temperature of -30 ºC. The condenser traps light organic vapours that have passed the quench and ESP which operate at higher temperatures. These vapours are condensed and collect in an oil pot which sits below the condenser.

6.1.8   Cotton wool filter

The cotton wool filter as the name implies is a filter that collects condensable liquids that may have passed the ESP and secondary condenser. The filter is a horizontally mounted, gas tight glass contraption that houses a mass of cotton wool. Any remaining vapours from the secondary condenser are trapped in the cotton wool.

6.1.9   Gas analysis system

The gas analysis system consists of the gas meter and the gas chromatographic system. The gas meter measures the volumetric throughput of the gas flow. Most of the non condensable part of the gas stream is vented off while a small part is sent to the GC for analysis. The GC uses different columns to analyse the gases from the process. The GC is conditioned and calibrated before runs to ensure that the analysis is done to an acceptable standard. A more detailed description of the GC has already been given in section 4.6.3.

6.2   SAFETY CONSIDERATIONS PRIOR TO COMMISSIONING

It was essential prior to commissioning of the unit to investigate, identify and familiarise the operator with certain hazards associated with the operation of a fast pyrolysis unit. The operation of a fast pyrolysis unit can constitute hazards that may be categorised in two groups. The hazards may be either of a toxic nature or a fire and explosive nature.

6.2.1   Toxic hazards

Fast pyrolysis units produce a certain number of hydrocarbons and other toxic compounds present in both the liquid and gaseous products. The product gas can contain high levels of carbon monoxide a colourless and odourless gas toxic to the human body in high proportions. Literature reports the long term occupational exposure limits to carbon monoxide to be 50ppm for an 8 hour working shift. The short term exposure limit for up to 10 minutes stands

at 400 ppm [177, 178]. The absorption of carbon monoxide into the blood stream leads to the formation of carboxyhaemoglobin whose effects in varying concentrations are detailed in Table 6-5.

Table 6-5 Symptoms of carboxyhaemoglobin levels in bloodstream [178]

% Carboxyhaemoglobin in blood	Symptoms
<20	Slight breathlessness
20-30	Flashing, headaches
30-40	Severe headache, nausea, impaired judgement
40-50	As above
50-60	Loss of consciousness
>60	Circulatory and respiratory system failure resulting in death

The other gaseous components of the non condensable pyrolysis gases are less toxic than carbon monoxide but also pose risks to the human body if present in large enough quantities. The effects of other pyrolysis gases are detailed in Table 6-6.

Table 6-6 OEL and toxic effects of pyrolysis gases [178]

Component	OEL (ppm)	Toxic Effects
Hydrogen	-	Asphyxiant
Carbon dioxide	5000	-
Nitrogen	-	Asphyxiant
Methane	-	Narcotic at high concentrations
C_2H_4, C_2H_6, C_3H_6 and C_3H_8	-	Asphyxiant and possible anaesthetic at high concentrations

*OEL-Occupational exposure limit, (ppm-part per million)

Other toxic hazards posed by products of the pyrolysis process come from the pyrolysis liquids and tars formed during the quenching of vapours. Certain compounds from the pyrolysis of coal and other mineral oils have been directly linked to the cause of scrotum cancer [179]. This is significant to the pyrolysis process as analogies with biomass pyrolysis liquids can be assumed.

6.2.2 Explosion and fire Hazards

Fast pyrolysis is a process that converts solid woody biomass fuel into liquid, solid and gaseous products. It is immediately apparent that there is a fire and explosion risk associated with the process. The solid char products of the process are known to have the tendency to self ignite if the conditions are suitable. This is particularly more likely if the char is of a

finer nature. The presence of nitrogen as part of the gaseous products however reduces the risk of explosion and fire but does not completely mitigate the risk of occurrence.

An added fire hazard associated with the process is the presence and storage of the biomass raw materials in the laboratory. The risk of a wood dust explosion from the materials is present where wood is stored. Literature from the Joint fire organisation presents the limits of an explosion between 360 for wood and 470 ℃ for wood pulp. This research does identify the risk of dust explosion although it can be said to be minimal. Dust is only generated during grinding and sieving and will not in sufficient quantities to pose the risk of an explosion [180].

6.3 SAFETY PRECAUTIONS

Safety measures were taken in three categories to minimise the inherent dangers associated with a fast pyrolysis process. The precautions were introduced in three forms described below.

6.3.1 Incorporation of safety devices into the process

It was noticed at the beginning of this research that the pyrolysis process was lacking any mechanism of relieving a build up of pressure in the system. The process is likely to form sticky tars and other products that may cause blockages in the process piping. It was decided to put pressure relief valves on the parts of the system that were most likely to encounter blockages. An assessment of the process areas most likely prone to blockages was undertaken. Based on this, it was decided to install relief valves on the reactor and the quench column. A relief valve was installed at the top of the reactor connected to the process vent line. Similarly, because bio-oils are sticky and tarry, a relief valve was also installed on the top of the quench column. This was in order to vent any pressure that may build if blockages occur due to tar formation.

The laboratory is equipped with a carbon monoxide alarm that sounds when the concentration of carbon monoxide in the lab rises above 50 ppm. As an added precaution however, personal carbon monoxide alarms worn on operator clothing were purchased to be used during experiments.

The idea of constructing a fume hood over the unit was also discussed but space and budget restrictions meant that the idea was dropped in consultation with the departmental safety officer. The safety precautions around the system were considered to be sufficient.

6.3.2 Operational procedure

An operational procedure contained in appendix 3 was written for the unit in collaboration with the departmental safety officer for general use by other researchers.

6.3.3 Supporting laboratory equipment

As part of laboratory procedure, an added number of equipment and safety measures independent of the fast pyrolysis unit were already in place and they included

1. Access: A clear path around the entire pyrolysis unit was maintained as a safety measure. Clear paths between the fast pyrolysis units and the laboratory exits were also established to ensure the swift evacuation of the laboratory if and when the need arises.

2. Laboratory breathing apparatus: Breathing apparatus with battery powered supply were in place for use during the pyrolysis runs. The apparatus also consisted of face screens as added protection for the system operators.

3. Feed Storage: The biomass samples to be pyrolysed were stored in plastic containers with tight lids to reduce any risk of ignition. Similarly, plastic bags already extant in the lab were designated as storage for any produced chars from the process.

4. Emergency procedures: It was also essential that the operator of the unit familiarised themselves with the laboratory and university safety procedures. This was undertaken prior to the commencement of any experiments. Emergency telephone numbers and evacuation paths and points were also noted.

6.4 COMMISIONING OF INDIVIDUAL SECTIONS OF 300G/H RIG

The system at the beginning of this study was an unproven one. As such, it had to be commissioned. The commissioning of the units happened in two separate phases. Cold and hot commissioning stages were carried out on the unit. The aims of the commissioning stages were to

- Test and observe the performance of individual units of the system.
- Test and observe the performance of the entire system
- To make amendments and modifications if necessary to individual units based on the tests
- To obtain and utilise data obtained for subsequent analysis of the system

- To help in coming up with a proper operating procedure of the unit for use by other researchers

The commissioning of the sections happened in the following order.

- Feed System
- Quench Unit
- Reactor unit
- Complete Unit commissioning (chapter 7)

The following section details the results from the commissioning phase of individual sections of the rig.

6.4.1 Cold commissioning tests

The cold commissioning phase encompassed the operation of individual pieces of equipment. The primary purpose was to ensure that sections of the unit performed satisfactorily. Other purposes were to calibrate the equipment and obtain the requisite experience required for purposeful operation. A summary of tests performed under the cold commissioning stage are presented in Table 6-7. The details of feed system commissioning are also described in full being a major part of the process.

Table 6-7 Summary of Cold commissioning tests

Equipment	Purpose of test	Observations/modifications	Cross reference to detailed discussion
Feed Screw	Rotation speed, calibration	Feeding screw bent. Straightening required. Calibration undertaken	6.4.2
Feed Hop	Leak Test	Leaks found. Gasket Change	
Inverter	Communication between inverter and motor	OK	
Flowmeters (entrain) , pressure indicators	Calibration	OK	
5 zone Multizone temperature controller	Communications with thermocouples. Temperature control	1 zone faulty. 4 others fully functional	
Reactor joints, Band Heaters	Leak Tests, Reactor Heating	No leaks observed. Recurring short circuits with band heaters. New band heaters with modified Steel jacket	
Distributor plate	Bed support and fluidisation	Visual observation of Fluidised sand bed. OK	
Cyclones	Leak test, solid separation	No leaks. Successful separation of bed material.	
Trace Heating tapes, control thermocouples	Pipework heating	OK. Trace heating reached required operational temperature	

Char-pots	Leak tests	OK. No leaks found	
System Pipework	Leak tests	Leaks found. New pipework and ferrules	
Quench Column	Leak tests	Leaks found. Gasket change	
	Quench Liquid Draining	Inefficient. Pyramidical Bottom	
Quench Liquid Pump	Recycle quench liquid	Pump failure. Replacement put in	
Recycle liquid flowmeter	Calibration	Successfully calibrated	
Quench Shell side cooling stream, flowmeters	Leak tests. Calibrations	No leaks found. Flowmeter calibrated.	
Column flooding	Calibration, liquid distribution.	OK. Excessive flooding observed at maximum pump rate. Quench plates modified for easier cascading of liquid	
Electrostatic Precipitator	Leak Tests, Current and voltage in nitrogen atmosphere	No leaks found. Stable operation. Constant voltage and current.	
Dry ice condensers	Leak tests	OK	

Cotton Wool Filter	Leak Tests	OK	
Gas Meter	Leak Tests, calibration checks	OK	

6.4.2 Feed System commissioning

The feed system commissioning involved feed rate tests on biomass samples relative to the drive motor setting. The operational principle of the feeder unit was based on being able to control the feed rate via the motor attached to the feed screw.

6.4.2.1 *Biomass feeder calibration*

To calibrate the feed system, a set-up was put in place as portrayed in Figure 6-12. The feed system calibration was carried out with the reactor detached from the face plate (figure 6-5) which holds it in place. A small flow of nitrogen (3 l/min) was passing through the feed hop. The calibration involved putting a pre-weighed collection vessel on a scale. By varying the speed of the motor by the setting on the inverter, the quantity of biomass conveyed by the screw through the reactor inlet into the receiving vessel over a fixed period of time was determined.
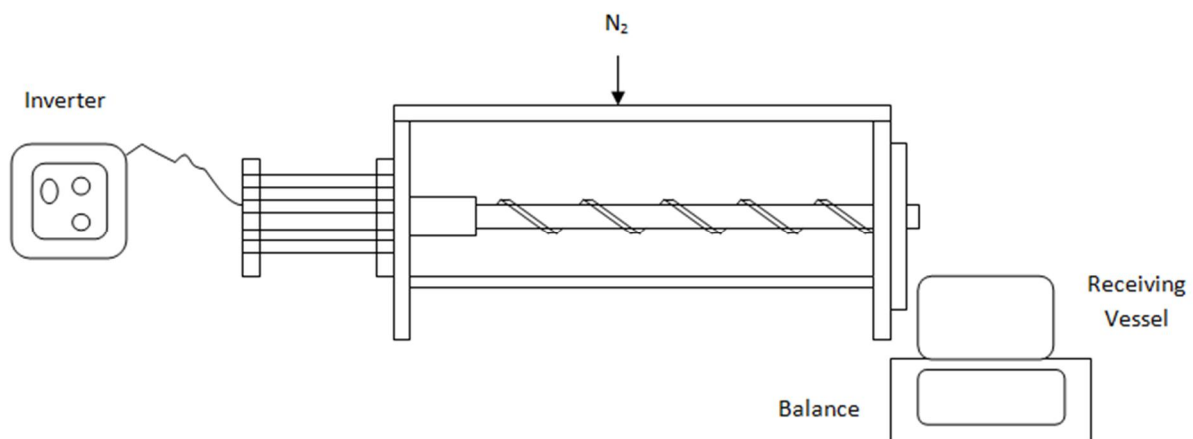
Figure 6-12 Feed system calibration set up

The commissioning of the feeder unit involved trials with using Beechwood. Table 6-8 shows the results of the feedstock tested at varying motor speeds.

Table 6-8 Calibration data for beech wood

Feeder Setting	Biomass feed rate (g/h)
5	125.40
10	243.60
20	501.60
30	762.60
40	1041.00
50	1396.20

The results are also presented as a calibration curve in Figure 6-13.
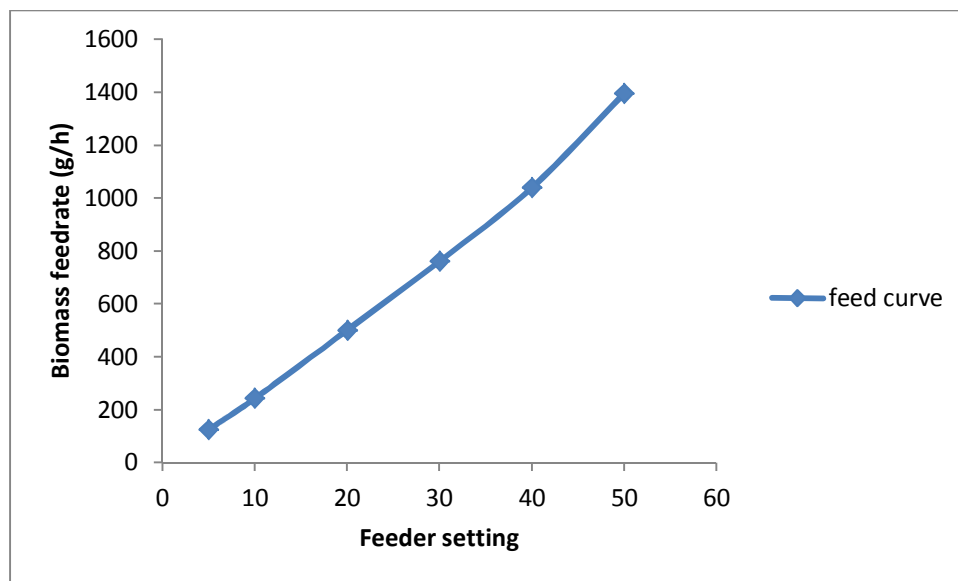
Figure 6-13 Biomass feed system calibration curve

6.4.3   Hot commissioning tests

The cold commissioning tests detailed in Table 6-7 though useful were limited in the kind of data they could provide. Performance of certain equipment could only be assessed under pyrolysis conditions. Equipment including the quench column and electrostatic precipitator can be operated individually but an assessment of their efficiency and limits could only be determined under actual pyrolysis conditions. Thus, the need for the hot commissioning tests. A summary of the hot commissioning tests are presented in Table 6-9.

Table 6-9 Summary of hot commissioning tests

Equipment	Purpose Of Test	Problems	Observations/Modifications	Cross Reference to detailed discussion
Pre-heater	Gas preheating	Short circuits.	Change to heating coil	
Reactor Heating	Get reactor to pyrolysis temperature.	Short circuits/Tripping	Unsuccessful. New heaters required. Modification to heating system. Observe new heaters and steel jacket	6.4.8
Quench column	Vapour quenching	Fouling. Blockages.	Heavy tars indicating improper quenching. Flooding of column. Modification of quench plates.	6.4.5
Reactor System	Feeding under pyrolysis conditions	Pre-pyrolysis	Poor fluidisation. Agglomeration. Char unable to leave reactor	7.6.2

6.4.4 Reactor commissioning tests

The aim of the reactor commissioning tests was to successfully get the reactor while operating as a fluidised bed to pyrolysis temperatures. The test also involved maintaining the reactor at the desired temperature (500 ℃) for a duration of at least 60 minutes. The tests involved operation of the band heaters with the temperature controller already described in section 6.1.3 of this report. Several attempts were made using the band heaters, but an outright failure of the equipment meant that pyrolysis temperature was never reached. The reactor was eventually commissioned after modifications and changes to the heating system. These are described in section 6.4.8.

6.4.4.1 *Vapour residence time calculation*

Peacocke [33] suggests that researchers should make the effort of explaining the method of residence time calculations. The rationale behind his suggestion was that reasonable comparisons can be made accurately since the residence time is an important parameter for fast pyrolysis.

Thus, the need arises to accurately define and estimate the vapour residence time for the system. In measuring the vapour residence time for fast pyrolysis, distinctions must first be made between the reactor only residence time and the total hot space residence time. The reactor only residence time describes the duration of the pyrolysis vapours in the actual reactor unit. The total hot space residence time on the other hand is a measure of the time the vapours spend in the total hot space of the unit. In the case of the 300 g/h unit, it includes the reactor volume from point of generation to the point of quenching (cyclones and transition pipes included). Based on the definitions of the residence times given, it can be concluded that the total hot space residence time is a more realistic measurement of the vapours residence time since the vapours pass through the heated cyclones and transfer lines prior to reaching the quenching unit. All residence times reported refer to the total hot space residence time.

The formula for calculating the residence time on the 300g/h unit during this research is shown in equation 6-1 [12, 40] below

$$ = \frac{\overline{\qquad}^{*} \qquad ^{*}}{^{*} \qquad ^{*}} \qquad \textbf{Eq 6-1}$$

Where

Volume$_{Totalhotspace}$	Volume of reactor, cyclones and transfer line	[cm^3]
W$_{sand}$	Weight of sand	[g]
T$_{measurement}$	ambient Temperature	[K]
T$_{Reactor}$	Average reactor temperature	[K]
Time	experiment duration	[s]
Volume$_{totalthroughput}$	Volumetric throughput	[l]

The formula used works based on the assumption that volume and density of the sand remain constant (a reasonable assumption since reactor operates blow through principle). It should also be mentioned that the total hot space of the reactor unit is the total volume above the distributor less the volume of the sand bed.

6.4.5 Quench system commissioning

The commissioning of the quench system of the 300 g/h unit happened before its actual reactor was functional. This was possible because the quench column could be adapted to run with the already extant 150 g/h reactor. This was necessary because the modifications to get the reactor unit fully operational involved steel fabrications which were time consuming (see section 6.4.8.2). It was also reasoned that because the reactor on the 300 g/h and the 150 g/h units were geometrically exact, the experiment would to a large extent be a reflection of fast pyrolysis process on the unit undergoing commissioning. The decision was then taken that the quench column be operated with the 150 g/h reactor unit as part of its commissioning. Several researchers have already described the 150 g/h unit [12, 40, 181-183] and the reader is referred for a full description of the unit. One experiment was undertaken with the 150 g/h unit reactor coupled to the 300 g/h unit quench column. The aim of the quench unit commissioning was to

- Observe the behaviour of the quench column and electrostatic precipitator under pyrolysis conditions.
- Develop a mass balance calculation method on the quench column

The commissioning configuration is shown in Figure 6-14.
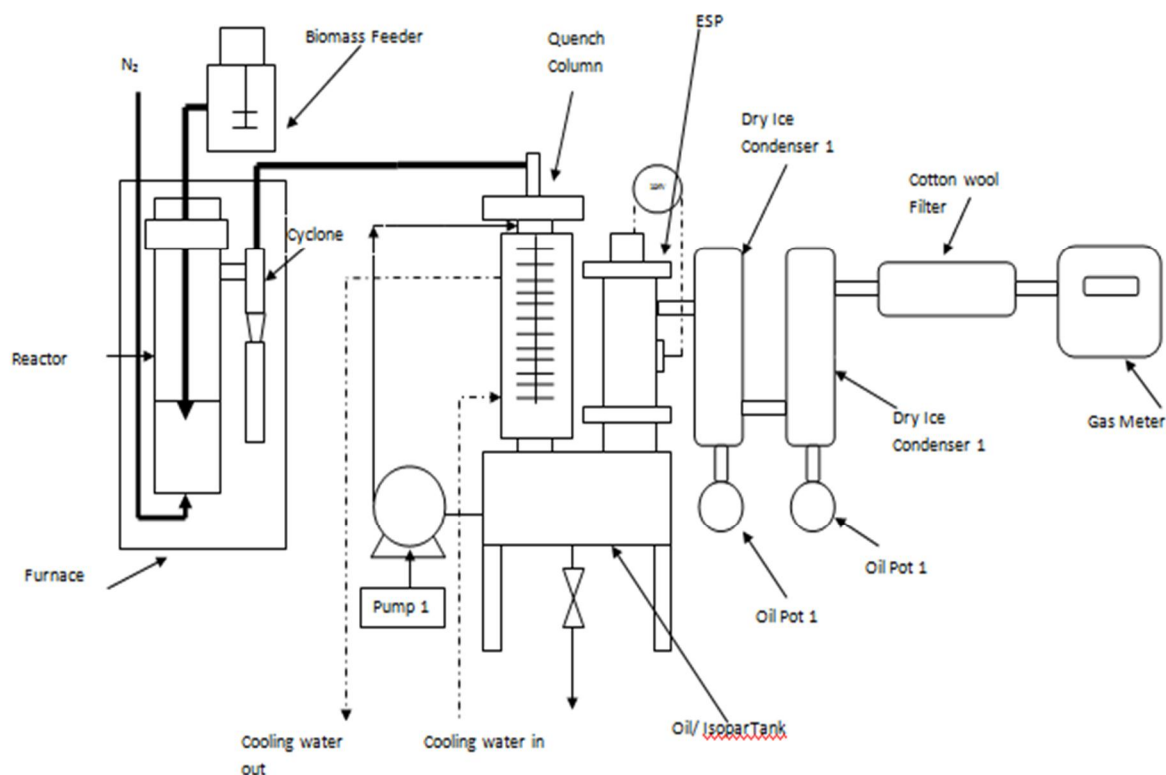
Figure 6-14 Hybrid configuration used for quench commissioning run

6.4.5.1 *Experiment QCOM-1-HYBRID*

Table 6-10 details relevant data for the commissioning run of the quench system.

Table 6-10 Quench unit commissioning test parameters

Parameter	unit	
Feedstock	-	Beech Wood
Test duration	min	110
feed rate	g/h	100.2
Target reactor temperature	°C	500
Particle size	µm	355-500

Run summary: Continuous feeding achieved with refilling of the hopper after 60 minutes. Slight smell emerged from the rig indicating a small leak but could not be detected. The target temperature was set at 500°C but was difficult to maintain due to overshooting of the furnace temperature. The flowmeter to measure isopar did not function. Thus, the maximum possible quench flowrate was determined by adjusting the pump with the quench column

open. A temporary transparent tube was connected at the quench top inlet to observe flow of the isopar level since flooding would cause isopar flow into the cyclones.

At the conclusion of the quench commissioning run, a procedure was put in place to attain the total mass of pyrolysis liquid in the quench vessel after the run. These main procedural steps include

- Recover oil from quench vessel
- Remove quench column, determine weight before and after cleaning with ethanol, filtration of ethanol washings to determine char.
- Remove tubes from the quench pump, drain off isopar and determine oil in tubes by weighting before and after cleaning.
- Remove ESP and determine weight difference before and after cleaning
- Wash quench vessel with ethanol. Evaporate Ethanol from the washing liquid to determine oil which was sticking on quench vessel.

After the commissioning run, it was observed that certain parts of the quench column were likely to retain some of the bio oil produced. Table 6-11 details sections of the unit and the mass of liquid retained from the quench commissioning run.

Table 6-11 Hold up in and around quench column

Part of Process	Mass of organic liquids retained (g)
Quench Lid	1.3
Quench Plates	10.22
Quench Column Walls	13.50
ESP Joint	1.3
Quench Recycle Pipes	0.4

The mass balance results from the quench commissioning run are shown in Table 6-12.

Table 6-12 Mass balance results for quench commissioning run

Feedstock in (g)	231.76		
CHAR			
Char in sand	6.74		
char from Quench Plates	1.5326		
Char Washings	1.4709		
Char pot	14.76		
		% char	10.57
OIL (g)			
cotton wool filter	1.21		
Oil Product Yield	100.48		
oil in Washings	13.50		
Dry Ice Condenser 2	0.24		
Oil pot 1	11.51		
Oil pot 2	0.91		
Quench plates	10.22		
EP	2.95		
Isopar tube2	0.16		
Isopar tube3	0.24	% oil	61.02
	165.95	**% mass in:**	**71.59**

It is worth noting that during the commissioning phase of the quench unit, the Gas Chromatograph was out of commission. As such, the gases produced during the course of this experiment were not analysed. The decision was taken to proceed with the commissioning anyway since the aim of the experiment was to observe the behaviour of the quench unit in terms of oil product recovery and collection. The gases were obtained by difference.

6.4.6   Mass balance calculation method

The second aim of the quench commissioning run of the 300 g/h system was to develop a mass balance calculation method on the quench part of the system. The mass balance calculation method needed to be able to estimate to a high degree of accuracy the

- Amount of pyrolysis liquids generated
- Amount of organic liquids generated
- Amount of char in the quench system and oil products
- Amount of water in the quench system and pyrolysis liquids

6.4.6.1 *Liquids yields determination*

In determining the total liquids yields in the quench system of the unit, it is necessary to first detail the points of at which pyrolysis liquids are collected. There are three main points of liquid collection on the quench unit of the rig as detailed in Table 6-13.

Table 6-13 Pyrolysis liquids collection points on 300g/h unit

Liquid Fraction	Point of collection
Bio-oil	Quench plates, Oil tank and ESP
Lighter fractions	Dry ice condenser and oil pot 1
Lighter fractions	Cotton wool filter

The main liquid fraction (bio-oil) which is a brownish black liquid from the system is collected in the oil tank below the quench column and the electrostatic precipitator. The amount of bio-oil (mixture of char, water and organic liquids) collected from the product collection tank during an experiment is determined by the difference between the mass of quench liquid at the start of the run, and mass of the total liquids at the end of the run. It should be noted that the pipework that conveys quench liquid from the oil collection tank to the top of the quench column retains some amount of quench liquid (~40 g). This is taken into account during the mass balance calculations. It is assumed that there is no bio-oil product in this stream as the quench stream outlet is connected higher up quench tank making it unlikely that any significant mass of oil finds its way into the stream since the bio-oil product collects at the bottom. This assumption is justified from the result of the quench commissioning run where over a 120 minute run where 231.76 g of biomass was fed, only 0.4 g of oil was found in the oil pipework. The mass increase of the electrostatic precipitator which is determined by gravimetric measurements before and after the experiment is assumed to be bio-oil of the same composition as the oil in the collection tank.

The second liquid fraction is collected in the dry ice condenser and oil pot below it. That liquid fraction usually contains more than 60 % water. It also contains lighter organic fractions condensed by the dry-ice acetone mixture. The colour of the lighter fraction is usually light brown but may differ depending on feedstock. At the end of every experiment the dry ice condenser is blocked with a rubber bung to ensure that there is minimal escape of vapours from the system. The dry ice condenser is usually weighed 16-18 hours after the experiment to ensure that the vapours condensed by the dry ice acetone mixture have collected in the oil pot below. The acetone in the dry ice condenser is then emptied and the

unit allowed to dry. The mass of the condenser is then obtained and the initial mass prior subtracted from the value to obtain the mass of any liquids that have collected on the walls of the DIC. The oil pot below the DIC is also weighed to determine the mass of liquids collected inside.

The final liquid fraction is collected in the cotton wool filter. The amount of liquid collected in the cotton wool filter is usually small when compared to other sections of the unit. It is absorbed in the cotton wool. This liquid is assumed to be of the same composition as the fraction collected in the dry ice condenser. Since this liquid is absorbed in the cotton wool, recovery is almost impossible and analysis is not carried out on it. The cotton wool filter is usually weighed immediately after the experiment because of the hygroscopic nature of cotton wool. If allowed to sit for long periods of time, there is a tendency for the cotton wool to absorb moisture from its surroundings which may cause erroneous mass balance calculations.

The total amount of pyrolysis liquids generated from the unit is the mass of oil collected in the main tank, ESP, quench plates, dry ice condensers and cotton wool filter. Up to 90% of total pyrolysis liquids are collected between the quench column and ESP while the remainder is collected in the dry ice condenser and cotton wool filter.

To determine the yield of organic liquids, the mass of water and char in the liquids are subtracted from the total liquids collected. Water contents of the fractions are determined using Karl Fischer titration described in section 4.7.1.5. The amount of char in the bio-oil is also subtracted after the char content of the oil fractions have been determined as described in section 4.7.1.6. Before this however, the mass of initial moisture in the biomass is obtained and subtracted. The mass balance is reported on a dry basis. Thus the initial feedstock moisture content must be discounted.

Bio-oil is usually high viscosity liquid containing water, chars and organic liquids. This invariably sticks to the wall of the quench columns. To quantify the amounts of oil on the walls of the quench unit, the quench unit is flushed with approximately 1.5 litres of ethanol after the Isopar and oil have been drained. The ethanol is able to dissolve the remaining oil and isopar sticking on the walls of the quench unit. A representative mixture of ethanol, water, isopar and oil mix is then taken and subjected to rotational vacuum evaporation. At the conclusion of that phase of the experiment, the only mix remaining is the oil and isopar as the ethanol and water are evaporated. The oil and Isopar are then phase separate based on their

immiscibility and difference in densities. The amount of oil is then calculated from the proportional ratio of pyrolysis liquids in the ethanol washing liquid. For the commissioning run QCOM-1-HYBRID, the amounts of oil remaining in the quench stood at 13.50 g. Later runs showed that for runs lasting more than an hour, the quench unit retained anywhere between 13 and 15 g of bio-oil.

6.4.6.2 Char yields determination

Most of the process char is collected before the quench unit and is a relatively straight forward process. To put a value on the amount of char produced, the mass increase in the fluidised bed reactor, char-pots and transition pipes are determined by gravimetric measurements. Any mass increase in all the components listed is solely attributed to char. This is because the operational temperatures are not expected to favour any condensation prior to the quench unit. Any increase in the reactor contents is assumed to be char that may not have been entrained during the experiment. This is obtained using a pre-weighed bag in a vacuum cleaner. Since the amount of char from the liquid fractions has already been quantified, they are added to the process char yields.

6.4.6.3 Gas yields determination

The accuracy of mass balances is hugely dependent on the accuracy of gas measurements. As shown, solids and liquid yields are primarily determined gravimetrically. The mass of gases are however obtained from the gas composition obtained from the micro GC and the total volumetric throughput of the experiments. As the gases are highly diluted with the nitrogen used as fluidising gas, the mass of nitrogen is discounted from the mass balance calculations.

In summary the distribution of pyrolysis products in the 300 g/h unit and methods of measurements are given in Table 6-14.

Table 6-14 Summary of product collection point and measurement methods

Product	Location	Measurement Method
Char	Primary and secondary Char pots, transition pipe	Mass Difference
Char	Reactor and coating on fluidising sand	Mass Difference
Char	Bio-oil	Solid contents determination
Char	Liquid Hold up in quench	Evaporation of ethanol washings
Reaction Water	Liquid Products	Karl Fischer Titration
Reaction Water	DIC liquid	Karl Fischer Titration
Reaction Water	Liquid Hold up in quench	Evaporation of ethanol washings
Organic liquids	Liquid Products	Mass of total Liquids ó Mass of Water in total liquids-Mass of char in total liquids
Organic liquids	Liquid Hold up in quench	Evaporation of ethanol washings
Gas	Vent System	Volume from Gas Meter and Gas Chromatography

The assumptions made as regards the calculation of a mass balance include

- All the char is recovered from the reactor when using the vacuum cleaner

- Any mass increase in the pipework is solely attributed to the presence of char. This is reasonable as the linking pipework is heated to 425 ºC during experiments reducing the possibility of any condensation to occur.

- The separation of the mass of the oil collected from the oil collection tank is efficient and sufficiently accurate to an extent that minimal quench liquid is present in the oil product. (Not mixed with isoparrafin).

- The washing of the quench column with ethanol is efficient enough to remove all the organic liquids and char retained by the quench unit.

6.4.7 Quenching system problems and modifications

6.4.7.1 Nature of problem

The commissioning of the quench unit was not without its problems. The holes on the plates of the quench column were initially 2 mm in diameter. With 6 holes on each plate, an open area of about 4.7% was on the surface of each plate. The size of the holes meant that the quench column was liable to flooding at high liquid flowrates. If the liquid flowrtate in the window area was high, the quench liquid was unable to cascade down the column quickly enough. This resulted in the flooding of the column. In altering the liquid flowrate to a lesser value, the problem of insufficient cooling arose from inadequate quench liquid contacting the vapours. This led to restricted operation of the quench since the only variable that could be altered was the quench liquid flowrate. The vapour residence time was controlled by the fluidising gas flowrate and could not be altered. A direct consequence of insufficient cooling is depicted in Figures 6-15 and 6-16. The photographs were taken after experiments using the quench column.

Figure 6-15 Fouling due to inefficient quenching
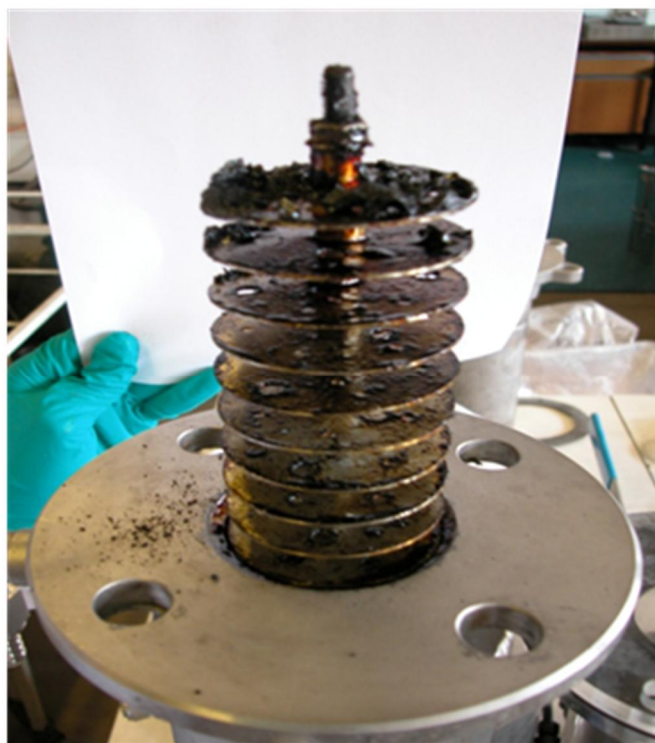
Figure 6-16 Heavy tars collection in quench column

6.4.7.2   Modifications to quench system

To reduce the likelihood of flooding, the open area of the quench plates was increased by machining the diameter of the holes in the quench plates to a larger diameter (3 mm). This allowed for easier flow of the quench liquid down the column while operating at desired flowrates. The likelihood of flooding was significantly reduced following the modifications. The larger diameter holes allowed for the easier cascading of the quench and pyrolysis liquids down the column.

Finally, it was noticed that the flat bottom of the oil collection tank made it was difficult to drain the oil product. The oil collection tank was modified based on design drawings developed during the early stages of this research. The new design as depicted in Figure 6-17 incorporated a pyramidical bottom for the oil collection tank. This meant the oil collected at the bottom of the tank at an angle of 60º. This facilitated easier draining of the liquid product aided by gravity. It completely removed the need for tilting of the unit as earlier practiced. Figure 6-18 also shows a digital photograph of the bottom of the quench column after the modification.

Figure 6-17 Dimensional drawings of modified quench column

Figure 6-18 Photograph of quench column after modification

6.4.8 Reactor heating problems and modifications

Section 6.4.4 highlighted the failure in getting the reactor to pyrolysis temperature using the initial band heaters. The heaters were three 250 W Watlow band heaters as shown in Figure 6-19.

Figure 6-19 Initial reactor heaters

6.4.8.1 *Nature of the problem*

The band heaters for the reactor heating to pyrolysis temperature were prone to absorbing moisture. Frequent short circuits were noticed in the early parts of testing the rig. The first step taken to circumvent the problem was to dry the band heaters in an oven at 105 ℃ prior to operation. This step proved to be partially successful as the heaters still failed after a couple of minutes of operation.

6.4.8.2 *Modifications to reactor heating system*

The original band heaters were never able to get the reactor to pyrolysis temperature even after numerous attempts. The decision was then taken to replace the band heaters. The ineffective band heaters were replaced by two Watlow ceramic knuckle band heaters with a power rating of 500 W and 850 W respectively as shown in Figure 6-20. These heaters were more powerful. They were however of a bigger diameter than the replaced heaters. As a

consequence, they did not fit the reactor. This necessitated further modifications in order to fill the void between the reactor and the new band heaters.

Figure 6-20 Replacement ceramic knuckle Watlow band heaters

A two part cylindrical steel jacket was built by the Mechanical Engineering Laboratory at Aston University based on design drawings developed and submitted. These two part jacket was for the upper section of the reactor. Another single cylindrical steel jacket was designed for the bottom section of the reactor. These fabrications were able to fill the void between the reactor and the new band heaters. Detailed dimensional drawings of the steel jackets are shown in Figure 6-21 and 6-22. Figure 6-23 shows a photograph of the top steel jackets after fabrication.
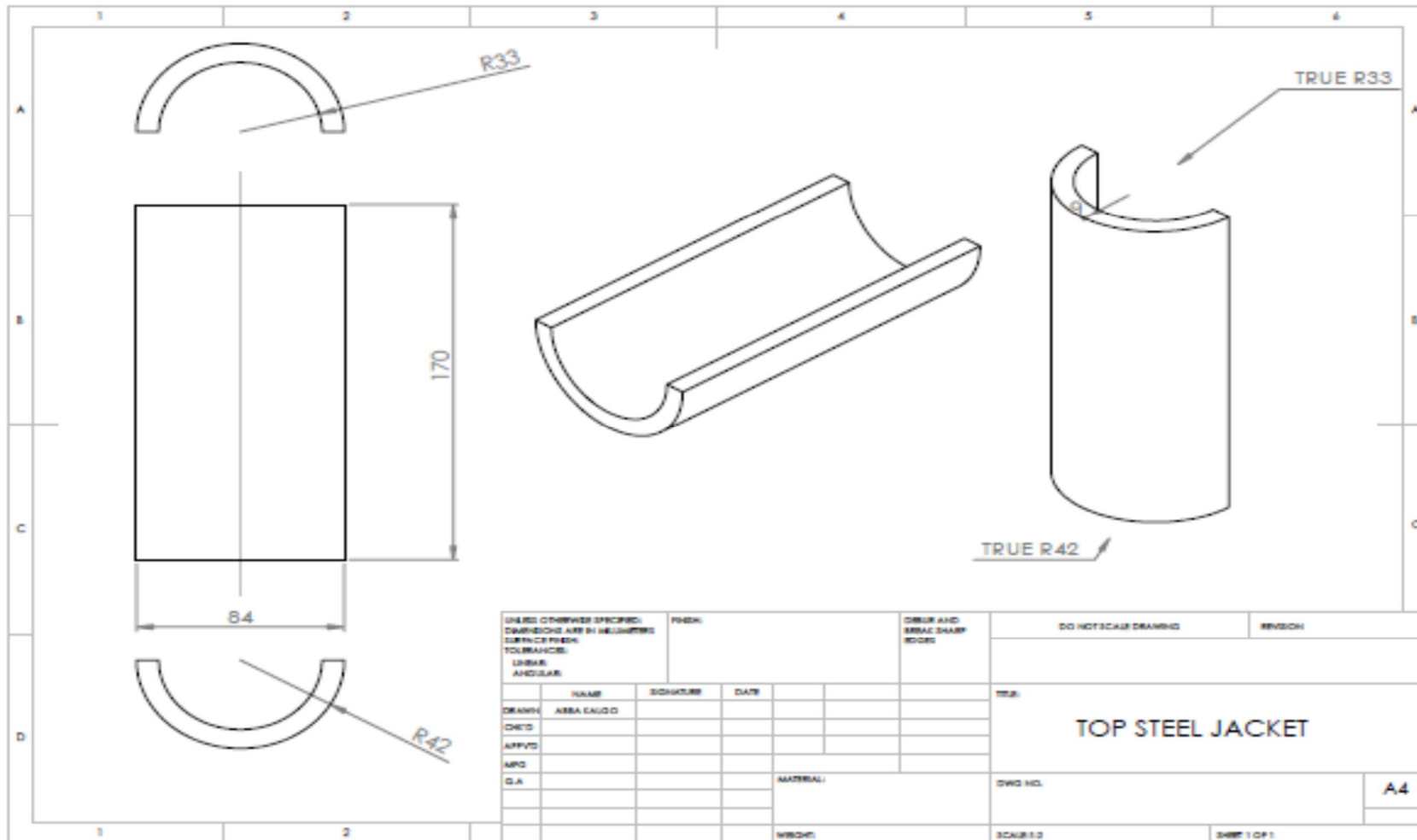
Figure 6-21 Dimensional drawings of top steel Jackets
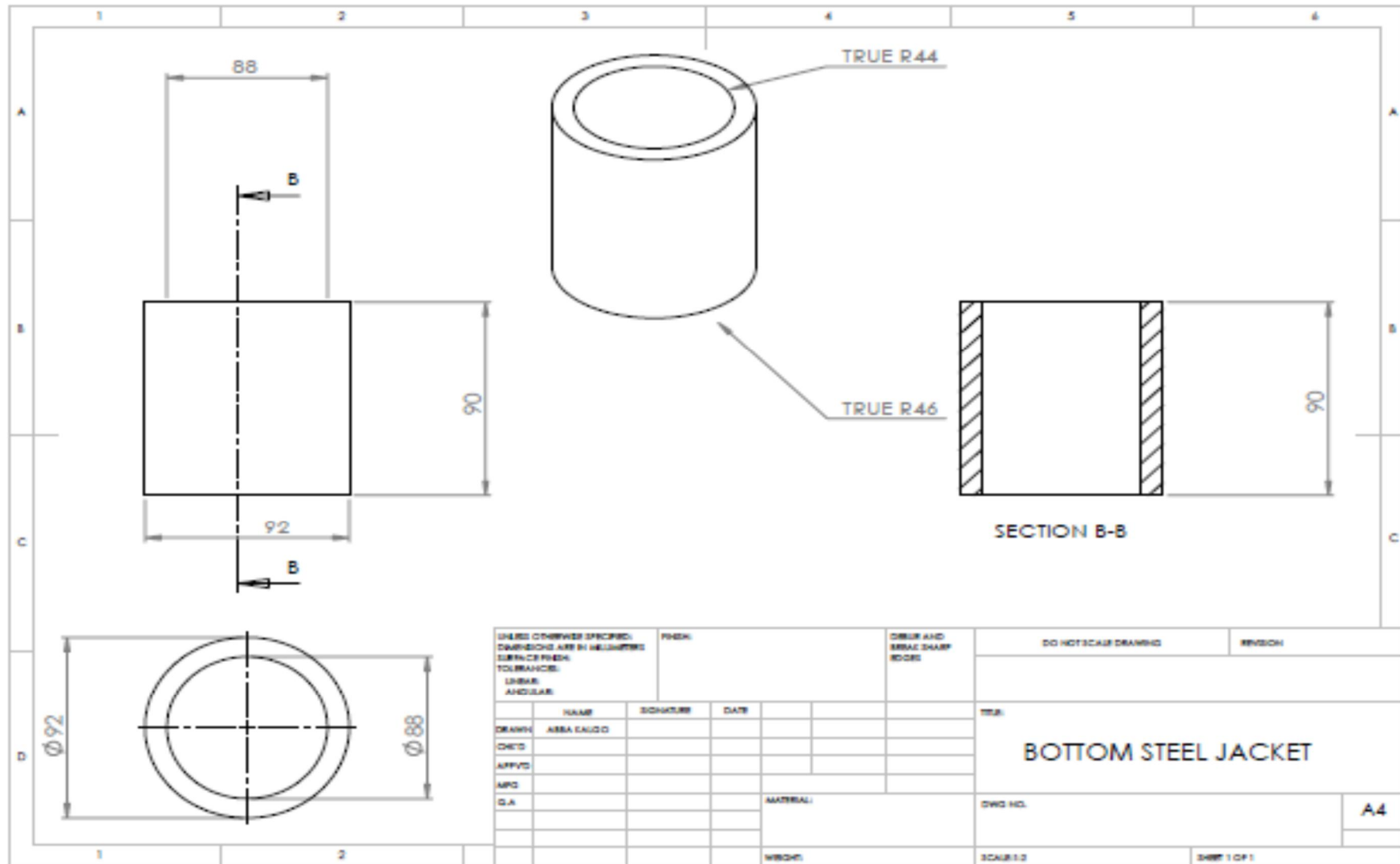
Figure 6-22 Dimensional drawings of bottom steel jacket

Figure 6-23 Photograph of steel jacket after fabrication

After installation of the steel jackets and the new band heaters, the modified heating system of the reactor was tested and operated successfully. Figure 6-24 shows the heating profile of the reactor with the modified heating system. It shows the reactor capable of reaching pyrolysis temperature within 70 minutes from the commencement of heating. A nitrogen flowrate of 6 l/min ($0.5U_{mf}$) was passed through the reactor. The mass of fluidising medium (sand) for this test was 300 g.
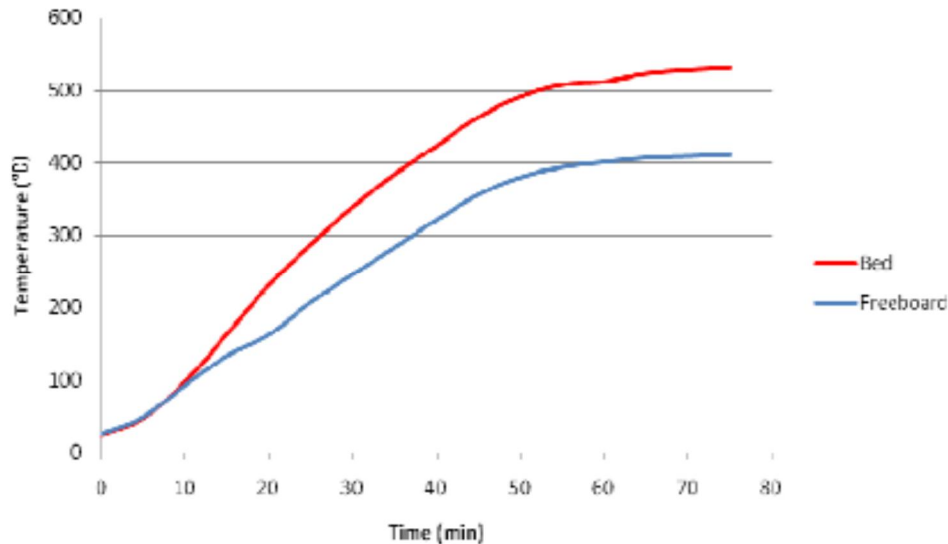
Figure 6-24 Reactor heating profile with modified heating system

6.5 SUMMARY

At this stage of the research, one of the primary objectives of the study had been met with the commissioning of the individual sections of the fast pyrolysis unit. The feed system, reactor system and liquid collection unit had all been put in working order. They were also confirmed to be capable of operating under fast pyrolysis conditions. The feed system has also been commissioned. A calibration method for the feed system has also been developed. A mass balance calculation method has also been developed over the complete unit.

7 FAST PYROLYSIS EXPERIMENTS ON 300g/hr RIG

The work described in this chapter reports 3 series of experiments. The first being the commissioning experiments using 4 different feedstocks. The second series of experiments investigates the impact of different particle sizes on the pyrolysis process. The final set of experiments explores the impact of temperature on process yields from the primary feedstocks. The chapter goes further to identify and discuss the post commissioning problems discovered during these experiments.

7.1 INTRODUCTION AND PARAMETERS FOR INVESTIGATION

Work undertaken so far has established that all the individual sections of the pyrolysis systems (feed system, reactor -solid collection system and the quench-oil collection system) are capable of operating under pyrolysis conditions. The next stage of the development of the pyrolysis system was to run the unit as a whole, under fast pyrolysis conditions.

As discussed in section 2.4 and 2.5, every fast pyrolysis process is dependent on a number of process variables including the feedstock and other process parameters. Table 7-1 gives a list of process parameters and variations possible for investigation using the commissioned process.

Table 7-1 Parameters for investigation

Parameter	Possible variation
Feed type	Beech, Pine, Miscanthus, Willow, Moringa (African and Indian), Jatropha (African and Indian)
Reaction Temperature	400-550 °C
Feed Particle size	0-1250µm
Feed moisture content	0-20 wt%
Vapour residence time	Variable, Ö2 s

While the parameters listed as part of Table 7-1 are not in any way near exhaustive, they are parameters shown by a number of researchers to influence the fast pyrolysis process [7, 9, 44, 94, 99, 184, 185]. Not all the parameters included in Table 7-1 could be investigated because of time constraints and equipment demand. As such, the selected variables discussed below were selected for investigation.

7.1.1 Feed type

The 300 g/h unit was to be used by several different researchers with various feedstocks. It was decided to test a wide array of feedstocks including the primary ones. Beechwood, Pine, Willow and Miscanthus were chosen because of availability and published data for comparison of process yields.

7.1.2 Particle size

Section 2.5.2 reviewed the literature on the impact of particle size on the pyrolysis process. The investigation of the effects of particle size was to be carried out using Beechwood as the base case feedstock. One of the major drawbacks of the existing 150 g/h unit is its inability to process a wide range of feed sizes as reported by several researchers [12, 40, 181, 183, 186]. Runs reported by all the researchers have shown a limitation of particle size to under 500 µm. It became imperative that the capability of the commissioned unit to handle a wider feed size range be investigated. The focus was on particle sizes larger than 500 µm which is the size limit of the 150 g/h unit.

7.1.3 Temperature

As in the case of particle size, reaction temperature has been shown to be the key parameter that influences the process particularly in terms of product distribution ratios and yields [5, 9, 11, 79, 80, 148, 167, 187-191]. As part of investigating the suitability of the primary feedstocks as raw materials for fast pyrolysis, the impact of temperature on process yields and distributions were to be studied. Two of the primary feedstocks namely African Moringa and Indian Jatropha were selected as the feedstocks. The aim was to investigate the effect of pyrolysis temperature on product distribution, liquid yields and gas compositions. The chosen target reaction temperatures were 400, 450, 500 and 550 ºC.

7.2 HYDRODYNAMIC PARAMETERS

Section 3.9 introduced the theory of fluidisation. A waterloo bubbling fluidised bed for fast pyrolysis works on the ‑blow throughø principle to achieve a continuous process [192]. Theoretically, the differences in particle sizes and densities mean that it is possible to blow out most of the char and any unreacted biomass particles while retaining the sand bed as the heat transfer medium in the reactor. Mathematically the successful operation of a bubbling fluidised bed for a fast pyrolysis processes should meet the criteria of equation 7-1.

$$\leq \qquad > \qquad > \qquad\qquad\qquad \textbf{Eq } 7\text{-}1$$

Where

U$_0$ is the operating velocity

Ut$_{sand}$ is terminal velocity of smallest sand particle

Ut$_{char}$ is Terminal velocity of largest char particle

Ut$_{biomass}$ is Terminal velocity of largest biomass particle

Also, from literature, the operational velocity of a bubbling bed should equal or be greater than $4U_{mf}$ [12, 193, 194] as shown in equation 7-2

$$\geq 4 \qquad\qquad\qquad \textbf{Eq } 7\text{-}2$$

The U_{mf} in this case would be that of the fluidising medium (sand) since the assumption is that the concentration of other reactor contents i.e. char would be significantly less than the sand as the fluidising medium such that

$$\gg \qquad\qquad\qquad \textbf{Eq } 7\text{-}3$$

Where

G_s is the flowrate of sand which should remain constant assuming there is no entrainment of sand from the reactor. G_{char} is the flowrate of char which should be continuously ejected from the reactor.

Additionally, the initial mass of sand to be used as the start of any experiment is obtained using the research group standard where the mass of fluidising medium is selected to be the same as the hourly nominal reactor throughput. For example, during experiments using the 1 kg/h unit, 1 kg of sand is used as the mass of fluidising medium in the reactor [40, 97, 181]. For a run on the 150 g/h unit, 150 g of sand is used [12, 117, 151, 181-183]. The same principle was thus applied to the commissioned reactor. Such that the mass of fluidising medium at the start experiments was selected to be 300 g of sand. No published literature to back up the amounts of sand used initially in the reactors has been found. Using such ratios will however lead to more predictable hydrodynamics of reactor contents. For example in a reactor processing 300 g/h of biomass, the flowrate of char in the reactor would be 0.4166 g/s assuming a worst case scenario where the residence time of a char particle is 5 seconds. Based on the example given, even for a ratio of char to sand particles of 0.4166:300, the

hydrodynamics of the bed may be calculated based on the physical properties of sand alone. The bed can be assumed to be homogenous because of the very low ratio of char to sand.

Table 7-2 gives the physical properties of the bed material (sand), Beechwood and char. Beechwood was selected as the commissioning feedstock. These calculations were to estimate the operational parameters of the reactor at pyrolysis reaction conditions.

Table 7-2 Commissioning data for hydrodynamic calculations

Particle	Particle Density (kg/m³)	Bulk Density (Kg/m³)	Voidage
Sand	2670	1650	0.4
Beechwood	680	300	0.6
Char	300	180	0.6

Table 7-3 gives the empirically determined fluidising properties of sand and Beechwood at pyrolysis reactor conditions. The data was obtained using correlations introduced in the latter parts of chapter 3.

Table 7-3 Calculated hydrodynamic parameters for Beechwood and sand

Parameter	unit	Sand (min)	Sand (Avg)	Sand (max)	Beech (min)	Beech (Avg)	Beech (max)
Particle Diameter	(µm)	355	427	710	355	427	1250
Particle Density	(kg/m³)	2670	2670	2670	780	780	780
Minimum Fluidising velocity	(m/s)	0.11	0.15	0.21	0.01	0.02	0.03
Terminal Velocity	(m/s)	3.52	4.24	4.96	1.42	1.70	1.99
Reynolds number at U_{mf}	-	2.31	4.02	18.50	0.16	0.29	7.34
Reynolds number at terminal velocity	-	4.19	5.11	8.51	1.60	2.10	7.26

Notes (a) Parameters calculated using nitrogen as fluidising gas with the following properties Density=0.442kg/m³, Viscosity = $2.821*10^{-5}$ kg/ms. Gas properties at 500 ºC

7.3 COMMISSIONING EXPERIMENTS (CR-300-001-CR-300-004)

A total of four commissioning experiments involving different feedstocks were carried out. These experiments have been detailed as the commissioning experiments. The feedstocks used were Beechwood, Pine, Willow and Miscanthus. Table 7-4 gives an overview of the process parameters for the experiments.

Table 7-4 Experimental Parameters for commissioning experiments

Run No	unit	CR-300-001	CR-300-002	CR-300-003	CR-300-004
Feedstock		Beech	Pine	Willow	Miscanthus
Run Duration	minutes	55	95	35	65
Target Reaction Temperature	(℃)	500	500	500	500
Feed Particle size	(µm)	<1250	355-500	355-500	355-500
Bed Particle size	(µm)	600-850	355-500	355-500	355-500
Fluidising gas Flowrate	(l/min	48	24	18	18

7.3.1   CR 300-001 (Beechwood)

Run CR300-001 was the first pyrolysis run carried out on the 300 g/h unit operating as a whole. The primary aim of run CR 300-001 was to observe the behaviour of the individually commissioned sections of the rig under fast pyrolysis conditions and bio-oil production.

The feed material for the run was beech wood of particle size 0-1250 mm. As the commissioning run, the parameters were set at the nominal designed throughput of the system. Feed rate was set to 300 g/h after calibration with the method described in section 6.4.2.1. The moisture content of the feed was 9.55 wt% and ash content was 1.0 wt%. The run lasted for 55 minutes of continuous feeding. The mass of sand as bed material was 300 g in line with research group methods.

A mass of 261.80 g was fed during the commissioning run. 89.77 g was determined to be char. The char value was determined by the increase in weight among the reactor contents, char-pots and transition pipes. Examination of the char-pots after the experiment showed that most of the fluidising medium from the bed had been entrained out of the reactor.

The char distribution showed that 96.28% of the process char was in the actual reactor with 2.23% distributed between the transition pipes and the char pots. The rest was contained in the oil products and other downstream equipment.

Also, the reactor contents contained some unreacted biomass particles that had fused with the fluidising medium indicating that the biomass feed rate was higher than the reactor could process.

By the end of the commissioning run, a number of conclusions could be reached. Oversized char clumps caused by the thermal decomposition of the biomass particles prior to reactor entry was present in the fluidised bed reactor. The fluidising gas flowrate of 48l/min which equated to $4U_{mf}$ for the particle size range used was deemed excessive. This was indicated by

the mass of sand in the char pots. 178.42 g of sand was recovered between the two char-pots of the system. This equated to more than 50% of the mass of fluidising sand placed in the reactor at the start of the experiment. That observation indicated high rates of entrainment of fluidising sand out of the reactor

Analysis of the run temperature profile of the fluidised bed and freeboard temperature showed behaviour uncharacteristic of a properly operating fluidised bed reactor (see section 7.6.2).

7.3.2   CR 300-002 (Pine)

Run CR 300-002 was the second commissioning experiments and the feedstock chosen for the experiment was Pine. The objective of the run was to explore the fast pyrolysis of pine using the commissioned 300 g/h unit to generate process yield data for comparison.

The run lasted 95 minutes at an average temperature of 513 ℃ over the experiment. Changes were made to the experimental parameters due to the excessive entrainment observed during run CR-300-001.The mass of fluidising medium was reduced to 150 g. The value of 150 g was chosen since the 300 g/h reactor was geometrically exact to 150 g/h unit reactor. The mass of sand used in that reactor for a standard run is 150 g. This meant a reduction in the initial bed height thus allowing more space in the reactor freeboard for bed expansion. The feed rate was also lowered as unreacted biomass in the reactor at the end of the experiment CR-300-001 indicated that the throughput into the reactor (300 g/h) was too high. The volumetric flowrate of fluidising gas was also lowered to 2.5 U_{mf} or 30 l/min of nitrogen in an attempt to reduce excessive entrainment of fluidising medium from the reactor.

At the conclusion of the run, 185.67 g of pine had been fed into the reactor. Mass balance analysis showed the 17.36 wt% of total feed was char, 23.45 wt% of biomass fed was gas and 43.36 wt% was liquids. Water generated during the experiment stood at 22.57 wt% while organic liquids were 25.79 wt% on dry basis.

Observations from the run included pre pyrolysis of biomass feedstock as in the first experiment. Entrainment of fluidising medium was evident from examination of the char-pots. 88 g of sand was recovered indicating that the fluidising gas flowrate used was still high enough to cause entrainment of bed material. The mass of fluidising medium entrained was determined by burning the contents of the char-pots at 900 ℃ in a muffle oven and weighing the remaining mass.

7.3.3 CR 300-003 (Willow)

The third commissioning run tagged CR 300-003 was a run involving willow as the feedstock. The objective of this run was to observe the behaviour of the fast pyrolysis unit while operating lower bulk density feedstock. The bulk density of the willow was found to be 290 kg/m^3. Again, the hydrodynamic parameters for this run had to be altered to mitigate the entrainment observed in Run CR 300-002. For this run, the fluidising gas flowrate was reduced to 18 l/min or 1.5 U$_{mf}$. The mass of fluidising medium was not altered however in order not to reduce the heat transfer occurring between bed material and biomass particles.

Mass balance analysis of this experimental run indicated that 29.66 wt% of the feed was converted into char. 33.89% was gaseous products while total liquid yields stood at 14.97 wt% of which 11.12 wt% was water on a dry basis. The high gas yield can be attributed to the high average pyrolysis temperature (586 ºC). This was due to the failure of the cooling water system around the feed system. This had been installed to reduce the extent of pre-pyrolysis observed during the first 2 commissioning runs. The run lasted 35 minutes.

Key observations during the run included intermittent feeding owing to bridge formation in the feed hop. The feeding resumed after operator intervention by application of external force on the hopper wall to collapse the bridges. This proved to be partially effective as bridge formation would occur again after a couple of minutes. This problem coupled with the failure of the make shift cooling system led to the eventual discontinuation of the run just. The bridging problem was deemed to be severe. The presence of fluidising medium in the char-pots observed during the first 2 commissioning runs did not occur during this experiment indicating that the fluidising gas flowrate was not high enough to entrain the sand from the reactor.

7.3.4 CR 300-004 (Miscanthus)

Experiment CR 300-004 involved the use of Miscanthus as the feedstock. The failure of run CR 300-003 which involved Willow was behind the decision to run the 300 g/h rig with a different low bulk density feed in this case Miscanthus. The bulk density of the Miscanthus was found to be 250 kg/m^3. The feed particle size for this run was 250-1000 µm.

Mass balance analysis showed that 84.80 g of Miscanthus was fed during the experiment. The product yields showed that 34.77 wt% of the feedstock on a dry basis was converted into liquids of which 23.82 wt% was water and 10.95 wt% was organic liquids. Char produced

over the entire run stood at 26.57 wt% while the product gas produced was 14.86 wt%. Total mass balance closure was 89.88 wt% of biomass on a dry basis.

Observations made during the run included intermittent feeding arising from bridge formation in the hopper. Operator intervention was required to collapse the bridges by application of external force to hopper wall to resume feeding. The intermittent feeding as a result of the bridging led to an alteration in the biomass feed rate from 90 g/h to 120 g/h. The average feed rate over the entire run was 84.80 g/h.

7.3.5 Results and discussions of commissioning experiments

Table 7-5 shows a complete summary of the mass balances obtained for the 4 commissioning runs using various feedstocks. The data in the Table also reports mass balance closures on the commissioning feedstocks from sources in literature for comparison purposes. For proper comparisons, the data obtained from this study and literature have been normalised.

Table 7-5 Mass balance overview for commissioning experiments

Experiment ID/Ref	Units	CR 300-001	QCOM-1-HYBRID	CR 300-002	SFB12 [12]	CR 300-003	141-06 [40]	CR 300-004	SFB 17 [12]
Feedstock		**Beech**	**Beech**	**Pine**	**Pine**	**Willow**	**Willow**	**Miscanthus**	**Miscanthus**
Particle size	(µm)	0-1250	355-500	355-500	355-500	355-500	250-350	250-1000	
Moisture content	(mf wt%)	9.55	9.55	10.17	10.04	8.25	7.76	4.81	8.46
Ash Content	(mf wt%)	0.97	0.97	0.97	0.23	0.97	1.34	1.79	3.16
Average Run Temperature	(°C)	504	503	512	505	586	515	502	493
Run duration	(minutes)	55	120	80	NA	35	60	40	NA
Average feed rate	(g/h)	285.60	100.2	82.62	80.0	122.40	62.59	130.46	89.0
Product Yields									
Liquids	(mf wt%)	**53.44**	**61.02**	**56.81**	**73.44**	**14.97**	**68.86**	**34.77**	**59.29**
Organics	(mf wt%)	40.16	52.41	43.36	66.64	3.85	52.93	10.95	51.68
Reaction water	(mf wt%)	13.28	8.61	22.57	6.80	14.97	15.93	23.82	7.61
Char	(mf wt%)	**19.71**	**10.57**	**19.68**	**11.03**	**29.66**	**20.92**	**26.57**	**19.40**
Gas	(mf wt%)	**11.48**	**28.41**[a]	**10.25**	**8.76**	**33.89**	**9.29**	**14.86**	**17.97**
Closure	(mf wt%)	**84.63**	**100.00**	**84.17**	**93.08**	**78.52**	**98.31**	**89.88**	**96.66**
<u>Normalised Yields</u>									
Liquids	(mf wt%)	**63.14**	**61.02**	**67.49**	**78.89**	**19.03**	**70.04**	**38.68**	**61.38**
Organics	(mf wt%)	47.45	52.41	51.51	71.59	4.90	53.89	12.18	53.46
Reaction water	(mf wt%)	15.69	8.61	26.81	7.30	19.06	16.20	26.50	7.87
Char	(mf wt%)	**23.28**	**10.57**	**23.38**	**11.85**	**37.77**	**21.27**	**29.56**	**20.07**
Gas	(mf wt%)	**13.56**	**28.41**[a]	**12.17**	**9.41**	**43.16**	**9.44**	**16.53**	**18.59**
Closure	(mf wt%)	**100.00**	**100.00**	**100.00**	**100.00**	**100.00**	**100.00**	**100.00**	**100.00**

Notes (a) Yield determined by difference, mf: moisture free

The first observation that can be made from the results with reference to the literature values is the low mass balance closures obtained for all four of the commissioning runs. The results show the actual mass balance closures to range between 84-89 % on a dry basis of fed biomass. An exhaustive and detailed discussion of the reason for the poor mass balance closures is given in section 7.6.2.3.

Similarly, it can be seen from the comparison of all mass balance results that organic yields from the commissioned 300 g/h unit experiments is significantly lower than values reported in literature for the concerned feedstocks. In the case of the beech wood run, yields were compared with run QCOM-1-HYBRID described in section 6.4.5.1. A hybrid configuration using the reactor system from the 150 g/h unit was used in conjunction with the commissioned quench unit of the 300 g/h unit. Results show that the char yield from the commissioned 300 g/h was nearly twice the value obtained from the beech run on the hybrid configuration. The total amount of liquids obtained from the 300 g/h unit was also lower than the liquid yield from the quench commissioning run. As highlighted in section 6.4.5.1 which reviewed the run QCOM-1-HYBRID, the gas analysis system was out of commission during the experiment and as such, gas yields were obtained by difference. The gas yield of the 300 g/h unit when compared to the yields from run QCOM-1-HYBRID was lower although the result from the run QCOM-1-HYBRID may not be an accurate representation of the actual yields since no gas analysis was made.

For the second commissioning run tagged CR-300-002 involving Pine as the feedstock pyrolysed, a comparison is made with work carried out by Hague [12] . Hague's run involved pine at 500 ºC on the 150 g/h unit.73.44 wt% representing total liquid yields on a dry basis. Organic yields from his work represented 66.64 wt% with reaction water being 6.80 wt%. The gas and char yields obtained from his work were 8.76 wt% and 11.03 wt% respectively with a mass balance closure of 93.08 wt% of total dry biomass fed. The pine run carried out during this research generated total liquid yields of 56.81 wt% on a dry basis with char and gas yields being 19.68 wt% and 10.25 wt% respectively on a dry basis. Of the total liquid yields from Run CR300-002, 43.36wt % was organic liquids while reaction water generated was 22.57 wt% of dry Pine. As was the case with the beech wood run, it can be seen that the mass of liquids obtained from the 150 g/h unit was significantly higher than the liquids generated during the run on the commissioned unit. It can also be seen from the distribution of organic and water yields that the 300 g/h unit tends to favour the formation of water during pyrolysis reactions. The amount of water generated from the 300 g/h was 3.6 times more than

the water generated from pyrolysis of pine on the 150 g/h unit published by Hague. The reason for this is discussed in section 7.6.2.2.

Fahmi [40] undertook the fast pyrolysis of Willow of particle size 250-350 µm for a duration of 60 minutes on the 150 g/h unit at an average pyrolysis temperature of 507 ºC. The Willow experiment from this research undertaken at an average temperature of 586 ºC for a duration of 35 minutes. As stated in the description and observations during experiment CR-300-003, the cooling mechanism of the reactor inlet failed during the experiment. This led to the abandonment of the experiment. The experiment had however, lasted long enough to attempt a mass balance calculation notwithstanding its premature end. Results from Fahmi's work show that a total liquid yield of 68.86 wt% was obtained on a dry basis of fed Willow. Of the biomass fed, 52.93 wt% was organic liquids while reaction water accounted for 15.93 wt%. Char yields were 20.92 wt% while gas yields 9.31 wt% of dry Willow. The mass balance closure was 98.31%. Run CR-300-003 from this study involving willow had a mass balance closure of 78.52%. This was the lowest closure from the commissioning experiments. Total liquid yields were 14.97 wt% of dry willow with char representing 29.66 wt%. Of the fed willow, only 3.85 wt% was organic liquids with the remainder of the liquids being water generated during pyrolysis reaction. The gas yield equated to 33.89 wt% which can be attributed to the high average temperature of the experiment which was 586 ºC.

Miscanthus sinensis was used as feedstock for run CR-300-004. It has been compared with published work by Hague [12]. The variant of Miscanthus used by Hague was Miscanthus sinensis. Mass balance results show strong variations in the ratio of pyrolysis products generated. The char yields from the Miscanthus run showed it to be 26.57 wt%. Hague reported char yields of 19.40 wt% on a dry basis. The biggest variation in results can however be seen in the yields and distribution of total liquids, organic liquids and reaction water. The work reported by Hague shows total liquid, organic yields and reaction water to be 59.29 wt%, 51.68 wt% and 7.61 wt% respectively. Experiment CR-300-004 shows total liquids, organic liquids and reaction water yields to be 34.77 wt%, 10.95 wt% and 23.82 wt% respectively. It can be seen from this comparison that the yields and ratio of distribution of pyrolysis products from the commissioned unit vary significantly in the case of Miscanthus. The gas yields when comparing the results show that higher gas yields were obtained from the experiment reported by Hague. The reader is referred to section 7.6.2.2 where the causes of these variations in yields and product distribution of pyrolysis products are exhaustively discussed.

7.4   SIZE INVESTIGATION EXPERIMENTS

The initial aim during the planning of the experiments tagged SIR was to investigate the impact of particle size on the process yields and product distribution using Beechwood. They became more necessary however, with the unexpected bridging and pre pyrolysis problem observed during the commissioning experiments. A second need for the experiments consequently arose. It became necessary in addition to the initial aim of investigating the impact of particle size on product yields, to observe if a variation in feed particle size could improve the bridging and pre-pyrolysis problem encountered during the commissioning experiments.

7.4.1   SIR 300-001 to SIR 300-004 (Beechwood)

Table 7-6 gives an overview of the mass balances calculated on the four experiments carried out with varying feed sizes. The particle size experiments were carried out using beech wood as the feedstock. The particle sizes investigated were in the range 355-500 µm, 600-850 µm, 850-1250 µm and 0-1250 µm.

Table 7-6 mass balance summary for SIR experiments

Run No	unit	SIR 300-001 (CR-300-001)	SIR 300-002	SIR 300-003	SIR 300-004
Feedstock		**Beech**	**Beech**	**Beech**	**Beech**
Particle size	µm	0-1250	355-500	600-850	850-1250
Moisture content	wt %	9.55	9.55	9.55	9.55
Ash Content	mf wt%	0.97	0.97	0.97	0.97
Average Run Temperature	°C	504	512	507	506
Vapour residence time	s	0.68	0.73	0.61	0.66
Feed rate	g/h	85.74	84.94	86.46	83.94
Run Duration	minutes	75	60	60	60
Product Yields					
Liquids	mf wt%	**53.44**	**57.47**	**55.52**	**52.17**
Organics		40.16	43.88	41.51	38.33
Reaction Water		13.28	13.59	14.01	13.84
Char	mf wt%	**19.71**	**21.05**	**22.49**	**26.54**
Gas	mf wt%	**11.48**	**10.16**	**10.58**	**8.83**
CO_2	Vol %	58.55	55.62	59.58	61.19
CO	Vol %	35.22	38.49	34.33	31.39
CH_4	Vol %	3.65	3.31	3.70	4.84
H_2	Vol %	1.01	1.07	1.10	1.18
C_2H_4	Vol %	0.44	0.42	0.31	0.45
C_2H_6	Vol %	0.33	0.35	0.32	0.27
C_3H_6	Vol %	0.43	0.36	0.30	0.31
C_3H_8	Vol %	0.37	0.38	0.36	0.37
Closure		**84.63**	**88.68**	**88.59**	**87.54**

Note: SIR 300-001 same as CR-300-001

7.4.2 SIR observations, results and discussions

7.4.2.1 *Mass Balance, product yields and distribution*

The series of experiments tagged SIR were conducted at a target pyrolysis temperature of 500 °C which has already been determined by Sitzmann and Salter [97, 117] to be the temperature at which maximum liquid yield from Beechwood is obtained. Flowrate of the fluidising gas through the reactor was limited to 18 l/min. That value equated to about 1.5 U_{mf} of the sand bed. The feed rate of the system was kept between 85-90g/h for all the experiments. For the size investigation runs, the first in the series of commissioning runs, CR-300-001 earlier reported in section 7.3.1 was also taken as the first of this series. The particle size range for CR-300-001was between 0-1250 µm of Beechwood and the target reaction temperature was 500 °C. Three further runs were undertaken with particle sizes 355-500, 600-850, 850-1250 µm.

Figure 7-1 shows the distribution of pyrolysis products from Beechwood as a function of particle size range at a target reaction temperature of 500 ºC
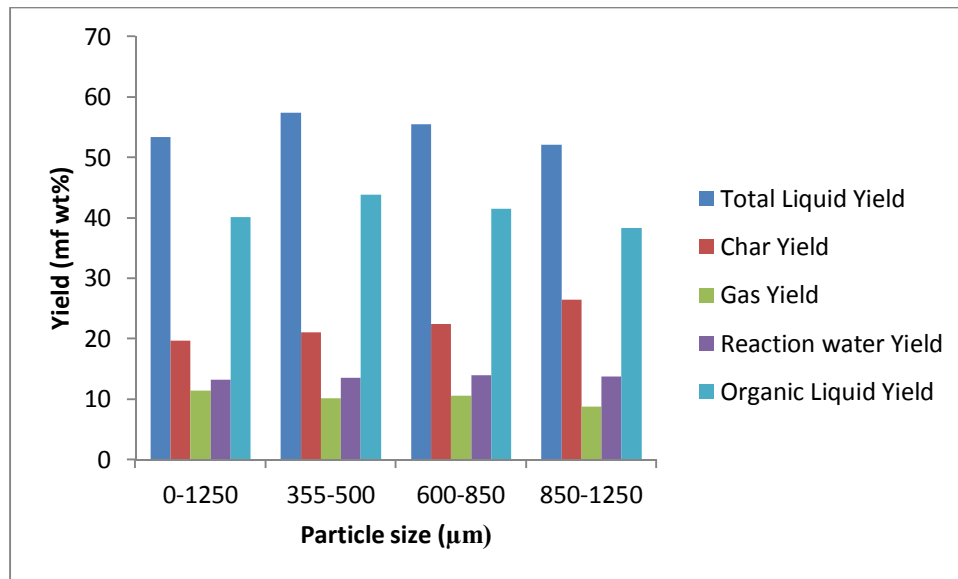
Figure 7-1 Pyrolysis product distribution as a function of particle size

Like the commissioning experiments, the mass balance closures for this series of experiments show closures to be between 84-89% of moisture free Beechwood. The reasons for the low mass balance closures are reviewed in section 7.6.2.3. As can be seen from the Table 7-6 and Figure 7-1, maximum total liquid yields and the maximum organic liquid yield of 57.47 wt% and 43.88 wt% were obtained from experiment SIR-002 where particle size was 355-500 µm. The results also show similarities in pyrolysis product yields between runs SIR-300-002 and SIR-300-003. The total liquid yields and gas yields were very similar for the two runs with SIR-300-003 producing slightly more char than the SIR-300-002.

The mass balance results for run SIR-003 showed slight variations between product yields and run SIR-002 from which maximum liquid and organic yields were obtained. While similar values for total liquid yields were reported for both experiments, the major discrepancy was in the yield of organic liquids where the run involving the smaller particle (355-500 µm) size range gave a higher organic yield than the run for the larger particle size (650-800 µm). Run SIR-300-003 when compared to SIR 300-002 also seemed to generate more water at the expense of organic liquids.

Results from run SIR300-004 which involved feeding beech of particle size 600-850 µm showed that it gave the lowest yield total liquids as well as of organic liquids when compared to the other experiments. This is not a surprising finding as previous results from studies in

literature have shown a trend between increasing particle size and lower organic liquid yields [195-197].

No clear trend was visible between varying particle size and reaction water generated during the experiments although it can be seen that the amount of water generated during all the experiments were between 13-14 wt% of moisture free Beechwood.

Regarding char yields from all the experiments, a trend can be seen between increasing particle size and an increase in process char yields. Again, this result is not unexpected as a number of studies published of different biomass feedstocks suggest a link between increasing particle size and an increase in the yield of char during fast pyrolysis [48, 196, 197].

An unexpected trend was noticed however from the results of the SIR experiments. This can be seen when the process gas yields are taken into account. While the results from SIR-002 and SIR-003 gave similar yields of gas i.e. 10.16 and 10.58 wt% respectively, experiment SIR-004 with the largest particle size of 850-120 µm gave a gas yield of 8.83 wt%. This result is unexpected because a higher char yield is in theory supposed to increase the extent of cracking of organic vapours into non condensable gases. While it cannot be said for certain what the cause of this unexpected decrease in gas yield is, the less than optimal operating conditions in the fluidised bed reactor may be responsible for this trend. As postulated by Bridgwater and Chen et al [7, 198, 199], fast pyrolysis is a series of complex reactions taking place simultaneously and in series. The exact mechanism of products generation cannot be explained with certainty.

Overall, it can be concluded that particle size does not play a significant role in product yields and distributions for particles under 1250 µm because the difference in yields across the runs can be considered as insignificant. This conclusion is however not robust. The pre-pyrolysis problem (see section 7.6.2) will most likely have played a part in the process yields.

7.4.2.2 *Impact of particle size on solid and water of pyrolysis liquids*

It was not part of the objectives of this research to characterise any product from the commissioning feedstocks. A complete mass balance could however not be obtained without the calculation of water content and solid contents of the bio-oil product generated. Thus, the data could be used to show the impact of particle sizes on the solids and water contents of liquids. Figures 7-2 and 7-3 char and water content based on the initial particle size. The

comparisons include data on run QCOM-1-HYBRID reviewed in section 6.4.5.1 where Beechwood was used.
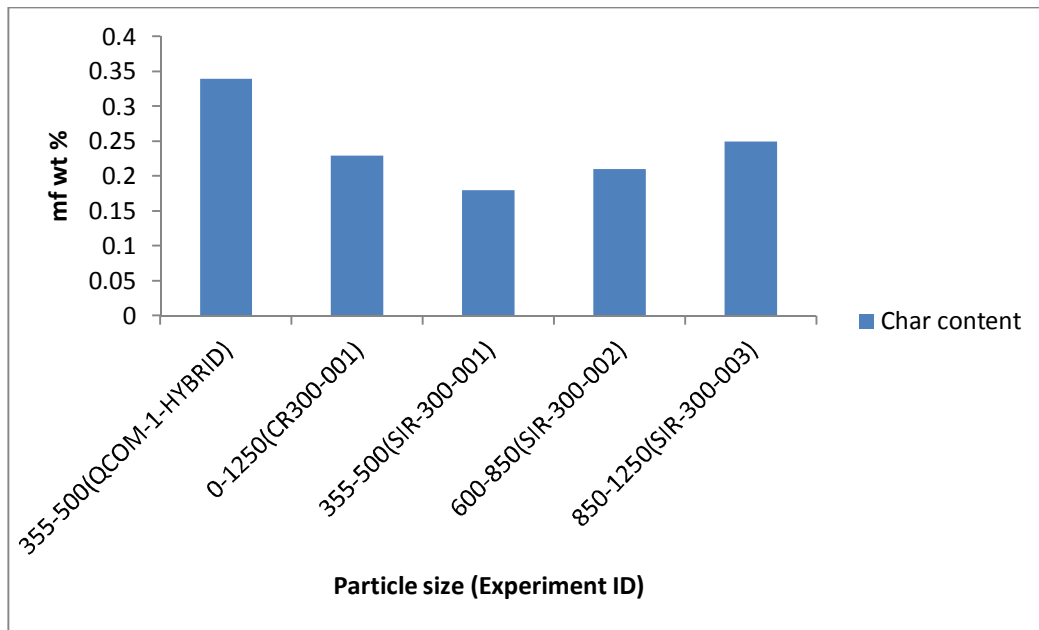
Figure 7-2 Bio-oil solid content as a function of particle size
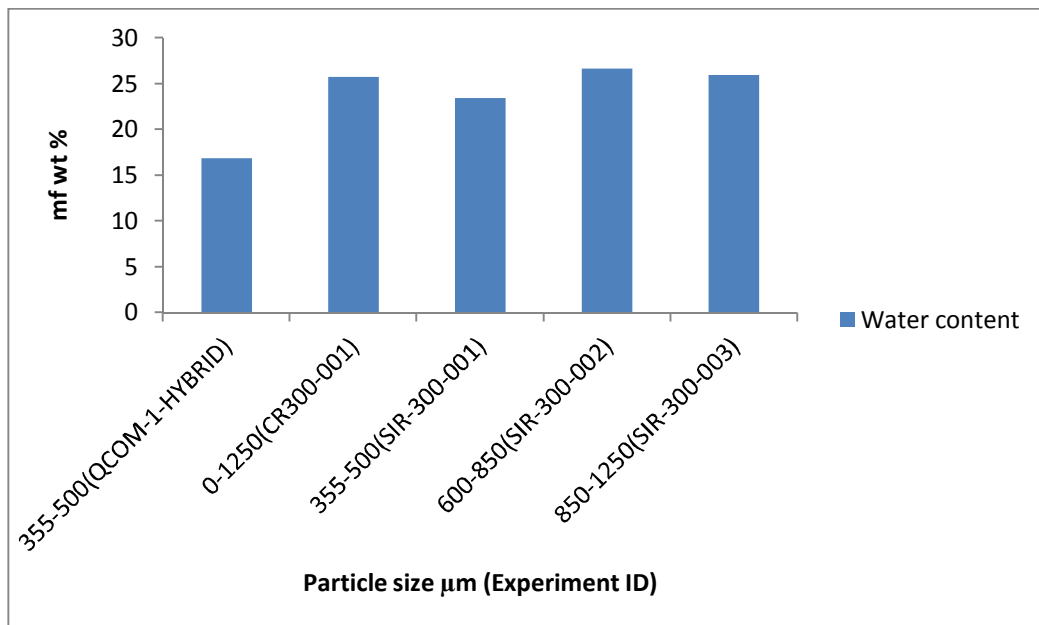
Figure 7-3 Bio-oil water content as a function of particle size

It can be seen from Figure 7-2, that the solid contents from the quench commissioning run QCOM-1-HYBRID was highest (0.34mf wt%.) when compared to oil from the other runs. This is due to the configuration used for the run. The 150 g/h unit reactor has only one cyclone attached to it making the solids separation less efficient. It increases the likelihood of solids carry-over into the quenching system. When comparing solid contents of bio-oil form

the other runs that used the main configuration of the 300 g/h unit, it is shown that oil from run SIR-300-001 where the particle size was 355-500 µm, gave the least amount of solid in the main oil product (0.18 mf wt%). Overall, it can be seen that oil from the main configuration had less solids than the run QCOM-1-HYBRID. This is also as a result of the pre-pyrolysis (see section 7.6.2.3) where biomass particles fuse together impacting on the amount and rate of removal of char.

Figure 7-3 shows the relationship between particle size and water contents of produced oils. Oil from run QCOM-1-HYBRID had lower water content than all the runs carried out using the main configuration. It is believed that the presence of high amounts of char in the reactor as a result of pre-pyrolysis (see section 7.6.2.1) was favouring water forming reactions during pyrolysis. This caused the water content of oils from the main configuration to be higher. As was the case with the solid contents, the run with particle size 355-500 µm gave the least amount of water in the bio-oil product amongst experiments that employed the main configuration.

Observations were also made during these sets of experiments as per the bridging problem observed during runs CR-300-003 and CR-300-004. Whereas the feeding was intermittent for those runs due to the bridges formed, these series of experiments showed the feeding was continuous for all the particle sizes investigated. This helped to reach a conclusion that the bridging problem is dependent to a large extent on the kind of feedstock being processed.

7.5   TEMPERATURE INVESTIGATION EXPERIMENTS

The results from the commissioning runs and particle size experiments using the 300 g/h unit were all characterised by low mass balance closures, and poor system operation. At this time, the decision had already been taken that a redesign of the process feed system would be necessary to improve and optimise the operation of the unit. It was reasoned however, that although the process in its operational state was less than optimal, the effects of temperature on the primary feedstocks i.e. Jatropha and Moringa could be studied. This was possible if all other process variables were kept constant and could be replicated over a series of experiments. The only variation was to be the process temperature. To study the effect of temperature on the primary feedstocks, a total of 8 experiments were performed on two of the primary feedstocks. They were African Moringa and Indian Jatropha. The choice of the primary feedstocks was dictated by availability at the time. An unexpected delay had occurred in obtaining African Jatropha from its suppliers. This ruled it out as a candidate for

the experiments. The decision to exclude Indian Moringa from these set of runs was taken because experimental attempts at running the system with the feedstock as part of supervision of an MENG project were problematic. The bridging problem already highlighted from the commissioning runs was very severe with the Indian Moringa feedstock. As a result, African Moringa and Indian Jatropha were selected as the feedstocks to be used for studying the effect of temperature on process yields of the primary feedstocks.

7.5.1   TIR 300-001 to TIR 300-008 (African Moringa & Indian Jatropha)

For the experiments TIR 001-008, the intended parameters for variation were the pyrolysis reaction temperature and the feedstock. They were to be subjected to fast pyrolysis in the commissioned unit at target pyrolysis temperatures of 400, 450, 500 and 550 ºC. The primary aim of these sets of experiments was to investigate the impact of temperature on the yields of pyrolysis products. The second aim was to determine the optimum pyrolysis temperature for maximum total liquid and maximum organic liquid yield for the feedstocks.

Table 7-7 details an overview of the process parameters, product yields, product distributions and mass balance closure results obtained from the experiments.

Table 7-7 Mass balance summary for TIR experiments

Run No	unit	TIR 300-001	TIR 300-002	TIR 300-003	TIR 300-004	TIR 300-005	TIR 300-006	TIR 300-007	TIR 300-008
Feedstock		African Moringa	African Moringa	African Moringa	African Moringa	Indian Jatropha	Indian Jatropha	Indian Jatropha	Indian Jatropha
Particle size	(µm)	355-849	355-849	355-849	355-849	355-849	355-849	355-849	355-849
Moisture content	(wt%)	6.19	6.19	6.19	6.19	8.07	8.07	8.07	8.07
Ash Content	(mf wt%)	5.53	5.53	5.53	5.53	9.26	9.26	9.26	9.26
Target Run Temperature	(°C)	400	450	500	550	400	450	500	550
Residence time	(s)	0.64	0.72	0.76	0.73	0.69	0.76	0.76	0.72
Feed rate	(g/h)	90.00	90.00	90.00	90.00	90.00	90.00	90.00	90.00
Run Duration	(Minutes)	60	60	60	60	60	60	60	60
Product Yields									
Liquids	(mf wt%)	**46.81**	**50.96**	**55.43**	**52.37**	**47.63**	**46.70**	**52.29**	**50.82**
Organics		36.63	37.36	38.47	38.15	30.22	31.10	35.72	38.70
Reaction Water		10.18	13.60	16.96	14.22	17.41	15.60	16.57	12.12
Char	(mf wt%)	**30.23**	**27.19**	**25.78**	**24.59**	**28.57**	**28.65**	**26.80**	**25.88**
Gas	(mf wt%)	**14.49**	**11.34**	**10.61**	**13.13**	**12.41**	**14.19**	**12.16**	**14.16**
CO_2	%vol	68.11	63.27	61.97	61.75	64.51	61.21	59.68	58.44
CO	%vol	26.53	31.81	32.78	34.18	29.67	32.92	33.41	35.44
CH_4	%vol	2.48	2.37	2.51	1.44	2.37	1.84	1.76	1.51
H_2	%vol	1.83	1.07	1.03	1.30	0.95	1.29	1.58	1.45
C_2H_4	%vol	0.79	0.81	0.77	0.54	1.10	0.89	1.08	1.19
C_2H_6	%vol	0.06	0.13	0.37	0.31	1.03	0.22	0.86	0.43
C_3H_6	%vol	0.11	0.42	0.22	0.20	0.86	0.99	0.84	0.76
C_3H_8	%vol	0.09	0.12	0.35	0.28	0.37	0.64	0.79	0.78
Closure		**91.53**	**89.49**	**91.82**	**90.09**	**88.61**	**89.54**	**91.25**	**90.86**

Mf: moisture free

7.5.2 TIR results, observations and discussions

7.5.2.1 *Mass balance, product yields and distribution*

Mass balances were calculated to observe the effect of temperature on the process yields. As explained in section 6.4.6 where the mass balance calculation was explained, liquid yield was determined primarily by gravimetric measurements. The gas yields were obtained from the gas volume and the gas composition obtained from the Gas Chromatograph. Char yield was also determined by mass differences. Figure 7-4 and 7-5 shows the distribution of pyrolysis products at temperatures of 400, 450, 500 and 550 ℃ for African Moringa and Indian Jatropha respectively.
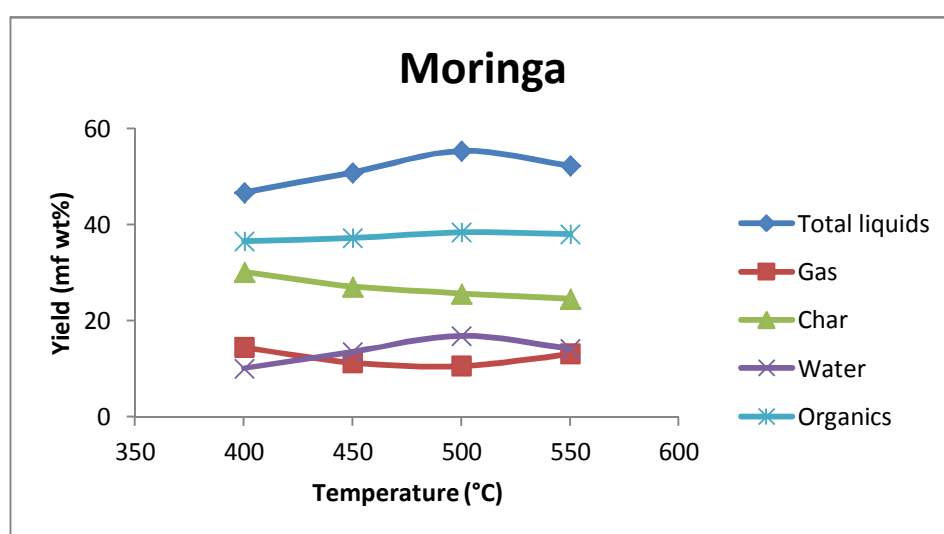
Figure 7-4 Moringa Pyrolysis product distribution as a function of temperature
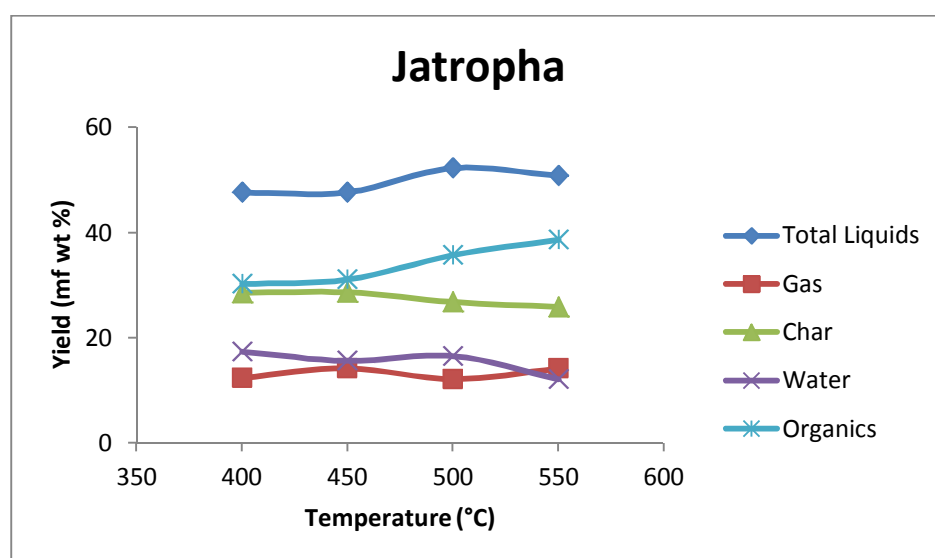
Figure 7-5 Jatropha pyrolysis product distribution as a function of temperature

For both African Moringa and Indian Jatropha, the maximum liquid yield was obtained at a pyrolysis temperature of 500 ℃. Maximum organic yield for Moringa was also obtained at 500 ℃. The results show however, that in the case of Jatropha, the optimum temperature for generating organic liquids is 550 ℃ even though maximum liquid yield was obtained at 500 ℃. Organic yields from Moringa were higher than that of Jatropha over the entire temperature range which can be attributed to its higher volatile matter (section 5.2.1). The effect of temperature on the yield of water in the bio-oil product is more pronounced in the case of Moringa than Jatropha. Figure 7-4 shows that there was an increase in reaction water yield for the Moringa experiments over the temperature range between 400-500 ℃ before a slight decline at 550 ℃. For Jatropha reference is made to Figure 7-5. The yield of water varied between 17.41 wt% at 400 ℃ and 12.12 wt% at 550 ℃. The lowest water yield for Jatropha was recorded at a pyrolysis temperature of 550 ℃

Analysis of the product gases for both feedstocks show them to be mainly composed of CO and CO_2. C_1-C_3 hydrocarbons and H_2 were detected in much smaller quantities than CO and CO_2. Figure 7-6 and 7-7 shows the temperature dependence of the gas composition in each feedstock over the range of gases detectable by the GC.
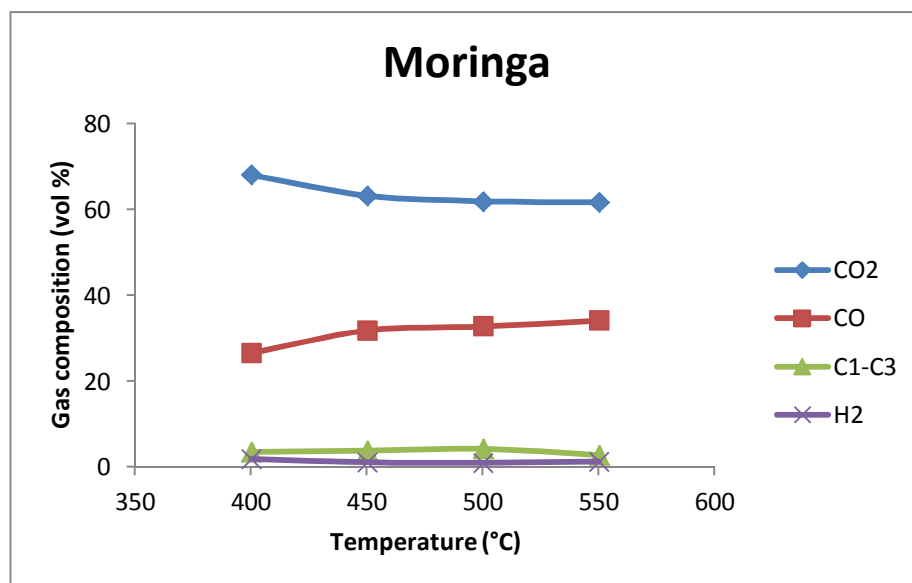
Figure 7-6 Moringa pyrolysis product gas composition a function of temperature
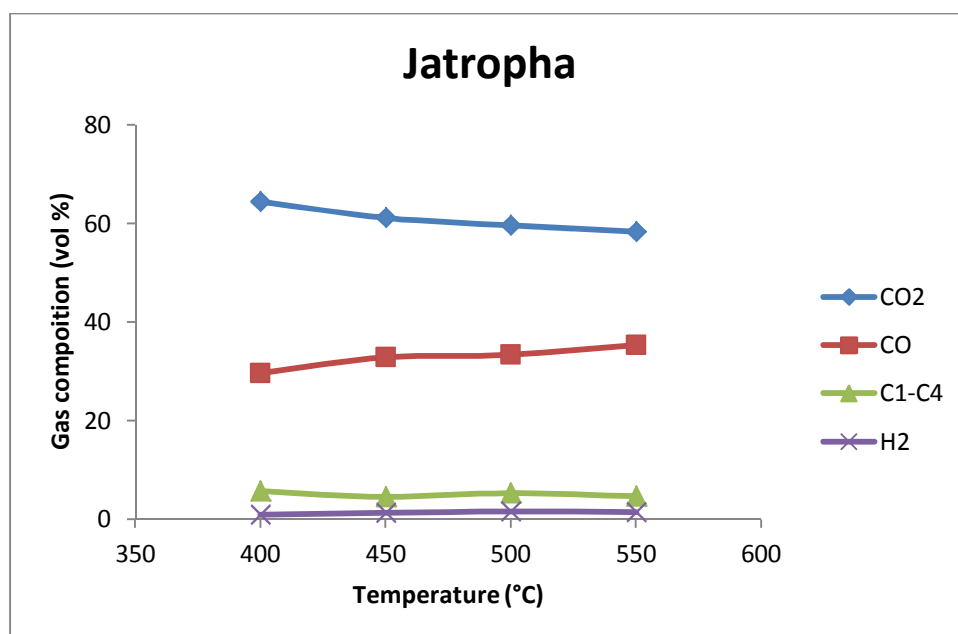
Figure 7-7 Jatropha pyrolysis product gas composition a function of temperature

The data represented the volume percent of each gas evolved during the experiments on a nitrogen free basis. The amount of hydrogen evolved was less than 2 vol% on all feedstocks at all temperatures. The gases for all feedstocks over the entire tested temperature ranges consisted primarily of CO_2 and CO. These results are strengthened by previous studies of different biomass where similar gas compositions have been reported [44, 99, 185, 200, 201]. The fast pyrolysis of Jatropha presscake at temperatures between 350 ó 550 ºC was carried out by Raja et al [152] . The main product gases in that study were CO and CO_2. In another study, rapeseed oil cake was pyrolysed at temperatures between 400 and 550 ºC. The major product gas was CO_2 similar to findings from this research [165].

For both feedstocks, the amount CO_2 produced decreased with an increase in temperature. Similarly, an increase in CO was noticed with an increase in pyrolysis temperature. The yield of C_1-C_3 hydrocarbons remained relatively constant between the studied temperature ranges with CH_4 being the dominant gas amongst the hydrocarbons for both feedstocks. The yields of CH_4 for Jatropha were lower than that for Moringa over the experimental temperature range.

In looking at the product yield curves from the pyrolysis of both feedstocks at various temperatures, it can be seen that the yield curves are not as pronounced as they are for conventional feedstocks. This research has however been sensitive to the fact that the pyrolysis products from the primary feedstocks may not necessarily follow trends observed

with regular biomass because of their composition. The fact that they have been pressed may also impact their thermal degradation in a manner not completely understood. In an attempt to compare process yields as a function of temperatures, results from one of the few studies of feedstock similar to Jatropha and Moringa press cakes have been reviewed. Hague undertook the fast pyrolysis of rape meal residue which is also a byproduct from oil seeds. When comparing results from this work to work by Hague, the shape of the yield curves though uncharacteristic, cannot be said to be totally unexpected [12]. Over a pyrolysis temperature range of 465-550 ºC, the process char yield of rape meal remained relatively constant at about 25% of biomass input before a slight decrease was noticed at temperatures over 500 ºC. Similarly, the organic liquid yield remained relatively constant over the temperature range at 47 wt%. The maximum organic yield from that study was 48 wt% on a dry basis. In comparing the water yields from this study with work by Hague, the same trend observed from Jatropha and Moringa were also observed by Hague. His work showed the water generated during pyrolysis to be stable around 10 wt% on a dry basis. Figure 7-8 shows, total liquid yields, organic yields and reaction water yields from Jatropha, Moringa and rape meal as reported by Hague.
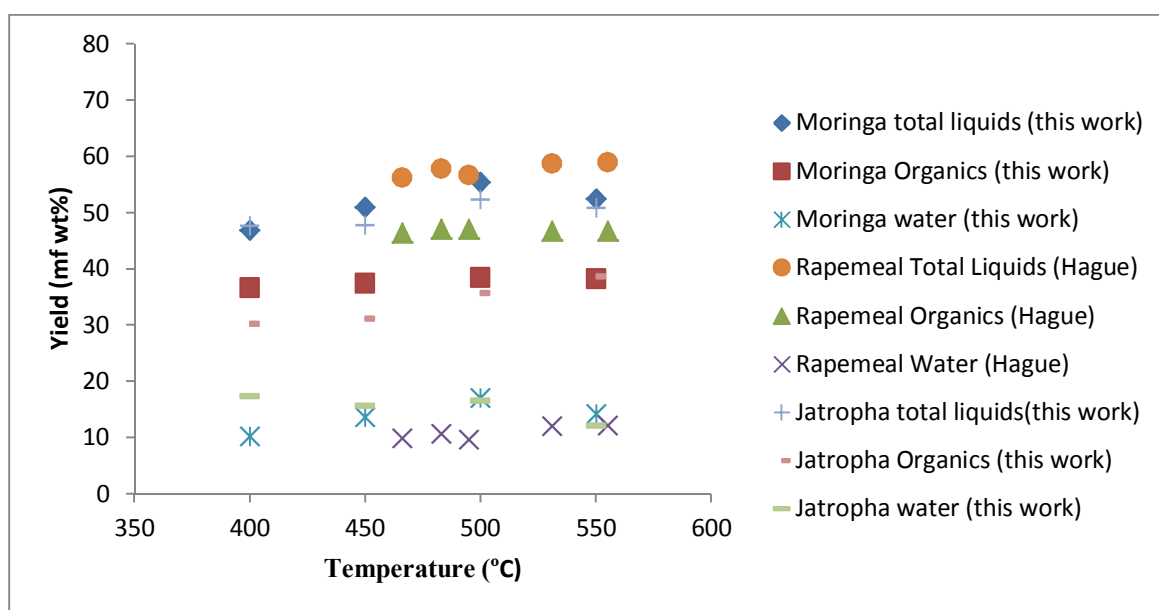
Figure 7-8 Moringa and Jatropha product yields in comparison with yields from the fast pyrolysis of Rape meal

The gas analysis carried out by Hague showed the major composition of the gas to be CO_2 and CO as observed during this study over the temperature range.

Overall, it can be concluded that although the organic yield curves are generally flatter than many feedstocks, it is in agreement with at least one published set of results on feedstocks from the pressing of oil seeds.

7.5.2.2 *Impact of temperature on solid and water contents of primary feedstocks liquids*

Solid and water content assessment of main pyrolysis liquid fractions at different temperatures were carried out and are reported as part of Table 7-8.

Table 7-8 Water and solid content of Jatropha and Moringa bio-oil as a function of temperature

Feedstock	Experiment Number	Pyrolysis Temperature (ºC)	Water Content (mf wt%)	Solid Content (mf wt%)
Moringa	TIR 300-001	400	22.41	0.38
	TIR 300-002	450	27.28	0.36
	TIR 300-003	500	28.19	0.39
	TIR 300-004	550	26.87	0.35
Jatropha	TIR 300-005	400	30.99	0.47
	TIR 300-006	450	31.68	0.41
	TIR 300-007	500	32.11	0.42
	TIR 300-008	550	31.72	0.41

mf: moisture free

With reference to the water contents of the Moringa pyrolysis liquids, there is an increase in the water content as temperature increased from 400 to 450ºC. The effect is however less visible at pyrolysis temperatures between 450 and 550ºC. In the case of Jatropha however, no direct relationship or conclusion can be drawn from the solid and water contents results as they relate to temperature. They all seem to fluctuate between 22 and 28 wt% for the Moringa feedstock and between 30 and 32 wt% for the Jatropha feedstock. The only trend that can be seen is that Jatropha seemed to contain higher water than Moringa over the temperature range investigated. This may be as a result of the higher amount of ash in the Jatropha feedstock suggesting that higher ash content in the feedstock may favour the formation of water.

Similarly, the solids contents of the pyrolysis liquids from both feedstocks suggest that pyrolysis temperature has no effect on the solid contents of the liquids. No relationship is seen between pyrolysis temperature and the final solid contents. Again, the only conclusion that can be made is that the Jatropha presscake seemed to produce more solids than the Moringa presscake. This may be also attributed to the higher ash content of the Jatropha feedstock.

7.6 PROBLEMS IDENTIFIED DURING COMMISSIONING EXPERMINENTS

During the 4 commissioning and subsequent runs on the 300 g/h unit, a number of operational problems were encountered on the unit. They included excessive entrainment of bed material, pre-pyrolysis, bridging in feed system and low mass balance closures. The problems limited the operational range of the process, particularly in terms of reactor hydrodynamics, quenching and more importantly, the organic liquid yield and mass balance closures. The problems are discussed exhaustively.

7.6.1 Feed System Problems

Bridges were formed continuously in the hopper that caused disruptions to continuous and steady state feeding for the process. The severity of the bridging problem varied depending on the feedstock being processed. The bridges could be collapsed by the application of an external force to the hopper walls. This proved ineffective in some cases, depending on the feedstock used. There were extremely difficult feedstocks whose bridges were difficult to break. This happened with Indian Moringa. As a result of this, the operator had to check feeding regularly to arrest the formation of bridges if continuous feeding processing was to be maintained.

In order to fully understand the bridging problem, the ±flowabilityø of bulk materials must first be defined. Prescott and Barnum [202] define flowability as the ability of granular and solid powders to flow. The flowability of any given material is known to depend on the physical characteristics of the material, environmental conditions and storage equipment. A number of physical and environmental parameters including moisture, temperature, pressure and particle size that affect flowability are discussed below.

Moisture: The hygroscopic nature of most biomass materials causes them to gain or lose moisture depending on the storage conditions. Johanson [203] showed that the cohesive strength and arching ability of bulk materials is affected by moisture. Similarly, Craik et al [204] and Moreya et al [205]showed that an increase in moisture content is usually accompanied by an increase adhesion and cohesion of bulk materials. Marinelli and Carson [206]also assert that even a minor change in the moisture content of bulk materials can significantly alter the frictional properties of the material.

Temperature: Temperature is also known to affect the flowability of materials although freezing conditions tend to have more severe effects. Researchers including Irani et al [207], Johanson [203] and Fitzpatrick et al [208] have all concluded that ice bonds formed as a result of low temperatures weaken the flow of bulk materials. Marinelli and Carson [206] also concluded that temperatures of the storage vessel and bulk material can have an impact on the friction angles of materials.

Pressure: Pressure as it relates to flowabiility is the increase in pressure of materials due to compaction. This compaction may be as a result of processing, transportation and vibrations. Pressure affects flow of materials in the sense that it increases the contact point between neighbouring particles and by extension, causes an increase in inter particle adhesion [207]. In the same vein, an increase in pressure will affect the critical arching dimensions of materials. The combined effects may eventually lead to a restriction of flow.

Particle size: Several studies conducted have shown that particle size and particle size distribution have a significant effect on the flowability of materials. Fitzpatrick et al [208]concluded that a decrease in particle size is associated with a decrease in flowability owing to an increase in surface are per unit mass. Yan and Barbosa [209]also concluded that an increase in particle size may be accompanied by an increase in compressibility. Marinelli and Carson [206] concluded finally that a smaller particle size and wider particle size range will lead to lower flowability and greater cohesive strength of particles.

Having identified the physical and environmental attributes that affect flowability of bulk materials, it is also important to identify additional parameters that may be used to quantify flowability. These parameters include angle of repose, internal friction and compressibility. They are discussed further.

Angle of repose: The angle of repose of any bulk material is defined as the angle between the horizontal and the slope of a heap of granular material dropped from an elevated position. Typically, the angle of repose of materials are determined experimentally by allowing the samples to flow onto a flat surface before measuring the heap angle with respect to the horizontal. Carr [210] suggests that the higher the angle of repose, the more difficult flowability is. Angles of between 50-60 show materials that will be difficult to flow.

Angle of Internal Friction: Johanson [203] defines the angle of internal friction as a measure of the force required to cause particles to move against each other. Stable slopes and restricted movements in storage vessels are hugely dependent on the angle of internal friction. The angle of internal friction is related to particle hardness, shape, size and surface friction. The identified properties relate in a complex manner to determine the angle of internal friction such that its determination is time consuming.

Compressibility: The compressibility of a material is related to pressure-density relationship of the material. In determining, compressibility the Hausner ratio -(ratio of loose bulk density to tapped bulk density) may be used. There are also empirical correlations that may be used to determine compressibility. Overall, the greater the compressibility value of a feedstock, the less flowable it is. Carr [210, 211] suggests compressibility of between 20-21% as the extreme values after which materials cannot be said to be freely flowable.

7.6.1.1   Bridging

The bridging problem encountered thus far is aggravated by the flawed design of the hopper. The hopper has a triangular cross section with a screw at the bottom as depicted in Figure 7-9.
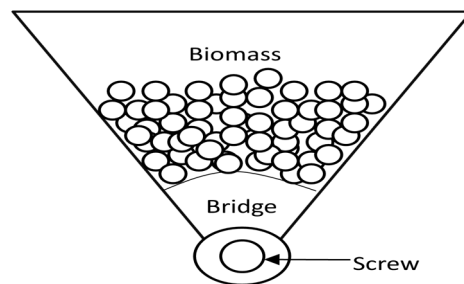
Figure 7-9: Schematic representation of bridging problem in feed system (adapted from [212])

Based on the discussions of flowability and its related parameters, materials that can be compacted will be compacted because of packing characteristics and the storage vessel shape. When this happens, an arch is formed that is able to withstand considerable stress. Depending on the material, the arch is able to transfer the load to the hopper walls. At that point, the kinematic coefficient of friction, F, which is a measure of coefficient of friction between the material and the wall of the hopper, becomes high. The end result is a situation where a bridge is formed and continuous flow through the feed system is stopped. External force then has to be applied to collapse the bridge and resume flow into the reactor. Maniatis [212] reports a similar problem after construction of a feed system for a gasification process.

Mathematically, the problem may be explained thus: When the strength of an arch, F, is exceeded by the internal stress, S, generated by a force above the arch, then flow occurs. Such that when

F<S   No flow Occurs

F=S   Critical point Reached

F>S   Flow Occurs

It is important to state at this point that the discussed physical parameters relate in complex ways with each other to contribute to flow. Such that each of the parameters may play a single or cumulative part in the extent of flow or lack of it.

An unsuccessful crude attempt was made at improving the feeding system. Two plates were inserted and taped onto the feed hop to increase the angle of slope for the biomass to reduce the bridging effect. The plates managed to slightly reduce the bridging effect but also reduced hopper capacity by more than 50 %.

7.6.2 Reactor problems

7.6.2.1 Pre-pyrolysis

A constant pre pyrolysis was prevalent as a consequence of the existing feed configuration. It is worthy of mention that the pre pyrolysis problem is a consequence of the manner of operation of the feed system although its effects are noticed in the reactor. Thus, the decision to label it as a reactor problem.

Experiments up to this point showed a problem of pre-pyrolysis where thermal decomposition of the biomass particles began prior to reaching the reactor. This pre-pyrolysis was as a result of heat from the band heaters conducting to the reactor inlet. The problem was further aggravated by the slow speed of the feeding screw into the reactor. Though it was possible to operate the screw at a higher speed, it was avoided because the screw that transports the biomass into the reactor also serves as the metering screw. At desired feed rates, the rotation speed of the screw is unable to transfer the biomass quickly enough into the reactor. This caused thermal decomposition to occur before the biomass particles reached the heated fluidised bed. Conversely, if the screw was operated at higher speeds, it would feed at a throughput greater than the capacity of the reactor. The consequence of this problem is depicted in Figure 7-10.
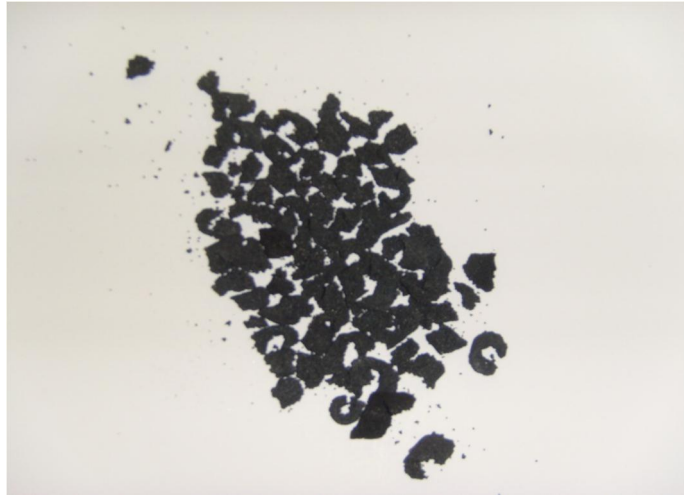
Figure 7-10: Pre-pyrolysed biomass feedstock resulting from poor feed system operation

The pre-pyrolysed biomass particles fused together in the reactor inlet tube and by the time the fused particles had reached the reactor, they were significantly larger than the bed particles that served as the heat transfer medium. This caused reduced heat transfer between the sand bed and the biomass particles. The reader may at this point, choose to recall the definition of fast pyrolysis attributed to Scott in section 3.10.1. The definition suggested that biomass particles should reach 90 % of target temperature in less than 2 seconds. Although the rate of heat transfer has not been measured, the sizes (up to 5mm in length) of the pre pyrolysed particles suggest that the criterion was not being met.

Another resulting effect of the fusion of the particles was that they negated the hydrodynamic calculations undertaken for char particles. Furthermore, even if the fused particles were able to be fluidised by increasing the gas flow rate, they had reached a size bigger than the outlet of the reactor. This meant they could not be ejected from the reactor into the char pot. These preceding actions meant that the sand bed would eventually defluidise causing the bed to behave as a fixed bed with continuous throughput. A direct consequence was a drop in reaction temperature. This would occur until the temperature was not conducive for pyrolysis. The reactor would also fill up with the fused particles causing an in pressure until the relief valve gave way.

Further evidence of the pre-pyrolysis problem and its effects in the reactor can be seen when analysing the heating profile of the reactor. Figures 6-19 and 6-20 display the temperatures recorded in the bed and freeboard of the reactor during two of the commissioning runs on the 300 g/h fast pyrolysis unit. In the case of CR-300-001, feeding was stopped after 55 minutes but temperature readings were taken over a 95 minute period. As can be seen, there is a

steady increase in the freeboard temperature from the point feeding begins. The charts indicate that the freeboard and bed temperature reach equal values after about 20 minutes of continuous operation.
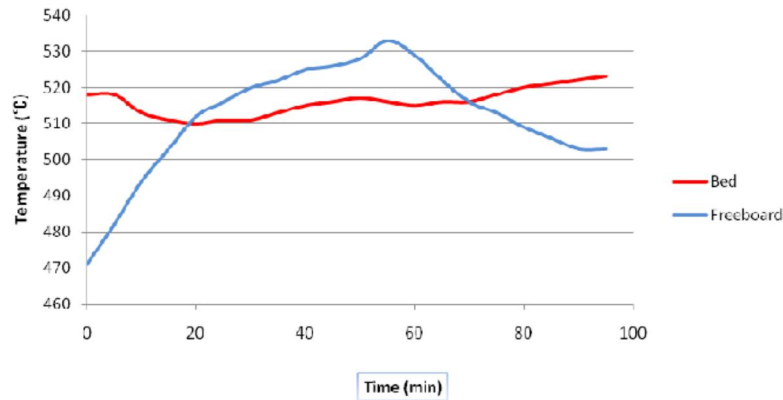
Figure 7-11: Heating profile for run CR-300-001 showing non-adiabatic operation of fluidised bed reactor
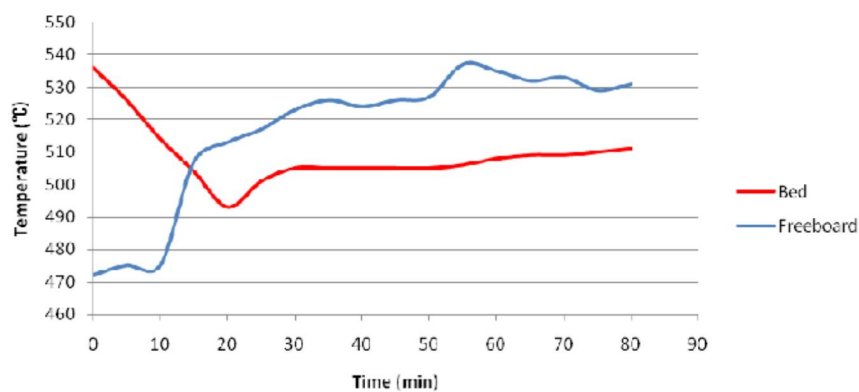
Figure 7-12: Heating profile for run CR-300-002 showing non-adiabatic operation of fluidised bed reactor

These temperature profiles are uncharacteristic of a properly operating bubbling fluidised bed reactor. Typical behaviour of a bubbling bed for fast pyrolysis should show a cooler freeboard temperature than the bed region as suggested by Piskorz et al [44]. This is because a bubbling fluidised bed unit should operate adiabatically. In practice, the freeboard region of a bubbling fluidised bed should be cooler than the bed region as is indicated on both charts at the beginning of the experiment. The absence of any heat transfer medium in the freeboard makes it cooler. The temperature in the fluidised bed region remains higher than the freeboard because of the presence of the fluidising sand which retains more heat.

The increase in temperature of the freeboard region after 15-20 minutes of operation can be attributed to the presence of the heat transfer medium or a build up of material that has the

ability to retain heat from its surroundings. Such that the temperature in the freeboard region may reach equal values and surpass the temperature in the bed region.

The reason that the freeboard temperature eventually surpasses the bed temperature is that the sand bed rises as the pre-pyrolysed particles build up at the bottom of the reactor raising the sand bed to the level of the freeboard thermocouple.

The final evidence of pre-pyrolysis is usually noticed at the end of a run. After the bed has cooled, inspection of the reactor contents show that the unit is filled to the brim since fused char particles were unable to leave the bed. An example of reactor contents is shown in Figure 7-13.

Figure 7-13 Reactor contents at the end of experiment CR-300-002

7.6.2.2 *Reduced organic yields*

Results from the experiments carried out so far on the commissioned unit show a reduced yield of organic liquids when compared to literature for feedstocks produced under similar processing conditions. This was the case for all the commissioning and subsequent experiments carried out where organic liquid yield comparisons were possible.

To understand the reason for the low organic yields, reference is made to section 2.4.5 where the effects of char and inorganic components of biomass on organic liquid yield of fast pyrolysis are reviewed. The inorganic constituents present in biomass particles (Alkali earth metals) are retained in the char product .The swift removal of char from reaction zones was identified as essential to prevent further cracking of organic vapours generated to maximise organic liquid yields.

As the chars formed during experiments on the commissioned unit are unable to be removed, the cracking of generated pyrolysis vapours continues unabated. This results in reduced organic liquid yields. It is also believed that the high amounts of char retained in the bed are responsible for the large amounts of reaction water generated. Extended pyrolysis vapour cracking has been shown to result in higher gas yields and reaction water [97].

Table 7-9 attempts to give a clearer picture of the peculiarity of the pre-pyrolysis and char retention problems identified in the reactor. This should show the extent to which the char retained plays impacts reduced organic liquid yields. A comparison has been made on the distribution of char produced from fast pyrolysis experiments on 3 functional fast pyrolysis units at BERG laboratories. The table shows the yields, location and distribution of char recorded after runs all involving Beechwood. The run on the 150 g/h unit was the quench commissioning run reviewed in section 6.4.5 while the 1 kg/h unit is from work reported by Sitzmann [97] involving Beechwood as feedstock for a fast pyrolysis experiment on the 1 kg/h unit.

Table 7-9 Char distribution on different fast pyrolysis rigs

	150g/h	1kg/h [97]	300g/h (CR-300-001)
Char Yield (wt%)	20.39	14.50	22.31
Char pots % char	92.18	97.3	2.23
Fluidised Bed % char	4.28	-	97.28
Oil Product % char	3.54	2.7	0.49

While up to 97 % of char produced on the 1kg and 150 g/h units are recovered from the process char-pots (where they should be), the reverse is the case on the commissioned 300 g/h unit. Up to 98 % of the char is recovered from the reactor itself. As more pyrolysis vapours come in contact with the produced char, the extent of cracking experienced by the vapours is increased.

The claim that reduced organic yields is due to char retention in the reactor is given more veracity by experimental work undertaken by Daugaard and Brown [213]. In a study to investigate the transport phase of pyrolysis liquids exiting a fluidised bed reactor, they used pure corn starch and a mixture of corn starch with 10% oak char as feedstock into a fluidised bed reactor under fast pyrolysis conditions. They recorded up to a 39 % reduction in the mass flowrate of pyrolysis aerosols leaving the reactor when feeding the mixture containing char

compared to pure corn starch. A 91 % increase in the mass flowrate of char was also observed while the mass flowrate of non condensable gases increased by 23 %.

Apart from the problem of increased vapour cracking due to the presence of char, it is postulated that the pre-pyrolysed particles in the reactor led to an increase in vapour residence time during the experiments. The manner of packing and rate of collection of the pre-pyrolysed particles in the reactor is not known and could not be determined. Such that a definite value on the increase in residence time of vapours could not be ascertained. It was concluded however, that as more char is collected in the reactor, the vapour residence time will increase due to a restriction to gas and vapour flow.

7.6.2.3 *Poor mass balance closure*

Results from all pyrolysis experiments showed that the highest mass balance closure obtained was 91.82 wt% on a dry basis. While the mass balances may be acceptable depending on the intended use of the data, closures higher than 95 % are preferred. The low mass balance closures were as a result of the construction of the feed system and the pre-pyrolysis problems already discussed. The Figure 7-14 below makes an attempt at clarifying why mass balance closures greater than 91 % were unable to be achieved using the commissioned unit.
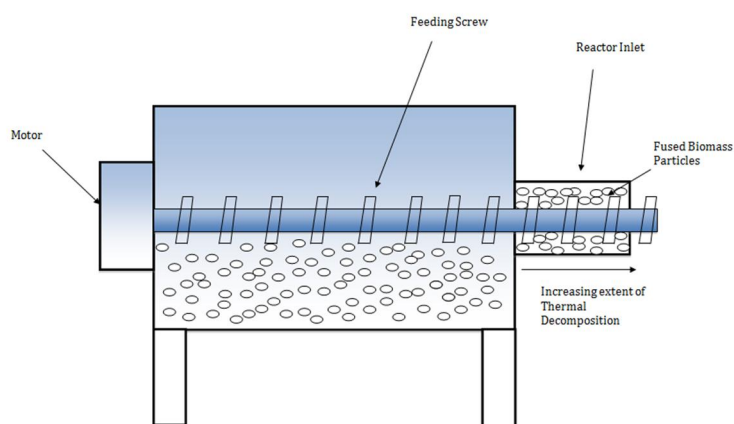
Figure 7-14 Biomass fusion in reactor inlet leading to poor mass balance closure

As can be seen from the Figure 7-14, the inlet into the reactor is able to retain some amount of biomass. This was the case unless all the biomass in the hopper was fed or the feed level in the hopper dropped below the feeding screw. This rarely happened as experiments could end abruptly because of defluidisation or a drop in temperature resulting from pre-pyrolysis and collection of char particles (explained in section 7.6.2.1). At the conclusion of most

experiments, biomass particles that had fused together because of heat conducted from the reactor to the reactor inlet remained in the pipe work that joined the reactor to the feed system. The mass retained in that space was usually between 7-12 g of biomass depending on the feedstock. The particles were difficult to retrieve. Practically, retrieval was only possible after the feed hopper had been emptied and the reactor had cooled down. The reactor contents were then emptied before the feeding screw was operated to push the biomass particles in the space into the reactor for recovery. The biomass particles in that space between reactor and feed system were found to have undergone thermal decomposition. The extent of thermal decomposition increased with the particles closest to the reactor.

Since the mass of particles retained in that space are yet to reach the reactor, they could not be considered to have undergone complete pyrolysis. Similarly, because the particles had started undergoing thermal decomposition, they could not be classified as unreacted biomass.

For the reasons highlighted, all the biomass particles retained in the space between the feed system and the reactor were classified as process losses. The only conclusion that could be reached with certainty regarding the particles left in the space between the feed system and the reactor was that they had been completely dehydrated. The extent of organic decomposition could not be ascertained with certainty. The fact that the particles had been dehydrated had little bearing on the mass balance closures since results are reported on a dry basis.

7.7 EXCESSIVE ENTRAINMENT AND COLD MODEL DEVELOPMENT

During the initial commissioning experiments on the 300 g/h unit operating at its designed capacity, one recurring characteristic was present. This was the presence of significant amounts of the fluidising medium (sand) in the char-pots after the reactor. This occurrence indicated that entrainment of the fluidising medium the reactor was taking place. This was an unwanted phenomenon as the reactor is supposed to operate based on the **'blow through'** principle where the particles of the biomass and pyrolysed char are ejected from the bubbling bed while the fluidising medium collapses back to bed. If excessive entrainment of the fluidising medium occurs, the sand bed which serves as the heat transfer medium will be ejected reducing the extent of heat transfer. Because of the excessive entrainment noticed during the first 2 commissioning experiments, all subsequent experiments were conducted at lower fluidisation velocities that equated to around 1.5 U_{mf}. While fluidisation is achieved at 1.5 U_{mf}, it can be said that the fluidisation velocity used during the experiments is very low

since values in literature show operational velocities for fluidised beds fast pyrolysis processes to be between 3-5 U_{mf} [12, 113, 117, 182, 193, 194, 214]. Modelling work carried out by Papadikis et al [194] on a reactor of exact dimensions as the one commissioned showed optimal operational velocity was $4U_{mf}$ [182]. A stronger case for higher operational fluidisation velocities in fluidised beds can also be made by making reference to work carried out by Martin [215]. The results of his study showed the relationship between fluidising velocity and the extent of bed to wall heat transfer in fluidised beds. Figure 7-15 shows the results presented by Martin.
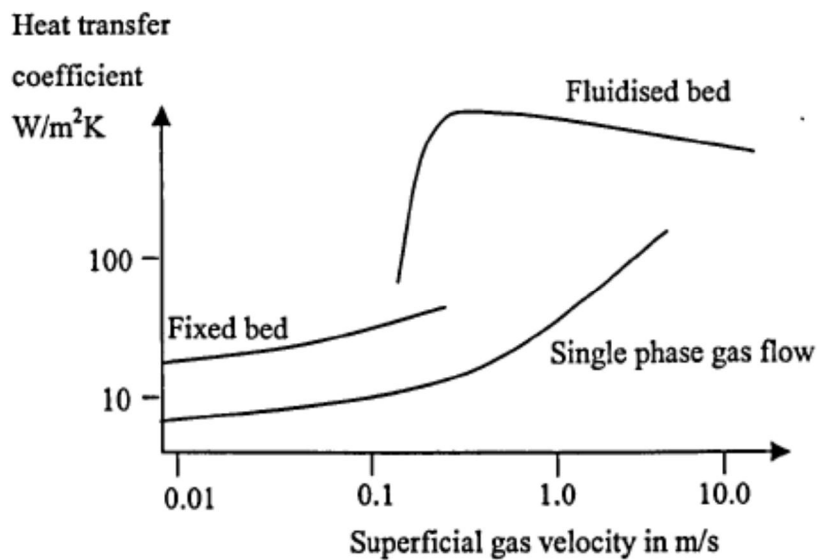
Figure 7-15 Heat transfer coefficient as a function of gas velocity in fixed and fluidised beds [215]

It can be seen from the Figure that a 4 fold increase in the velocity of fluidised bed leads to more than a 10 fold increase in the heat transfer coefficient. The findings of this work are in qualitative and quantitative agreement to modelling work carried out by Gerhauser [98] on heat transfer in bubbling fluidised beds.

Going back to the excessive entrainment observed during the first 2 commissioning runs, it was theorised that the presence of the fluidising medium in the char-pots was the result of one of two possibilities which were

1. Wrong hydrodynamic calculations for the fluidised bed
2. Reactor geometry unable to allow for the optimum fluidising conditions as determined by the hydrodynamic calculations due to reactor outlet being lower than the transport disengaging height

As the hydrodynamic calculations were checked, the only other conclusion that could be reached for the entrainment of the fluidising medium was that the reactor geometry could not support the optimum operational parameters.

To further understand the effect of the reactor geometry on entrainment, the reader is referred back to section 3.9.5 where entrainment and elutriation from fluidised beds were reviewed. In that section, the extent of solids loading and carry over in a fluidised bed reactor was shown to reduce with increasing freeboard height and become almost constant when the freeboard of the reactor exceeded a parameter known introduced as the transport disengaging height. It then became necessary to check if the outlet of the commissioned reactor was located at a point higher than the appropriate transport disengaging height.

To check the TDH of the reactor, a method proposed by Weil and Zen was employed [114, 123]. The method estimates the TDH based on the relationship between fluidising velocity, and reactor dimensions. This method was successfully used by Ramirez [216] in the design of a bubbling fluidised bed reactor for a gasification process using a bed of quartz sand of mean particle size of 385 µm. Figure 7-16 shows the relationship between reactor diameter, and the ratio of reactor diameter to TDH as function of fluidising velocity. For the commissioned 300 g/h reactor, the bed diameter is 41mm and the minimum fluidisation velocity for bed material 355-500 µm is 0.15 m/s which at 4 U_{mf} equates to 0.60m/s.
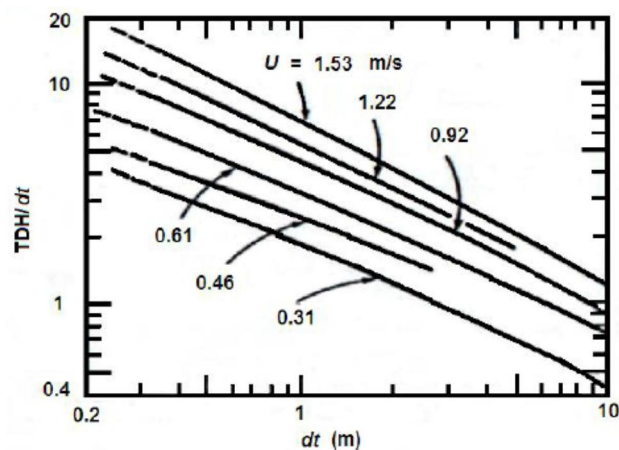
Figure 7-16 TDH calculation chart as proposed by Weil and Zen [114]

From the chart, it can be seen that for the fluidisation velocity in question (0.60 m/s) the ratio of TDH:D_R for a reactor diameter of 41mm equates to 8. Such that if this method were used in selecting a value for the TDH of a reactor of 0.041 m, the selected value for the TDH should be 0.328 m not including the height of the static bed. It should be recalled that the

outlet of the commissioned reactor is located 254 mm from the distributor plate (see Figure 6-6). What this simple check suggests is that the outlet of the reactor is located significantly below the recommended TDH. This suggests that the entrainment of fluidising sand of the reactor is because of the reactor geometry.

The absence of the original design calculations for the 300 g/h reactor unit also meant that to confidently examine the behaviour of the reactor, the research needed to find a means of understanding the hydrodynamics occurring in the reactor. The use of empirical correlations to estimate and predict hydrodynamics has already been employed but as Kunii[114] reports, empirical correlations can give unreliable results when they are varied from the experimental conditions from which they are derived. Similarly, a study carried out during an MENG project at Aston University by Thong [125], tested empirical correlations for entrainment presented by Kunii and found that the results are unreliable. In some cases, they gave negative rates of entrainment. This suggests that empirical correlations should be used with caution.

Cold models of fluidised bed reactors have long been used as a valuable tool for examining fluidised bed reactor hydrodynamics and understanding bed behaviour. Boukis [5] in research of circulating fluidised bed fast pyrolysis showed that the cold model can be used to facilitate the visual inspections of bed behaviour. Similarly, Latif [193] used cold models in a study of developing fluidised bed reactors for the gasification of Almond Shells.

Based on the excessive entrainment and a need to observe the hydrodynamics of the reactor, it was decided to construct a cold model of the 300 g/h unit with exact geometric dimensions. A cold model of the reactor was built from a tubular piece of Perspex. The diameter of the tube was 41mm to match the exact diameter of the reactor. The length of the body of the cold model was 260mm. A Pyrex sintered Borscite filter disc with porosity rating 2 was used as the distributor plate of the cold model. As explained in section 6.1.2, the 300 g/h unit distributor plate was made of Inconel with 100µm pore size and 3mm thickness. The pores of the disc used as the distributor was 100 µm pore size and the thickness of the disc was 3mm. A plenum chamber for the reactor was also made from another piece of see through Perspex. The length of the plenum was 50 mm and the diameter was 41mm matching the exact dimensions of the 300 g/h reactor. A 6.25 mm outlet was drilled 254 mm from the distributor plate also to replicate the outlet of the actual reactor. The fluidising gas inlet was drilled through the base of the plenum chamber with a diameter of 6.35 mm and fitted with a quarter

inch Swagelock fitting to allow for the connection of the fluidising gas inlet pipe. Again these dimensions are exactly as on the actual reactor. The only difference between the cold model and the actual reactor is that because the biomass inlet of the reactor was on the side, there was an opening with a cylindrical steel block where the bolts that hold the reactor unit to the feed system face plate are fastened. It is unlikely that this feature would negate any observations or conclusions drawn from experiments on the cold model. Figure 7-17 shows the cold model reactor set up.

Figure 7-17 Cold model set up for hydrodynamic experiments

7.7.1   Hydrodynamic experiments using cold model

Having constructed the cold model to the exact specifications as the actual reactor, the cold model was equipped with a line supplying the fluidising gas through a calibrated nitrogen flowmeter to measure the volumetric flowrate of fluidising gas going into the unit. The cold model was also equipped with a pressure indicator measuring the pressure drop across the bed. Experiments was carried out using the unit. The aims of these experiments were to visually observe the bed hydrodynamics under the chosen optimal conditions and also to study the relationship between the mass of fluidising medium, bed height and the fluidising gas flowrate on bed voidage and bed density at STP. Based on an initial bed mass of 300 g of sand of particle size range 355-500 µm, the values reported in Table 6-10 were obtained from the cold model.

Table 7-10 Data obtained from cold model experiment @ STP

Parameter	Unit	Observed Value
Static bed Height	mm	175
Minimum fluidising velocity	l/min	20
Minimum Bubbling Velocity	l/min	Same as U_{mf}
Expanded Bed Height at minimum fluidising conditions	mm	178
Expanded Bed Height @ Operational Velocity of $4U_{mf}$	m	> 0.260

The extent of bed expansion at varying fluidising gas flowrates the bed were recorded from the cold model. Digital photography was employed for this. A series of digital photographs (usually >12) were taken using a Sony 350 camera capable of taking continuous still photographs. The value of the bed expansion was obtained from the average expanded bed height of the pictures taken.

Data presented in Table 7-10 show visual observations of the expanded bed height at a fluidisation velocity of 4 U_{mf} to be capable of reaching 260 mm. It is believed that the expanded bed height would exceed this value if length of the body of the cold model (260 mm) was any higher. Again, the reader is reminded that outlet of the reactor is situated 254 mm from the distributor plate of the reactor. Based on these initial findings, it was immediately concluded that the reactor was geometrically incapable of handling volumetric gas flowrates of up to 4 U_{mf} if an initial bed mass of 300 g was used and explains the entrainment observed during the initial commissioning runs.

The extent of heat transfer in fluidised beds is known to be dependent on the average voidage in the reactor. As postulated by Kojima et al and Van Ommen [217, 218], the average voidage in a fluidised bed may be calculated from the pressure gradient as long as the friction between the gas-wall and solids-wall are neglected. The voidage may be calculated from equation 7-4

$$ = — \qquad \textbf{Eq 7-4}$$

Where

      P   is pressure drop across the fluidised bed $[kg/ms^2]$

      $_{bed}$ average fluidised bed density $[kg/m^3]$

      g   is acceleration due to gravity $[m/s^2]$

h   expanded bed height   [m]

And the average bed voidage is related to the average bed density by equation 7-5

$$= 1 - \text{⬜} \quad .(\quad - \quad) \qquad \textbf{Eq 7-5}$$

Where

$_{bed}$	average fluidised bed density	[kg/m^3]
$_s$	Particle density	[kg/m^3]
$_g$	fluidising gas density	[kg/m^3]
$⬜_{avg}$	average bed voidage	[-]

The pressure drop   P, across the reactor was measured using a pressure gauge between the top and the bottom of the cold model. To study the effects of varying fluidising gas flowrate on the overall bed voidage and the average bed bulk density in the reactor, the parameters detailed in Table 7-11 were used. The voidage and bed density across 3 varying bed (100, 200 and 300g) masses which by extension increase the height of the bed were observed and data derived for use with equations 7-4 and 7-5.

Table 7-11Cold model experiments parameters

Parameter	unit	Value	Value	Value
Bed Mass	(g)	100	200	300
Fluidising gas flowrate	(l/min)	20, 25, 30, 35	20, 25, 30, 35	20, 25, 30, 35
Expanded Bed Height	(mm)	53, 74, 99, 125	109, 132, 164, 197	157, 180, 210, 254

By inserting the values obtained for the pressure drops across the reactor in equation 7-4, at varying flowrates, values were obtained for the average voidage across the reactor at different bed masses and bed heights. The values obtained are plotted as part of Figure 7-18
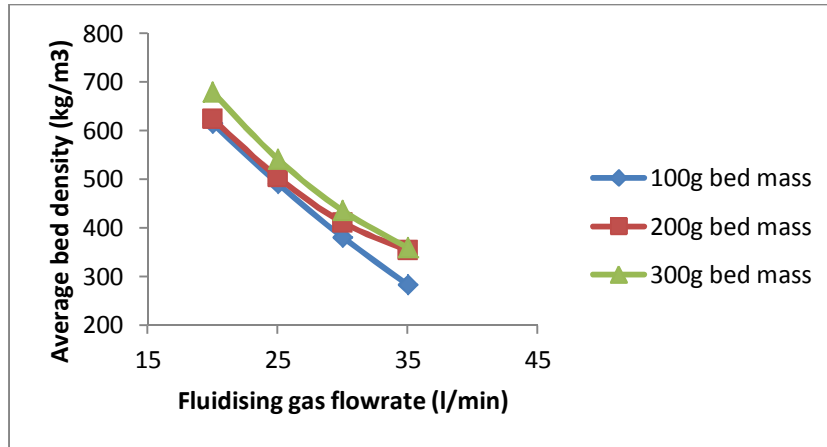
Figure 7-18 Average bed density as a function of bed mass and fluidising gas flowrate

Figure 7-18 shows clearly that for a given bed mass, the average bed density can be lowered by an increase in the fluidising gas flowrate.

By putting in values obtained for average bed density in equation 7-5, values are obtained for the average bed voidage across the reactor. The values obtained are plotted in Figure 7-19
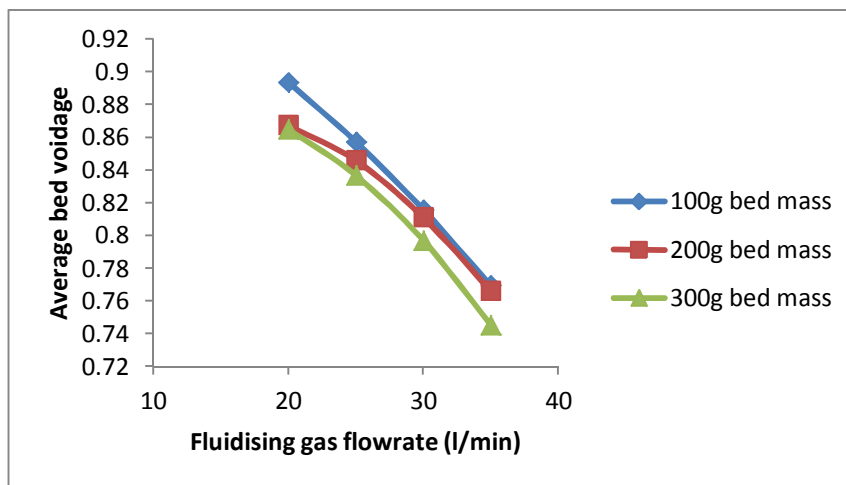
Figure 7-19 Reactor average voidage as a function of bed mass and fluidising gas flowrate

As can be seen from Figure 7-19, the average voidage across the bed also decreases with an increase in fluidising gas flowrate. This indicates that a higher rate of heat transfer across the existing reactor may be achieved by an increase in the fluidising gas flowrate for a constant bed mass.

It can be concluded from Figures 7-18 and 7-19 that the extent of heat transfer is function of initial mass of the bed and flowrate. Higher bed mass and gas flowrates resulted in lower average voidage and lower bed density.

These results show conclusively that by operating the reactor at a flowrate of 18 l/min or 1.5 U_{mf} as was the case in all the experiments carried out after CR-300-002, the extent of heat transfer is limited and leaves room for substantial improvement if the reactor geometry would allow for higher fluidising gas flowrates without excessive entrainment of sand from the reactor. By increasing the fluidising gas flowrate by less than a factor of 2, the average bed density has been more than halved.

7.8 SUMMARY

This chapter has explored the production of bio-oil using the commissioned 300 g/h fast pyrolysis units. 15 experiments were carried out and have been reported. 4 of the experiments were commissioning experiments using Beechwood, Miscanthus, Pine and Willow as feedstocks. Mass balances were calculated and compared with experimental results of similar feedstocks from literature. The results showed that although bio-oil could be generated with the unit, the liquid and organic yields were significantly less than reported values in literature indicating that there was room for improvement in the process. A further 3 experiments were carried out to investigate the impact of particle size on product yields and distributions during which mass balances were calculated and the impact of particle size on solid and water contents were investigated.

African Moringa and Indian Jatropha were also processed in the commissioned unit over a temperature range of 400-550 ℃ to determine the optimum pyrolysis temperature for generating maximum liquid and organic liquid yields from the feedstocks. A total of 8 experiments were carried out. For both feedstocks, it was discovered that maximum liquid yield was obtained at a pyrolysis temperature of 500 ℃.

During the experiments carried out using the commissioned unit, operational problems were discovered that included pre-pyrolysis, bridging in the feed system, poor mass balance closures and hydrodynamic limitations. The causes of all the major problems were identified and their impacts on the process reviewed extensively.

As per the hydrodynamics of the reactor, a cold model of the reactor unit was developed and tested. Results from the cold model showed that the extent of heat transfer in the existing reactor was limited by reactor geometry. The experiments also showed that the extent of heat transfer in the reactor could be improved if a bigger reactor could be designed and built.

The true operational limits of the downstream equipment which include the quench column and electrostatic precipitator are yet to be determined because of the limitations imposed by poor feeding and reactor operation.

At the end of this phase of the research, it was concluded that there is room for improvement to the commissioned system. Alternative feed and reactor systems are necessary to optimise the process.

8 DEVELOPMENT OF ALTERNATIVE FEEDING SYSTEM

This chapter encompasses the development of an alternative feed system, and peripheral equipment as part of optimising the commissioned fast pyrolysis process.

8.1 INTRODUCTION

Part of the objectives of this study was to optimise the operation of the commissioned unit should the need arise. The feed system has been identified as the major culprit for the poor operation of the entire system. The pre-pyrolysis problem has been linked to the deficient design of the process section. The bridging problem explained in section 7.6.1.is also as a result of the poor design of the feed system. This made an alternative feeding system a necessity.

8.2 CONSIDERATIONS FOR FEED SYSTEMS

Several types of biomass feed systems are currently in use for fluidised bed systems. These feed systems are there to transfer the biomass from storage to the processing stage. The most common feed systems in use are rotary valve systems, pneumatic feed systems and screw feed systems. Rotary valve systems are expensive and are rarely used for small scale applications [219]. Their use is limited to large scale and industrial systems. Pneumatic feeders are used in small and lab scale operations (150 g/h unit) but their major drawback is the complex design and extra equipment like blowers and stirrers. There is also an added need for a transport gas increasing the operating costs associated with such units. Screw feed systems are the most commonly used for biomass processing. Their ease of use and adaptability to the volumetric control of material flow from bins and hoppers make them popular. They can be enclosed and hence lock vapours and gases.

A list of screw feeders and their characteristics is shown in the Table 8-1below. These feeders reviewed by Levelton [220] are appropriate for biomass feed systems. They can also be used at low pressures and for feed sizes between 1-6 mm.

Table 8-1: Types of screw feeder Configurations [220]

No	Screw Feeder Type	Comments
1	Constant Cross Section	Common Design, Proven for many materials
2	Variable Cross Section	Frequently used for pressure applications
3	Choked Screws	Complicated design. Delivers plugs of solids. Needs further development
4	Plug Screws	Screw jamming for large materials
5	Multiple Screws	Proven design. Common for larger units

A proper biomass feeder design is essential to the performance of any biomass conversion process. The key essential elements of a biomass feeding system [206, 221] are

- A storage unit that is able to exhibit the right flow pattern for the required material. This may be in form of a bin, silo or hopper.
- A conveying system that will allow unhindered delivery of the material to the reactor unit while accurately metering the required amount of feed.

Other important requirements that an efficient feeder system should be able to deliver for a fast pyrolysis process include

- Uniform distribution of biomass into the reactor unit. In the case of the proposed unit, this should be achieved easily as the proposed reactor will be no larger than 65mm in diameter (see chapter 9). This size should allow for easy distribution of the biomass across the entire cross sectional area of the unit.
- A leak proof system that will ensure that the pyrolysis gases and vapours do not leak. It should be able to prevent back flow of any gases into the feed system or escape to the surroundings
- Accurate metering and transport of the biomass to the fluidised bed reactor.

8.2.1 Flow of bulk materials

Flow is defined as the relative movement of bulk particles in proximity to neighbouring particles along the wall of the containing vessel. Flowability studies are important to ensure steady and reliable flow of granular solids. Flowability is known to be a combination of the physical properties a material, environmental factors and storage equipment. The following factors impact the flowability of materials and must be taken into account when studying feed systems [219].

Moisture content and humidity: Most agricultural and organic materials are hygroscopic, they have the tendency to lose and gain moisture with changing environments. The moisture content of materials affects the cohesive strength of the particles and impact on arching. Marinelli and Carson [206] report that small changes in moisture contents can change the frictional properties of bulk solids. Increases in moisture increase the compressibility of materials. Humidity is also known to increase the angle of repose of certain materials and should be considered in feed system design [222].

Temperature: Freezing temperatures are reported to increase the possibility of formation of ice bridges reducing the flowability of materials. Ice bridges form as a result of high moisture and low temperatures in the feed system. The feeding of materials should be kept at relatively moderate temperatures and extremes should be avoided [223].

Particle size and shape: The size and shape of the particles determines the ease with which bulk solids can be conveyed. Smaller particles are generally easier to convey but it has been found that reduction in particle size of powders in particular, worsens the flowability of the material. This is due to increased cohesion arising from an increase in surface area per unit mass [206, 224].

8.2.2 Material consideration

In designing a biomass feed system, the initial step is to consider and analyse the type of material that will be fed through the feed system. This analysis should take into account the physical characteristics of the material focusing on bulk density, particle size, particle shape and moisture content [221]. These factors play a role in the precise metering and transport of the biomass. As the biomass feed system proposed will handle various types of biomass including grasses, woods and agricultural residue, the physical characteristics of a range of materials have to be taken into consideration. Table 8-2 below assesses the type of biomass that may be fed through the system and their characteristics.

Table 8-2: Properties of biomass considered for feeding[220, 225]

	Material	Bulk Density (kg/m^3)	Typical Sizes (d_p in mm)	Flowability	Other Properties
1	Stalks	250-440	$d_p<1$	Free flowing	Light, fluffy
2	Sawdust	200-350	$d_p<1$	Very sluggish	Hygroscopic
3	Cake Pressing	580-1400	$d_p<1$	sluggish	Packs under pressure
4	Wood Chips	160-800	$d_p<1$	Free flowing	Light, may agglomerate
5	Wood Shavings	100-150	$d_p<1$	Free flowing	Light, may agglomerate
6	Grasses	200-400	$d_p<1$	Free flowing	Light, packs under pressure

8.3 PROPOSED FEED SYSTEM CONFIGURATION

Based on existing fast pyrolysis units in literature and experience from the use of existing lab and pilot scale units, one the most promising alternatives identified and thought to be applicable within the context of this research is the dual screw feed system.

In coming up with an alternative biomass feed system, the transport and metering components of the system could have been encased in a single unit. That decision would however, increase the complexity of the design as a screw feeder that will accomplish both functions will be difficult to design, fabricate and operate as seen with the initial design. For added flexibility and ease of use, a dual screw feed system was chosen for the alternative feed system. The first screw will adjust accurately the biomass feed rate. The second screw which will operate at higher speeds will facilitate rapid and unhindered transportation of the biomass to the reactor.

This dual screw feed system is common with fast pyrolysis systems and is currently in use on the 1 kg/h and 5 kg/h units at Aston university. Dual screw feed systems operate on the principle that the first screw is responsible for metering and that must be the screw used for calibration purposes. A similar system used by Ramirez et al [216] is shown in figure 8-1.

Aston University

Illustration removed for copyright restrictions

Figure 8-1 Dual screw feed system as employed by Ramirez et al [216]

The following components were to be the key parts of the new feed system

8.3.1 Feed hopper

Levelton [220] proposed designing biomass feed hoppers in cylindrical or vertical cuboids shapes instead of cones. The proposed hopper should have a capacity of at least 0.05 m^3 to allow for longer experiments. The storage vessel should be made of stainless steel for durability. The feed system should also have an inlet for an inert purge stream.

8.3.2 Metering screw

The discharge of the biomass at the desired rate will be regulated by the metering device in this case a screw. The metering device will be situated at the bottom of the feed hopper to allow metering of the biomass housed in the hopper. The metering screw was to be a strengthened screw with carefully controlled diameter, pitch and thickness. Figure 8-2 shows a schematic representation of a typical metering screw.
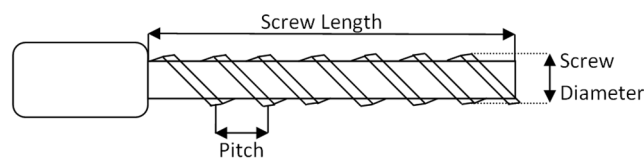
Figure 8-2 Schematic representation of a feeding/metering screw

The feed system may be equipped with gravimetric capabilities to record loss in weight as the biomass is fed. These systems are more accurate than volumetric feeders.

8.3.3 Feeding screw

The feeding screw should be situated below the metering screw. The screw is to be positioned horizontally and its length should stop just at the inlet of the fluidised bed reactor to prevent material carry over from inside the reactor. The screw will be encased in order to prevent any leakages of pyrolysis gases and vapours.

8.4 K-TRON KT-20

The literature and principles of biomass feeder operation have been well understood. However, the design of biomass feeding systems can be a complex and time consuming exercise. The limited time demanded that any alternative design be reliable and operational with minimal problems. As such, minimal room for error was permissible. Previous studies carried out at the research group by Boukis and Maniatis [5, 212] have shown that although

an understanding of feeding systems can be achieved, their designs may still pose problems that need constant changes and modifications. For the identified reasons, the decision was taken to use an off the shelf system from a commercial provider for metering of the biomass. Stemming from the decision, the author of this thesis in collaboration with engineers from K-TRON chose a gravimetric feed system capable of meeting the requirements for biomass feeding. After a series of interactions with the feed system providers, 3 different biomass samples of differing bulk densities and sizes were sent to the providers. The physical data from the samples sent are shown in Table 8-3.

Table 8-3 Feedstocks considered in selecting off the shelf feed system

	Particle Size(µm)	Bulk Density(kg/m^3)	Moisture Content (wt %)
Beechwood	355-849	300	9.55
African Moringa	355-849	430	8.26
Indian Moringa	355-849	590	6.33

The model chosen was a K-TRON KT-20 with a loss in weight system shown in Figure 8-3. This feed system had the advantage of being able to tell the operator at any given time during the experiment the amount of biomass fed and the amount of biomass left in the system. It also allowed the operator to alter the feed rate to a desired value by simply altering the set point on the onboard computer. The feed system also meant that the calculations of mass balances were further simplified as the need to weigh the feed before and after had been totally eliminated. The onboard computer was capable of providing the information on its display panel.

Aston University

Illustration removed for copyright restrictions

Figure 8-3 Schematic diagram of K-TRON KT-20 loss in weight feed system [226]

A brief description of the K-TRON KT-20, its principle of operation is detailed below while a digital photograph of the actual unit is shown in Figure 8-4.

Figure 8-4 Digital photograph of K-TRON KT 20 and mobile stand

The K-TRON KT 20 is equipped with a hopper for storage of the biomass. A horizontal agitator for bridge breaking is encased within the hopper to ensure continuous feeding while twin auger screws for metering and discharge of the materials are situated at the bottom. Table 8-4 details the relevant data for the K-TRON KT 20 as specified by the author

Table 8-4 Operational parameters for K-TRON KT 20 loss in weight feed system

Parameter	Unit	Value
Motor		Baldor 0.095kW 180V DC 0.65A 2000RPM
Bulk Material		Wood pellets
Minimum Feed rate	(g/h)	0.1
Maximum Feed rate	(g/h)	0.5
Discharge tools		13mm double fine auger screws
Hopper Volume	(l)	20

8.4.1   Gravimetric system

The gravimetric weighing system of the KT20 is equipped with a smart force transducer sensor. The weighing system is equipped with three load cells mounted on a frame. Its operation is based on a vibrating wire principle as shown in Figure 8-5.

Figure 8-5 K-TRON smart force transducer principle of operation for loss in weight system [226]

Using mechanical means, any applied load on the scale is transmitted to a wire causing a change to its resonance frequency. The value of the load is then computed by an onboard microprocessor. The signal sent to the controller is a fully calibrated temperature compensated signal via a RS 458 serial communication port. The weight data is sent at a speed of between 2400 ó 34800 bps.

8.4.2 See through outlet

The K-TRON Kt 20 unit comes equipped with horizontal spout as outlet for material discharge as standard. An option of a vertical outlet is also available for downwards feeding as was to be employed with the alternative feed system. This option was chosen during the procurement of the unit. The vertical outlet was however open ended and would not provide the gas tight requirements of a pyrolysis process. For this reason, a modification was made where a see through gas tight contraption was to be installed on the feed outlet. This had the advantage of

- Letting the user know when material was being discharged
- Letting the user know if there was any blockage in the fast screw system as a material build up would be noticed

For the see through unit, a machined cylindrical top base and cap for the top and bottom of the outlet were fabricated based on design drawings submitted during the research. Figure 8-6 shows a digital photograph of the unit with the see through contraption installed. Figure 8-7 shows the dimensional drawings of the vertical outlet.

Figure 8-6 Installed see through outlet on K-TRON KT-20 metering system

Similarly, a throat made of stainless steel (Appendix 4) was fabricated which would connect the see through unit to the fast screw system via a flexible bellow.
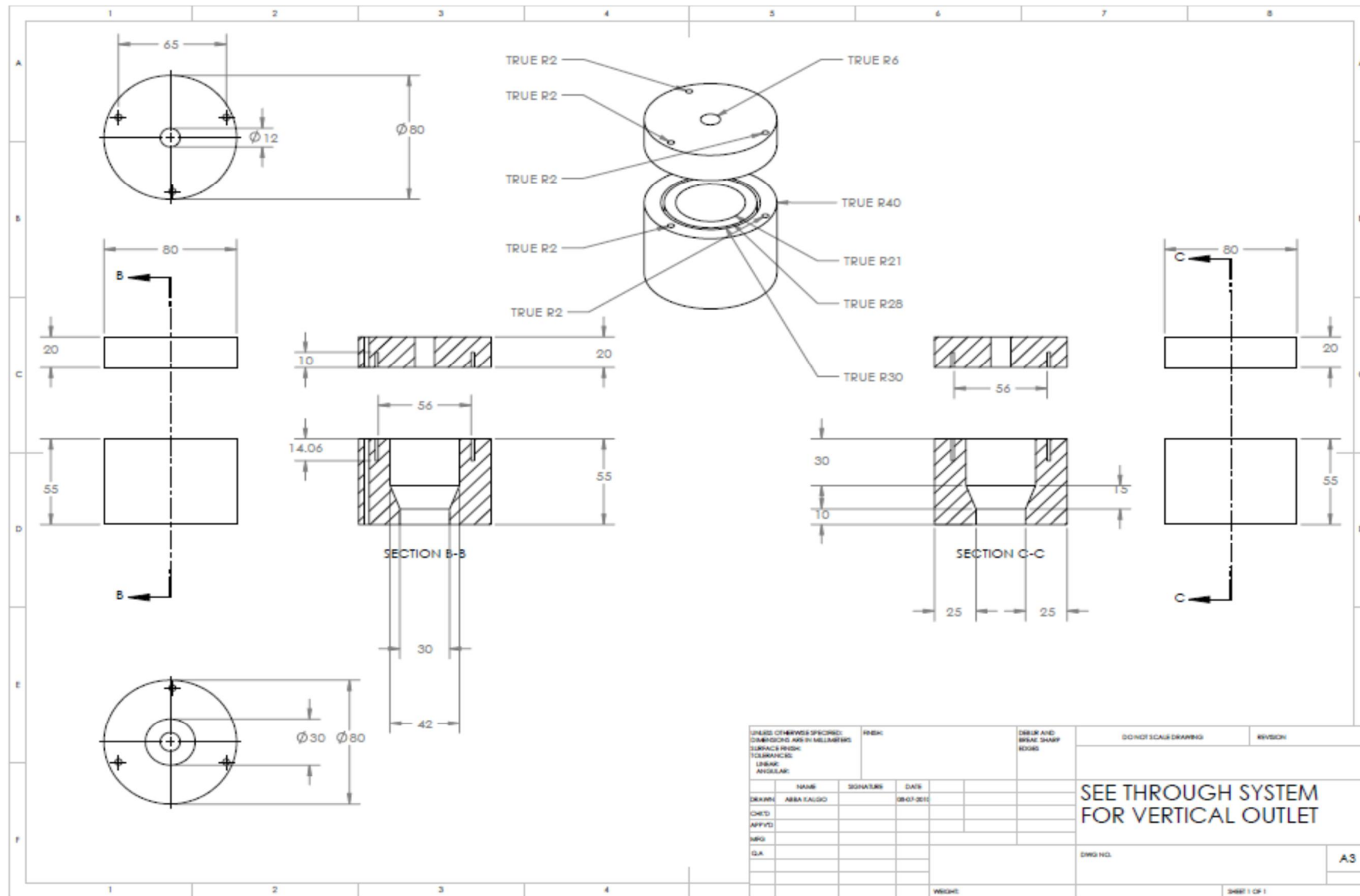
Figure 8-7 Dimensional drawings for see through feed outlet

8.5   COMMISSIONING OF K-TRON KT-20 FEED SYSTEM

To commission the KT-20, a series of tests were conducted using Beechwood as the reference material. The aims of the commissioning tests were to

- Evaluate the accuracy of the scale on the loss in weight system
- Evaluate the accuracy of discharge of the metering system on the procured unit
- To evaluate the operation of the metering unit in conjunction with the fast screw system to assess suitability for use with a fast pyrolysis system

8.5.1   Scale tests

To test the accuracy of the weighing system, 8 measurements of pre-weighed biomass were placed in the feed hopper at 500 g increments to observe the response of the scale. The results obtained are shown in Table 8-5.

Table 8-5 Commissioning scale tests for K-TRON KT 20

	Mass recorded on scale (g)	Mass recorded by KT-20 (g)
Test 1	500.00	500.2
Test 2	1000.00	1000.4
Test 3	1500.00	1499.8
Test 4	2000.00	2000.3
Test 5	2500.00	2500.1
Test 6	3000.00	3000.4
Test 7	3500.00	3500.3
Test 8	4000.00	4000.1

8.5.2   Metering tests

A second set of tests were carried out in order to observe the accuracy of discharge from the KT-20 based on the operator setting. These tests were to observe the accuracy of metering. Settings were varied between 100 to 500 g/h which was the maximum feed rate of the system. The tests were carried out by collecting the mass discharged from the system in a pre-weighed vessel and comparing the reported discharged value from the on board computer to the values recorded in the pre-weighed vessel. The results of the tests are shown in Table 8-6.

Table 8-6 Commissioning discharge tests for K-TRON KT-20

Biomass feeder set point (g/h)	Actual mass flowrate (g/h)
100	100.2
200	200.1
300	300.4
400	400.1
500	500.2

8.6 MODIFIED FEEDING SCREW CONFIGURATION

This part of this study involved converting the initial single screw feed system to a fast screw for conveying biomass swiftly into the reactor. A detailed description of the existing feed system has already been given in section 6.1.1. To cut costs, the alternative feed system was to make use of the existing single screw system components as part of the dual screw design.

From the description already given of the gearbox and motor of the existing system, it is evident that the existing single screw configuration may be employed at very high speeds that will allow for its operation as a fast screw system.

The modification needed to allow for gas tight operation of the fast screw into the reactor coupled to the KT-20. Figure 8-8 shows the eventual design adopted. Figure 8-9 shows the dimensional drawings of the fast screw base.
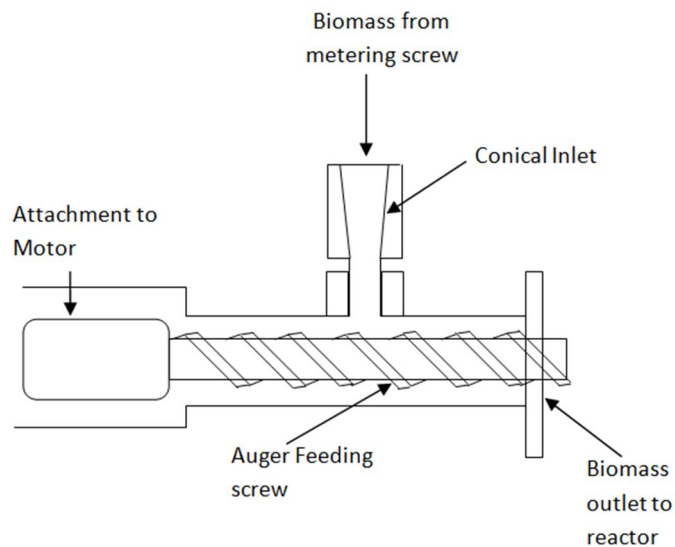
Figure 8-8 New fast screw feed configuration
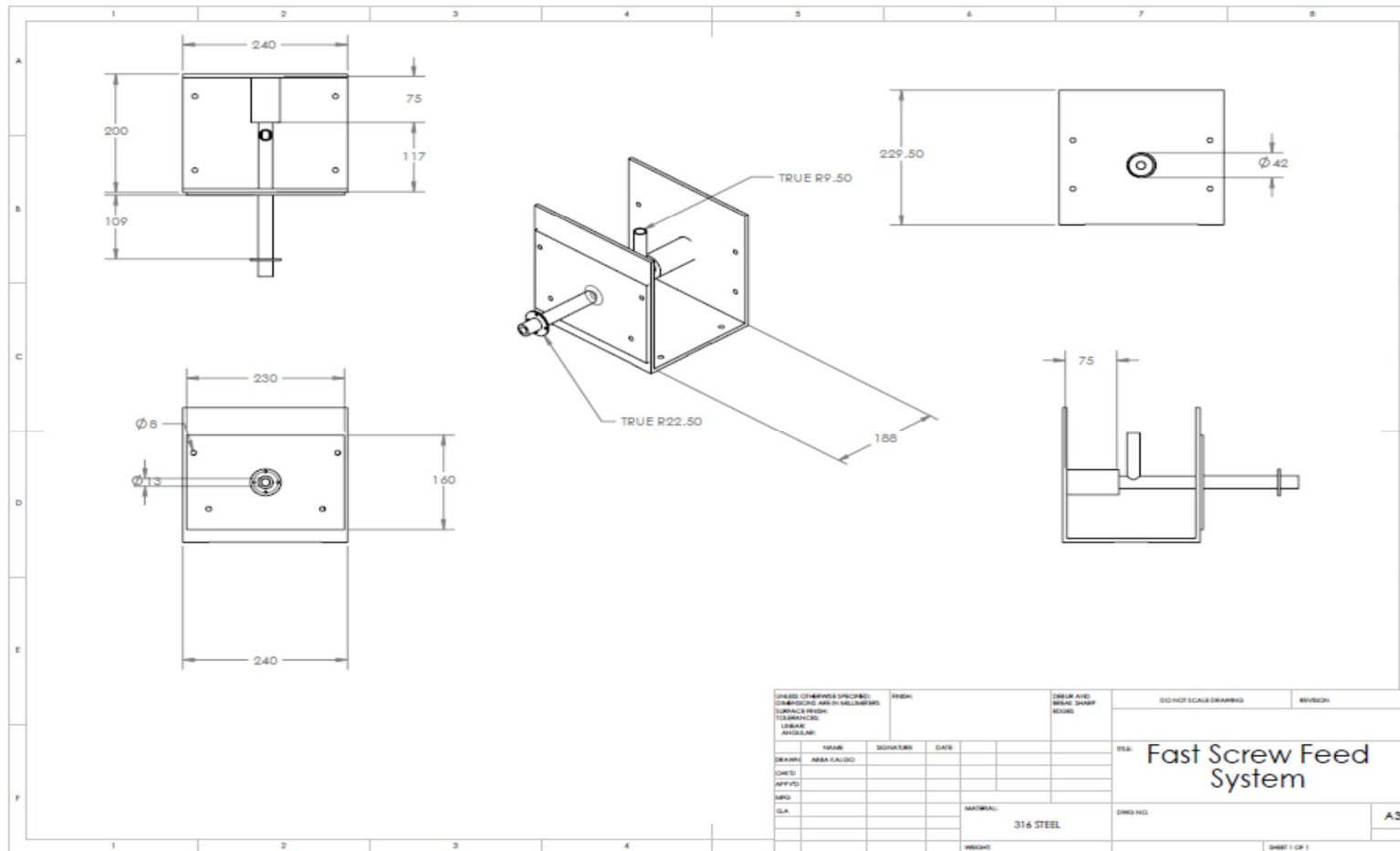
Figure 8-9 Dimensional drawings for fast screw feed system

Figure 8-10 shows a photograph of the fast screw configuration after construction. Two 6 mm reinforcement plates were added to increase the robustness of the fast screw system since it would support the weight of the motor and gearbox.
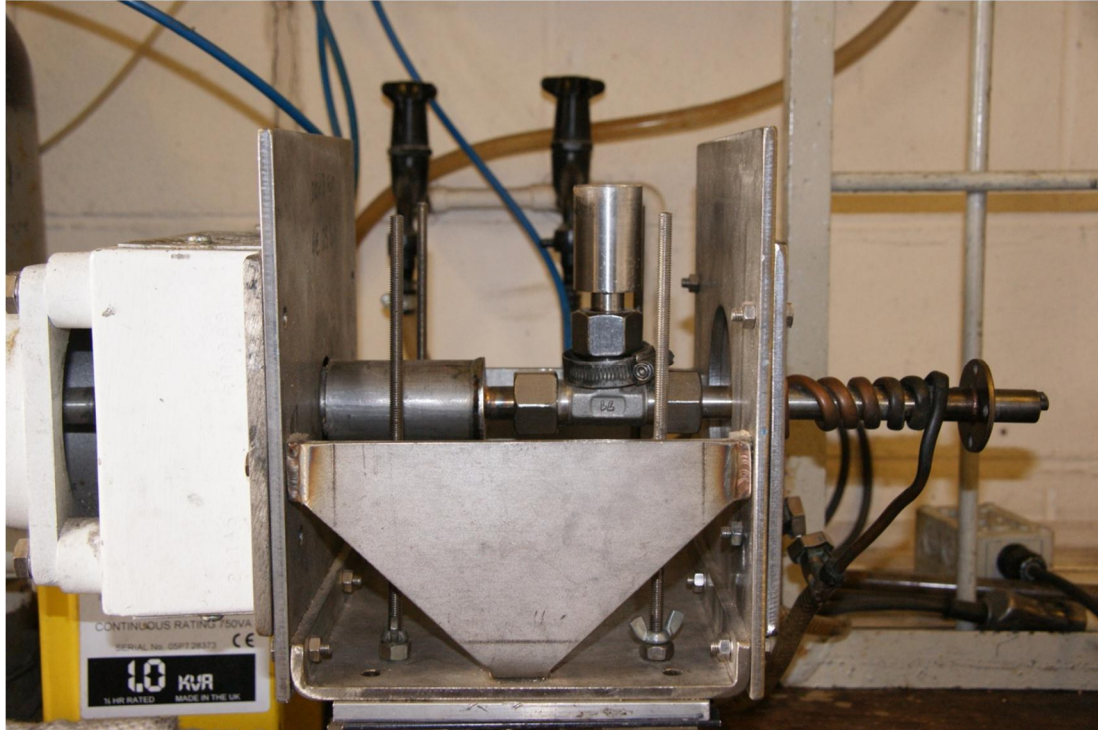
Figure 8-10 Photograph of constructed fast screw system

8.7   COMMISSIONING OF ALTERNATIVE FEED SYSTEM

Having tested the weighing and metering systems of the K-TRON KT-20 feeding system, the next set of tests carried out were to observe and assess the behaviour of the unit operating as a whole i.e. KT-20 metering system connected to the fast screw. The key requirement to be met by the feed system operating as a whole was that the speed of the fast screw should have minimal impact on the rate of discharge of biomass from the fast screw. To properly assess this, tests were carried out where the setpoint of the metering system was kept constant while only the speed of the fast screw was varied. The tests were carries out at fast screw settings of 40, 80, 120 and 150.

Figure 8-11 shows the relationship between feed rate and fast screw setting on the alternative feed system. As can be seen from the Figure, the requirement that the feed rate be independent of fast screw speed has been met.
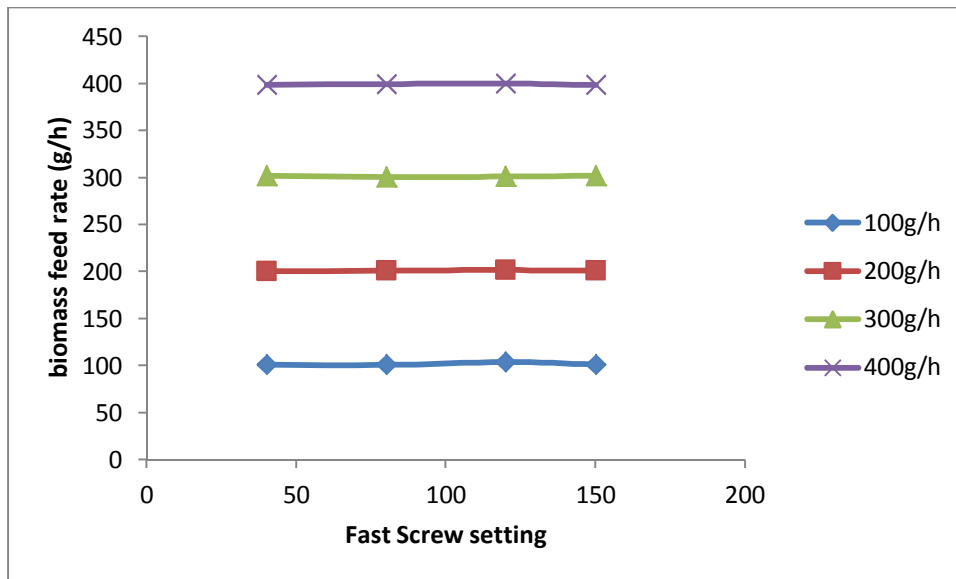
Figure 8-11 Effect of fast screw on biomass feedrate

8.8 SUMMARY

The design of an alternative fast pyrolysis feed system has been reported in this chapter. The design involved changing the existing single screw system into a dual fast screw feed system. An alternative biomass feed system with gravimetric capabilities has been commissioned. The feed system has been shown to be able to meter and effectively convey biomass with high degrees of accuracy.

9 DESIGN OF AN ALTERNATIVE FLUIDISED BED REACTOR

This chapter details the design of a new bubbling fluidised bed reactor. The designs of the distributor plate and plenum chamber are also detailed in this chapter.

9.1 INTRODUCTION

Observations during the commissioning stage of the 300 g/h reactor showed that a number of optimal conditions for reactor operation including operating at between 3-5 times the minimum fluidisation velocity were not met. Cold model experiments carried out on a scale model of the unit further reinforced the conclusion that the reactor could not be operated at the intended optimum conditions. It was decided after the cold model tests to design and construct a new reactor unit. The reactor is to allow for a wider range of operating conditions and higher throughput than the initial unit.

9.1.1 Justification for new reactor development

The following discussions present justifications for the design of a new reactor unit.

9.1.1.1 Hydrodynamic limitations of initial reactor

The hot commissioning phase and cold model tests showed conclusively that the existing 300g/h reactor could not operate at the required throughput because of geometric limitations. A bubbling fluidised bed fast pyrolysis process should be able to achieve selective entrainment of particles. It is required that the hydrodynamic parameters of the bed should be able to entrain char and unreacted biomass particles but allow the fluidising medium to collapse back to the bed. These operational limits are a function of reactor geometry mainly the Transport disengaging height (TDH), operational velocity and the expanded bed height. The optimum operational velocity of fluid bed reactors particularly for fast pyrolysis is between 3-4 U_{mf}. The static bed height with 300 g of sand in the initial reactor stood at 15 cm. This did not allow for operation at velocities larger than 1.5 U_{mf}. The cold model also showed that the reactor geometry allowed minimal space for bed expansion at the optimal operational conditions. This led to excessive entrainment of the fluidising sand which serves as the heat transfer medium to the biomass particles. As entrainment of sand occurred, the extent of heat transfer to the biomass particles is significantly reduced. This leads to reduced yields and a reduction in char pot capacity since the fluidising medium ends up in the char pot. Similarly operating at lower velocities limits the ability of the system to eject bigger particle and higher density materials like the primary feedstocks.

9.1.1.2 *Operational Limit of downstream equipment*

Another reason to develop a new reactor stems from the need to determine the operational limits of the downstream equipment. The quench column and the electrostatic precipitator were designed to carry vapour loads from the processing of 300 g/h of biomass [227]. The commissioning phase experiments cannot be said to have determined their operational limits since the existing reactor was never operated at its designed capacity.

9.1.1.3 *Improvements to mass balances and process yields*

One reoccurring characteristic of experiments carried out during the commissioning phase was low mass balance closures. The low mass balance closures were attributed to the feeding problems and hydrodynamic limitations of the commissioned unit as described in section 7.6. Another reason for the low mass balance closures was the short duration of the experiments carried out. It was theorised that the hold up in the quench unit will increase over the duration of the run until it reached a constant value. In order to reduce the errors in the mass balance calculations caused by the hold up, it is necessary to carry experiments at extended durations of time.

9.2 BUBBLING FLUIDISED BED REACTOR DESIGN STEPS

To design the new reactor, the research delved into existing literature to help choose steps that consider the most important parameters that impact on maximum liquid yield from a fast pyrolysis process. At this point, it should be pointed out that the literature for design of fluidised bed equipment is vast. Several studies have been reported on the design of bubbling fluid bed systems for both gasification and pyrolysis.

Ramirez [216] reports the design of a bubbling fluidised bed gasifier for the gasification of rice husk. The method involved a combination of empirical correlations and innovations by the research group under which the development was carried out. At the conclusion of the study, a fluidised bed gasifier of 0.3 m internal diameter and 3 m height was constructed and operated successfully. The model for the development of the reactor was basic and focused reactor sizing based on experience and empirical correlations.

In a 1986 study by Maniatis [212], a fluidised bed gasifier was also constructed from first principles for the gasification of biomass. The diameter of the reactor was 0.8 m. The study was based primarily on empirical correlations for the reactor design and prediction of the reactor performance.

Van den Enden [228] also proposed a design methodology for the development of fluidised bed gasifiers which was reiterative in nature. The methodology involved design using modelling software.

For this research, a design methodology developed by Boukis et al [229] has been employed. Boukis method was developed for a circulating fluidised bed with a char combustor. The method has however been adapted for a conventional bubbling bed. In addition, the design of the reactor distributor plate and windbox is based on proven correlations from the vast fluidised bed equipment literature. The method incorporates the key requirements for fast pyrolysis namely

- Short Vapour residence time
- Moderate reaction Temperature
- High heat transfer rates

The design method for the bubbling fluidised bed reactor aims to match energy and mass balances to proven reaction kinetics and hydrodynamic parameters.

In addition to these parameters, Scott et al [192] suggest that the blow through principle as seen in the commissioned reactor be retained as it is very effective in removing char from fluidised beds during fast pyrolysis. All these factors have been taken into account for the design of the new reactor. Figure 9-1 shows the various design steps as adapted for a bubbling bed.
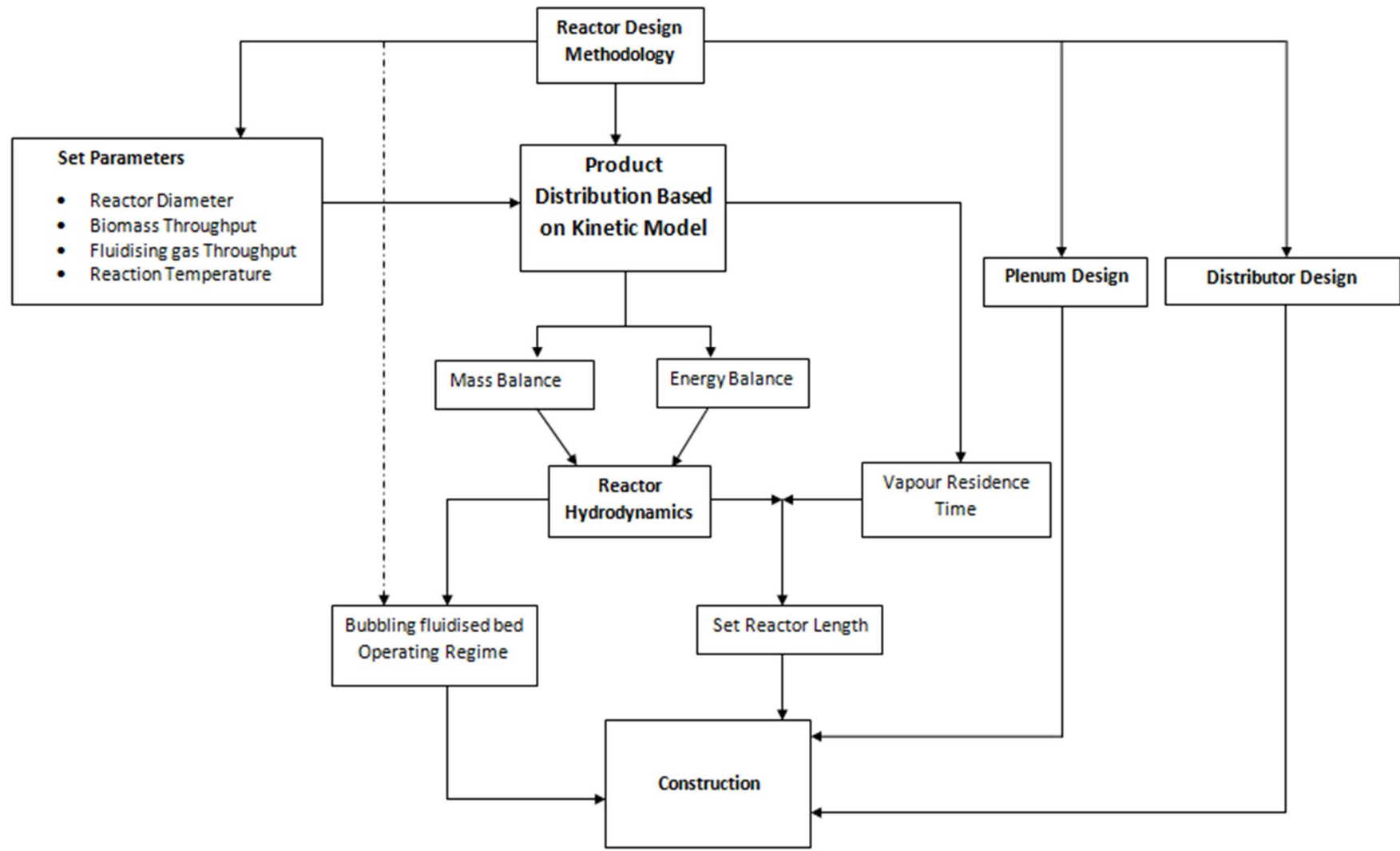
Figure 9-1Bubbling fluid bed reactor design method (adapted from [228])

9.2.1 Bubbling fluidised bed operating regime

The first step is to define the reactor operating regime. Over the years, certain parameters associated with fluidisation have been developed and accepted as standards for use. This includes the Geldart classification of particles reviewed in section 3.9. Another widely accepted starting point for defining the operating regime of any fluidised system is the Grace diagram shown in Figure 9-1.

Aston University

Illustration removed for copyright restrictions

Figure 9-2Grace Diagram for fluidised systems [230]

The Grace Diagram identifies flow regimes for fluidised systems by relating gas and particle properties. The diagram proposes flow regimes based on two dimensionless parameters. The dimensionless parameters are d* which represents the dimensionless particle size and u* which represents the dimensionless gas velocity. The parameters are defined by the equations 9-1 and 9-2.

$$\cdot \qquad * \qquad\qquad /\mu \quad \cdot \quad \overline{\qquad} \quad \cdot \qquad \textbf{Eq 9-1}$$

$$\overline{\qquad}_{\cdot} \qquad * \qquad\qquad \mu \quad \cdot \quad 3 \quad /4 \quad \cdot \qquad \textbf{Eq 9-2}$$

Where

$d*$	dimensionless particle size defined by equation 9-1	[-]
$u*$	dimensionless gas velocity defined by equation 9-2	[-]
d_p	particle Diameter	[m]
U_0	operational Gas Velocity	[m/s]
g	gas density	[kg/m^3]
s	solid density	[kg/m^3]
g	acceleration due to gravity	[m/s]
μ_g	Gas viscosity	[kg/sm]
Re_p	Particle Reynolds number	[-]
Ar	Archimedes number	[-]
C_D	drag coefficient	[-]

Where C_D is obtained by the expression in equation 9-3

$$4 \quad - \quad /(3 \quad) \qquad \textbf{Eq 9-3}$$

The function Re_p/C_D relates the particle Reynolds number with the drag coefficient to characterise the gas velocity. The Archimedes number characterises the relationship between the solid particle and the action of the gas on it. The dimensionless parameters u* and d* are particularly useful in design of fluidised systems as each parameter is representative of two process characteristics namely gas velocity and the particle diameter raised to the first power. These parameters are able to characterise the hydrodynamics of any gas solid system in a unified approach and are independent of other process variables.

Based on the discussion of the Grace Diagram, any system designed must be able to operate within the limits imposed. If the system is operational within these limits, then the criterion of good heat and mass transfer as well as more controlled hydrodynamics will be met. The Grace diagram has been introduced as the first step of the design process. The eventual reactor operation must allow for the system to operate within the limits imposed by the Grace diagram.

9.2.2 Set design parameters

Some of the design parameters were fixed. The reactor was to be fabricated from a standard 2.5 inch steel pipe with an internal diameter of 65 mm. This was to minimize costs considering the tight research budget. It was safe to proceed with this pipe size as it is larger than the existing reactor with 41 mm I.D and less than the 1 kg/h reactor which has an I.D of 75mm. Another advantage of the relatively small diameter chosen is that it would ease the distribution of particles of biomass across the entire fluidised bed.

It was also decided that the reactor should be capable of processing up to 500 g/h of biomass. The throughput value was chosen in order that the actual operational limits of the downstream equipment (quench and ESP) of the existing 300g/h unit be ascertained. It was also reasoned that should there ever be a need to scale up the system, only the quench system would be included.

9.2.3 Kinetic model for product ratios and distribution

The reader may choose to recall the discussion in section 2.2 which reviewed kinetic models for pyrolysis. It showed that many models exist to predict product yields. However, very few of them have been tested. One of the few models that has been tested and verified is the model proposed by Liden. The Liden model is accepted as one of the most reliable kinetic models to predict fast pyrolysis product yields over a wide temperature range. The strength of the model is reinforced by its ability to predict liquid yields which is the primary aim of fast pyrolysis as shown by Samolada et al [231]. The data presented in Table 9-1 shows a product distribution sourced from work carried out by Scott et al [134] for Eastern Maple. The product distribution is based on the kinetic model by Liden. These product yields and distribution form the basis for the energy and mass balance for the proposed reactor.

Table 9-1 Product distribution based on work carried out by Scott [134]

Reaction products	wt% (dry basis)	wt% (wet basis) 7.5% wt H_2O, 0.5% ash
Organic Liquids	60.00	55.20
Charcoal	15.00	13.80
Non-condensable gases	14.50	13.34
Reaction Water	10.50	9.66
Feedstock Water	0.00	7.50
Ash	0.00	0.50
Total	100.00	100.00

The product distribution is valid for a feedstock with 7.5% moisture and 0.5% ash content at a reaction temperature of 500 ºC.

Having already set the biomass throughput of the proposed reactor at 0.5 kg/h, it is possible to present the fluidising gas flowrate into the reactor as a function of the biomass throughput. Table 9-2 presents biomass to feed ratio for existing fluidised bed reactors systems for fast pyrolysis.

Table 9-2 Ratio of feedstock to gas throughput of fast pyrolysis systems

	Diameter (mm)	Throughput (kg/h)	Gas to feed ratio	
Aston University 150g/h	41	0.15	8-10	measured
Aston University 1kg/h	75	1.0	6-9	measured

Based on the Table above, it can be seen that the gas to feed ratio for fluidised bed fast pyrolysis is around 10 irrespective of the reactor throughput. Thus, a value of 10 has been selected for the proposed reactor such that the mass flowrate of fluidising gas G_G into the reactor may be expressed as $G_G=10G_{B+MA}$ where G_{B+MA} is the throughput of biomass into the reactor including moisture and ash. Scott et al [192] in other work suggested that lower biomass to gas ratio be employed for fluidised bed reactor design for fast pyrolysis.

9.2.4 Mass of Bed Material and Reactor Throughput

Having selected an appropriate kinetic model to be used for prediction of product yields and decided on reactor throughput. The next step was to decide the mass of fluidising medium. Reference is made to the research group standard that relates reactor throughput to the amount of heat transfer medium. As the capacity of the proposed reactor would be 500 g/h, the mass of the heat transfer medium in the reactor is also set to 500 g.

9.2.5 Energy Balance

The proposed reactor will have a throughput of preheated nitrogen as the fluidising gas. This will cause the gas to enter the reactor typically at between 450- 500 ºC. The energy requirements of the pre-heater are however, not included in the energy balance of the reactor system as the preheating unit is operating independently of the reactor. The entry temperature of the preheated gas is however taken into account in the energy balance calculations since it will reduce the required amount of the external energy input required.

Also the energy balance calculations are based on the assumption that the mass of the fluidising medium (quartz sand) remains constant i.e. there is no entrainment of the bed material. This assumption is necessary to maintain a constant rate of heat transfer from the bed. While this may be difficult to achieve in reality, the rate of entrainment of the bed material out of the reactor can be controlled if a single narrow particle size range of heat transfer medium is used.

The energy balance also works on the assumption that the bed particles attain and maintain the same temperature of the preheated gas entering the reactor. This assumption is justified based a review of temperature effects on heat transfer in fluidized beds by Yates [116]. He asserted that heat transfer between gases and solids is very efficient as a result of high surface area of the particulate phase in fluid beds. Yates further estimates that 1 m^3 of 100 µm particle can have a surface area of up to 30000 m^2 and concluded that gas to particle heat transfer is rarely a limiting factor in gas-solid fluid bed heat transfer.

The overall energy balance in the proposed reactor may be presented as equation 9-4

$$
[\qquad\qquad\qquad] +
$$
$$
+
$$
$$
[\qquad\qquad\qquad\qquad] =
$$
$$
+
$$
$$
[\qquad\qquad]\qquad\qquad\qquad\qquad \textbf{Eq 9-4}
$$

From the equation that represents the overall energy balance in the proposed reactor, it can be seen that the required external energy input can only be calculated after the remaining parameters in the equation have been obtained.

To estimate the energy provided by the entraining gas, the term in equation 9-5 which represents the energy provided by the fluidising gas can be calculated by

$$
=\qquad\qquad -\qquad \textbf{Eq 9-5}
$$

Where G_G is the mass flowrate of fluidising medium and C_{Pn2} is specific heat capacity of Nitrogen at 500 °C. T_2 and T_R represent fluidising gas entry temperature and reaction temperature which are 723 K and 773 K respectively

The term G_G in equation 9-6 is equated to $10G_{B+MA}$ such that equation 9-5 becomes

$$= 10 \quad (\quad - \quad) \qquad \textbf{Eq 9-6}$$

It should be noted that the ratio of fluidising gas to biomass throughput can be validated based using equations 9-1and 9-2 in conjunction with the Grace diagram. If the operational regime of the bubbling bed is found to lie between the region of bubbling bed operation from in the Grace diagram based on the dimensionless parameters d* and u*, it may be concluded that the value chosen is valid.

The energy provided by the heat transfer medium (bubbling sand bed) is

$$= \quad (\quad - \quad) \qquad \textbf{Eq 9-7}$$

Where G_S and C_{PS} are mass flowrates and specific heat capacity of quartz sand at reaction conditions.

The energy lost from the system has been estimated to be 10% of the total energy input into the system such that it may be expressed in the form of equation 9-8

$$=$$

$$0.1\{ \qquad\qquad + \qquad\qquad\qquad +$$

$$\} \qquad \textbf{Eq 9-8}$$

On substituting equation 9-6 and 9-7 into equation 9-8, equation 9-9 is obtained.

$$=$$

$$0.1[\qquad\qquad + 10 \qquad - \quad + \qquad - \quad]$$

$$\textbf{Eq 9-9}$$

The other term in the overall energy balance calculation is the heat required for the complete devolatisation of biomass to organics. To obtain an exact measure of the energy required for this term, detailed analysis of the thermal decomposition of biomass is required. Biomass decomposition under fast pyrolysis conditions has already been defined as a set of complex reactions without a clear decomposition mechanism. An alternative means of estimating the heat requirements must be employed.

This research has been sensitive to the fact that any mechanism employed to estimate the heat requirements of biomass fast pyrolysis must give a reasonable measure of the heat requirements to thermally decompose biomass particles to organic vapours, bio-char and product gases. There exists in literature various values for the heat of pyrolysis reactions with varying estimates. The reasons for the variations from different researchers can be attributed to difference in feed stocks, experimental configurations, reaction conditions and also the extent to which the studies have permitted the reactions to occur.

Despite these variations in the values for heat of pyrolysis reactions, researchers are generally in agreement that the fast pyrolysis process is as a whole endothermic. To estimate the energy requirements for pyrolysis, it is first of all necessary to define the energy demands during fast pyrolysis. The energy requirements for pyrolysis are a combination of two enthalpies. The sensible enthalpy which refers to the energy required to raise the temperature of the biomass and the reaction enthalpy which refers to the energy required to drive the pyrolysis reaction from biomass to pyrolysis products [232].

Several researchers including Reed and Gaur [233] have attempted to estimate the energy requirements for pyrolysis. They estimated the energy requirements to be between 2.9-3.5 MJ/kg of biomass. Their study employed a reducing flame to heat the biomass samples and the experiments lasted up to 50 seconds. The time taken to obtain their results however is not representative of a fast pyrolysis process and is unlikely to be a representation of energy requirements for a fast pyrolysis process.

Similarly, Morris et al [234] presented values of 2.5 MJ/kg of oil produced. If an assumption of 70% oil conversion is used, that would imply an energy requirement of 1.75 MJ/kg of biomass. They however failed to give details of their calculations and assumptions.

Daugaard and Brown [232] measured the energy requirement for the fast pyrolysis of several kinds of biomass. The method employed accounted for heat losses and took into account the moisture content of the various feedstocks. Based on their results, they obtained average energy requirements of 1.5 MJ/kg over four different biomass types. Based on the clarity of the methods used to derive the values, the energy requirements for fast pyrolysis in the proposed reactor has been selected to be 1.5 MJ/kg of biomass in agreement with the published study by Daugaard.

To obtain the energy requirements for the reactor system, the formula shown in equation 9-10 is derived by substituting equations 9-6, 9-7 and 9-9 into equation 9-4.

[+ 10   ,   −   +   −   ] = ——— +

0.1[+ 10   −   +   −   ] **Eq 9-10**

Table 9-3 lists the actual values used in calculating the energy requirements of the proposed reactor with at a biomass throughput of 0.5 kg/h.

Table 9-3 Parameters to determine external energy required for proposed reactor

Parameter	Unit	Value
G_G= Fluidising gas flowrate	Kg/h	5
$G_{B+MA=}$ Biomass flowrate	Kg/h	0.5
G_S= Sand flowrate	Kg/h	0.5
C_{PS} = Specific heat capacity of sand	___	0.80
C_{Pn2}= Specific heat capacity of nitrogen at 500 ºC	___	1.056
T_2= gas entry temperature	K	723
T_R= pyrolysis temperature	K	773
Energy for biomass devolatisation	kJ/Kg	1500

Solving for equation 9-10 with a biomass throughput of 0.5 kg/h, a required energy input of 1950 KJ/h or 0.54 kW is required to meet the energy requirements of the system.

9.2.6   Mass balance

For the mass balance, data presented in Table 9-4 is assumed to be the inputs and outputs of the pyrolysis reactor as a function of biomass throughput. This is based on the product distribution presented in Table 9-1. Values for output on a moisture and ash free basis have been obtained by multiplying percentage product yields by a moisture ash free correction factor (MAFCF) obtained from equation 9-11 below.

$$= \frac{[\quad . \quad . \quad]}{\quad} = 0.92 \qquad \textbf{Eq 9-11}$$

223

All inputs and outputs have also been presented as a function of biomass on as received basis and a moisture ash free basis.

Table 9-4 Distribution of pyrolysis products as a function of biomass throughput (kg/h)

Component	Input	Output as a function of moisture ash free biomass	Output as function of biomass as received
Biomass as received	G_{B+MA}	-	-
Biomass (maf)	G_B	-	-
Fluidising gas	$G_G=10G_{B+MA}$	-	$10G_{B+MA}$
Ash	$0.005G_{B+MA}$	-	$0.0050\,G_{B+MA}$
Feed water	$0.075G_{B+MA}$	-	$0.0750\,G_{B+MA}$
Reaction water		$0.105\,G_B$	$0.0966\,G_{B+MA}$
Organic liquids		$0.60\,G_B$	$0.552\,G_{B+MA}$
Char		$0.150\,G_B$	$0.1380\,G_{B+MA}$
Non condensable gases		$0.145\,G_B$	$0.1334\,G_{B+MA}$

maf: moisture ash free

Again, it should be noted that the product distribution is for biomass fast pyrolysis for a feedstock with 5% ash content, 7.5% moisture content occurring at 500 °C with a vapour residence time of 0.5 second. From the data presented in Table 9-4 the mass throughputs of the system in kg/h are shown in Table 9-5.

Table 9-5 Actual reactor throughput values for proposed 0.5kg/h reactor

Component	Input	Output as a function of moisture ash free biomass(kg/h)	Output as function of biomass as received (kg/h)
Biomass as received	0.5	-	-
Biomass (maf)	0.46	-	-
Fluidising gas	5	-	5
Ash	0.0025	-	0.0025
Feed water	0.15	-	0.15
Reaction water		0.0483	0.0444
Organic liquids		0.2760	0.2532
Char		0.069	0.0634
Non condensable gases		0.066	0.0613

maf: moisture ash free

9.3 ADJUSTING REACTOR HYDRODYNAMICS FOR THROUGHPUTS

Having completed the mass and energy balance of the reactor, the next step was to match the hydrodynamic parameters of the system to its throughputs. The hydrodynamics are governed by the volumetric fluidising gas flowrate, pyrolysis gas and vapour flowrate at reaction conditions.

For simplification purposes, the calculations assume isothermal operation in the fluidised bed reactor at 500 ºC. While this may not be the case in reality, the assumption will not have a negative effect on the proposed reactor since adiabatic operation is a favourable occurrence in terms of fast pyrolysis [192].

The hydrodynamics have to take into account the formation of pyrolysis products in the reactor since decomposition of the biomass will lead to pyrolysis vapour formation and non condensable gases.

The diagram shown in Figure 9-3 attempts to clarify the vapour velocities at different points in the proposed reactor. The terms U_R at point A and U_R at Point B are gas and vapour velocities at reaction conditions where A is the point above the distributor plate and B is the exit of the reactor. The gas velocity at the bottom of the reactor relates to only N_2 being the fluidising gas. At the top of the reactor however, pyrolysis products in the form of vapours and non condensable gases will have been generated. This means that the vapour velocity at point B must include the inert fluidising nitrogen gas from point A and generated products at point B.
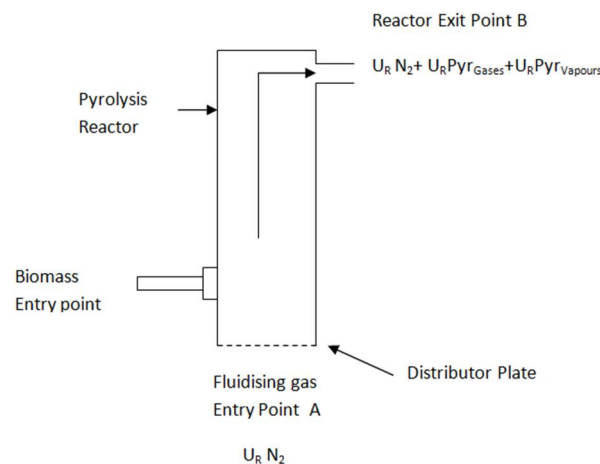
Figure 9-3 Velocity diagram for bottom and top of proposed reactor

225

To determine the vapour velocities at the different points in the reactor, the volumetric flowrates of fluidising gas, pyrolysis gases and organic vapours at the reactor inlet and exit must be known. This can be obtained from the mass flowrates and densities of the vapours and gases. Assumptions for the densities of steam, pyrolysis vapours and pyrolysis gas have been made based from steam tables and published data by Liden and Reed [58, 235]. The value for the pyrolysis gas density is based on an assumption that the gases consist only of CH_4, CO and CO_2 at ratios of 13%, 60% and 27% respectively at reaction conditions.

$\rho_{pg}=0.48kg/m^3$ Liden [58]

$\rho_{pv}=2.3kg/m^3$ Reed [235]

$\rho_{st}=0.284kg/m^3$ Steam density at 500 ºC and atmospheric pressure

Table 9-6 below summarises the volumetric flowrates in the reactor at the bottom of the reactor and the top according to Figure 9-4 and the mass balance presented in Table 9-5. Note that the steam value includes the initial feed moisture content.

Table 9-6 Volumetric flowrates at bottom and top of proposed reactor (m^3/h)

	N_2	Organic Vapours	Pyrolysis Gas	Steam
Point A	5	-	-	-
Point B	5	0.6(0.46)	0.145 (0.46)	0.19(0.46)

Based on the data in the Table 9-6 and assumptions for the gas and vapour densities, an equation for the velocity of fluidising gas, pyrolysis gas, pyrolysis vapours and reaction water in the form of steam at the exit of the reactor based on reactor diameter and biomass throughput is derived as equation 9-12

$$ = + \frac{(0.46)}{0.0325} \frac{1}{\left(\frac{0.6}{2.3} + \frac{0.145}{0.48} + \frac{0.19}{0.284}\right)} $$

$$ = + \frac{(\ .\ \ )}{.} \frac{}{(\ .\ \ \ )} = + 116.16 - \qquad \textbf{Eq 9-12} $$

226

as a velocity term based on reactor cross sectional area and the density of N_2 at 500 ºC $= 0.442$ kg/m^3 is obtained from

$$= \frac{\quad}{\cdot \quad (\;\cdot\;)} = 3427.27 - \qquad\qquad \textbf{Eq 9-13}$$

Such that the volumetric gas flowrate at the exit of the reactor becomes

$$3427.27 + 116.16 = 3454.43 \text{ m}^3/\text{h}.$$

The value for the vapour velocity in the entire reactor now equates to 0.982 m/s by dividing the volumetric gas flowrate by the cross sectional area.

9.3.1 Determining reactor length

The proposed reactor length may now be determined by relating the vapour residence time to the reactor volume and the mean gas flowrate. Equation 9-14 below shows the relationship between vapour residence time, reactor volume and volumetric gas flowrate.

$$= \overline{\quad} \qquad\qquad \textbf{Eq 9-14}$$

Where

t_{res}	vapour residence time	[s]
V_R	Reactor Operational Volume	[m^3]
	Mean volumetric gas flowrate including pyrolysis vapours and gases	[m^3/s]

As already stated, the kinetic model on which the reactor product distribution is based has a residence time of 0.5 seconds. For this reason, the value of the residence time is set to 0.5s.

The gas velocity has also been obtained and set at 0.982 m/s which through a cylinder with 0.065 m diameter gives a volumetric flowrate of 0.003240 m^3/s

It is important to state at this point that the residence time calculation is based on the time taken from the point of generation of products and vapours to the point of quenching. This includes the time elapsed for the vapours to pass through the cyclone and peripheral equipment prior to the condensation stage. An assumption has been made that the volume of the cyclones and other pipe work equates to 15% of the actual reactor volume such that an expression for the operational volume may be presented as equation 9-15

$$= \quad + 0.15 \quad = 1.15 \qquad \textbf{Eq 9-15}$$

Where

A_R reactor cross sectional area $[m^2]$

L_R length of reactor $[m]$

By inserting equation 9-15into equation 9-14, the relationship between flowrate, residence time and reactor volume can be presented as equation 9-16

$$= \quad = \quad + 0.15 \quad = 1.15 \qquad \textbf{Eq 9-16}$$

Substituting the values of 0.5 s, 0.00324 m^3/s and 0.0033 m^2 for residence time, volumetric flowrate, cross sectional area into equation 9-16 and solving for L_R, a value of 0.426 m is obtained for the reactor length.

9.4   DESIGN VERIFICATION

In order to verify the design, the dimensionless parameters from the Grace diagram presented as equation 9-1 and 9-2 were used to check if the reactor will operate as a bubbling bed. Table 9-7 shows the calculated values for the dimensionless parameter d* (equation 9-1) for sand particles sizes 355, 500, 710and 850 µm. The parameters were calculated using the gas properties of N_2 at 500 ºC and quartz sand density.

The corresponding u* range for the particles to operate in bubbling mode obtained from the Grace diagram are also presented.

Table 9-7 Dimensionless parameters d*and u* values from Grace diagram

Average particle size(µm)	Calculated d*	Bubbling U* Range	Calculated U*	SGDL
355	8.65	0.22-1.8	0.26	Yes
500	12.19	0.3-1.95	0.53	Yes
710	17.31	0.38-2	1.07	Yes
850	20.72	0.45-2.3	1.53	Yes

SGDL- Satisfies Grace Diagram Limits?

It can be seen from the Table 9-7 that the range of values presented for U*from the grace diagram are between 0.22 and 2.3. The mean gas velocity obtained was 0.982 m/s. By inserting the value of the gas velocity into equation 9-2, values for U* have been calculated and are also presented in Table 9-7.

The results of the design verification show that at a gas velocity of 0.982 m/s, sand particle sizes of between 355 and 850 µm will operate as a bubbling bed. Thus, efficient heat transfer and bubbling bed behavior may be expected from the designed reactor at designed throughputs.

Also, the operational velocity of 0.982 m/s is below the terminal velocity of the smallest particle size in Table 9-7. This also shows that the bed material will not be blown out of the reactor provided the length of the free board is higher than the transport disengaging height (TDH).

9.5   GAS DISTRIBUTOR DESIGN

As stated earlier, the key features of a fluidised bed system include excellent mixing capacity with high heat and mass transfer rates. The quality of mixing and extent of heat and mass transfer is to a large extent determined by the bubbling characteristics of the gas and fluidising medium. According to Botterill and Whitehead [129, 236], a proper fluidised bed gas distributor should be able to achieve

- Even gas distribution across the fluidising bed
- Produce effective gas-solid contact and maximise particle movement
- Minimise channelling
- Minimise dead zones on the distributor
- Minimise blocking tendencies of the plate
- Minimise particle flow back into the plenum during operation
- Minimise attrition caused by fluidised particles
- Support forces due to pressure drop during operation and weight of the bed when not operational.

Geldart and Baeyerns [237] assert that the performance of a gas distributor can determine the extent of success or failure of a fluidised bed. They conclude that improper design of gas distributor is mainly responsible for difficulties encountered in the operation of gas fluidised systems. Uniform gas distribution, small bubbles at the distributor plate are essential for optimum operation of gas fluidised beds. Figure 9-4 shows types of distributor plates for fluidised systems.

Figure 9-4 Types of distributor plate and their effects on fluidisation [212]

Distributor design is still a largely empirical procedure though the results obtained may be used with confidence as data obtained from them show good agreement with experimental values [238, 239]. The relatively small diameter of the proposed reactor and budget restrictions played a part in the decision to equip the new reactor with a sintered plate to serve as the distributor.

An early rule of thumb estimates the pressure drop across the distributor as a ratio of the pressure drop across the entire bed. This pressure drop across the bed may be obtained by equation 9-19 by Harrison and Davidson [240]. Equations 9-18 and 9-19 estimate the pressure drop across the distributor depending on direction of flow.

$$\Delta \qquad\qquad 1 \qquad\qquad\qquad \textbf{Eq 9-17}$$

Where, for downwardly directed flow

$$\Delta \qquad 0.1\Delta \qquad\qquad\qquad \textbf{Eq 9-18}$$

And for upward and laterally directed flow as is the case for the proposed reactor [241]

$$\Delta \qquad 0.3\Delta \qquad\qquad\qquad \textbf{Eq 9-19}$$

Where

ΔP_{bed} pressure drop across fluidised bed $[kg/ms^2]$

ΔP_d pressure drop across distributor $[kg/ms^2]$

$_s$ solid density at reaction conditions $[kg/m^3]$

	gas density at reaction conditions	$[kg/m^3]$
g	acceleration due to gravity	$[m/s]$
H_{mf}	Bed height at minimum fluidising conditions	$[m]$
	Bed voidage	$[-]$

For distributor plates of the sintered type, flowrates are proportional to the applied pressure until the onset of turbulence. The Darcy equation in equation 9-20 is used to express the relationship between the variables up to the limit of proportionality

$$= \frac{\quad}{\quad} \qquad \textbf{Eq 9-20}$$

Where

P_d	pressure drop across distributor	$[mm\ H_2O]$
Q_g	volumetric gas flowrate	$[cm^3/s]$
D	Permeability of material	$[cm^2]$
t_p	plate thickness	$[cm]$
A_p	Plate area	$[cm^2]$
μ_g	Gas viscosity	$[poise]$

From the value obtained, an appropriate grade degree of porosity for the distributor plate may be obtained based on data shown in Table 9-8

Table 9-8 Relationship between permeability and grades of porous distributor plates [193]

| Grade | Pore size Distribution | | | Permeability Darcies x 10^{-8} | Density (g/cm^3) | Minimum Thickness (mm) | Porosity (%) | |
	Min	Mean	Max				Solid	Void
B 05	0.75	2	9	1.0	6.0-7.5	1.5	75	25
B 10	2.50	6	25	2.5	6.0-7.0	2.0	70	30
B20	7.50	20	85	7.0	5.0-6.0	2.5	60	40
B 30	10.0	35	150	30	5.0-6.0	3.0	60	40
B 40	15.0	50	250	90	5.0-6.0	3.5	60	40
B 50	20.0	75	320	150	4.5-5.5	4.0	55	45

To evaluate the pressure drop across the distributor, the pressure drop across the entire bed must be obtained and equated 0.3 of the value obtained. The operational parameters of the reactor at pyrolysis conditions are given in Table 9-9

Table 9-9 Design parameters for distributor plate

Parameter	Unit	Value
Particle Density	kg/m^3	2670
Gas Density	kg/m^3	0.442
Gas Viscosity	kg/ms	2.81*10^{-5}
Operating temperature	°C	500
Mean Particle size	µm	427
Bed voidage	-	0.4
Sphericity	-	0.86
Bed Height at minimum fluidising conditions	m	0.10
Bed diameter	m	0.065
Operational velocity	m/s	0.95

*All Gas parameters are of N_2 @ 500 °C

It should be noted that in order to determine the bed height at minimum fluidisation to be used in equation 9-17, a restriction imposed by Kunii and Levenspiel [114] on the ratio between the expanded bed height and the bed height at minimum fluidising conditions presented in equation 9-21 is used

$$1.2 < \frac{}{\phantom{H_{mf}}} < 1.4 \qquad \textbf{Eq 9-21}$$

Where H is maximum expanded bed height and H_{mf} is bed height at minimum fluidisation velocity. The maximum expanded bed height is assumed to be twice the internal diameter of the reactor so that H= 0.13 m. By choosing a value of 1.3 for H/H_{mf} based on equation 9-21, the bed height at minimum fluidisation velocity is estimated to be 0.1 m.

The pressure drop across the bed may now be obtained by inserting the appropriate values into equation 9-17.

$$\Delta = 2670 - 0.442 * 1 - 0.4 * 9.81 * 0.1$$

$$= 1965 \text{ N/m}^2$$

$$= 200.37 \text{ mm } H_2O$$

To estimate the value of the pressure drop across the distributor plate, a ratio of 0.3 of the pressure drop across the entire bed is selected based on equation 9-19.

$$\Delta \geq 0.3\Delta$$

$$\Delta = 0.3 * 200 = 60 = 5884 \quad /$$

For a bed diameter of 0.065mm at operating condition, the volumetric flowrate is

$$( ) = 0.95 * (0.0325) = 0.00315 = 3150$$

Rearranging equation 9-20 and inserting appropriate values where

P_d	pressure drop across distributor	=5884 dynes/cm^2
Q_g	gas flowrate	=3150 cm^3/s
T_p	plate thickness	= 0.3 cm
A_p	Plate area	= 33.18 cm^2
μ_g	Gas viscosity	=2.81*10-4 poise

$$= \frac{\mu}{}$$

$$= \frac{3250 * 2.81 * 10 \quad * 0.4}{7114 * 33.18} = 150 * 10$$

From Table 9-8, the distributor plate to give the nearest pressure drop is grade 50 i.e. 7114 dynes/cm^2. This satisfies the criterion that $P_d \times 0.3 \quad P_{bed.}$ When it came to ordering the plate however, a distributor of that specification required expensive fabrication. Thus, an off the shelf sintered plate with 3 mm thickness and 70 mm diameter was used instead. Interestingly, if the thickness of the grade 50 plate is reduced to 3mm in the Darcy equation, the value obtained for the pressure drop across the distributor is 5335 dynes/cm^2. That value is 90% of the estimated pressure drop of across the distributor. The material of construction of the distributor plate was to be chosen to be Hastelloy X. The chosen material has a maximum operating temperature limit of 930 ℃. Table 9-10 gives the composition of Hastelloy X.

Table 9-10 Elemental composition of Hastelloy X

Element	Amount %
Fe	17.0-20.0
Cr	20.5-22.5
Ni	bal
C	<0.15
Mo	8.0-10.0
Co	0.5-2.5
W	0.2-1.0

Maximum operating temperature 930 ℃

9.6 PLENUM DESIGN

The effect of the plenum chamber on successful operation of fluidised beds systems is often absent from literature on fluidised bed hydrodynamics. Work carried out by Grace and Vakhshouri [242] concluded that the proper design of a plenum for fluidised bed systems also affects to a large extent the quality of fluidisation bed hydrodynamics. The study concluded and recommended that details of plenum volume and design be provided for research concerning fluidised bed design.

The function of a plenum on a fluidised bed reactor is to distribute the gas under the distributor as uniformly as possible. Litz [243] concluded from a study on the analysis of fluidised bed plenums that its operation is dependent on a complicated three dimensional flow. The study also concluded that the complications of the flow may be simplified by designing the chamber to a volume that is large enough to accommodate any acceleration effects the gas may encounter. In the same vein, it concluded that even if the plenum is large enough for the gas pressures to equalise, the gas entry nozzle must also be positioned carefully to avoid maldistribution of the fluidising gas. Figure 9-5 shows typical plenum configurations.

Aston University

Illustration removed for copyright restrictions

Figure 9-5 Gas entry configurations into plenum chambers [244]

For horizontal entry into a vertical vessel, the high velocity gas stream expands until

1. It hits the opposite wall
2. It dissipates itself at about 100 times the nozzle diameter [245]
3. It hits the base of the distributor plate

The distributor plate should be situated at a distance H_w according to equation 9-22 and 9-23 [246], above the gas nozzle to prevent maldistribution where

H_w length of the windbox   [m]

D_w diameter of the windbox   [m]

D_{noz} diameter of the gas inlet   [m]

$$= 0.2 \quad + 0.5 \quad\quad - \quad\quad > \frac{}{100}$$

$$= 18 \quad\quad - \quad\quad < \frac{}{100}$$

For vertical Entry into a vertical vessel (as is the case with the proposed reactor) through a centred nozzle, the high velocity gas stream expands until

1. The diameter of the gas jet coincides with the vessel diameter
2. The gas dissipates itself
3. Hits the central portion of the distributor plate

The nozzle should be placed at a distance H_w [246] below the distributor plate to prevent maldistribution where

$$= 3 \quad - \quad\quad - \quad\quad > \frac{}{36}$$

$$= 100 \quad\quad - \quad\quad < \frac{}{36}$$

The limitations imposed by equations 9-24 and 9-25 were used to determine the appropriate equation to calculate H_W. The gas supply was to be passed through a 0.25 inch pipe. The diameter of the pipe equates to 6.35 mm. The reactor diameter is the same as the plenum diameter and is 65 mm. Therefore,

$$\frac{}{36} = \frac{0.065}{36} = 0.0018$$

As can be seen, the ratio of $D_w/36$ is less than the nozzle diameter such that equation 9-23 is appropriate for the estimation. The height of the reactor wind box H_w is

$$= 3\ 0.065 - 0.00635\ = 0.175$$

The appropriate height for the wind box based on the method proposed by Zenz [246] is 175.95 mm. Because of space considerations on the bench, a lesser value had to be considered. The value was reduced to 150 mm which equates to a 17.3% reduction in the calculated height of the plenum chamber.

Figure 9-6 shows the final reactor dimensional drawings. All dimensions are in millimetres.
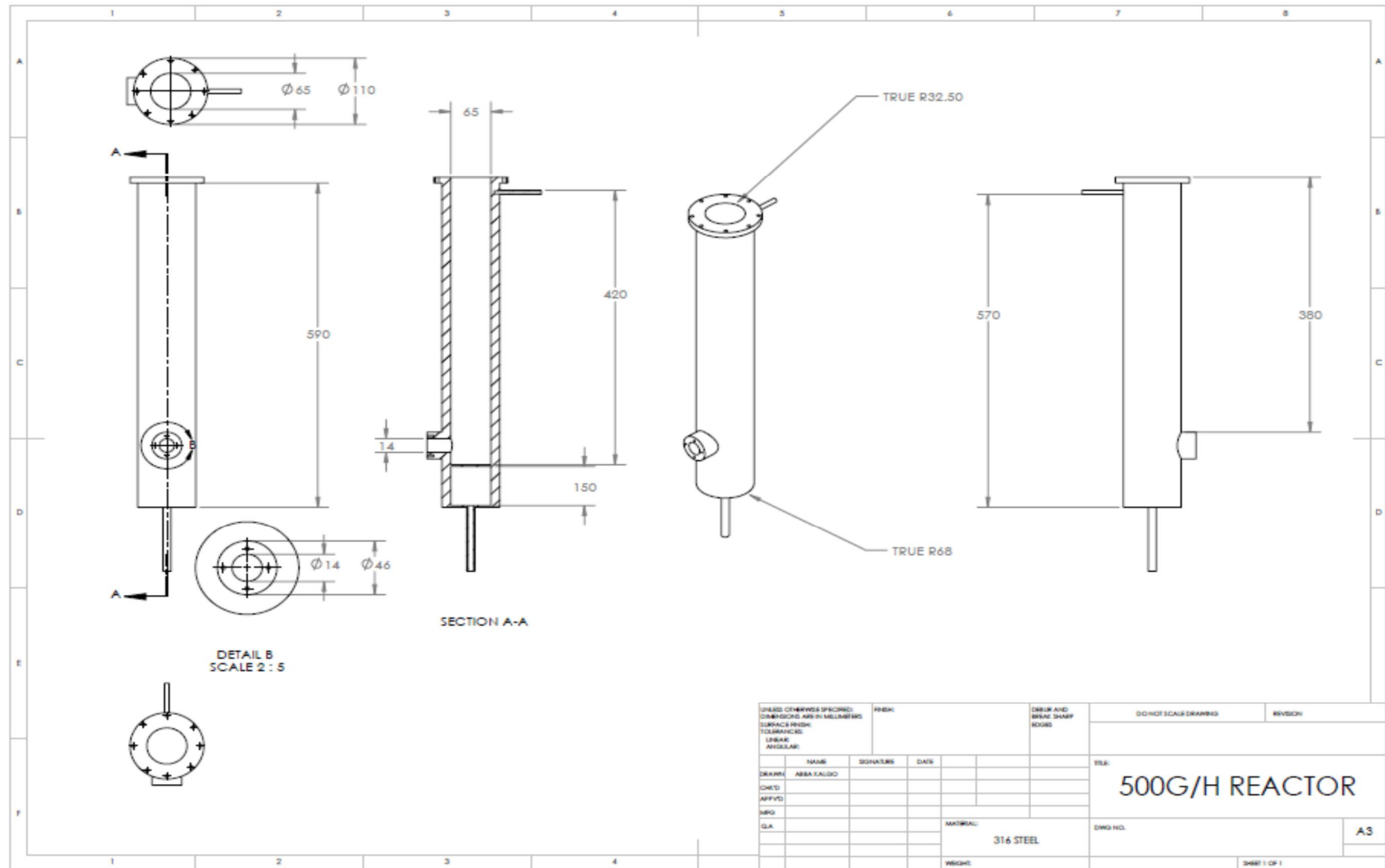
Figure 9-6 Dimensional drawings of 500g/h reactor

9.7   REACTOR COVER PLATE

For indication purposes on the designed reactor, thermocouples and analogue pressure meters were to be used. It was decided that all the probes be attached from the top of the unit. For that reason, the cover plate of the fluidised bed was machined from stainless steel with appropriate connections. The connections allowed for the use of Swagelock fittings with appropriate ferrules. The cover plate was to sit on top the reactor vessel with a high temperature gasket in between for sealing purposes. A schematic of the reactor cover plate is depicted in Figure 9-7.
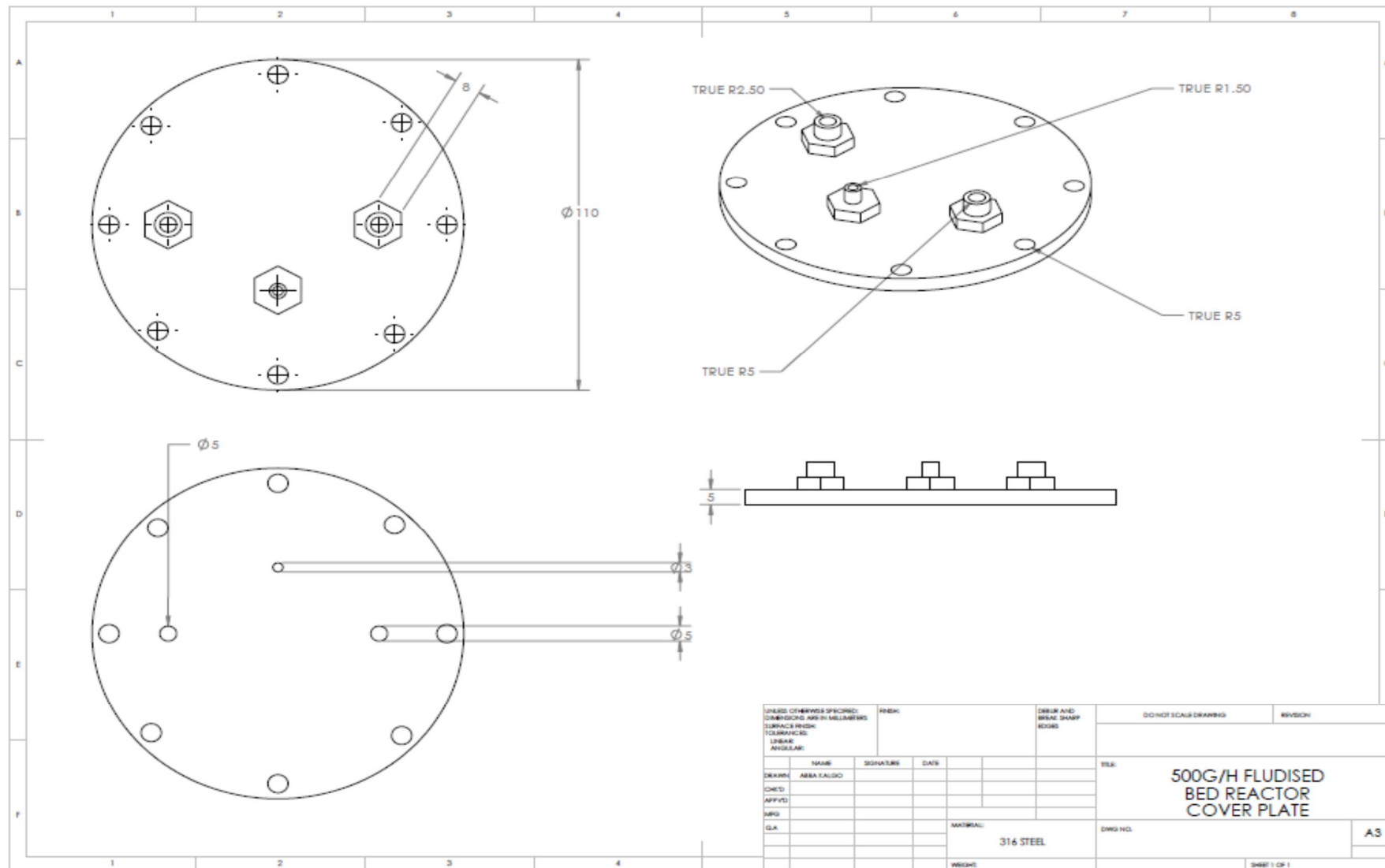
Figure 9-7 Dimensional drawings of fluidised bed reactor cover plate

9.8 OPTIMISED MULTIPOINT THERMOCOUPLE

For indication on the designed 500 g/h reactor, an optimised multipoint thermocouple was used. One of the characteristics of the 300 g/h reactor was the need for the operator to constantly take temperature readings at regular time intervals. This was usually time consuming and was prone to errors as the timings could not be exact. It was decided that a system capable of being connected to a data logging system be incorporated to the development of the new reactor to automate the collection of temperature data during experiments.

Since many laboratory and pilot scale systems are used for scale up purposes, it is essential that as many temperature readings as possible be obtained over the length of the reactor. This can be particularly useful in obtaining temperature profiles along the entire reactor for modelling and future reactor design. In most conventional lab scale units, this is achieved by a number of thermocouples inserted at different points along the reactor as is the case on the BERG 7 kg/h, 1 kg/h and 150 g/h fast pyrolysis units at Aston University. This method of data collection is also used on the commissioned 300 g/h unit reactor.

The major disadvantage with this system lies in the fact that the hydrodynamic behaviour in fluidised beds particularly those less than 100 mm diameter can be altered by having too many probes particularly in the fluidised bed region. The bubble formation in fluidised beds can be altered by probes inserted through the cross section of the bubbling bed. This can lead to poor fluidisation and irregular hydrodynamic behaviour which are unwanted characteristics.

Based on the disadvantages of having too many probes and the need to be able to collect reliable temperature data from the reactor, the need to find a reliable data collection system with as few numbers of probes in the reactor arose.

This was achieved by the use of an optimised multipoint thermocouple. The thermocouple was fabricated by Idaho labs in the United States. The probe was designed especially for the 500 g/h unit based on dimensions obtained during this research.

The optimised multipoint thermocouple is a single probe, with multiple measurement points across the length of the probe. The thermocouple used in the reactor had seven measuring points across its entire length. Its photograph is shown in Figure 9-8. The points on the probe

were chosen based on a cold model (not shown) of the reactor to choose precise points of interest along the reactor length.

The thermocouple was held in place through the reactor lid through a Swagelok fitting through steel ferrules that allowed for movement in the vertical direction for cleaning and straightening when the need arises.
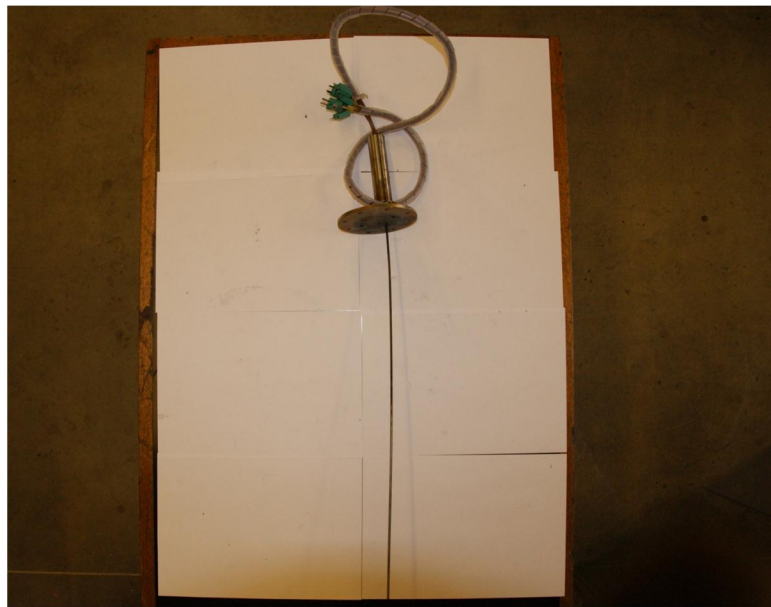
Figure 9-8 Digital photograph of OMPT attached with reactor cover plate

The points are located based on the data presented in Table 9-11

Table 9-11 Optimised multipoint thermocouple data

Thermocouple Point	Distance on Probe (inches)	Point of Measurement
1	0	Distributor/ Gas Entry Temperature
2	2	Biomass Entry Point
3	3	Fluidised Bed
4	5.5	Fluidised Bed
5	10.5	Freeboard
6	14.5	Freeboard
7	16.5	Reactor /Gas/Vapour Exit

9.8.1   Commissioning of optimised multipoint thermocouple

The optimised Multipoint thermocouple commissioning was undertaken after the unit was connected to a data logging system via the necessary cabling. It was necessary to observe the OMPT behaviour at elevated temperatures under which fast pyrolysis occurs. One hot commissioning test was carried out on the OMPT. The test involved heating the 500 g/h reactor with a bed of quartz sand at the proposed operational conditions. This included

heating the reactor to pyrolysis temperature with a pre-heated stream of nitrogen (450 ℃) as fluidising gas. The data obtained from this experiment is shown in Figure 9-9.
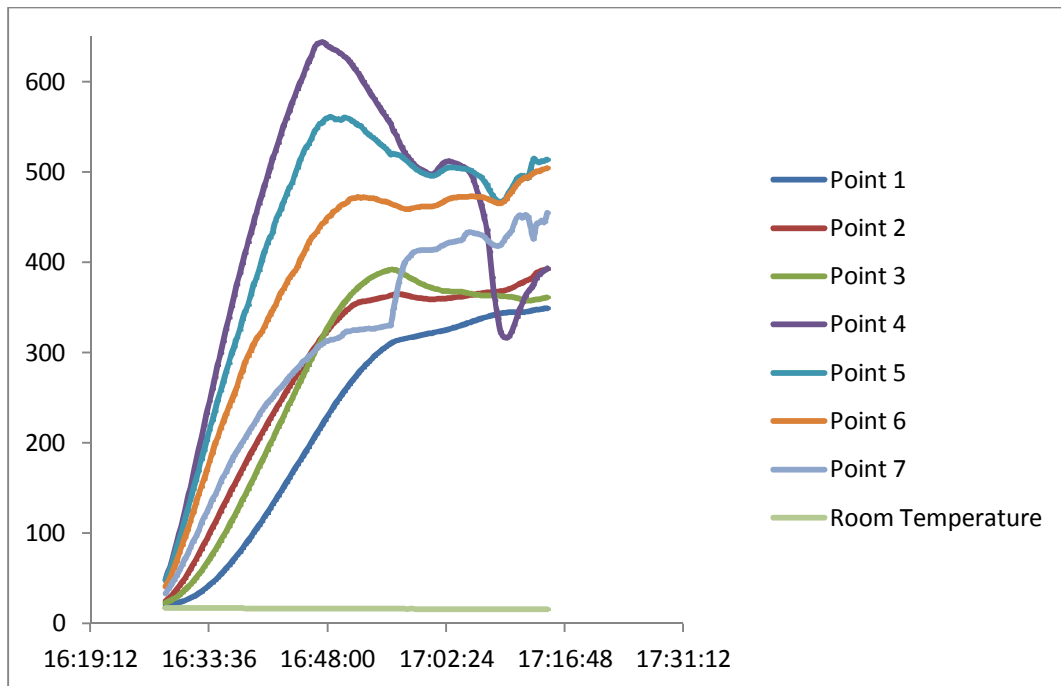
Figure 9-9 500g/h reactor temperature profile as measured by OMPT

The data obtained also proved to be important as it gave an indication of the time required for the bubbling fluidised bed to reach pyrolysis temperature. The time observed was however taken in the winter and this may vary during warmer periods of the year. The material and amount of thermal insulation is also certain to have an effect on the time taken for the reactor to reach pyrolysis temperature. The data obtained from the commissioning test indicated clearly the OMPT is functional and capable of giving accurate temperature measurements along the entire length of the 500 g/h bubbling bed reactor

10 OPTIMISED SYSTEM FAST PYROLYSIS

This chapter describes the fast pyrolysis experiments carried out using the optimised fast pyrolysis system. 5 experiments were undertaken. The chapter also reports the characterisation and quality assessment of pyrolysis products from the primary feedstocks produced using the optimised configuration.

10.1 INTRODUCTION

The two previous chapters have detailed the design and commissioning studies of the optimised feed system and the new fast pyrolysis reactor. One feature of the alternative feed system is the possibility of operating either the initial reactor at the beginning of the study or the new reactor developed in chapter 9. The feed system was easily adaptable because of the relatively small difference between the reactor diameters i.e. 41 and 65 mm. This ensures that an even distribution of biomass particles across the bed can be maintained. Figure 10-1 shows a photograph of both reactors side by side with their band heaters attached. From the photograph, it is apparent that the new reactor is bigger than the initial reactor. This should by extension, be able to handle higher biomass throughputs and possess a wider hydrodynamic operational range.

Figure 10-1 Photograph of new and initial reactor units

10.2 OPTIMISED FAST PYROLYSIS CONFIGURATION

As a result of the optimisation of the feed system, the process configuration was changed. The new configuration as shown in Figure 10-2 shows the dual screw feed system. The configuration depicted was used for the rest of the research.
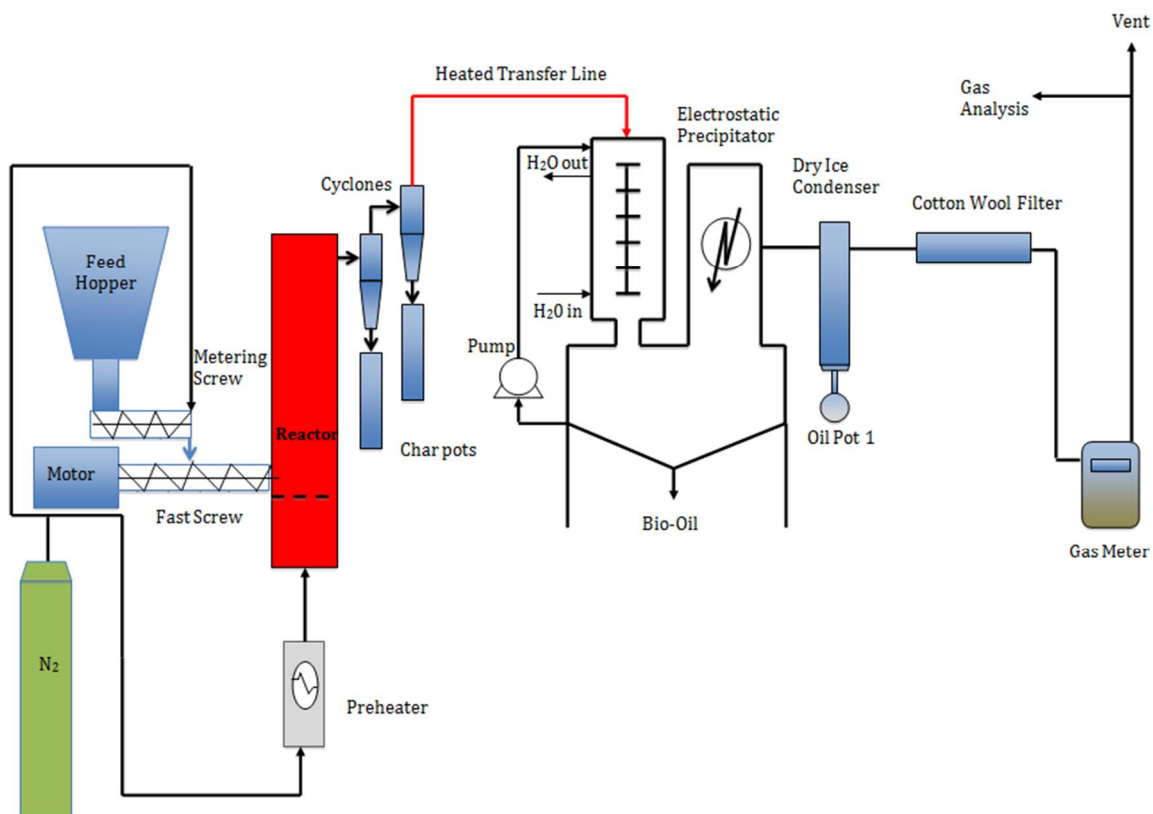
Figure 10-2 Optimised system flowsheet

As already highlighted, the fast pyrolysis runs described in this chapter report 5 experiments carried out using the optimised system.   One of the fast pyrolysis experiments was undertaken using Beechwood as feedstock. Beechwood was the base case feed at the beginning of experimental work. The remaining four experiments involved each of the primary feedstocks.

10.3 FAST PYROLYSIS EXPERIMENTS USING OPTIMISED SYSTEM

The primary aims of these experiments were to

- Commission the new reactor and alternative feed system under fast pyrolysis conditions

- Observe product distribution using the optimised system at higher throughputs

- Produce pyrolysis products under optimum conditions for quality assessment and characterisation

Figure 10-3 shows a photograph of the optimised fast pyrolysis system as used for this set of experiments. The gravimetric K-TRON KT 20 feed system is not included in the photograph.

Figure 10-3 Photograph of optimised rig showing alternative feed system and 500g/h reactor

The parameters set out in Table 10-1 were set as the operating conditions for the optimised system.

Table 10-1 Operational parameters for optimised system experiments

Parameters	unit	Value
Reaction Temperature	(℃)	500
Fluidising gas flowrate	(l/min)	48
Mass of fluidising medium	(g)	300-500
Biomass Feed Particle size	(µm)	355-849
Biomass feed rate	(g/h)	300-450
Fluidising medium particle size	(µm)	600-850

Table 10-2 is a summary of the mass balances for the experiments undertaken using the optimised system.

Table 10-2 Mass balance results for experiments carried out on 500g/h reactor

Run Number	500BW	500 AM	500 IM	500 AJ	500 IJ
Feedstock	**Beech Wood**	**African Moringa**	**Indian Moringa**	**African Jatropha**	**Indian Jatropha**
Average Reaction Temperature(℃)	507	504	430	512	508
Feed Rate(g/h)	450	300	250	300	300
Moisture content (mf wt%)	9.55	6.19	6.35	7.36	8.07
Ash (mf wt%)	1.0	5.53	5.62	5.27	9.26
Particle size (μm)	355-849	355-849	355-849	355-849	355-849
Run Time (minutes)	90	90	60	90	90
INPUT (g) Wet Feed Dry Feed Feed water	675.30 610.80 64.50	450.80 423.89 26.91	249.87 234.70 15.17	451.13 417.92 33.21	451.92 410.77 41.15
YIELDS (mf wt%) **Total Liquids** Organics Reaction Water **Char** **Gas**	**60.96** 51.83 9.13 **18.51** **17.53**	**60.17** 42.75 17.42 **22.29** **14.80**	**58.83** 37.78 17.05 **20.11** **19.87**	**66.92** 51.26 15.66 **13.49** **18.03**	**58.22** 38.94 19.28 **24.57** **15.01**
Closure	**97.06**	**97.26**	**94.51**	**98.44**	**97.80**
Gas composition (vol %)* H_2 CO CO_2 CH_4 C_2H_4 C_2H_6 C_3H_6 C_3H_8	1.11 32.34 59.21 6.63 1.88 0.93 0.55 0.21	1.26 21.62 72.81 3.54 0.08 0.59 0.04 0.06	2.86 48.21 49.50 3.14 0.04 0.02 0.03 0.06	0.78 26.54 66.11 4.57 1.01 0.02 0.94 0.03	1.69 31.49 61.42 3.57 0.14 0.41 0.15 0.13

mf: moisture free;

10.3.1 Observations, results and discussions

In terms of the pre-pyrolysis problem discussed in section 7.6.2.1, the alternative feed system proved very effective in eliminating it. No pre-pyrolysis was noticed after all the experiments undertaken with the modified feed system. Only the run involving Indian Moringa (500IM) showed problems with agglomeration in the reactor and was discontinued after 60 minutes. The temperature had dropped to a value not suitable for fast pyrolysis. All other experiments lasted for 90 minutes with high mass balance (>95%) closures obtained for them.

The first run of this series involved Beechwood as the feedstock. The biomass feed rate was set at 450 g/h in order to test higher biomass throughputs with the new reactor. The run lasted for 90 minutes. Although no feeding problems were noticed, the electrostatic precipitator after the quench column seemed unable to handle the higher gas and vapour flowrates. A problem of re-entrainment of aerosols captured by the ESP was noticed at the higher biomass and fluidising gas throughputs. Evidence of this was present from the dry ice condenser as drops of bio-oil were found in the oil pot below it. The efficiency of the ESP also seemed to drop as fluctuations in the operational voltage were noticed with the higher biomass throughput.

The problem of re-entrainment of aerosols captured in the ESP meant that all subsequent runs were limited to throughputs of no more than 300 g/h. If the re-entrainment observed is excluded, the experiment can be deemed successful as it lasted 90 minutes at a throughput of 450 g/h. The mass balance closure for the Beechwood run was 97.06 % with a total liquid yield of 60.96 wt% of dry Beechwood.

Another observation made when assessing the mass balance results from the optimised system is the increase in organic yields compared to the initial fast pyrolysis process. In the case of beech wood from experiment 500 BW, an increase in total liquid and organic liquid yield is observed when compared to experiments carried out prior to optimisation of the system (see section 7.4.1). The same trend can be seen for African Moringa and Indian Jatropha experiments. An increase in the organic liquid yields has occurred for runs undertaken with the same particle size and temperature. Figure 10-4 compares the pyrolysis product yields for Beechwood, African Moringa and Indian Jatropha using the initial fast pyrolysis configuration and the optimised system. The runs compared include TIR-003 and TIR-007. The reader may recall that these experiments were carried out at 500 ºC (see section 7.5.1). The organic yields increases seem to have come from a reduction in char generated.
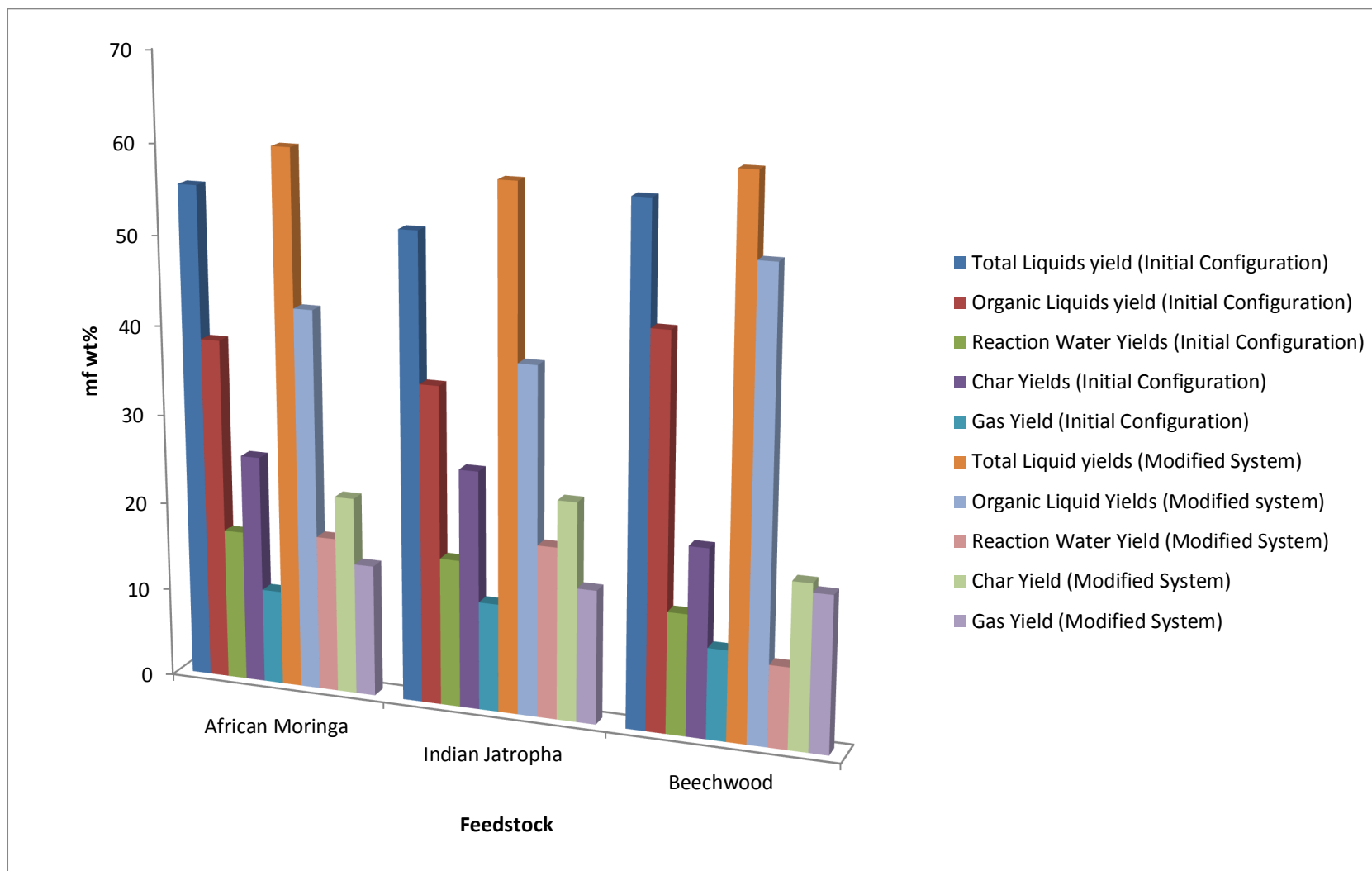
Figure 10-4 Comparison of product yields for initial and optimised process

Another trend can be observed from the mass balance results presented in Table 10-2 as per the composition of the product gases. The yield of methane from the non condensable gases is shown to have increased when compared to the experiments carried out using the initial configuration. What the observation suggests is that a reduced extent of pyrolysis vapour cracking favours the formation of methane as a non condensable gas. It cannot be said for certain if the increases in methane yields are as a result of a reduction in vapour residence time or the absence of char in the reactor. Also, the low yields of C_2-C_4 gases suggest the presence of other gases not detectable by the gas chromatograph. The higher than usual sulphur contents in the feedstocks suggest the formation of gases like H_2S and SO_X at the expense of hydrocarbons.

With regards to the product yields from the primary feedstocks, African Jatropha is shown to give the highest yield of both organic (51.26 mf wt%) and total liquids (66.92 mf wt%). 451.13 g of African Jatropha was fed during the experiment. The experiment lasted for 90 minutes and ended with no problems. The highest yields of Organic and total liquids from African Jatropha was a surprising and unexpected result since the volatile content obtained for the original African Jatropha feedstock reported in section 5.2 was not the highest amongst the primary feedstocks. Char yield was 22.29 wt% while gas yields were 17.53 wt%.

It can also be seen that Indian Moringa gave the lowest yield of organic liquids of all the primary feedstocks. This is a result of the agglomeration observed with the feedstock. As can be seen from the Table 10-2, the run lasted for 60 minutes while all the others lasted for 90 minutes. The run had to be ended prematurely as there was a swift drop in pyrolysis temperature to under 400 ℃ just before the end of the experiment. The biomass feed rate during the experiment also had to be reduced as a blockage occurred in the fast screw system. The shorter duration of the run is also responsible for the lower mass balance closure obtained although a 94.51% closure may be considered as acceptable.

African Moringa gave a total liquid yield of 60.17 wt% on a moisture free basis. A total of 450.80 g of African Moringa was fed on a wet basis. The feed moisture content was 6.19 wt% meaning that 422.89 g of dry African Moringa was processed during the run. The total organic yields from the experiment was 42.75 wt% on a dry basis while 17.42 wt% of African Moringa was reaction water generated on a dry basis. 22.29 wt% of the total feedstock was converted to char while gas yield obtained stood at 14.80 wt%. The total mass

balance closure of the experiment was 95.96 % and the experiment lasted 90minutes with no problems reported.

The run involving Indian Jatropha as feedstock also lasted for 90 minutes and ended successfully. Total pyrolysis liquid yield obtained were 58.22 wt% of Indian Moringa on a dry basis. The reaction water generated was 19.28 wt % which was the highest reaction water yield of this series of experiments. Char yield was 24.57 wt% while total gas yield was 15.01 wt%. The gas analysis of the product gas showed that Indian Jatropha had similar gas composition to its African counterpart. Its organic yields were significantly less however. Indian Moringa produced the highest amount of char of the primary feedstocks.

10.4 CHARACTERISATION OF PYROLYSIS LIQUIDS

The pyrolysis products from this batch of experiments were fully characterised using the techniques reported in section 4.7. The choice to completely characterise the products from this set of experiments was because they were the products generated under optimum pyrolysis conditions. As such, they were the products most suitable for characterisation and quality assessment.

10.4.1 Water and solids content

In section 7.5.2.2, the solids and water contents of the oils produced were measured. The results though accurate were not likely to be actual representation of water and solid contents because of the feeding and pre-pyrolysis problems encountered with the fast pyrolysis configuration at the time. For that reason, the samples of the primary feedstocks produced from the optimised system were analysed for solid and water contents. This batch of oils was produced with the new feed system, under reaction conditions that may be considered as ideal for a fast pyrolysis process. Table 10-3 shows the water and solid contents measured. The table also includes the water content of the oils produced from African Moringa and Indian Jatropha (experiment TIR-300-003 and TIR-300-007) at a target pyrolysis temperature of 500 °C using the initial configuration.

Table 10-3 Water and solid contents of pyrolysis liquids from primary feedstocks

Feedstock	Experiment Number	Water Content (wt%)	Solid Content (wt%)
Indian Moringa	500IM	7.18	0.42
Indian Jatropha	500IJ	12.01	0.51
African Moringa	500AM	8.42	0.49
African Jatropha	500AJ	6.70	0.38
African Moringa	TIR-300-003	28.19	0.39
Indian Jatropha	TIR-300-007	32.11	0.41

It can be seen from the table that the water contents for the main bio-oils produced from the 500 series experiments range between 6-12 wt%. The values reported are average values over triplicate measurements. The water content results show that the oils from the primary feedstocks contain less water than conventional biomass which is reported to be between 15-30% for wood [247]. The low water content of the bio-oils seems to be typical of press cake residues. Ozcimen [160] reports bio-oil with as little as 0.001 vol% water from the pyrolysis of rapeseed residues. Smets et al [139] report bio-oil with 8.4 and 6.7 wt% from pyrolysis of rapeseed at 450 and 500 ºC respectively.

When comparing the water content of oil from the initial and optimised configuration, it can be seen, that there is a reduction in the values. Water content of African Moringa and Indian Jatropha oil decreased from 28.19 wt% and 32.11 wt% to 8.42 wt% and 12.01 wt% respectively. This reinforces the conclusion reached in section 7.5.2.2 where it was suggested that the presence of char in the reactor was encouraging water retention reactions since the char was not leaving the reactor.

The water content of bio-oils is reported to be both advantageous and disadvantageous to its use as a fuel [247]. While a higher water content may reduce the viscosity and have a positive impact on pumping costs, it is also capable of reducing the heating values of the oil and impact negatively on its energy content as a fuel.

The solid content of bio-oils is an important parameter since it may cause blockages in fuel systems. Pipes, pumps, valves and nozzles are all at risk of being blocked if high solid content oils are passed through them.

As per the solids content, all the oils show solid contents to range between 0.38 and 0.44 wt%. As already mentioned, the efficiency of solids removal on the current process is a function of cyclone efficiency which drops significantly when particle sizes of less than 10 µm pass through. This is the reason that no visible reduction in oil solid content is noticed when oils from experiment TIR-300-003 and TIR-300-007 are compared to 500AM and 500IJ. Even though the char formed during TIR-300-003 and TIR-300-007 did not leave the bed, some form of attrition possibly from the feeding screw rubbing across the char particles was causing formation small char particles. That is a possible explanation as to why no reduction in solid content is noticed between oils from the initial configuration and the optimised one.

The solid contents of bio-oil may be reduced using a number of techniques notable amongst which is hot vapour filtration. A recent study by Sitzmann [97] of hot vapour filtration undertaken at Aston University demonstrated that solid contents of 0.01 wt% may be achieved if organic vapours from fast pyrolysis are subjected to hot vapour filtration prior to quenching. This may be a very efficient way of reducing the solid contents in bio-oil depending on its intended use. It should be noted however that, reduction in solids content using hot vapour filtration is at the expense of organic liquid yield since an increase in residence time is characteristic of the technique. That causes extended cracking of organic vapours reducing liquid yield as concluded by Sitzmann.

10.4.2 Elemental Composition, heating values and pH

The elemental compositions of bio-oils from all the primary feedstocks are presented as part of Table 10-4. The pH and heating values obtained using bomb calorimetry and estimated based on elemental composition are also reported in the same Table 10-4.

Table 10-4 Properties of Pyrolysis liquids from primary feedstocks

Experiment No	500IM	500IJ	500AM	500AJ	[139]	[247]
Feedstock	Indian Moringa	Indian Jatropha	African Moringa	African Jatropha	Rape meal	Wood
Elemental Composition (wt%, mf)						
Carbon	66.33	67.64	65.02	64.90	70.20	54-58
Hydrogen	9.61	9.32	12.98	8.54	10.00	5.5-7.0
Nitrogen	7.06	8.26	2.65	7.82	5.10	0-0.2
Oxygen	15.97	14.39	18.91	18.36	14.10	35-40
Sulphur	1.03	0.39	0.44	0.38	0.60	-
H/C molar ratio	1.74	1.65	2.40	1.58	1.71	-
O/C molar ratio	0.18	0.16	0.22	0.21	0.15	-
Empirical Formula	$CH_{1.74}N_{0.09}O_{0.18}S_{0.005}$	$CH_{1.65}N_{0.10}O_{0.16}S_{0.002}$	$CH_{2.40}N_{0.035}O_{0.22}S_{0.002}$	$CH_{1.58}N_{0.10}O_{0.21}S_{0.002}$	$CH_{1.71}N_{0.06}O_{0.15}S_{0.003}$	-
Heating Values (MJ/Kg)						
HHV calorimeter	27.57	24.11	26.62	28.89	33.17	-
HHV calculated	26.93	27.11	28.82	25.81	-	17.3
LHV	24.84	25.07	25.99	23.95	-	-
pH						
Main Bio-Oil	7.1	6.8	7.1	6.8	6.9	2.5
DIC liquid	6.7	6.8	6.9	6.3	6.4	-

In assessing the result of the elemental compositions of the bio-oils from the primary feedstock, it is apparent that they are very similar. As can be seen from the Table 10-4, carbon contents between 64-68 wt% are present in all the bio-oils. This is indicative of high energy contents of the oils. The carbon contents of all oils from the primary feedstocks also indicate a high level of carbon conversion efficiency which is defined as the amount of feedstock carbon present in the bio-oil product.

Not surprisingly, the bio-oils from the Indian feedstocks have lower oxygen content than their African counterparts. This is an expected result as the ultimate analysis in chapter 4 showed that the original African feedstocks had higher oxygen contents than the Indian ones. Of the primary feedstocks, oil from Indian Jatropha had the lowest oxygen content while African Moringa oil exhibited the highest oxygen content of 18.36 wt%. Indian Moringa and African Jatropha had oxygen contents of 15.97 and 18.36 wt% respectively.

They also contain significantly lower amounts of oxygen when compared to bio-oil from conventional bio-oil from cellulosic feedstocks. Typically, bio-oil from cellulosic feedstocks would contain 40-50 wt% oxygen [247]. The reason for the low oxygen content in the bio-oils from the primary feedstocks cannot be theorised with certainty although a possible explanation is that the decomposition of the residual oil and proteins in the feedstock is causing oxygen rejection by the pyrolysis vapours.

In terms of hydrogen distribution, African Moringa seemed can be seen to possess the highest amounts of hydrogen amongst oil from the primary feedstocks at 12.98 wt%. All others bio-oils had hydrogen contents between 8-10 wt%.

Similarly, the entire oils exhibit high nitrogen contents which again are not unexpected with the originally high amounts of nitrogen in the initial biomass feedstocks. Indian Moringa, Indian Jatropha and African Jatropha all had similar nitrogen contents between 7-8 wt% while the oil from African Moringa had a nitrogen content of 2.65 wt%.

The measure of pH goes a long way in determining the suitability of any bio-oil as a potential fuel. Bridgwater [10] reports that pH is responsible for corrosion and care must be taken when using high pH bio-oils as fuels. Corrosion resistant materials like stainless steel and olefin polymers are preferred to reduce corrosion. The presence of carboxylic compounds including formic and acetic acids are responsible for high pH in bio-oil.

pH values show the bio-oils from the primary feedstocks to be almost neutral. This is unusual with bio-oil since as most bio-oils are acidic with pH values between 2-3 [248]. A possible explanation for the pH values is the decomposition of crude protein into basic compounds to neutralize the acids in the bio-oils.

Table 10-4 also makes reference to bio-oil from a rape meal study by Smets et al [139]. It can be seen based on their data that the exhibited characteristics of bio-oil from the primary feedstocks may not be limited to Jatropha and Moringa press cakes but bio-oils from press cakes as a whole.

10.4.3 Molecular weight distribution and stability

Despite the promise shown by bio-oil as a potential fuel, one of the major drawbacks associated with its use is its stability. The stability of a bio-oil is measured primarily by the extent of an increase in viscosity over time. Typically, the viscosity of bio-oil increases with storage and is an unwanted characteristic [248]. The stability of bio-oil is affected by the high levels of oxygen and water present.

The molecular weight distribution of bio-oils produced from all the primary feedstocks were analysed using the GPC technique described in section 4.7.1.2.

The tests carried on molecular weight distribution of the primary feedstocks involved analysis of freshly produced bio-oils and aged bio-oil. The freshly produced bio-oils refer to oils subjected to GPC no later than 7 days after production and stored in a fridge a temperature of 4 °C after collection. The aging of the bio-oils were carried out using a method proposed by Oasmaa and Meier [249] which equates the storage of bio-oil at 80 °C for 24 hours to storing bio-oil at normal room conditions for a year. The aging of the bio-oils were achieved by putting the samples in a sealed vessel for 24 hours at 80 °C in an oven.

The results from the GPC analysis were presented in form of the weight average molecular weight (Mw), number average molecular weight (Mn), molecular weight at highest peak (Mp) and the polydipersity (PD). The importance of measuring the molecular weight distribution of bio-oils is that it has a close correlation with the viscosity which is another important parameter in terms of bio-oil quality.

Table 10-5 shows the GPC results of fresh and aged oils from all 4 primary feedstocks. For Comparison purposes, the Table 10-5 also includes data on the molecular weight distribution of fresh and aged bio-oils for more conventional feedstocks measured using GPC. Also, the GPC results of press cakes similar to the primary feedstocks i.e. Pennycress and Camelina from literature [250] are included.

Table 10-5 Data from GPC studies on oils from primary feedstocks

	Feedstock	African Jatropha	African Moringa	Indian Jatropha	Indian Moringa	Beechwood [97]	Camelina Presscake [250]	Pennycress presscake [250]	Cassava stalk [183]
Molecular Weight									
Fresh	**Mw**	261	246	289	190	325	250	410	369
	Mn	163	161	180	126	NA	178	255	247
	Mp	402	177	393	179	NA	NA	NA	172
	PD	1.60	1.52	1.60	1.50	NA	NA	NA	1.49
Aged	**Mw**	258	240	301	192	525	248	408	778
	Mn	162	160	179	130	NA	176	253	347
	Mp	402	177	402	179	NA	NA	NA	172
	PD	1.59	1.50	1.68	1.47	NA	NA	NA	2.24

NA: Not Available

Figures 10-5 and 10-6 shows the curves for Mw and Mn of all the fresh and aged bio-oils listed in Table 10-5. It is pertinent to note that the steeper the curve between the fresh and aged bio-oils of any given sample, the less stable it is.
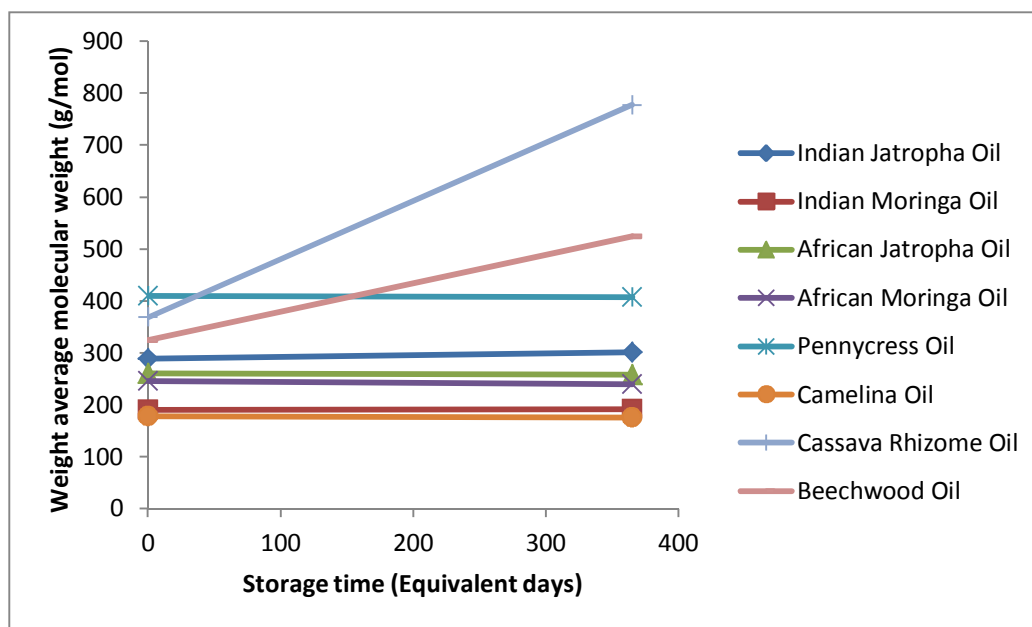
Figure 10-5 Impact of aging on weight average molecular weight of oils from primary feedstocks
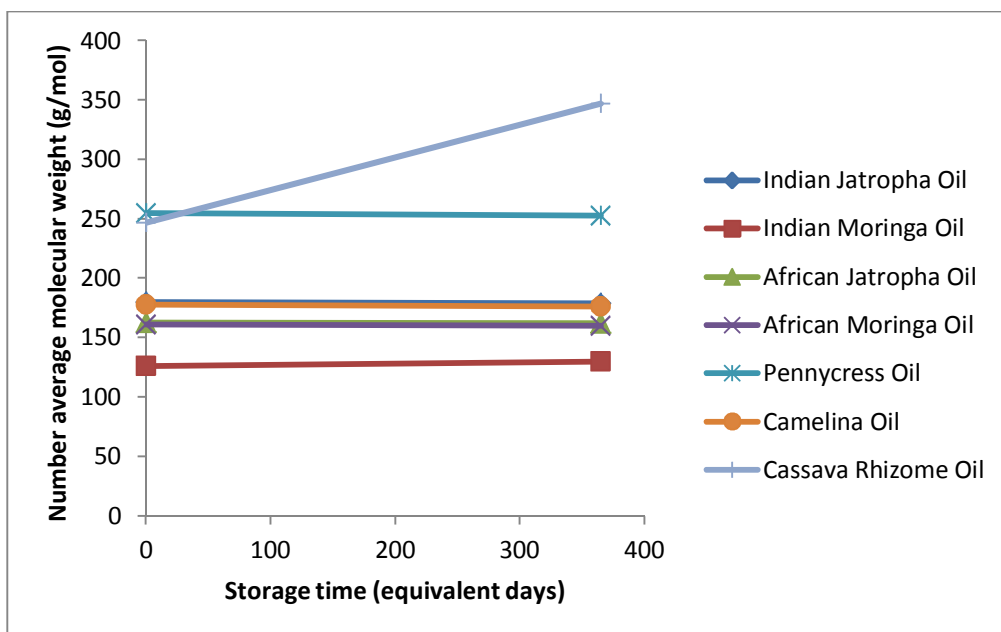
Figure 10-6 Impact of aging on number average molecular weight of oils from primary feedstocks

The results of the GPC analysis shows that the bio-oils produced from the primary feedstocks have a high degree of stability. Despite the accelerated aging the samples were subjected to, they remained very stable with results of African Jatropha and African Moringa oil showing an increase of stability with age as the average molecular weight decreased for both feedstocks. In the case of the Jatropha feedstocks, a slight increase in the molecular weight was noticed from 289 to 301 g/mol for Indian Jatropha while the molecular weight of Indian Moringa increased from 190 to 192 g/mol after accelerated aging.

To emphasise the unconventional high levels of stability exhibited by oils from the primary feedstocks, comparisons have been made with fresh and aged bio-oil produced from beech wood and cassava rhizome [97, 183]. They were also subjected to GPC analysis before and after accelerated aging. The weight average molecular weight for freshly produced bio-oils from beech and cassava were 325 and 369 g/mol respectively. After accelerated aging, the values increased to 525 and 778 g/mol for beech and cassava rhizome respectively. This is almost a two fold increase in the weight average molecular weight indicating substantial changes resulting from polymerisation and oligomerisation reactions. These increases in molecular weights noticed in oil from Beechwood and cassava rhizome are typical characteristic behavior of bio-oil aging with conventional feedstocks used for fast pyrolysis.

Not many studies on bio-oil stability from the fast pyrolysis of press cakes are available. A 2010 study by Boateng et al [250] reported unusually high stability of bio-oil produced from press cakes of oil seeds from the mustard family. The study reported GPC analysis of fresh and aged bio-oils of Pennycress and Camelina press cakes. The oils were aged using the same methods employed during this research. The results of the study are in strong agreement with findings from this research. They also reported an increase in stability after aging of bio-oil from Pennycress and Camelina press cakes. The results of the study are also plotted as part of Figures 10-6 and 10-7.

A comparison of the elemental composition of the primary feedstocks with the feedstocks from the study by Boateng revealed striking similarities in terms of nitrogen, hydrogen, carbon and oxygen contents. They exhibited high nitrogen contents (>5%) indicative of high protein content as the primary feedstocks of this research (see section 5.2).

When comparing the primary feedstocks against one another, it can be seen from Figures 10-5and 10-6, there is a strong resemblance in molecular weights of the bio-oils produced from African Moringa and African Jatropha. The values for the Weight average Molecular Weight and the number average molecular weight are almost identical. This suggests that the co-pyrolysis of both feedstocks could be explored as a part of a complete bio-refinery concept.

The values for polydipersity, PD have also been reported in Table 10-5. The PD is a measure of the molecular homogeneity of any given sample. It is a representation of the ratio of the weight average molecular weight to the number average molecular weight (Mw/Mn). Values of PD are always greater than 1 and a higher PD value is representative of lower molecular homogeneity. PD values for the fresh oil from all primary feedstocks show them to be in the range between 1.50-1.60. The PD values after aging show that the highest change in polydipersity was in the case of Indian Jatropha which showed an increase from 1.60 to 1.68. All the other oils showed a reduction in polydipersity indicating that the level of molecular homogeneity increased after aging. To give an indication of a typical change in polydipersity, the change in polydipersity change between fresh and aged bio-oil from cassava rhizome was from 1.49-2.24 [183]. That is an increase of more than 50 % in its value. The highest change in PD from the primary feedstocks was 5% in Indian Jatropha while all the other feedstocks showed a PD value shift in the negative.

The results of the GPC analysis suggests that an increase in viscosity associated with bio-oils as they age may not be noticed with bio-oils produced from the primary feedstocks.

10.4.4 GC/MS analysis of pyrolysis liquids

Bio-oils produced from the fast pyrolysis of the primary feedstocks were further subjected to GC/MS analysis, the method for which has already been reviewed in section 4.7.1.4. The aim of the analysis was to identify and quantify the main compounds present in the pyrolysis liquids since products from the feedstocks are scarcely reported in literature.

Tables 10-6 to 10-9 list the major compounds identified in the pyrolysis liquid fractions for each of the 4 primary feedstocks along with their quantities as calculated from the integrated peaks of the chromatographs.

Table 10-6 Major GC detectable compounds in Indian Moringa pyrolysis liquids

Compound	% peak Area	
	Main oil	**DIC liquid**
Pyrrole	9.766	0.00
3-pyridine carboxyaldehyde,o-acetyloximine	2.011	0.75
2-hydroxtethylhydrazine	1.870	0.00
phenol	4.19	0.00
Phenol 4-methyl	4.35	0.00
Propanenitrile,2-methylthiol	1.001	4.79
2,4-imadazolidinedione 5,5 dimetthyl	0.00	43.12
2,4-imadazolidinedione 5ethyl-5 metthyl	0.00	25.87
Sulfur	0.00	0.86
Furfuryl alcohol	0.258	0.00
3,4 dimethyl pentanol	2.208	0.00
Dodecane 2,6,10-trimethyl	0.941	0.00
Heptadecane 2.6,10,15 tetramethyl	0.847	0.00
Heneicosane	0.144	0.00
Benzeneacetonitrile, 4-hydroxy	6.254	0.00
Cyclic octaatomic sulfur	0.683	17.40
Hexadecenoic acid, ethyl ester	2.314	2.3
9-octadecenoic acid (Z) tetradecyl ester	40.819	0.00
Oleic acid	4.60	1.004
Total	82.255	96.094

Table 10-7 Major GC detectable compounds in African Jatropha pyrolysis liquids

Compound	% peak Area	
	Main oil	DIC liquid
Pyrrole	1.096	0.511
Dimethyltrisulfide	1.041	0.00
Piperdine 2,3-dimethyl	7.654	0.141
Pyridine 2,4,6 trimethyl	3.447	0.00
Indole	1.751	2.514
Crestomycin	3.086	0.00
2-methyl-1-ethylpyrrolidine	1.189	4.108
Furfuryl alcohol	0.590	0.00
Dimethylhydantoin	0.00	4.099
5-isopropyl-2,4-imidazolidinedione	4.876	6.157
Phenol	2.024	0.00
Mequinol	0.465	0.00
2 methyl phenol	0.644	0.00
Carbamic acid	0.250	0.00
3 ethyl phenol	1.646	0.00
2 methoxy 4 vinyl phenol	2.493	0.00
3,4 dimethylphenol	0.993	0.00
2,6 dimethoxyphenol	0.851	0.00
3-ethylphenol	0.487	0.00
Oleic acid	32.077	22.489
Phorbol	3.100	11.622
Total	69.76	51.641

Table 10-8 Major GC detectable compounds in African Moringa pyrolysis liquids

Compound	% peak area	
	Main Oil	**DIC liquid**
Acetic acid methyl ester	0.212	0.00
Pyrrole	7.843	3.482
Triopilidine	0.529	0.00
5-Amino-2H-tetrazole	5.591	1.247
Pyrazole 1,4 dimethyl	2.021	0.121
Indole	0.923	7.554
Dimethylhydantoin	0.846	0.00
Carbamic acid phenyl ester	1.71	0.00
Phenol 2 methyl	0.147	0.00
Furfuryl alcohol	1.840	0.00
Phenol, 4 methyl	0.755	0.00
Phenol, 4-ethyl-2-methoxy	3.134	0.00
Phenol 2,5 dimethyl	0.722	0.00
Phenol, 2-methoxy-4-methyl	4.026	0.00
2-methoxy-4-vinyl phenol	0.750	0.00
Mequinol	0.599	0.00
2,3 anhydro D galactosan	1.841	3.854
Phenol, 2,6 dimethoxy	0.249	0.00
Lysidine	0.947	5.214
Phenol, 3-methyl	21.35	0.00
Hexadecenoic acid	8.20	0.00
Benzeneacetonitrile, 4-hydroxy	18.074	2.174
Cyclic octaatomic sulfur	0.00	11.087
Oleic acid	14.363	54.128
Total	96.672	88.861

Compound	% peak area	
	Main Oil	**DIC liquid**
Pyridine	3.40	4.225
hexanitrile	0.00	2.94
Pyridine 2,4,6 trimethyl	1.24	0.00
1 H-Azepine, hexahydro-3,3,5-trimethyl	5.096	0.00
9-oxobicyclo 1 6 olnon-4-one	0.00	1.63
Dimethyltrisulfide	0.934	0.00
Pyrrole -2,5-dione, 1-2,5-dimethoxyphenyl	0.750	0.00
Piperdine 2,3-dimethyl	5.436	7.200
Piperdine-4-one, 1-ethyl-2,3-dimethyl	7.095	1.588
5-ethyl-5-methylhydantoin	7.74	3.014
caldine	0.00	6.44
Phenol, 4-ethyl-2-methoxy	0.627	0.00
Phenol 2,5 dimethyl	0.818	0.00
Phenol, 2-methoxy-4-methyl	1.550	0.00
2-methoxy-4-vinyl phenol	1.088	0.00
Furfuryl alcohol	2.145	0.00
4-piperdinone, 2, 2, 6, 6-tetramethyl	0.599	0.00
Glycine, N [N-glycyl-l-Leucyl]	11.493	0.00
Morpholine, 4-oxiranymethyl	3.599	16.41
2h-pyran-2-one, 6-hexytetrahydro	0.00	15.41
2-myristynol pantethiene	0.00	4.9
Morpholinopropane sulfuric acid	3.599	0.00
Oleic acid tetradecyl ester	18.442	0.00
Phorbol	2.330	6.417
Total	**77.98**	**70.174**

Typical pyrolysis liquids are usually composed of aldehydes, ketones, furans, esters, carboxylic acids and phenolic compounds. These compounds are formed as a result of the degradation of the hemicellulose, cellulose and lignin component of the biomass. The quantity of each group of compounds is also known to be a function of the amount of the original building block in the biomass.

GC-MS analysis of pyrolysis oils from the primary feedstocks show the presence of phenolic compounds derived from the pyrolysis of the lignin constituent of the feedstocks. Phenols, methoxy phenols and dimethoxy phenols were present in the main pyrolysis liquids.

The results of the GC-MS analysis of the pyrolysis liquids from the press cakes also show a preponderance of nitrogen containing organic compounds. These compounds are in the form of cyclic amines, pyrroles, piperidines, diazoles, indoles, pyridines and their derivatives. They also show the oils to be composed of organic compounds from the thermal

decomposition of triglycerides. Compounds like oleic acid and its esters are found to be present in significant quantities. These results agree with the PY-GC/MS results of the primary feedstocks from section 5.2.5. Oleic acid has also been shown to be the major constituent of Jatropha and Moringa oil by many researchers including Akintayo, Augustus et al, Azam et al and Sarin et al [251-254].

The presence of these organic nitrogen compounds like indole, pyridine and pyrrole which are basic account for the higher than usual pH exhibited by the pyrolysis liquids from the press cakes. The nitrogen containing compounds look to have the beneficial effect of increasing the pH of the pyrolysis liquids.

The results of the GC-MS analysis also show the different fractions of the pyrolysis liquids to be chemically different. In the case of Indian Moringa, it can be seen that the secondary liquid fraction collected from the dry ice condenser is composed primarily of sulphur. This finding is in line with the result of the elemental analysis where Indian Moringa exhibited a high sulphur content of 3.03 wt% on a dry basis. The African Moringa lighter fraction is mainly composed of sulphur and oleic acid with traces of other nitrogen containing organic compounds.

The light fractions of the Indian Jatropha show that it is composed mainly of a morpholine derivative. Morpholine is used in industry to for pH adjustments in fossil fuels. The other major compounds are piperdine derivatives. The three most abundant compounds in the lighter fractions from African Jatropha are oleic acid, phorbol and 5-isopropyl-2,4-imidazolidinedione.

Finally, the stability exhibited by the feedstocks may be explained by the presence of compounds like furfuryl alcohol. Alcohols have been added to bio-oil to increase stability [66]. The presence of naturally occurring alcohols is likely to contribute to the stability observed after aging. Similarly, the absence of compounds like hydroxyacetaldehde and maltol may also play a role. Diebold [66] has identified these as compounds responsible for aging in bio-oils.

10.5 SUMMARY

The optimised fast pyrolysis system has been operated under fast pyrolysis conditions. The alternative feed system has solved the feeding problems of its predecessor unit. Similarly, the alternative reactor developed has allowed for longer fast pyrolysis experiments at higher throughputs and wider hydrodynamic conditions. Higher mass balance closures and increased organic liquid yields have been obtained using the optimised system. The reactor intended to process 500 g/h of biomass has however not been run at its designed capacity due to limitations of the ESP.

11 CONCLUSIONS AND RECOMMENDATIONS

Based on the work reported in this thesis, a number of conclusions have been reached and are presented. Similarly, recommendations on further work that should be undertaken in continuation to this research are also presented. The nature of the study meant that two sets of conclusions were reached. The first concerns the commissioned and optimised process. The second relates to the unreported biomass feedstocks and their products. It is appropriate to present the initial objectives as research questions.

11.1 COMMISSIONED PROCESS CONCLUSIONS

Was the 300 g/h rig at the commencement of research capable of producing pyrolysis liquids via fast pyrolysis?

The 300 g/h unit which was unproven was commissioned and shown to be capable of performing fast pyrolysis experiments. Modifications carried out showed that the initial design of the system was indeed capable of processing biomass to liquids. The results from the commissioning studies also showed that there were reduced organic liquid yields as a result of poor operation caused by design flaws.

Was there room for improvement to individual units of the process?

The poor operation of the feed system greatly hampered the operability of the unit. The premature pyrolysis of biomass prior to reactor entry was caused by the design of the feed system.

The initial reactor on the commissioned unit was shown to be limited by its geometry and size. This meant that optimum hydrodynamic parameters were never achieved using the reactor. A nominal throughput of 300 g/h unit as designed for the process was never achieved using the initial reactor.

The operation of the quenching unit of the process was also problematic due to the fabrication of the peripheral equipment inside the quench unit. Modifications were made to the quench plates and oil collection tank to improve its performance and ease product collection.

Was there room for improvement to the process as a whole?

The less than optimal operation of the feed and reactor systems meant that the unit as whole operated very poorly. One of the lessons of this research is that the poor design of individual units of a process can hamper the operability of an entire process. Great care must be taken in design and operation of processing units.

As a result of the feeding problems, an idea for an alternative feed system design incorporating parts of the initial feed system was conceived and developed. The alternative design incorporated a metering unit with gravimetric capabilities and a fast screw for efficient feeding. The alternative feed system was able to eliminate the problems caused by its predecessor unit.

A new reactor was designed with a nominal throughput of 500 g/h of biomass. The design was based on experience gained using the initial fast pyrolysis unit and established principles from literature. The unit was successfully tested up to a throughput of 300 g/h of biomass. The reactor was never run at its maximum capacity due to limitations imposed by the quenching unit.

Experiments using the designed reactor and alternative feed systems showed improvements in terms of process yields and product quality. The improved results in terms of yields and product quality were testament to successful optimisation of the fast pyrolysis unit at the commencement of this research.

11.2 FEEDSTOCK CONCLUSIONS

Are press cakes from the oil seeds from Jatropha and Moringa appropriate feedstocks for a fast pyrolysis process?

African Moringa, African Jatropha, Indian Moringa and Indian Jatropha were characterised in terms of elemental composition, heating values and thermal degradation behaviours. The results showed that although the feedstocks had high ash contents compared to more conventional biomass, the energy contents were also higher than conventional biomass feedstocks. The characterisation results also showed that all the feedstocks contained volatile matter of more than 70 % that can be exploited for energy purposes. The thermal degradation behaviours investigated via thermogravimetric analysis during this research also showed that fast pyrolysis is an appropriate technology in exploiting the energy potential of all the press cakes.

Can bio-fuels mainly pyrolysis liquids from press cakes of Moringa and Jatropha be produced from fast pyrolysis?

Over the temperature range investigated (400-550 ºC), it was shown that 500 ºC was the optimum temperature for obtaining maximum liquid yields for Jatropha and Moringa. In the case of Jatropha however, maximum organic liquid yield was obtained at a pyrolysis temperature of 550 ºC.

Of what quality were the bio-fuels produced?

The main bio-oil product from all the feedstocks showed high energy contents above 25 MJ/kg of oil product. The heating values for the bio-oils showed that bio-oil from the press cakes contained higher energy for exploitation than bio-oil obtained from more conventional feedstocks.

Analysis of all the oils also showed unusually high levels of stability after aging of the bio-oil products. One of the major drawbacks of bio-oil for energy use is the change in physical characteristics observed during aging. Results from this research show that the bio-oil from these feedstocks show great potential as difficulties due to aging are expected to be minimal. In the same vein, the pH values of the bio-oils showed them to be neutral and slightly basic. This is also a promising find since conventional bio-oils are acidic and have a tendency to corrode storage materials. Elemental analysis of the oils also show that the feedstocks have a high carbon conversion efficiency leading to reduced oxygen content in the bio-oils.

11.3 PROCESS RECOMMENDATIONS

The design of feed systems using a single screw for metering and feeding on fast pyrolysis processes should be avoided at all times. Any cost savings associated with the single screw feed system will be eroded and characterised by poor operation of the entire unit.

The optimised feed system has been designed to operate with the initial reactor at the commencement of this research. This may be beneficial for feedstocks where minute quantities are available.

The optimised reactor was designed to handle a throughput of 500 g/h. This was not achieved because of limitations of the quench system mainly the electrostatic precipitator. It is recommended that the design of the electrostatic precipitator of the unit be changed to a wet walled system. This will allow the optimised reactor to operate at its designed throughput.

Results from the analysis of the feedstocks showed the presence of sulphur. The current gas analysis system does not allow for the measurement of gases like sulphur oxides and hydrogen sulphide. It is recommended that the gas analysis system be upgraded to detect a wider range of gases. The need for fast pyrolysis process development units to detect sulphur containing gases cannot be over emphasised.

11.4 FEEDSTOCK RECOMMENDATIONS

Based on the findings, it is suggested that a thorough and detailed study on the economic feasibility of Jatropha and Moringa press cakes as large scale fast pyrolysis feedstocks be undertaken. This may help in determining the economic potential of the feedstocks.

Similarly, the co-pyrolysis of the primary feedstocks used during this research and oil press cakes as a whole be explored as means of maximising their use as feedstocks.

While this research has explored the quality of the pyrolysis liquids from the primary feedstocks, it has not explored the potential of the bio-char as an energy source. For this reason, it is recommended that a complete characterisation of the bio-chars from the process be undertaken to assess their energy potential.

The press cakes used were all subjected to cold pressing and as such contained residual oil. A larger process will most likely use solvent extraction to oil retrieval from seeds ensuring less oil in the actual press cakes. This may have an impact on the energy contents of the press cakes and their subsequent products. For this reason, it is recommended that fast pyrolysis of de-oiled press cakes be undertaken. This will allow for the impact of the residual oil on the fuel quality to be assessed.

The high ash contents of the feedstocks may have had an impact on the yields of organic liquids generated. The effect of pre-treatment on the organic liquid yields should be investigated. The use of hot water pre-treatment or mild acid washing to reduce the alkali metal contents will very likely have a positive impact on the yields of organic liquids.

During this research, only African Moringa and Indian Jatropha were processed over a temperature range. The impact of temperature was not explored on Indian Moringa and African Jatropha. It is recommended that the impact of temperature on the feedstocks be investigated as they may behave differently from their counterparts.

With regards to the stability exhibited by pyrolysis oils from the press cakes, it is recommended that more analytical techniques be employed in order to understand the chemistry of the reactions in the oils. An extended insight into the chemistry of bio-oils from the press cakes will be very beneficial to the upgrading of pyrolysis liquids.

It was the intention of this research to measure the viscosity of the main bio-oils before and after aging. Equipment failure however meant that this was not possible. The results of the GPC analysis suggest that no increase in viscosity should be noticed. This should be confirmed by undertaking viscosity measurements on the pyrolysis liquids.

This research has shown that presscakes from oil seeds do not firmly sit in the category of lignocellulosic biomass. The application of lignocellulosic assumptions and knowledge to presscakes may not be an actual representation of their behaviours particularly in terms of thermal degradation. For this reason, it is recommended that the thermal degradation of presscakes be further studied so that they may be further understood in terms of pyrolysis.

12 REFERENCES

1. United, N. *Status of Ratification of the Kyoto Protocol*. 2011 [cited 2011 June 5th]; Available from:
   http://unfccc.int/kyoto_protocol/status_of_ratification/items/2613.php.

2. Bridge, S.A., *Flash Pyrolysis of Biomass for Liquid Fuels.* Aston University, M.Phil Thesis, 1991.

3. Coombs, J., *Macmillan Dictionary of Biotechnology*. 1986, Macmillan Press Limited: London and Basingstoke.

4. Balat, M., Balat, Mehmet., Kirtay, E., Balat, H., *Main routes for the thermo-conversion of biomass into fuels and chemicals. Part 1: Pyrolysis systems.* Energy Conversion and Management, 2009. **50**(12): p. 3147-3157.

5. Boukis, I.P., *Fast Pyrolysis of Biomass in a Circulating Fluidised Bed Reactor.* Aston University, Ph.D Thesis, 1997: p. 361.

6. Bridgwater, A.V. and G.V.C. Peacocke, *Fast pyrolysis processes for biomass.* Renewable and Sustainable Energy Reviews, 2000. **4**(1): p. 1-73.

7. Bridgwater, A.V., Bridge, S.A, *A Review of Biomass Pyrolysis and Pyrolysis Technologies*, in *Biomass Pyrolysis Liquids Upgrading and Utilisation*, A.V. Bridgwater, Grassi, G., Editor. 1991, Elsevier Applied Science: London and New York.

8. Robinson, M.N., *Design, Modelling and Construction of a Novel Ablative Fast Pyrolysis Reactor and Product Collection System.* Aston University, Ph.D Thesis, 2000: p. 246.

9. Bridgwater, A.V., D. Meier, and D. Radlein, *An overview of fast pyrolysis of biomass.* Organic Geochemistry, 1999. **30**(12): p. 1479-1493.

10. Bridgwater, A., V., *Fast Pyrolysis of Biomass*, in *Thermal Biomass Conversion*, A.V. Bridgwater, Hofbauer, H., Van Loo, S., Editor. 2009, CPL press: Newbury. p. 37-78.

11. Bridgwater, A.V., *Principles and practice of biomass fast pyrolysis processes for liquids.* Journal of Analytical and Applied Pyrolysis, 1999. **51**(1-2): p. 3-22.

12. Hague, A.R., *The Pre-Treatment and Pyrolysis of Biomass for the Production of Liquids for Fuels and Speciality Chemicals.* Aston University, Ph.D Thesis, 1998.

13. Martín, C., Moure, A., Martín, G., Carrillo, E., Domínguez, H., Parajó, J., *Fractional characterisation of jatropha, neem, moringa, trisperma, castor and candlenut seeds*

as potential feedstocks for biodiesel production in Cuba. Biomass and Bioenergy, 2010.

14. Gübitz, G.M., M. Mittelbach, and M. Trabi, *Exploitation of the tropical oil seed plant Jatropha curcas L.* Bioresource Technology, 1999. **67**(1): p. 73-82.

15. Bridgwater, A., V., *Review of Fast pyrolysis of Biomass and Product Upgrading.* Biomass and Bioenergy, 2011: p. 1-27.

16. Jain, S. and M.P. Sharma, *Prospects of biodiesel from Jatropha in India: A review.* Renewable and Sustainable Energy Reviews, 2010. **14**(2): p. 763-771.

17. Dehgan, B., *Phylogenetic Significance of Interspecific Hybridization in Jatropha (Euphorbiceae.* Systematic Botany, 1984. **9**(4): p. 467-478.

18. Estrin, A., *Development of the Jatropha cultivation and biodiesel production: case study of Karnataka State, India.* Imperial College Ph.D. Thesis, 2009: p. 584.

19. Thurmond, W., *Biodiesel 2020: Global Market Survey, Feedstock Trends and Forecasts.* 2008. p. 685.

20. BBC. *Could Jatropha be a biofuel panacea?* 2007 [cited 2010 4th March]; Available from: http://news.bbc.co.uk/1/hi/6278140.stm.

21. Filemon, A., *Biofuels from plant oils.* 2010, Jakarta: ASEAN Foundation. 165.

22. Tewari, D.N., *Jatropha & Biodiesel.* Vol. 1. 2007, New Delhi: Ocean Books Limited.

23. Achten, W.M.J., Verchot, L., Franken, Y. J., Mathijs, E., Singh, V. P., Aerts, R., Muys, B., *Jatropha bio-diesel production and use.* Biomass and Bioenergy, 2008. **32**(12): p. 1063-1084.

24. Staubman, R., *Bio-gas production from Jatropha curcas Press cake* Applied Biochemistry and Biotechnology, 1997. **63-65**: p. 457-467.

25. Lopez O, N. Foidi, and G. Foidi, *Production of Biogas from Jatropha curcas fruit shells*, in *Symposium on Jatropha 97*. 1997, Austrian Ministry of Foreign Affairs: Austria.

26. Morton, J.F., *The horseradish tree, Moringa pterigosperma (Moringaceae). A boon to arid lands.* Econ. Bot., 1991. **45**: p. 318-333.

27. Sengupta, M.A., Gupta, M.P, *Studies on the seed fat composition of Moringaceae family.* Fette, Seifen, Anstrichim, 1970. **72**: p. 6-10.

28. Karmakar, A., S. Karmakar, and S. Mukherjee, *Properties of various plants and animals feedstocks for biodiesel production.* Bioresource Technology, 2010. **101**(19): p. 7201-7210.

29.   Rashid, U., Anwar, F., Moser, B.R., Knothe, G.,, *Moringa oleifera oil: A possible source of biodiesel.* Bioresource Technology, 2008. **99**(17): p. 8175-8179.

30.   Kibazohi, O. and R.S. Sangwan, *Vegetable oil production potential from Jatropha curcas, Croton megalocarpus, Aleurites moluccana, Moringa oleifera and Pachira glabra: Assessment of renewable energy resources for bio-energy production in Africa.* Biomass and Bioenergy, 2011.

31.   Foidi, N. and H.P.S. Makkar, *The potential of Moringa and Oilifiera for Agricultural and industrial uses*, in *The Miracle tree: The multiple attributes of Moringa*, L.J. Fugile, Editor. 2001, Church World Service: Dakar. p. 45-76.

32.   Mohan, D., C.U. Pittman, and P.H. Steele, *Pyrolysis of Wood/Biomass for Bio-oil: A Critical Review.* Energy & Fuels, 2006. **20**(3): p. 848-889.

33.   Peacocke, G.V.C., *Ablative Pyrolysis of Biomass.* Aston University, Ph.D Thesis, 1994.

34.   Rossi, A., *Fuel characteristics of wood and nonwood Biomass Fuels*. Progress in Biomass Conversion, ed. D.A. Tillman. Vol. 5. 1984, New York: Academic Press.

35.   Chan, W.R., Kelbon, M, , *Modelling and Experimental verification of physical and Chemical processes of large biomass particles.* Fuel, 1985. **64**: p. 1505-1513.

36.   Chan, W.R., Kelbon, M,, *Single Particle biomass pyrolysis.* Ind. Eng. Chem. Proc. Res. Dev, 1988. **27**: p. 2261-2275.

37.   Goos, A.W., *The Thermal Decomposition of Wood*, in *Wood Chemistry*, L.E.a.J. Wise, E.C., Editor. 1952, Reinhold: New York.

38.   Antal, M.J., *Biomass Pyrolysis: A review of the Literature Part 1- Carbohydrate Pyrolysis*. Vol. 1. 1983: Plenum Press.

39.   Byrne, G.A., D. Gardener, and F. Holmes, H., *The pyrolysis of Cellulose and the Action of Flame Retardants.* Journal of Applied Chemistry, 1966. **16**: p. 81-88.

40.   Fahmi, R., *The Characterisation and Optimisation of Modified Herbaceous Grasses for Identifying Pyrolysis* Aston University, Ph.D Thesis, 2007: p. 228.

41.   Kilzer, F.J., *Speculation on the nature of cellulose pyrolysis.* Pyrodynamics, 1965. **2**(1): p. 151.

42.   Shafizadeh, F., *Pyrolysis and Combustion of Cellulosic Material.* Advanced Carbohydrate Chemistry, 1968. **23**: p. 419-474.

43.   Liden, A.G., Berruti, F and Scott, D.S, *A Kinetic Model for the Production of Liquids from the Flash Pyrolysis of Biomass.* Chem. Eng. Comm., 1988. **65**: p. 207-221.

44.   Piskorz, J., Radlein, D., Madjerski, P., Scott, D.S, *The Waterloo fast pyrolysis process*, in *Bio-Oil production and utilisation: Procceedings of 2nd EU-Canada workshop on bio-oil thermal processing*, E.N. Hogan, Bridgwater, A.V., Editor. 1997, CPL press: Newbury. p. 22-27.

45.   Piskorz, J., D. Radlein, and D.S. Scott, *On the mechanism of the rapid pyrolysis of cellulose.* Journal of Analytical and Applied Pyrolysis, 1986. **9**(2): p. 121-137.

46.   Di Blasi, C., *Modeling chemical and physical processes of wood and biomass pyrolysis.* Progress in Energy and Combustion Science, 2008. **34**(1): p. 47-90.

47.   Demirbas, A., *Mechanisms of Liquefaction and Pyrolysis Reaction of Biomass.* Energy Conversion and Management, 2000. **41**: p. 633-646.

48.   Demirbas, A., *Effects of temperature and particle size on bio-char yield from pyrolysis of agricultural residues.* Journal of Analytical and Applied Pyrolysis, 2004. **72**(2): p. 243-248.

49.   Shafizadeh, F., *Introduction to Pyrolysis of Biomass.* Journal of Analytical and Applied Pyrolysis, 1982. **3**: p. 283-305.

50.   Evans, R.J., Milne, T.A., *Molecular Characterisation of of the Pyrolysis of Biomass.* Energy and Fuels, 1987. **1**(4): p. 311-319.

51.   Alen, R., Kuoppala E, Oesch, P, *Formation of the Main Degradation Compound Groups from Wood and its Components during Pyrolysis.* Journal of Analytical and Applied Pyrolysis, 1996. **36**: p. 137-148.

52.   Nowakowski, D.J., Bridgwater, A. V., Elliott, D. C., Meier, D., de Wild, P., *Lignin fast pyrolysis: Results from an international collaboration.* Journal of Analytical and Applied Pyrolysis, 2010. **88**(1): p. 53-72.

53.   Antal, M.J., *Biomass Pyrolysis: A review of the Literature. Part 2- Lignocellulose Pyrolysis.* Advances in Solar Energy; K.W Boer and J.A Duffe. 1985, New York: Plenum Press.

54.   Nunn, T.R., *Product Composition and Kinetics in the rapid pyrolysis of sweet gumhardwood.* Ind. Eng. Chem. Proc. Des. Dev, 1985. **24**: p. 836-844.

55.   Shafizadeh, F. and P. Chin, P,S., *Thermal deterioration of wood*, in *172nd National American Chemical Society Meeting*. 1976: Washington, D.C. p. 57.

56.   Graham, G., R., *A Characterization of the Fast Pyrolysis of Cellulose and Wood Biomass.* University of Waterloo, Ph.D Thesis, 1993. **Waterloo**.

57. Di Blasi, C., *Comparison of semi-global mechanisms for primary pyrolysis of lignocellulosic fuels.* Journal of Analytical and Applied Pyrolysis, 1998. **47**(1): p. 43-64.

58. Liden, A.G., *A kinetic and heat transfer modelling study of wood pyrolysis in a fluidized bed.* University of Waterloo, M.Sc Thesis, 1985.

59. Williams, P.T., Besler, S., *Thermogravimetric analysis of the components of biomass*, in *Advances in Thermochemical Biomass Conversion*, A. Bridgwater, V., Editor. 1994, Blackie Academic & Professional: Glasgow. p. 771-783.

60. Bradbury, A., Sakai, Y, Shafizadeh, F, *A kinetic model for the pyrolysis of cellulose.* Journal of Applied Polymer Science, 1979. **23**(1): p. 3271-3280.

61. Shafizadeh, F., Furneaux, R.H., Cochran, T.G., Scholl, J.P, *Production of Levoglucosan and Glucose from the pyrolysis of Cellulosis Materials.* Journal of Applied Polymer Science, 1979. **23**: p. 3525-3539.

62. Diebold, J.P., *The Cracking Kinetics of Depolymerized Biomass Vapors in a Continuous Tubular Reactor.* Colorado School of Mines, M.Sc Thesis, 1985.

63. Diebold, J.P., *A unified, global model for the pyrolysis of cellulose.* Biomass and Bioenergy, 1994. **7**(1-6): p. 75-85.

64. Gorton, C.W., Knight, J.A. *Oil from Biomass Pyrolysis by Entrained-Flow Pyrolysis.* in *Biotech and Bioeng Symposium*. 1984.

65. Piskorz, J., D.S. Scott, and D. Radlein, *Composition of Oils Obtained by Fast Pyrolysis of Different Woods*, in *Pyrolysis Oils from Biomass*. 1988, American Chemical Society. p. 167-178.

66. Diebold, J.P., *A review of the Chemical and Physical Stability of Fast Pyrolysis Bio-Oils*, in *Fast Pyrolysis of Biomass: A Handbook*, A. Bridgwater, V., Editor. 2002, CPL Scientific Publishing: Newbury. p. 243-292.

67. Diebold, J.P., Bridgwater, A.V, *Overview of Flash Pyrolysis of Biomass for the Production of Liquid Fuels.* Developments in thermochemical conversion of biomass, ed. A.V. Bridgwater. Vol. 1. 1994, London: Blackie Academic and Professional.

68. Sipila, K., Kuoppala, E., Fagernäs, L., Oasmaa, A., *Characterisation of biomass based flash pyrolysis oils.* Biomass and Bioenergy, 1998. **14**: p. 103-113.

69. Scholze, B., C. Hanser, and D. Meier, *Characterisation of the water-insoluble fraction from fast pyrolysis liquids (pyrolytic lignin) Part II. GPC, carbonyl groups and C-13-NMR.* Journal of Analytical and Applied Pyrolysis, 2001. **58**: p. 387-400.

70.	Fratini, E., Bonini, M., Oasmaa, A., Solantausta, Y., Teixera, J., *SANS analysis of microstructural evolution during the aging of pyrolysis oils from biomass.* Langmuir, 2006. **22**: p. 306-312.

71.	Oasmaa, A. and E. Kuoppala, *Fast Pyrolysis of forestry residue. Storage stability of liquid fuel.* Energy and Fuels, 2003. **17**: p. 1075-1084.

72.	Diebold, J.P. and S. Czernik, *Additives to lower and stabilize the viscosity of pyrolysis oils during storage.* Energy and Fuels, 1997. **11**: p. 1081-1091.

73.	Stoikos, T., *Upgrading of biomass Pyrolysis Liquids to High-Value Chemicals and Fuel Additives*, in *Biomass pyrolysis liquids upgrading and utilisation*, A. Bridgwater, V., Grassi, G., Editor. 1991, Elsevier Science Publishers: Barking. p. 227-242.

74.	Goyal, H.B., D. Seal, and R.C. Saxena, *Bio-fuels from thermochemical conversion of renewable resources: A review.* Renewable and Sustainable Energy Reviews, 2008. **12**(2): p. 504-517.

75.	Huber, G.W., S. Iborra, and A. Corma, *Sysnthesis of transportation fuels from biomass: Chemistry, catalysts and engineering.* Chem Rev, 2006. **106**: p. 4044-4098.

76.	Lédé, J., *Comparison of contact and radiant ablative pyrolysis of biomass.* Journal of Analytical and Applied Pyrolysis, 2003. **70**(2): p. 601-618.

77.	Lédé, J., Broust, F., Ndiaye, F.T., Ferrer, M., , *Properties of bio-oils produced by biomass fast pyrolysis in a cyclone reactor.* Fuel, 2007. **86**(12-13): p. 1800-1810.

78.	Samolada, M.C. and I.A. Vasalos, *Effect of experimental conditions on the comopsition of gases and liquids from biomass pyrolysis*, in *Advances in Thermochemical Biomass Conversion*, A. Bridgwater, V., Editor. 1994, Blackie Academic & Professional: Glasgow. p. 859-873.

79.	Azeez, A.M., D. Meier, and J. Odermatt, *Temperature dependence of fast pyrolysis volatile products from European and African biomasses.* Journal of Analytical and Applied Pyrolysis, 2010.

80.	Heo, H.S., Park, H.J., Park, Y.K., Ryu, C., Suh, D.j., Suh, Y.W., Yim, J.H., Kim, S.S., , *Bio-oil production from fast pyrolysis of waste furniture sawdust in a fluidized bed.* Bioresource Technology, 2010. **101**(1, Supplement 1): p. S91-S96.

81.	Pattiya, A., J.O. Titiloye, and A.V. Bridgwater, *Fast pyrolysis of cassava rhizome in the presence of catalysts.* Journal of Analytical and Applied Pyrolysis, 2008. **81**(1): p. 72-79.

82. Piskorz, J., Majerski, P., Radlein, D., Scott, D., .Bridgwater, A. V., *Fast pyrolysis of sweet sorghum and sweet sorghum bagasse.* Journal of Analytical and Applied Pyrolysis, 1998. **46**(1): p. 15-29.

83. Uzun, B.B., A.E. Pütün, and E. Pütün, *Fast pyrolysis of soybean cake: Product yields and compositions.* Bioresource Technology, 2006. **97**(4): p. 569-576.

84. Zheng, J.-L., *Pyrolysis oil from fast pyrolysis of maize stalk.* Journal of Analytical and Applied Pyrolysis, 2008. **83**(2): p. 205-212.

85. Jones, J.M., Williams, A., Darvell, L, I., Nawaz, M., Baxter, X., *The role of metals in biomass pyrolysis, char formation and char properties*, in *Science in Thermal and Chemical Biomass Conversion*, A. Bridgwater, V., Boocock, D, G, Editor. 2006, CPL press: Newbury. p. 1203-1214.

86. Agblevor, F.A. and S. Besler, *Inorganic Compounds in Biomass Feedstocks. 1. Effect on the Quality of Fast Pyrolysis Oils.* Energy & Fuels, 1996. **10**(2): p. 293-298.

87. Franz, F.P., *Principles of wood science and technology.* 1968, New York: Springer.

88. Renu Kumar, R., Kolar, A, J., *Effect of fuel particle shape and size on devolatization time of Casaurina wood*, in *Science in Thermal and Chemical Biomass Conversion*, A. Bridgwater, V., Boocock, D, G, Editor. 2006, CPL press: Newbury. p. 1251-1264.

89. Nan, L., Best, G, Neto, *Integrated Energy Systems in China-The Cold Northeastern Region Experience.* 1994, Food and Agriculture Organisation of the United Nations: Rome.

90. Maschio, G., A. Lucchesi, and C. Koufopanos, *Study of Kinetic and Transfer Phenomena in the Pyrolysis of Biomass Particles*, in *Advances in Thermochemical Biomass Conversion*, A. Bridgwater, V., Editor. 1994, Blackie Academic & Professional: Glasgow. p. 746-759.

91. Bilbao, R., A. Millera, and M. Murillo, B., *Heat transfer and weight loss in the thermal decomposition of large wood particles*, in *Advances in Thermochemical Biomass Conversion*, A. Bridgwater, V., Editor. 1994, Blackie Academic & Professional: Glasgow. p. 833-845.

92. Scott, D., S., Piskorz, J., *The flash Pyrolysis of Aspen-Poplar wood.* The Canadian Journal of Chemical Engineering, 1982. **60**: p. 666-674.

93. Kelbon, M., Bousman, S, *Conditions that Favour Tar Production from Pyrolysis of Large moist wood Particles*, in *Pyrolysis Oils from Biomass, Producing, Analyzing and Upgrading*, J.a.M. Soltes E, T.A, Editor. 1988: Washington DC.

94. Maniatis, K.a.B., A., *Fast Pyrolysis of Biomass*, in *Research in Thermochemcial Biomass Conversion*, A.V.a.K. Bridgwater, J.L, Editor. 1988, Elsevier Science: New York.

95. Van de Velden, M., Baeyens, J., Brems, A., Janssens, B., Dewil, R., , *Fundamentals, kinetics and endothermicity of the biomass pyrolysis reaction.* Renewable Energy, 2010. **35**(1): p. 232-242.

96. Cuevas, A., Rebollo, L., Scott, D., Reinoso, C., *Union Fenosa fast pyrolysis development*, in *Bio-Oil production and utilisation: Proccedings of 2nd EU-Canada workshop on bio-oil thermal processing*, E.N. Hogan, Bridgwater, A.V., Editor. 1997, CPL press: Newbury. p. 82-85.

97. Sitzmann, J., *Upgrading of Fast Pyrolysis Oils by Hot Vapour filtration.* Aston University, Ph.D Thesis, 2009.

98. Gerhauser, H., *CFD Applied to the Fast Pyrolysis of Biomass in Fluidised Beds.* Aston University, Ph.D Thesis, 2003.

99. Peacocke, G.V.C., Bridgwater, A.V., *Ablative fast pyrolysis of biomass: results and analyses*, in *Bio-Oil production and utilisation: Proccedings of 2nd EU-Canada workshop on bio-oil thermal processing*, E.N. Hogan, Bridgwater, A.V., Editor. 1997, CPL press: Newbury. p. 35-48.

100. Scholl, S., Klaubert, H., Meier, D., *Bio-Oil from a new ablative pyrolyser*, in *Science in Thermal and Chemical Biomass Conversion*, A. Bridgwater, V., Boocock, D, G, Editor. 2006, CPL press: Newbury. p. 1372-1379.

101. Rossi, C., Graham, R., *Fast pyrolysis at ENEL*, in *Biomass Gasification and Pyrolysis: State of the Art and future prospects*, M. Kaltschmitt, Bridgwater, A.V., Editor. 1997, CPL press: Newbury. p. 300-307.

102. Freel, B.A., Graham, G., Huffman, D., *Commercial aspects of Rapid Thermal Processing*, in *Bio-Oil production and utilisation: Proccedings of 2nd EU-Canada workshop on bio-oil thermal processing*, E.N. Hogan, Bridgwater, A.V., Editor. 1997, CPL press: Newbury. p. 86-95.

103. Maniatis, K., Baeyens, J., Peeters, H., Roggeman, G., *The Egemin Flash Pyrolysis Process*, in *Advances in thermochemical BIomass Conversion*, A. Bridgwater, V., Editor. 1994, Blackie Glasgow.

104. Boukis, I.P., *Practical implications during operation of a CFB air blown pyrolyser*, in *Bio-Oil production and utilisation: Proccedings of 2nd EU-Canada workshop on bio-*

oil thermal processing, E.N. Hogan, Bridgwater, A.V., Editor. 1997, CPL press: Newbury. p. 49-65.

105. Boukis, I.P., Bezergianni, S., Grammelis, P., Bridgwater, A. V., *CFB air-blown flash pyrolysis. Part II: Operation and experimental results.* Fuel, 2007. **86**(10-11): p. 1387-1395.

106. Roy, C., Morin, D., Dube, F., *The biomass pyrocycling process*, in *Biomass Gasification and Pyrolysis: State of the Art and future prospects*, M. Kaltschmitt, Bridgwater, A.V., Editor. 1997, CPL press: Newbury. p. 307-316.

107. Roy, C., Yang, Y., Blanchette, D., de Caumia, B., Korving, L., *Development of a novel vacuum pyrolysis reactor with improved heat transfer potential*, in *Developments in thermochemical conversion of biomass*, A.V. Bridgwater, Boocock, D.G, Editor. 1997, Blackie academic & professional: London. p. 351-368.

108. Wagenaar, B.M., Prins, W., *Review of rotating cone technology for flash pyrolysis of biomass*, in *Biomass Gasification and Pyrolysis: State of the Art and future prospects*, M. Kaltschmitt, Bridgwater, A.V., Editor. 1997, CPL press: Newbury. p. 316-327.

109. BTG-BTL. *http://www.btg-btl.com/index.php?r=technology*. 2011 [cited 2011 March 11th].

110. Luo, Z., Wang, S., Liao, Y., Zhou, J., Gu, Y., Cen, K., , *Research on biomass fast pyrolysis for liquid fuel.* Biomass and Bioenergy, 2004. **26**(5): p. 455-462.

111. Zheng, J.-L., *Bio-oil Production from cotton stalk.* Energy Conversion and Management, 2008. **49**: p. 1724-1730.

112. Weerasinhe, C.R., *Fluidised Bed pyrolysis of Coal.* Imperial College M.Sc Thesis, 1981.

113. Zhuo, Y., *Development of a Bench Scale High Pressure Fluidised Bed Reactor for the Processing of Coal and Biomass.* Imperial College of Science, Technology and Medicine, University of London, Ph.D. Thesis, 1999.

114. Kunii, D. and O. Levenspiel, *Fluidization Engineering*. 1991, Newton: Butterworth-Heinemann. 491.

115. Geldart, D., *Types of gas fluidization.* Powder Technology, 1973. **7**: p. 285-292.

116. Yates, J.G., *Effects of temperature and pressure on gas-solid fluidization.* Chemical Engineering Science, 1996. **51**(2): p. 167-205.

117. Salter, E.H., *Catalytic Pyrolysis of Biomass for improved Liquid Fuel Quality.* Aston University, Ph.D Thesis, 2001.

118. Howard, J.R., *Fluidized Bed Technology: principles and applications*. 1989, New York: Adam Higler.

119. Subramani, H.J., M.B. Mothivel Balaiyya, and L.R. Miranda, *Minimum fluidization velocity at elevated temperatures for Geldart's group-B powders.* Experimental Thermal and Fluid Science, 2007. **32**(1): p. 166-173.

120. Rowe, P.N., *Comment on minimum fluidizing velocity of coal-derived chars at elevated temperatures.* Chemical Engineering Science, 1985. **40**(10): p. 2003-2003.

121. Yates, J.G., *Handbook of Fluidization and Fluid-Particle Systems*, W.-C. Yang, Editor. 2003, Marcell Decker. p. 861.

122. Werther, J.a.E.-U., H., *Handbook of Fluidization and Fluid-Particle Systems*, W.-C. Yang, Editor. 2003, Marcell Decker.

123. Kunii, D.a.L., O., *Entrainment and Elutriation from fluidised beds.* Journal of Chemical Engineering of Japan, 1969. **2**: p. 84-88.

124. Zenz, F.A., Weil, N.A, *A theoretical-Empirical approach to the mechanism of particle entrainment from fluidized beds.* American Institute of Chemical Engineering Journal, 1958. **4**: p. 472-479.

125. Thong, J., *Modelling of Entrainment in a Fluidised Bed Syatem.* Aston University, MEng Thesis, 1999.

126. Kettering, K.N., Mansfield, E.L., Smith, J.M, Chem. Eng. Prog., 1950. **46**: p. 139.

127. Heertjes, P.M., McKibbins, S.W., Chem. Eng. Sci., 1956. **5**: p. 161.

128. Heertjes, P.M., De Boer, H.G.J and De Haas Van Dorsser, A.H, Chem. Eng. Sci., 1953. **2**: p. 97.

129. Botterill, J.S.M., *Fluid Bed Heat Transfer*. 1975, New York: Academic Press.

130. Mostafa, I., *Studies on Fluidised Bed Drying.* Imperial College Ph.D. Thesis, 1977.

131. Baerg, A., Klassen, J. and Gishler, P.E, Canadian Journal of Research, 1950. **28**: p. 287.

132. Gomes, J., L, M., *Modelling Heat and Mass Transfer in Gas-Solid Fluidized Beds Using the Two-Fluid Granular Temperature Approach*, in *Chemical Engineering and Chemical Technology*. 2004, Imperial College, University of London: London.

133. Scott, D., S., Piskorz, J., Graham, R.G., Grinshpun, A., *The Effect of Temperature on Liquid Product Compositionfrom Fast Pyrolysis of Cellulose.* American Chemical Society. Division of Fuel Chemistry, 1987. **32**(2): p. 1-11.

134.   Scott, D., Piskorz, J., Bergougnou, M., Graham, R., Overend, R., *The role of temperature in the fast pyrolysis of cellulose and wood.* Industrial & Engineering Chemistry Research, 1988. **27**(1): p. 8-15.

135.   Sheng, C. and J. Azevedo, L, T., *Estimating the higher heating value of biomass fuels from basic analysis data.* Biomass and Bioenergy, 2005(28): p. 499-507.

136.   Phyllis, *Database for biomass and Waste.* Energy research centre of the Netherlands (ECN), 2005.

137.   Wang, J.C. and J.E. Kinsella, *Functional properties novel proteins: Alfafa leaf protein.* Food Science, 1976. **41**: p. 286.

138.   Beerens, P., *Screw-Pressing of Jatropha Seeds for Fueling Purposes in Less Developed Countries.* Eindhoven University of Technology, M.Sc Thesis, 2007.

139.   Smets, K., Adriaensens, P., Reggers, G., Schreurs, S., Carleer, R., Yperman, J., *Flash pyrolysis of rapeseed cake: Influence of temperature on the yield and the characteristics of the pyrolysis liquid.* Journal of Analytical and Applied Pyrolysis, 2011. **90**(2): p. 118-125.

140.   Tkachuk, R., *Nitrogen-tto-protein conversion factors for cereals and oilseed meals.* Cereal Chemistry, 1969. **46**.

141.   Mosse, J., *Nitrogen to protein conversion factor for ten cereals and six legumes or oil seeds. A reappraisal of its definition and determination: variation according to species and to seed protein content.* Journal of Agricultural and Food Chemistry, 1990. **38**: p. 18-24.

142.   Milton, K., Dintzis, F, R., *Nitrogen -to-protein conversion factors for tropical plant samples.* Biotropica, 1981. **13**(3): p. 177-181.

143.   Yeoh, H., H., Wee, Y, O., *Leaf protein contents and nitrogen-to-protein conversion factors for 90 plant species.* Food Chemistry, 1994. **49**: p. 245-250.

144.   Ezeagu, I.E., Petzke, J. K., Metges, C. C., Akinsoyinu, A. O., Ologhobo, A. D., *Seed protein contents and nitrogen-to-protein conversion factors for some uncultivated tropical plant seeds.* Food Chemistry, 2002. **78**(1): p. 105-109.

145.   Elmer, P., *Perkins Elmer Pyris 1 TGA manual.* Vol. 1. 2001. 1-59.

146.   Meier, D., Oasmaa, O., Peacocke, G.V.C., *Properties of fast pyrolysis liquids: status of test methods*, in *Developments in thermochemical conversion of biomass*, A.V. Bridgwater, Boocock, D.G, Editor. 1997, Blackie academic & professional: London. p. 391-409.

147. Chen, M., Wang, J., Zhang, M., Chen, M., Zhu, X., Min, F., Tan, Z., , *Catalytic effects of eight inorganic additives on pyrolysis of pine wood sawdust by microwave heating.* Journal of Analytical and Applied Pyrolysis, 2008. **82**(1): p. 145-150.

148. Kang, B., Lee, K., Park, H., Park, Y., Kim, J., *Fast pyrolysis of radiata pine in a bench scale plant with a fluidized bed: Influence of a char separation system and reaction conditions on the production of bio-oil.* Journal of Analytical and Applied Pyrolysis, 2006. **76**(1-2): p. 32-37.

149. Park, H.J., Y.-K. Park, and J.S. Kim, *Influence of reaction conditions and the char separation system on the production of bio-oil from radiata pine sawdust by fast pyrolysis.* Fuel Processing Technology, 2008. **89**(8): p. 797-802.

150. Fahmi, R., Bridgwater, A. V., Darvell, L. I., Jones, J. M., Yates, N., Thain, S., Donnison, I. S., *The effect of alkali metals on combustion and pyrolysis of Lolium and Festuca grasses, switchgrass and willow.* Fuel, 2007. **86**(10-11): p. 1560-1569.

151. Cooke, L.A., *The Effect of a ZSM-5 Containing Catalyst on the Fluidised Bed Fast Pyrolysis of Pine Wood.* Aston University, Ph.D Thesis, 1999: p. 244.

152. Raja, S., Kennedy, Z., Pillai, B. C., Lee, C., Lindon R., , *Flash pyrolysis of jatropha oil cake in electrically heated fluidized bed reactor.* Energy. **35**(7): p. 2819-2823.

153. Demirbas, A., *Trace Metal Concentrations in ashes from Various Types of Biomass Species.* Energy Sources, 2003. **25**: p. 743-751.

154. Monti, A., N. Virgilio, D., and G. Venturi, *Mineral Composition and Ash Contents of Six Major Energy Crops.* Biomass and Bioenergy, 2008. **32**: p. 216-223.

155. Werkelin, J., Skrifvars B-J., and M. Hupa, *Ash-Forming Elements in Four Scandanavian Wood Species. Part 1. Summer Harvest.* Biomass and Bioenergy, 2005. **29**: p. 451-466.

156. Vassilev, S., Baxter, D., Andersen, L., Vassileva, C., , *An overview of the chemical composition of biomass.* Fuel, 2010. **89**(5): p. 913-933.

157. Kantarelis, E. and A. Zabaniotou, *Valorization of cotton stalks by fast pyrolysis and fixed bed air gasification for syngas production as precursor of second generation biofuels and sustainable agriculture.* Bioresource Technology, 2009. **100**(2): p. 942-947.

158. Gerçel, H.F., *The production and evaluation of bio-oils from the pyrolysis of sunflower-oil cake.* Biomass and Bioenergy, 2002. **23**(4): p. 307-314.

159. Özbay, N., A.E. Pütün, and E. Pütün, *Structural analysis of bio-oils from pyrolysis and steam pyrolysis of cottonseed cake.* Journal of Analytical and Applied Pyrolysis, 2001. **60**(1): p. 89-101.

160. Özçimen, D. and F. Karaosmanoglu, *Production and characterization of bio-oil and biochar from rapeseed cake.* Renewable Energy, 2004. **29**(5): p. 779-787.

161. Pütün, A.E., E. Apaydin, and E. Pütün, *Bio-oil production from pyrolysis and steam pyrolysis of soybean-cake: product yields and composition.* Energy, 2002. **27**(7): p. 703-713.

162. Ramachandran, S., Singh, S., Larroche, C., Soccol, C., Pandey, A.,, *Oil cakes and their biotechnological applications - A review.* Bioresource Technology, 2007. **98**(10): p. 2000-2009.

163. Sensöz, S. and D. AngIn, *Pyrolysis of safflower (Charthamus tinctorius L.) seed press cake in a fixed-bed reactor: Part 2. Structural characterization of pyrolysis bio-oils.* Bioresource Technology, 2008. **99**(13): p. 5498-5504.

164. Yorgun, S., S. Sensöz, and Ö.M. Koçkar, *Flash pyrolysis of sunflower oil cake for production of liquid fuels.* Journal of Analytical and Applied Pyrolysis, 2001. **60**(1): p. 1-12.

165. Ucar, S. and A.R. Ozkan, *Characterization of products from the pyrolysis of rapeseed oil cake.* Bioresource Technology, 2008. **99**(18): p. 8771-8776.

166. Tsai, W.T., M.K. Lee, and Y.M. Chang, *Fast pyrolysis of rice husk: Product yields and compositions.* Bioresource Technology, 2007. **98**(1): p. 22-28.

167. Ji-lu, Z., *Bio-oil from fast pyrolysis of rice husk: Yields and related properties and improvement of the pyrolysis system.* Journal of Analytical and Applied Pyrolysis, 2007. **80**(1): p. 30-35.

168. Pütün, E., B.B. Uzun, and A.E. Pütün, *Fixed-bed catalytic pyrolysis of cotton-seed cake: Effects of pyrolysis temperature, natural zeolite content and sweeping gas flow rate.* Bioresource Technology, 2006. **97**(5): p. 701-710.

169. Uzun, B.B., A.E. Pütün, and E. Pütün, *Composition of products obtained via fast pyrolysis of olive-oil residue: Effect of pyrolysis temperature.* Journal of Analytical and Applied Pyrolysis, 2007. **79**(1-2): p. 147-153.

170. Ghetti, P., L. Ricca, and L. Angelini, *Thermal Analysis of Biomass and Corresponding Pyrolysis products.* Fuel, 1996. **75**: p. 565-573.

171. Demirbas, A. and M. Demirbas, F., *Biomass and Wastes: Upgrading Alternative fuels.* Energy Sources, 2003. **25**(3): p. 317-329.

172. Yoshida, T., Tetsuya S., Yamamoto, K., Hambali, E. *Characterisation of Pellet from Oil Palm and Jatropha Residues*. in *Sixth Biomass-Asia Workshop*. 2009. Hiroshima.

173. Yang, H., Yan, R., Chen, H., Lee, D., Zheng, C., , *Characteristics of hemicellulose, cellulose and lignin pyrolysis*. Fuel, 2007. **86**(12-13): p. 1781-1788.

174. Vlahov, G., P.K. Chepkwony, and P.K. Ndalut, *13C NMR Characterization of Triacylglycerols of Moringa oleifera Seed Oil: An Oleic-Vaccenic Acid Oil*. Journal of Agricultural and Food Chemistry, 2002. **50**(5): p. 970-975.

175. Peacocke, G.V.C., *Dicussion on 300g/h Unit*, A.S. Kalgo, Editor. 2007: Birmingham.

176. Metals, S., *Physical constraints and thermal properties of inconel 600*. 2008: Special Metals.

177. Anon, *Occupational exposure limits*, in *EH 40/87*, HMSO, Editor. 1987.

178. Anon, *Carbon Monoxide Poisoniong: Causes and Prevention*, in *Health and Safety at Work notice No.29, HMSO, 1971.*, HMSO, Editor. 1971.

179. Anon, *Industry fails to Heed Cancer Advice*. Plant Engineering and Maintainence, 1988. **26**.

180. Anon, *Explosibility tests for Industrial Dusts*, HMSO, Editor. 1975.

181. Abdullah, N., *An Assessment of Pyrolysis for Processing Empty Fruit Bunches*. Aston University, Ph.D Thesis, 2005.

182. Papadikis, K., *Computational Modelling of the Fast Pyrolysis of Biomass in Bubbling Fluidised Bed Reactors*. Aston University, Ph.D Thesis, 2009.

183. Pattiya, A., *Catalytic Pyrolysis of Agricultural Residues for Bio-Oil Production*. Aston University, Ph.D Thesis, 2007.

184. Diebold, J.P., Bridgwater, A.V, *Overview of Flash Pyrolysis of Biomass for the Production of Liquid Fuels*. Developments in thermochemical conversion of biomass, ed. A.V. Bridgwater. Vol. 1. 1997, London: Blackie Academic and Professional.

185. Peacocke, G.V.C., Dick, M.C., Hague, R.A., Cooke, L.A., Bridgwater, A.V., *Comparison of ablative and fluidised bed fast pyrolysis products: Yields and analyses*, in *Developments in thermochemical conversion of biomass*, A.V. Bridgwater, Boocock, D.G, Editor. 1997, Blackie academic & Professional: London. p. 191-206.

186. Liu, P., *Improvement of Bio-oil stability in wood pyrolysis process*, in *Chemical Engineering and Applied Chemistry*. 2003, Aston University: Birmingham. p. 175.

187. AcIkgoz, C., O. Onay, and O.M. Kockar, *Fast pyrolysis of linseed: product yields and compositions*. Journal of Analytical and Applied Pyrolysis, 2004. **71**(2): p. 417-429.

188.   Agblevor, F.A., Beis, S., Kim, S. S., Tarrant, R., Mante, N. O., *Biocrude oils from the fast pyrolysis of poultry litter and hardwood.* Waste Management, 2010. **30**(2): p. 298-307.

189.   Blin, J., Volle, G., Girard, P., Bridgwater, A.V., Meier, D., , *Biodegradability of biomass pyrolysis oils: Comparison to conventional petroleum fuels and alternatives fuels in current use.* Fuel, 2007. **86**(17-18): p. 2679-2686.

190.   Heo, H., Park, H., Yim, J., Sohn, J., Park, J., Kim, S., Ryu, C., Jeon, J., Park, Y., , *Influence of operation variables on fast pyrolysis of Miscanthus sinensis var. purpurascens.* Bioresource Technology, 2010.

191.   Jung, S.-H., B.-S. Kang, and J.-S. Kim, *Production of bio-oil from rice straw and bamboo sawdust under various reaction conditions in a fast pyrolysis plant equipped with a fluidized bed and a char separation system.* Journal of Analytical and Applied Pyrolysis, 2008. **82**(2): p. 240-247.

192.   Scott, D., Majerski, P., Piskorz, J., Radlein, D., , *A second look at fast pyrolysis of biomass--the RTI process.* Journal of Analytical and Applied Pyrolysis, 1999. **51**(1-2): p. 23-37.

193.   Latif, A., *A Study of the Design of Fluidised Bed Reactors for Biomass Gasification.* University of London, Ph.D. Thesis, 1999: p. 232.

194.   Papadikis, K., S. Gu, and A.V. Bridgwater, *A CFD approach on the effect of particle size on char entrainment in bubbling fluidised bed reactors.* Biomass and Bioenergy, 2009. **34**(1): p. 21-29.

195.   Encinar, J.M., et al., *Pyrolysis of two agricultural residues: Olive and grape bagasse. Influence of particle size and temperature.* Biomass and Bioenergy, 1996. **11**(5): p. 397-409.

196.   Shen, J., et al., *Effects of particle size on the fast pyrolysis of oil mallee woody biomass.* Fuel, 2009. **88**(10): p. 1810-1817.

197.   Encinar, J.M., Beltrán, F. J., Bernalte, A., Ramiro, A., González, J. F., *Pyrolysis of two agricultural residues: Olive and grape bagasse. Influence of particle size and temperature.* Biomass and Bioenergy, 1996. **11**(5): p. 397-409.

198.   Bridgwater, A.V., *Personal Communication*, A. Kalgo, Editor. 2010: Birmingham.

199.   Chen, M.-Q., Ren, Zheng-Wei., Li, Ting-Chen., Yao, Yun-Jin., Yan, Yong-jie, *Mathematical model for pyrolysis of biomass in a Spout-fluidized bed reactor*, in *Science in Thermal and Chemical Biomass Conversion*, A. Bridgwater, V., Boocock, D, G, Editor. 2006, CPL press: Newbury. p. 1342-1370.

200. Manurung, R., et al., *Valorisation of Jatropha curcas L. plant parts: Nut shell conversion to fast pyrolysis oil.* Food and Bioproducts Processing, 2009. **87**(3): p. 187-196.

201. Onay, Ö., S.H. Beis, and Ö.M. Koçkar, *Fast pyrolysis of rape seed in a well-swept fixed-bed reactor.* Journal of Analytical and Applied Pyrolysis, 2001. **58-59**: p. 995-1007.

202. Prescott, J., Barnum, R., *On Powder Flowability.* Pharmaceutical Technology, 2000: p. 60-84.

203. Johanson, R., *Know your material-HOw to predict and use the bulk properties of solids.* Chemical Engineering, 1978: p. 9-17 (Desk book issue).

204. Craik, D., Miller, B., *The flow properties of powders under humid conditions.* Journal of pharmacy and pharmacology, 1958. **10**: p. 136-144.

205. Moreyra, R., Peleg, M., *Effect of equillibrium water activity on the bulk properties of selected food powders.* Journal of Food Science, 1981. **46**: p. 1918-1922.

206. Marinelli, J., Carson, J.W., *Solve Solids Flow Problems in Bins, Hoppers and Feeders.* Chemical Engineering Progress, 1992: p. 22-28.

207. Irani, R., Callis, C., Liu, T., *Flow conditioning and anti caking agents.* Industrial & Engineering Chemistry, 1959. **51**(10): p. 1285-1288.

208. Fitzpatrick, J., Iqbal, T., Delaney, C., Twomey, T., Keogh, M., *Effect of powder properties and storage conditions on the flowability of milk powders with different fat contents.* Journal of food Engineering, 2004. **64**(4): p. 435-444.

209. Yan, H., Barbosa, G., *Compression characteristics of agglomerated food powders; effect of agglomerate size and water activity.* Food Science and Technology International, 1997. **3**(5): p. 351-359.

210. Carr, J., R.L., *Classifying flow properties of solids.* Chemical Engineering, 1965. **72**(3): p. 69-72.

211. Carr, J., R.L., *Evaluating flow properties of solids.* Chemical Engineering, 1965. **72**(3): p. 163-168.

212. Maniatis, K., *Fluidized Bed Gasification of Biomass.* Aston University, Ph.D Thesis, 1986.

213. Daugaard, D., E., Brown, R, C., *The transport phase of pyrolytic oil exiting a fluidized bed reactor*, in *Science in Thermal and Chemical Biomass Conversion*, A. Bridgwater, V., Boocock, D, G, Editor. 2006, CPL press: Newbury. p. 1189-1202.

214. Van Berkel, A., Brem, G., *A novel method to measure bioimass reactivity in a fluidised bed*, in *Science in Thermal and Chemical Biomass Conversion*, A. Bridgwater, V., Boocock, D, G, Editor. 2006, CPL press: Newbury. p. 1148-1162.

215. Martin, H., *Heat and Mass transfer in fluidised beds.* International Chemical Engineering, 1982. **22**(1): p. 30-43.

216. Ramirez, J., J., Martinez, J.D., Petro, S.L., *Basic Design of a Fluidized Bed Gasifier for Rice Husk on a Pilot Scale.* Latin American Applied Research, 2007. **37**: p. 299-306.

217. Kojima, T., Ishihara, K., Kuramoto, M., Furusawa, T. in *World congress III of Chemical Engineering*. 1986. Tokyo.

218. van ommen, R., J. and R. Mudde, F. *Measuring the Gas-Solids Distribution in Fluidized Beds-A review.* in *New Horizons in Fluidization Engineering*. 2007. Vancouver.

219. Bortolamasi, M., Fottner, J. *Design and Sizing of Screw Feeders*. in *International Congress for Particle Technology*. 2001. Nurumberg, Germany.

220. Levelton, B.H.A.L., *Status of Biomass Feeder Technology*, in *ENFOR Project*. 1982.

221. Carson, J.W., Greg Petro, G.E., *How to Design Efficient and Reliable Feeders for Bulk Solids*, J.J. Incorporated, Editor.

222. Carson, J.W., Royal, T.A., Goodwill, D.J, *Understanding and Eliminating Particle Segregation Problems.* Bulk Solids Handling, 1986. **6**(1): p. 139-144.

223. Carson, J.W., Purutyan, H., Royal, T.A. *Uniform Conditioning of Bulk Solids in Processing Vessels*. in *12th International Congress of Chemical and Process Engineering*. 1996. Prague.

224. Marinelli, J., Carson, J.W., *Use Screw Feeders Effectively.* Chemical Engineering Progress, 1992: p. 47-51.

225. Dai, J. and J.R. Grace, *Biomass screw feeding with tapered and extended sections.* Powder Technology, 2008. **186**(1): p. 56-64.

226. K-Tron, *Kt-20 Operation Manual*. Vol. 1. 2010: K-Tron. 497.

227. Peacocke, G.V.C., *Personal Communication*. 2008.

228. van den Enden, P.J. and E.S. Lora, *Design approach for a biomass fed fluidized bed gasifier using the simulation software CSFB.* Biomass and Bioenergy, 2004. **26**(3): p. 281-287.

229. Boukis, I.P., Grammelis, P., Bezergianni, S., Bridgwater, A. V., *CFB air-blown flash pyrolysis. Part I: Engineering design and cold model performance.* Fuel, 2007. **86**(10-11): p. 1372-1386.

230. Yang, W.-C., *Bubbling Fluidized Beds*, in *Handbook of Fluidization and Fluid Particle Systems*, W.-C. Yang, Editor. 2003, Marcell Dekker: New York.

231. Samolada, M.C. and I.A. Vasalos, *A kinetic approach to the flash pyrolysis of biomass in a fluidized bed reactor.* Fuel, 1991. **70**(7): p. 883-889.

232. Daugaard, D.E. and R.C. Brown, *Enthalpy for Pyrolysis for Several Types of Biomass.* Energy & Fuels, 2003. **17**(4): p. 934-939.

233. Reed, T.B., Gaur, S., *The High heat of Fast Pyrolysis for for Large Particles*, in *Developments in Thermochmeical Biomass Conversion*, A. Bridgwater, V., Boocock, D, G, Editor. 1997: New York. p. 97-103.

234. Morris, K., W. Johnson, and R. Thamburaj. *Fast Pyrolysis of Biomass for Green Power generation*. in *1st World Conference and Exhibition on Biomass for Energy and Industry*. 2000. Seville, Spain.

235. Reed, T.B., J.P. Diebold, and R. Desrosiers, *Perspectives in heat transfer requirements and mechanisms for fast pyrolysis*, in *Specialists' Workshop on Fast Pyrolysis*. 1980: Copper Mountain. p. 7-19.

236. Whitehead, A.B., *Fluidization*, H. Davidson, Editor. 1971, Academic Press. p. 781-814.

237. Geldart, D. and J. Baeyens, *Design of Distributors for Gas Fluidized beds.* Powder Technology, 1985. **42**(1): p. 67-78.

238. Chatterjee, A. and A.R. Shankar, *Fluidized Bed Gas Distributors.* Chemical Age of India, 1982. **33**(9): p. 487-490.

239. Basu, P., *Fluidized Bed Boilers-Design and Applications*, in *Design of Gas Distributors for Fluid Bed Boilers*, P. Basu, Editor. 1984, Pergamon Press: Toronto.

240. Davidson, J.F. and D. Harrison, *Fluidization*. 1971, London: Academic Press.

241. Agarwal, J.C., W.L. Davis, and D.T. King, *Gas Distribution in Fluidized Beds.* Chemical Engineering Progress, 1962. **58**(85).

242. Grace, J.R. and K. Vakhshouri, *Effects of Plenum Chamber Volume and Distributor Geometry on Fluidized Beds.* Particuology, 2010. **8**: p. 2-12.

243. Litz, W.J., *Design of Gas Distributors.* Chemical Engineering, 1972. **13**(162-166).

244. Werther, J. and S.B. Reddy Karri, *Gas Distributor and Plenum Design in Fluidized Beds*, in *Handbook of Fluidization and Fluid-Particle Systems*, W.-C. Yang, Editor. 2003, Marcel Dekker A G: New York. p. 164-179.

245. Perry, H.R., *Perry's Chemical Engineer's Handbook.* 1997: McGraw-Hill.

246. Zenz, F.A., *Fluidization and Fluid Particle Systems.* Nelsonville, Pemm-Corp Publication, 1989: p. 101-109.

247. Czernik, S. and A.V. Bridgwater, *Overview of Applications of Biomass Fast Pyrolysis Oil.* Energy & Fuels, 2004. **18**(2): p. 590-598.

248. Oasmaa, A. and S. Czernik, *Fuel Oil Quality of Biomass Pyrolysis OilsState of the Art for the End Users.* Energy & Fuels, 1999. **13**(4): p. 914-921.

249. Oasmaa, A. and D. Meier, *Norms and standards for fast pyrolysis liquids: 1. Round robin test.* Journal of Analytical and Applied Pyrolysis, 2005. **73**(2): p. 323-334.

250. Boateng, A.A., C.A. Mullen, and N.M. Goldberg, *Producing Stable Pyrolysis Liquids from the Oil-Seed Presscakes of Mustard Family Plants: Pennycress (Thlaspi arvense L.) and Camelina (Camelina sativa).* Energy & Fuels, 2010. **24**(12): p. 6624-6632.

251. Akintayo, E.T., *Characteristics and composition of Parkia biglobbossa and Jatropha curcas oils and cakes.* Bioresource Technology, 2004. **92**(3): p. 307-310.

252. Augustus, G.D.P.S., M. Jayabalan, and G.J. Seiler, *Evaluation and bioinduction of energy components of Jatropha curcas.* Biomass and Bioenergy, 2002. **23**(3): p. 161-164.

253. Mohibbe Azam, M., A. Waris, and N.M. Nahar, *Prospects and potential of fatty acid methyl esters of some non-traditional seed oils for use as biodiesel in India.* Biomass and Bioenergy, 2005. **29**(4): p. 293-302.

254. Sarin, R., Sharma, M., Sinharay, S., Malhotra, R., , *Jatropha-Palm biodiesel blends: An optimum mix for Asia.* Fuel, 2010. **86**(10-11): p. 1365-1371.

NOMENCLATURE

A_P	area of Plate	[cm^2]
Ar	Archimedes number	[-]
A_R	reactor cross sectional area	[m^2]
C_D	drag coefficient	[-]
C_{pn2}	Specific heat capacity of nitrogen	[kJ/kg K]
C_{ps}	specific heat capacity of sand	[kJ/kg K]
d*	dimensionless particle number	[-]
d_p	diameter of particle	[m]
D_{noz}	gas nozzle internal diameter	[m]
D_R	reactor internal diameter	[m]
D_w	diameter of windbox	[m]
g	acceleration due to gravity	[m/s^2]
G_B	biomass through (moisture ash free)	[kg/h]
G_{B+MA}	Biomass throughput (wet+ash)	[kg/h]
G_G	fluidising gas mass flowrate	[kg/h]
G_S	fluidising gas mass flowrate	[kg/h]
H	bed height at operational velocity	[m]
H_{mf}	bed height at minimum fluidising conditions	[m]
L_R	length of reactor	[m]
Q_g	gas flowrate at distributor plate	[m^3/s, cm^3/s]
	gas flowrate at reactor exit	[m^3/s]
Re	Reynolds number	[-]

t_p	distributor plate thickness	[cm]
t_{res}	vapour residence time at reactor conditions	[s]
T_2	temperature of fluidising gas	[K]
T_R	pyrolysis temperature	[K]
U_0	reactor operational velocity	[m/s]
U_{mf}	minimum fluidising velocity	[m/s]
U^*	dimensionless gas velocity	[-]
$U_R(A)$	gas velocity at distributor plate	[m/s]
$U_R(B)$	gas/products velocity at reactor exit	[m/s]
V_R	reactor operational volume	[m^3]
$_{pg}$	average pyrolysis gases density	[kg/m^3]
$_{pv}$	average pyrolysis vapour density	[kg/m^3]
$_s$	sand particle density	[kg/m^3]
$_g$	nitrogen gas density at reactor conditions	[kg/m^3]
μ_g	nitrogen viscosity at reactor conditions	[poise, kg/ms]
P_{bed}	pressure drop across fluidised bed	[N/m^2, mm H$_2$O]
P_d	pressure drop across distributor	[N/m^2, mm H$_2$O]
	bed voidage	[-]
$_D$	permeability of porous plate	[cm^2]

APPENDIX 1 - PUBLICATIONS

The list below details publications arising from this research.

Kalgo, A.S and Titiloye, J.O. Fast Pyrolysis of Jatropha curcas and Moringa olifiera seed cakes: Part I. Characterisation, oil content determination and thermal degradation study, Bioten Conference. Birmingham, United Kingdom, 2010: P 89

Kalgo, A.S and Titiloye, J.O. Bio-oil Production from Fast Pyrolysis of Jatropha curcas and Moringa olifiera Press Cakes, 19th European Biomass Conference and Exhibition. Berlin, Germany, 2011. P 35

Kalgo, A.S and Titiloye, J.O. Development of a fluidised bed fast pyrolysis process and its subsequent optimisation. Energy & Fuels (2011). Submitted for publication.

Kalgo, A.S and Titiloye, J.O. The impact of temperature on the fast pyrolysis of Moringa and Jatropha press cakes. Journal of Analytical and Applied Pyrolysis (2011). Submitted for publication.

APPENDIX 2 - TGA OF OILED AND DE-OILED PRESS CAKES

This appendix presents the TGA study of the primary feedstocks before and after oil extraction. The oil was extracted using the techniques described in section 4.4.8. In section 5.2.4 certain parts of the DTG curves were attributed to the decomposition of the residual oil in the press cakes. The figures below show the TG and DTG curves of press cakes as received and after oil extraction.
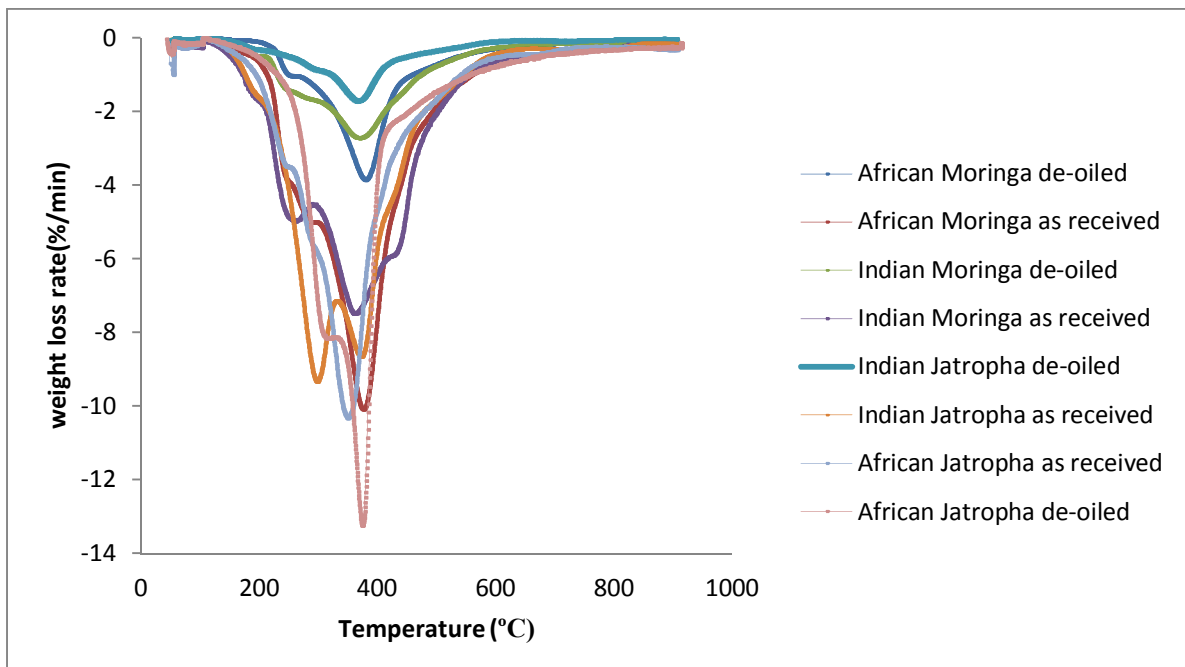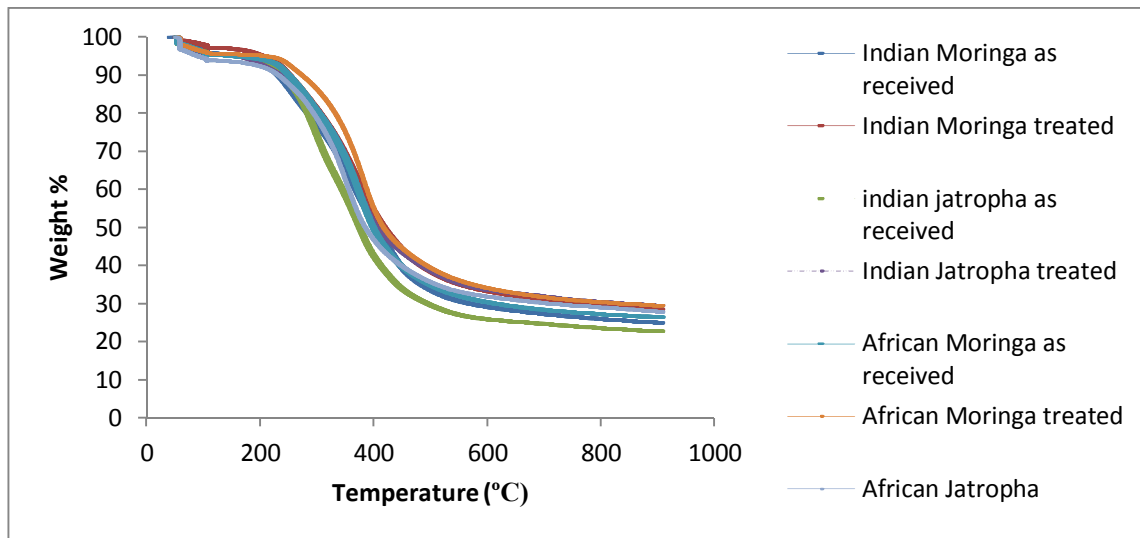
APPENDIX 3 - 300G/H OPERATING PROCEDURE

(Abba Kalgo and Guzhon Jiang)

Set Up

The diagram below shows the set up for the 300 g/hr pyrolysis rig in Aston University.

Pre-Start up

1. Put a pre-determined amount of biomass to be pyrolysed into the feeder and close it.
2. Put a measured amount of sand (about 150g, particle size: 355 - 500µm) into the reactor and then close it.
3. Weigh char pots 1 and 2 and attach them to the reactor (Anti-seize is applied to all the joints of the reactor and the metal components i.e. the char pot, the reactor threading and also to the ball and socket joint between the transition pipe and the metal transition pipe. This is done to prevent the glassware and metal components from getting stuck after the run.).
4. Sufficiently insulate the reactor to avoid any significant heat losses to the surroundings.
5. Ensure there are no combustible materials e.g. paper, organic solvent etc. around the vicinity of the rig.
6. Ensure rig is clean and properly assembled; all nuts and bolts should be tight enough and clamps should be used where appropriate to prevent leakages.
7. Open fluidising gas and set flow rate to 6l/min.
8. Open the feeder top nitrogen gas and set flow rate to 2 l/min.
9. Using a leak detector or soap solution, check for leakages at all joints and connections.
10. Ensure that all temperature and pressure displays are identified.

11. Ensure that the electric insulation plastics of all wires are not contacted with hot surface.

12. Check that all electric connections are appropriate and are isolated from the hot area of the fluidised bed

13. Check that the entire system is adequately earthed.

14. Check that the venting system connected to the rig is working. A piece of paper can be placed near the port, if the paper is sucked in, the venting system is working.

15. Check the Micro GC to make sure it is ready to accept gas samples.

16. Make sure the electrostatic precipitator is connected and properly earthed.

17. Make sure that the secondary condenser is filled with dry-ice/acetone mixture.

Start up

1. Open the cooling water valve. The flow rate should be set to make sure that the wall of the wall of the feeder close to the reactor is not more than $50^{o}C$.

2. Switch on the first slip-on heater, wait for about 2 minutes and switch on the second slip-on heater. The temperature of the heaters should be set to about $620^{o}C$ as this will allow the bed attain pyrolysis temperature of $550^{o}C$.

3. Allow enough time for the bed temperature to become stable at $550^{o}C$, usually takes between 1-2 hours.

4. Turn on the trace heating and let the temperature reach set point of about $450^{o}C$. This will usually take just a few minutes.

5. Turn on the electrostatic precipitator and set the voltage to 15KV (the current is at about 0.5A at this voltage)

6. When the reactor temperature becomes steady at pyrolysis temperature, turn on the screw feeder and adjust to a pre-determined rotating speed (Simultaneously, start a stop watch to monitor the time of the experiment). For a feedstock of 0.28g/ml bulk density, a rotating speed of 6 rpm is required to obtain a feeding rate of 1.5g/min. The feeding rate is proportional to the rotating speed and inversely proportional to the bulk density of the feedstock. An adequate rotating speed can then be calculated according to the bulk density of the feedstock.

Operation

1. Record the system parameters every 3 minutes. The items to be recorded are bed temperature, freeboard temperature, feeder pressure, pressure difference across the bed, EP voltage and current.

2. Check the screw feeder regularly to make sure there is no noise.

3. Take sensible actions according to the physical observations and measurements during the running period such as the nitrogen flow rates. Valves can be adjusted manually to correct such changes.

4. A high feeder pressure indicates a blockage in the system. The rig must be stopped according to the emergency shutdown procedure.

Shut down

1. Turn off the slip-on heaters.
2. Close all nitrogen gas flow.
3. Turn off the GC pump.
4. Pour out the mixture of acetone and dry-ice into a beaker. After drying, the mass of the condenser is measured.
5. Close the cooling water valve.
6. Separate the glass transition pipe from the metal transition pipe as it may otherwise become stuck.
7. Leave the system to cool down to room temperature.

Dismantling and cleaning

1. Take off all insulation material from the rig.
2. Dismantle char pots and transition pipe from the condenser.
3. Weigh all parts of the rig for mass balance purposes.

Emergency shut down

1. Turn off feeder screw.
2. Turn of the power from the mains.
3. Follow procedure for normal shut down.

APPENDIX 4 - DIMENSIONAL DRAWINGS OF PERIPHERAL EQUIPMENT

32

TRUE R14

TRUE R16

A

56

28

A

SECTION A-A

10

14

Ø28

TITLE:

Fast Screw Inlet

MATERIAL:

DWG NO.

A3

WEIGHT:

SCALE:1:1

SHEET 1 OF 1

297

50

Ø26 Ø30 Ø70

50

50

26

A

8

70

70

A

30

TRUE R35

TRUE R2

30

8

8

8

80

70

TRUE R15

SECTION A-A

	NAME	SIGNATURE	DATE		
DRAWN	ABBA KALGO		08-07-2015		
CHK'D					
APP'VD					
MFG					
Q.A					

UNLESS OTHERWISE SPECIFIED:
DIMENSIONS ARE IN MILLIMETERS
SURFACE FINISH:
TOLERANCES:
 LINEAR:
 ANGULAR:

FINISH:

DEBUR AND
BREAK SHARP
EDGES

DO NOT SCALE DRAWING

REVISION

TITLE:FEED OUTLET THROAT

MATERIAL: 316 STEEL

DWG NO.

A3

WEIGHT:

SCALE:1:1

SHEET 1 OF 1

298

Feed System Stand

(TRUE R35)

$\emptyset 70$

A

A

C

D

A

SECTION A-A

(335)

$\emptyset 70$

	NAME	SIGNATURE	DATE	
DRAWN	ABBA T.ALGO		30-04-2010	
CHK'D				
APP'VD				
MFG				
Q.A				

TITLE:500g/h
SCREWBASE CHARPOT

MATERIAL:316
STEEL

DWG NO.

A3